



**HAL**  
open science

# Heavy-light meson properties from lattice QCD

Antoine Gerardin

► **To cite this version:**

Antoine Gerardin. Heavy-light meson properties from lattice QCD. General Physics [physics.gen-ph]. Université Paris Sud - Paris XI, 2014. English. NNT : 2014PA112185 . tel-01126879

**HAL Id: tel-01126879**

**<https://theses.hal.science/tel-01126879>**

Submitted on 6 Mar 2015

**HAL** is a multi-disciplinary open access archive for the deposit and dissemination of scientific research documents, whether they are published or not. The documents may come from teaching and research institutions in France or abroad, or from public or private research centers.

L'archive ouverte pluridisciplinaire **HAL**, est destinée au dépôt et à la diffusion de documents scientifiques de niveau recherche, publiés ou non, émanant des établissements d'enseignement et de recherche français ou étrangers, des laboratoires publics ou privés.



Comprendre le monde,  
construire l'avenir®



**Thèse de doctorat**  
Spécialité: **Physique**

École Doctorale Physique en Ile-de-France - ED 564  
Laboratoire de physique théorique d'Orsay

---

**Heavy-light meson properties from lattice  
QCD**

---

Présentée par **Antoine Gérardin**

pour obtenir le grade de

DOCTEUR EN SCIENCES DE  
L'UNIVERSITÉ PARIS-SUD XI

Thèse soutenue publiquement le 23 septembre 2014 devant la Commission d'examen :

Dr. Benoît	BLOSSIER	(Directeur de thèse)
Dr. Diego	GUADAGNOLI	(Rapporteur)
Dr. Andreas	JUETTNER	(Examineur)
Pr. Vittorio	LUBICZ	(Rapporteur)
Pr. Vincent	MORENAS	(Examineur)
Dr. Marie-Hélène	SCHUNE	(Examineur)



Thèse préparée au  
**Laboratoire de Physique Théorique d'Orsay**  
Bâtiment 210, Université Paris-Sud 11  
91 405 Orsay CEDEX

## Abstract

Heavy-light mesons play an important role in the search of new physics beyond the Standard Model. In particular  $B$ -mesons properties can be used to put constraints on the matrix elements of the Cabibbo-Kobayashi-Maskawa (CKM) mixing matrix governing flavour-changing weak decays.

The dynamics of quarks and gluons are described by Quantum Chromodynamic (QCD). This theory predicts that, at low energies, the associated coupling constant increases, making the use of perturbative methods ineffective. Lattice QCD is a non-perturbative regularization scheme of QCD, suitable for numerical simulations. However, studying heavy-light mesons remains a challenging task due to the many different energy scales that must be considered simultaneously on the lattice. In this work, I use the Heavy Quark Effective Theory (HQET), which consists in a systematic expansion of the QCD Lagrangian and correlation functions in  $1/m$  where  $m$  is the mass of the heavy quark.

After a presentation of the main techniques used in lattice simulations, a computation of the  $b$ -quark mass with  $N_f = 2$  dynamical quarks is presented. All the steps are performed non-perturbatively, offering an important cross-check of the value cited in the PDG which mainly relies on perturbation theory. A computation of the  $B$ -meson decay constant at static and first orders in HQET will be also presented and phenomenological implication are discussed.

In the second part of this thesis, after introducing the Heavy Meson Chiral Lagrangians and its different couplings, I present the lattice computation of two such couplings. The first one is associated to the hadronic transition  $B^{*'} \rightarrow B\pi$  where  $B^{*'}$  is the radial excitation of the vector  $B$  meson. The Generalized Eigenvalue Problem (GEVP) will be used to extract information about the excited state from the ratio of three-point to two-point correlation functions and I will discuss the phenomenological implications of our results. Then, I will present the computation of the coupling  $h$  between the scalar and the pseudoscalar  $B$  mesons using two-point correlation functions. This coupling enters the formulae used to guide the chiral extrapolations when positive parity states are taken into account. We will see that  $h$  is large compared to the other couplings and that  $B$  meson orbital excitation degrees of freedom cannot be missed in chiral loops.

Finally, I will present the lattice computation of the mass and decay constant of the first radial excitation of the  $D$  meson. The mass will be compared with the recently observed state by the BaBar Collaboration and I show how the decay constant can help to solve the so-called “1/2 vs. 3/2” puzzle. In this work, the GEVP is used to control the contribution from higher excited states and continuum and chiral extrapolations are performed to take into account systematic errors.

**Keywords:** Lattice QCD, non-perturbative, HQET, B physics, heavy-light mesons



## Résumé

Les mésons lourd-légers jouent un rôle majeur dans la recherche de nouvelle physique au delà du modèle standard. En particulier, les propriétés du méson  $B$  sont utilisées pour contraindre la matrice Cabibbo-Kobayashi-Maskawa (CKM) qui décrit les changements de saveur d'un quark lors d'une interaction faible.

Les interactions entre quarks et gluons sont décrites par la théorie de l'interaction forte (QCD). Cette dernière prédit, qu'à faible énergie, le couplage de la théorie croît rendant tout traitement perturbatif impossible. La QCD sur réseau est une régularisation non-perturbative de la QCD adaptée aux simulations numériques. Néanmoins, l'étude des mésons lourd-légers est particulièrement délicate puisqu'elle nécessite la prise en compte de nombreuses échelles d'énergies. La théorie effective des quarks lourds (HQET) peut alors être utilisée : elle consiste en une expansion systématique du Lagrangien QCD et des fonctions de corrélation en puissance de  $1/m$  où  $m$  est la masse du quark lourd.

Après avoir présenté les outils de la QCD sur réseau, un calcul de la masse du quark  $b$  avec  $N_f = 2$  quarks dynamiques est présentée. Toutes les étapes sont réalisées de manière non-perturbative et le résultat est une importante vérification de la valeur actuellement citée par le PDG et qui repose essentiellement sur des calculs perturbatifs.

Dans la seconde partie de la thèse, après avoir présenté les Lagrangiens décrivant les mésons lourd-légers dans la limite chirale, je présente le calcul de deux couplages. Le premier couplage est associé à la transition hadronique  $B^{*l} \rightarrow B\pi$  où  $B^{*l}$  est la première excitation radiale du méson  $B$  vecteur. Il est obtenu en étudiant le rapport de fonctions de corrélation à trois et deux points et le problème aux valeurs propres généralisées (GEVP) est utilisé pour isoler la contribution de l'état excité. Dans un second temps, le couplage  $h$  qui décrit la transition entre des mésons  $B$  scalaire et pseudoscalaire est calculé. Ce couplage intervient dans les extrapolations chirales de différentes quantités, comme la constante de désintégration du méson  $B$  scalaire. Nous verrons que le couplage  $h$  est important et qu'il ne peut pas être négligé.

Finalement, je présenterai nos résultats concernant le calcul de la masse et de la constante d'annihilation de la première excitation radiale du méson  $D$ . Je comparerai la masse obtenue avec celle du nouvel état récemment découvert par la Collaboration BaBar et j'expliquerai comment le calcul de la constante d'annihilation peut aider dans la résolution du fameux problème "1/2 vs. 3/2". Tout au long de ce travail, le GEVP est utilisé pour réduire la contribution des états excités. De plus, les extrapolations chirales et la limite du continu sont étudiées afin de tenir compte des différentes sources d'erreurs systématiques.

**Mots clés** : QCD sur réseau, HQET, mésons  $B$ , mésons lourd-léger



# Contents

<b>Introduction</b>	<b>9</b>
<b>1 Lattice QCD</b>	<b>11</b>
1.1 QCD in the continuum . . . . .	12
1.2 From Minkowski to Euclidean space-time . . . . .	16
1.3 Discretization of the action . . . . .	16
1.4 The gauge action . . . . .	18
1.5 The fermionic action . . . . .	19
<b>2 Computation of observables in lattice QCD</b>	<b>25</b>
2.1 Path integrals in Lattice QCD . . . . .	26
2.2 Monte Carlo simulations . . . . .	28
2.3 The quark propagator . . . . .	32
2.4 Correlators . . . . .	35
2.5 The Generalized Eigenvalues Problem . . . . .	38
2.6 Smearing . . . . .	39
2.7 Error estimation . . . . .	41
2.8 Setting the scale and the continuum limit . . . . .	45
2.9 Discussion of systematic errors . . . . .	46
<b>3 Computation of <math>m_b</math> and <math>f_B</math></b>	<b>49</b>
Introduction . . . . .	51
3.1 The Heavy Quark Effective Theory . . . . .	52
3.2 Correlations functions in the framework of HQET . . . . .	58
3.3 Matching with QCD . . . . .	59
3.4 The axial current and $\mathcal{O}(a)$ improvement . . . . .	62
3.5 Computation of $\mathbf{m}_B$ and $\mathbf{f}_B$ in HQET at order $1/m$ . . . . .	64
3.6 The Generalized Eigenvalue Problem . . . . .	66
3.7 Simulation parameters . . . . .	69
3.8 Determination of the RGI $\mathbf{b}$ -quark mass $\mathbf{M}_b$ . . . . .	70
3.9 Conversion to the $\overline{\text{MS}}$ scheme . . . . .	73
3.10 Computation of the $\mathbf{B}$ meson decay constants $\mathbf{f}_B$ and $\mathbf{f}_{B_s}$ . . . . .	77
Conclusion . . . . .	83
<b>4 On the <math>B^{*'} \rightarrow B\pi</math> transition</b>	<b>85</b>
Introduction . . . . .	86
4.1 Heavy Meson Chiral Lagrangians . . . . .	87
4.2 The $g_{B^{*'}B\pi}$ coupling . . . . .	94
4.3 Computation on the Lattice . . . . .	97

4.4	Simulation parameters . . . . .	101
4.5	Lattice results . . . . .	102
4.6	Decay thresholds . . . . .	105
4.7	Diagonal couplings $\mathbf{g}_{11}$ and $\mathbf{g}_{22}$ . . . . .	105
	Conclusion . . . . .	107
<b>5</b>	<b>Computation of the soft pion coupling <math>h</math></b>	<b>109</b>
	Introduction . . . . .	110
5.1	Strategy . . . . .	111
5.2	Lattice setup . . . . .	114
5.3	Signal analysis . . . . .	120
5.4	Results . . . . .	122
5.5	Discussions . . . . .	126
	Conclusion . . . . .	127
<b>6</b>	<b>Mass and decay constant of the radially excited <math>D</math> meson</b>	<b>129</b>
	Introduction . . . . .	130
6.1	Computation of the masses and decay constants of $D_{(s)}$ and $D'_{(s)}$ . . . . .	131
6.2	Simulation details . . . . .	133
6.3	Results . . . . .	134
	Conclusion . . . . .	142
	<b>Conclusion</b>	<b>145</b>
	<b>Appendices</b>	<b>147</b>
<b>A</b>	<b>Definitions and conventions</b>	<b>149</b>
<b>B</b>	<b>Convergence rate in the sGEVP</b>	<b>153</b>
<b>C</b>	<b>Wick contractions</b>	<b>159</b>
<b>D</b>	<b>Renormalization</b>	<b>163</b>

# Introduction

In this thesis, I will focus on the heavy-light  $B$  and  $D$  mesons composed of a heavy quark,  $b$  or  $c$ , and one light quark where *heavy* and *light* refer to the natural scale of QCD given by the lambda parameter  $\Lambda \approx 200$  MeV. The theory that describes interactions between quarks and gluons is Quantum ChromoDynamics (QCD). At high energy scales, the strong coupling constant goes to zero such that a perturbative expansion of the correlation functions in the coupling constant is justified, this is called asymptotic freedom and quarks and gluons are weakly interacting. However, at low energy, the strong coupling increases and perturbation theory is no longer applicable: quarks and gluons cannot be seen as asymptotic states but hadronize into mesons and baryons observed in experiments. Lattice QCD allows to do QCD calculations, from first principles, in a non-perturbative way. It corresponds to a specific regularization of the QCD Lagrangian, convenient for numerical studies, where space-time is discretized into a hypercubic lattice. The spatial extent  $L$  plays the role of an infrared cutoff and the lattice spacing  $a$  corresponds to the ultraviolet cutoff making the path integral formulation of the theory well-defined. Taking the limit of infinite volume and zero lattice spacing, one then recovers QCD. However, we will see that some difficulties appear when dealing with heavy-light systems due to the many different scales that must be treated simultaneously on the lattice.

In particular, I will present a non-perturbative computation of the  $b$ -quark mass [1] which is one of the fundamental parameters of the Standard Model (SM). This provides an important cross-check since the result cited by the PDG [2] mainly relies on perturbative computations. The  $b$ -quark mass also enters in the determination of the Cabibbo-Kobayashi-Maskawa (CKM) matrix element  $|V_{ub}|$  from inclusive decays  $\bar{B} \rightarrow X_u \ell \bar{\nu}_\ell$  and contributes significantly to the total error. The CKM matrix is a unitary matrix which parametrizes flavour-changing quark transitions in the Standard Model. It plays a major role in the precision tests of the flavour sector of the Standard Model and the search for new physics since deviations from unitarity could be a sign of new physics. Then, I will present the computation of the  $B$  meson decay constant [3] which governs the weak decays of the  $B$  meson. In particular, it enters as a lattice input in the extraction of the matrix element  $|V_{ub}|$  from exclusive decays  $B \rightarrow \tau \nu$ . Finally, I will compare this result with the other exclusive determination of  $|V_{ub}|$  based on  $B \rightarrow \pi \ell \bar{\nu}$  which uses the form factor  $B \rightarrow \pi$  as an input.

In the second part of this thesis, I will present the Heavy Mesons Chiral Lagrangians which combine both the Heavy Quarks Effective field Theory (HQET) for the heavy quarks and chiral perturbation theory for the light quarks. To reduce the computational cost, many lattice simulations are performed at unphysical quark masses such that the pion mass is above its physical value. To estimate the associated systematic error, different simulations at several pion masses are performed and this effective field theory

is used to extrapolate the result to the chiral limit. At static order in HQET and first order in the pion momentum, this Lagrangian for negative and positive parity states is parametrized by a few coupling constants  $\hat{g}$ ,  $\tilde{g}$  and  $h$  which can be computed on the lattice. The coupling  $g$  between the two low lying pseudoscalar and vector  $B$  mesons has been studied in several works but very little is known about the couplings with excited states. In Chapter 4, I will present a first lattice computation of the coupling which parametrizes the hadronic transition  $B^{*'} \rightarrow B\pi$  between the radial excitation and the ground state  $B$  meson [131]. We will argue that excited states may play an important role in the interpretation of experimental data. Indeed, sum rules calculations of the coupling  $g_{D^*D\pi}$  failed to reproduce the experimental data unless one explicitly introduce the contribution of the first radial excitation. Since we work in the static limit, our work is a first hint of this statement even if  $1/m$  corrections in the HQET expansion are expected to be sizable in the case of  $D$  mesons. As a by-product of our work, we also have access to the coupling  $\hat{g}$ . Then, I present our lattice study of the scalar  $B$  meson and in particular, I present a computation of the soft pion coupling  $h$  which parametrizes the decay of the scalar  $B$  meson into the ground state  $B$  meson using two point correlation functions.

Finally, I will present our results on the computation of the mass and decay constant of the radial excitation of the  $D$  meson [5]. I will compare our results with the recently measured state by the BaBar Collaboration [6] and potentially compatible with the  $D'$  meson. I will also present the results on the computation of the decay constant  $f_{D'}$  and show how it can help to solve the so-called “1/2 vs. 3/2” puzzle [7, 5].

In the case of the  $B$  meson, the lattice simulations used in this work are performed using a subset of the CLS (coordinated lattice simulation) gauge configurations based on the Wilson-Clover action with two-dynamical quarks and the HYP smearing for the heavy quark. This lattice regularization is  $\mathcal{O}(a)$ -improved and lattice artifacts are quadratic on the lattice spacing. Moreover large volumes are used, satisfying the condition  $Lm_\pi > 4$ , such that volume effects are expected to be small. In the last chapter, which concerns the properties of the radial excitation of the  $D$  meson, ensembles from the ETM Collaboration are used. They are based on an alternative choice of regularization, called Twisted Mass QCD at maximal twist such that  $\mathcal{O}(a)$ -improvement is automatically fulfilled for physical quantities.

This thesis is organized as follows. In the first two chapters, I introduce the basic ingredients of a lattice QCD simulation which will be useful in the next chapters. In particular, I explain how the QCD Lagrangian can be regularized on the lattice and I introduce the Monte Carlo algorithm used to evaluate the path integral. Finally, I discuss the different sources of systematic errors. In Chapter 3, I explain how the heavy b-quark can be handled in lattice simulations using the Heavy Quark Effective field Theory (HQET) and I present the non-perturbative computation of b-quark mass and B meson decay constant which governs the weak decays of the meson. Then in Chapter 4, I present the first computation of the coupling associated to the hadronic transition  $B^{*'} \rightarrow B\pi$  between the first radial excitation and the ground state  $B$  mesons and in chapter 5, I compute the soft pion coupling  $h$  which parametrizes the hadronic transition of the scalar  $B$  meson (orbital excitation) into the ground state  $B$  meson  $B_0^* \rightarrow B\pi$ . Finally, in the last chapter, I present our results on the mass and decay constant of the radially excited  $D'$  meson.

# Chapter 1

## Lattice QCD

### Contents

---

<b>1.1</b>	<b>QCD in the continuum</b> . . . . .	<b>12</b>
1.1.1	The Lagrangian . . . . .	12
1.1.2	Wilson loops . . . . .	13
1.1.3	Symmetries . . . . .	14
<b>1.2</b>	<b>From Minkowski to Euclidean space-time</b> . . . . .	<b>16</b>
<b>1.3</b>	<b>Discretization of the action</b> . . . . .	<b>16</b>
<b>1.4</b>	<b>The gauge action</b> . . . . .	<b>18</b>
<b>1.5</b>	<b>The fermionic action</b> . . . . .	<b>19</b>
1.5.1	Naïve formulation and the doubling problem . . . . .	19
1.5.2	Wilson Fermions . . . . .	20
1.5.3	Improvement of the Wilson action . . . . .	21
1.5.4	Properties of Wilson Fermions . . . . .	22
1.5.5	Twisted Mass Fermions . . . . .	23

---

Quantum Chromodynamics (QCD) is the theory of the strong interaction between quarks and gluons. The associated coupling constant  $g$  has the particularity to decrease at high energies, or equivalently at short distances, so that perturbation theory is reliable. This is called asymptotic freedom. On the contrary, at low energies, or long distances, the coupling constant becomes large and a perturbative treatment is no longer possible: this is the confinement phase of QCD which explains why quarks are never observed as asymptotic states. Lattice QCD aims to compute QCD observables non-perturbatively, from first principles. In this chapter, I will start with a brief introduction of the theory in the continuum and recall its main properties which will be useful in the next chapters. For a more comprehensive introduction, the subject is introduced in standard textbooks [8, 9, 10]. Then, I will explain how the theory can be regularized on the lattice, starting with the gauge action and, in a second step, with the fermionic action. Finally, I will discuss the main symmetries of the lattice action.

## 1.1 QCD in the continuum

### 1.1.1 The Lagrangian

Quantum Chromodynamics is a relativistic gauge field theory based on the non-abelian  $SU(3)$  group. Its basic degrees of freedom are the quarks (fermions) and the gluons (bosons).

The quarks are represented by 4-components Dirac spinor fields  $\psi(x)$  which belong to the fundamental representation of the gauge group. The fields depend on the space-time position  $x$  and carry Dirac ( $\alpha = 1, 2, 3, 4$ ) and color ( $a = 1, 2, 3$ ) indices<sup>1</sup>. In the Standard Model, there are  $N_f = 6$  different flavours of quarks called up (u), down (d), strange (s), charm (c), bottom (b) and top (t), therefore, the fields  $\psi_f$  are labeled by a flavour index  $f = 1, \dots, 6$ .

	$\mu$	$\overline{m}^{\overline{\text{MS}}}(\mu)$
up ( $u$ )	2 GeV	$2.3^{+0.7}_{-0.5}$ MeV
down ( $d$ )	2 GeV	$4.8^{+0.5}_{-0.3}$ MeV
strange ( $s$ )	2 GeV	$95 \pm 5$ MeV
charm ( $c$ )	$\overline{m}_c^{\overline{\text{MS}}}$	$1.275 \pm 0.025$ GeV
bottom ( $b$ )	$\overline{m}_b^{\overline{\text{MS}}}$	$4.18 \pm 0.03$ GeV
top ( $t$ )	$\overline{m}_t^{\overline{\text{MS}}}$	$173.07 \pm 0.52 \pm 0.72$ GeV

Table 1.1 – Quark masses in the  $\overline{\text{MS}}$  scheme [2]. The parameter  $\mu$  corresponds to the renormalization scale.

The gluons are represented by the Lorentz vector gauge field  $A_\mu(x)$ . Each space-time component  $A_\mu(x)$ , labeled by a Dirac index  $\mu$ , is an element of the  $su(3)$  Lie Algebra

1. Here and in the following, Dirac indices are denoted by Greek indices ( $\alpha, \beta, \dots$ ) and color by Latin indices ( $a, b, c, \dots$ )

and carries one color index  $a$ . Therefore, one can write

$$A_\mu(x) = \sum_{a=1}^8 A_\mu^a(x) T_a, \quad (1.1)$$

where  $T_a$  are the generators of the  $\text{su}(3)$  Lie algebra (Appendix A). In terms of these fields, the continuum Lagrangian of Quantum Chromodynamics in Minkowski space-time is given by

$$\mathcal{L}_{\text{QCD}} = -\frac{1}{2} \text{Tr} [F^{\mu\nu} F_{\mu\nu}] + \sum_{f=1}^{N_f} \bar{\psi}_f(x) (i\mathcal{D} - m_f) \psi_f(x), \quad (1.2)$$

where color and Dirac indices are omitted for simplicity. The antiquark field  $\bar{\psi}_f$  is defined by  $\bar{\psi}_f = \psi_f^\dagger \gamma_0$  where  $\gamma_0$  is the  $\gamma$ -matrix associated with time (Appendix A). The bare quark mass of flavour  $f$  is  $m_f$  and the covariant derivative  $\mathcal{D}$  is defined by

$$\mathcal{D} = \gamma^\mu D_\mu = \gamma^\mu (\partial_\mu - ig_0 A_\mu), \quad (1.3)$$

where  $g_0$  is the strong coupling constant. Here as in the following, summation over repeated indices is understood except if stated otherwise and the metric convention is given in Appendix A. Finally, the field strength tensor is given by

$$F_{\mu\nu}(x) = \frac{i}{g_0} [D_\mu(x), D_\nu(x)] = \partial_\mu A_\nu(x) - \partial_\nu A_\mu(x) - ig_0 [A_\mu(x), A_\nu(x)], \quad (1.4)$$

and is an element of the  $\text{SU}(3)$  gauge group

$$F_{\mu\nu}(x) = \sum_{a=1}^8 F_{\mu\nu}^a(x) T_a. \quad (1.5)$$

The commutator in eq. (1.4) is non zero due to the non-abelian nature of the gauge group. Therefore, gluons interact with themselves as well as with quarks: this feature is responsible for the non-perturbative aspects of QCD.

Finally, the theory is defined by its generating functional  $Z$  in terms of which we can compute any correlation functions. In the functional integral formalism,  $Z$  is given by an integral over fermion and gauge fields  $\psi, \bar{\psi}, A_\mu$

$$Z = \int D[A_\mu] D[\psi] D[\bar{\psi}] e^{iS_{\text{QCD}}}, \quad S_{\text{QCD}} = \int d^4x \mathcal{L}_{\text{QCD}},$$

where  $S_{\text{QCD}}$  is the QCD action. A precise definition of the associated measure will be given in the second chapter where the theory is regularized on the lattice.

### 1.1.2 Wilson loops

In the continuum theory, we can define the *Wilson line* along a path  $P$  that runs from  $y$  to  $z$

$$U_P(z, y) = \mathcal{P} \exp \left[ ig_0 \int_P A_\mu(x) dx^\mu \right], \quad (1.6)$$

where the label  $P$  indicates that the Wilson line depends on the path and  $\mathcal{P}$  stands for path-ordering to take into account the non-commutativity of the gauge field  $A_\mu(x)$ . In particular, when the path is closed, it defines a Wilson loop:

$$U_P(y, y) = \mathcal{P} \exp \left[ i g_0 \oint_P A_\mu(x) dx^\mu \right]. \quad (1.7)$$

For Abelian groups, like  $U(1)$  in QED, the path ordering is not necessary and Stokes' theorem can be used to express the Wilson loop as the flux of the field strength through the surface  $S$  which spans the closed loop  $\mathcal{P}$

$$U_P(y, y) = \exp \left[ i \frac{g_0}{2} \oint_S F_{\mu\nu}(x) d\sigma^{\mu\nu} \right]. \quad (1.8)$$

Even if this is not easily extended to non-abelian groups, this geometrical interpretation of the field strength will be useful when introducing the regularized version of QCD.

### 1.1.3 Symmetries

As a relativistic theory, the QCD Lagrangian is invariant under standard Lorentz transformations. In addition, I will discuss two other symmetries which will be useful in the next sections: the gauge invariance and the chiral symmetry in the massless limit.

#### Gauge invariance

Gauge invariance is one of the main features of QCD: it means that the Lagrangian is invariant under local rotations in color space. More precisely, a local gauge transformation, acting on both spinor and gauge fields, is defined by

$$\begin{aligned} \psi(x) &\longrightarrow \psi'(x) = \Omega(x)\psi(x), \\ \bar{\psi}(x) &\longrightarrow \bar{\psi}'(x) = \bar{\psi}(x)\Omega^\dagger(x), \\ A_\mu(x) &\longrightarrow A'_\mu(x) = \Omega(x)A_\mu(x)\Omega^\dagger(x) - \frac{i}{g_0} (\partial_\mu\Omega(x))\Omega^\dagger(x), \end{aligned}$$

where the field  $\Omega(x) = \exp(i\omega^a(x)T_a) \in SU(3)$  depends on the space-time position  $x$ . In particular, the covariant derivative obeys the simple transformation rule  $D_\mu(x) \rightarrow D'_\mu(x) = \Omega(x)D_\mu(x)\Omega^\dagger(x)$ . Finally, it is useful to notice that the Wilson line also transforms similarly,  $U_P(x, y) \rightarrow U'_P(x, y) = \Omega(x)U_P(x, y)\Omega^\dagger(y)$ , so that the Wilson loop is a gauge invariant quantity.

#### Chiral symmetry

Another important feature of the QCD Lagrangian is the chiral symmetry in the limit of vanishing quark masses. In this context, it is useful to introduce the left and right components of a spinor by

$$\psi = \psi_L + \psi_R = P_L\psi + P_R\psi,$$

where left and right projectors are given by

$$P_L = \frac{1 - \gamma_5}{2} \psi, \quad P_R = \frac{1 + \gamma_5}{2} \psi,$$

and satisfy the relations  $P_L + P_R = 1$ ,  $P_L^2 = P_L$ ,  $P_R^2 = P_R$  and  $P_R P_L = P_L P_R = 0$ . Then, in the massless limit, the fermionic part of the QCD Lagrangian can be decomposed into the sum of two terms, each one involving only one chirality  $L$  or  $R$ . Considering only one flavour ( $N_f = 1$ ), eq. (1.2) becomes

$$\mathcal{L}_{\text{QCD}} = -\frac{1}{2} \text{Tr} [F^{\mu\nu} F_{\mu\nu}] + \bar{\psi}_L(x) \not{D} \psi_L(x) + \bar{\psi}_R(x) \not{D} \psi_R(x).$$

A mass term  $m\bar{\psi}\psi = m(\bar{\psi}_R\psi_L + \bar{\psi}_L\psi_R)$  would break this symmetry since it mixes both left and right chiralities. An immediate consequence of this decomposition is that the massless Lagrangian is invariant under a global chiral phase transformation parametrized by the two angles  $\theta_L$  and  $\theta_R$  and acting on the Dirac components of the spinor:

$$\psi_L(x) \rightarrow \psi'_L(x) = e^{i\theta_L} \psi_L(x) \quad , \quad \bar{\psi}_L(x) \rightarrow \bar{\psi}'_L(x) = \bar{\psi}_L(x) e^{i\theta_L}, \quad (1.9)$$

$$\psi_R(x) \rightarrow \psi'_R(x) = e^{i\theta_R} \psi_R(x) \quad , \quad \bar{\psi}_R(x) \rightarrow \bar{\psi}'_R(x) = \bar{\psi}_R(x) e^{i\theta_R}. \quad (1.10)$$

Using linear combinations of the previous transformations where the full spinor is rotated with the same angle or where each chirality is rotated with an opposite angle, this  $U(1) \otimes U(1)$  symmetry can be more conveniently parametrized into  $U(1) \otimes U(1)_A$  where the transformations now read

$$\psi(x) \rightarrow \psi'(x) = e^{i\theta} \psi(x), \quad (1.11)$$

$$\psi(x) \rightarrow \psi'(x) = e^{i\theta_A \gamma_5} \psi(x). \quad (1.12)$$

The first  $U(1)$  transformation is associated with the baryon number conservation and the second, with the subscript  $A$ , stands for axial transformation. This is a symmetry of the Lagrangian but the associated symmetry is anomalously broken at the quantum level of the theory (this is the axial anomaly [11, 12]).

In nature, up and down quarks (and the strange quark to a certain extent) happen to have relatively small masses when compared to the natural scale of QCD given by the lambda parameter  $\Lambda \approx 200$  MeV. Then, we can generalize the previous discussion with  $N = 2$  or  $3$  flavours of massless quarks. In addition to the previous symmetry, we can rotate independently the left and right components of the spinor in flavour space (this is the isospin symmetry which also holds for non-zero but degenerate masses). The full symmetry for vanishing quark masses becomes

$$\psi_L(x) \rightarrow \psi'_L(x) = U_L \psi_L(x), \quad (1.13)$$

$$\psi_R(x) \rightarrow \psi'_R(x) = U_R \psi_R(x), \quad (1.14)$$

where  $U_L, U_R \in U(N)$  are independent unitary matrices. Again, we can more conveniently write this as  $SU(N)_V \otimes SU(N)_A \otimes U(1) \otimes U(1)_A$  where the  $SU(N)_V \otimes SU(N)_A$  transformations are given by :

$$\psi(x) \rightarrow \psi'(x) = e^{\vec{\alpha}_V \cdot \vec{\tau}} \psi(x) \quad (\text{vector transformation}) \quad (1.15)$$

$$\psi(x) \rightarrow \psi'(x) = e^{\vec{\alpha}_A \cdot \vec{\tau} \gamma_5} \psi(x) \quad (\text{axial transformation}) \quad (1.16)$$

where  $\tau$  are the generators of the  $SU(N)$  group. In the case of  $SU(2)$  they are given by  $\tau_i = i\sigma_i/2$  where  $\sigma_i$  are the Pauli matrices.

Since axial transformations mix states of opposite parity, we would expect an exact degeneracy in the spectrum for states with the same quantum numbers but opposite parity. This is obviously not the case in experiments. First, the quark mass term breaks explicitly the chiral symmetry, however this breaking term does not explain the large mass difference between, for example, the  $\rho$  meson and the  $a_1$  meson. This leads to the conclusion that chiral symmetry is also spontaneously broken. Chiral symmetry will be useful in Chapter 4 to describe heavy-light mesons and their exchange of soft pions.

## 1.2 From Minkowski to Euclidean space-time

Correlation functions are usually expressed in terms of path integrals. In this formalism, the weight associated to each path is given by  $e^{iS_{\text{QCD}}}$  where  $S_{\text{QCD}}$  is the classical action evaluated along the path. From a numerical point of view, the presence of the complex variable  $i$  is problematic since the integrand oscillates rapidly. The way to overcome this problem is to work in Euclidean space-time after performing a Wick rotation defined by the formal substitution

$$x_0 \rightarrow -ix_4 \quad , \quad x_i \rightarrow x_i .$$

In Euclidean space-time, the weight associated to each path becomes  $e^{-S_E}$  where the Euclidean action is given by

$$S_E = \int d^4x \left( \frac{1}{2} \text{Tr} [F^{\mu\nu} F_{\mu\nu}] + \bar{\psi}(x) (\gamma_\mu^E D_\mu + m) \psi(x) \right) . \quad (1.17)$$

Here, the scalar product is the usual euclidean scalar product  $a^\mu b_\mu = \sum_{\mu=1}^4 a_\mu b_\mu$  and the Euclidean gamma matrices  $\gamma_\mu^E$  are given in Appendix A.

The correspondence between Euclidean and Minkowski correlation functions is given by the Wightman axioms [13] and the Osterwalder-Schrader theorem [14, 15, 16]. The Wightman axioms allow for an analytic continuation from Minkowski to Euclidean space-time while the Osterwalder-Schrader theorem states that, given some assumptions, the reverse operation is also justified. When working with the Euclidean formulation, the physical results are obtained by rotating back to Minkowski space-time but, fortunately, many interesting quantities like masses or some space-like matrix elements are directly accessible from Euclidean correlation functions avoiding the delicate analytic continuation back to Minkowski space-time. Nevertheless, this problem can occur, in particular when dealing with unstable particles or off-shell matrix elements [17].

In the following, I will always work in Euclidean space-time and I will drop the subscript  $E$ . The scalar product is also understood to be the usual Euclidean scalar product except stated otherwise.

## 1.3 Discretization of the action

The idea of lattice QCD is to discretize the theory on a finite hypercubic lattice  $\Lambda$ , of size  $L^3 \times T$ , with a lattice spacing  $a$

$$\Lambda \equiv \{ x = (n_1, n_2, n_3, n_4)a \quad , \quad (n_1, n_2, n_3) \in [0, L] \quad , \quad n_4 \in [0, T] \} .$$

More general lattices, with a lattice spacing depending on the space-time directions could also be considered but only isotropic lattices will be used in this work. Finally, we would like to maintain as many symmetries as possible in the discrete version of the theory. In particular, since gauge invariance plays a major role in modern physics we would like to conserve it.

### Spinor fields

Following the ideas of Wilson [18], spinor fields are replaced by Grassmann vectors on each site of the lattice  $\psi(x), \bar{\psi}(x)$ ,  $x \in \Lambda$  with Dirac and color indices as in the continuum.

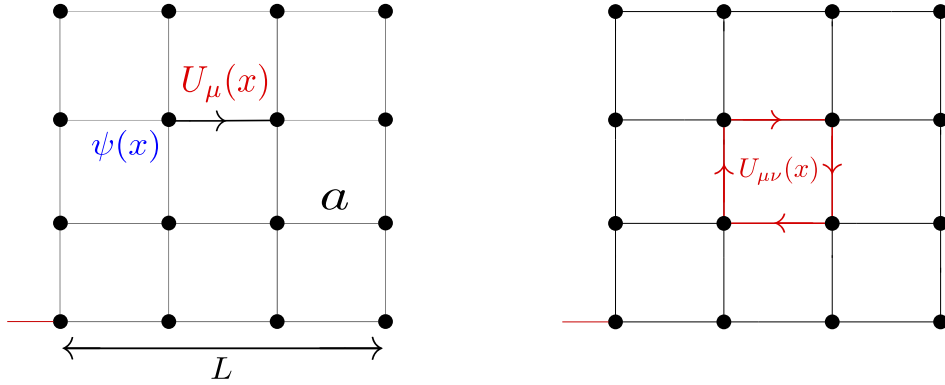


Figure 1.1 – Notations used for the fermionic field  $\psi(x)$  and the link variable  $U_\mu(x)$ .  $L$  is the spatial extent of the lattice and  $a$  is the lattice spacing.  $U_{\mu\nu}(x)$  is the plaquette associated to the site  $x$ .

### Gauge field

For the gluons, it is not convenient to use a discretized version of the vector field  $A_\mu(x)$  since it would make it difficult to implement gauge invariance. In the previous section, we have noticed that *Wilson loops* transforms trivially under gauge transformations. Therefore, we associate one *link variable*  $U_\mu(x) \in \text{SU}(3)$  to each link of the lattice: it corresponds to the parallel transporter from  $x + \hat{\mu}$  to  $x$  where  $\hat{\mu}$  is the unit vector in the direction of  $\mu$ . It can be related to the continuum gauge field  $A_\mu(x)$  using relation (1.6).

### Symmetries

A gauge transformation on the lattice is defined by

$$\psi(x) \longrightarrow \psi'(x) = \Omega(x)\psi(x), \quad (1.18)$$

$$\bar{\psi}(x) \longrightarrow \bar{\psi}'(x) = \bar{\psi}(x)\Omega^\dagger(x), \quad (1.19)$$

$$U_\mu(x) \longrightarrow U'_\mu(x) = \Omega(x)U_\mu(x)\Omega^\dagger(x + a\hat{\mu}), \quad (1.20)$$

where  $\Omega(x)$  is an  $\text{SU}(3)$  group element defined on each site of the lattice.

While gauge symmetry is implemented in an exact way, the translational and rotational invariance of the theory are reduced to discrete translational and rotational invariance (translations have to be a multiple of the lattice spacing  $a$  and only rotations with an angle of  $\pi/2$  are allowed). However, as the lattice spacing  $a$  goes to zero, these transformations get closer to their continuum analog.

### Boundary conditions

For the gauge field, one can choose periodic boundary conditions in space and time. For the quarks, however, one choose anti-periodic boundary conditions in the time direction and periodic boundary conditions in space directions. This difference is necessary for the formal reconstruction of the Hilbert space for the Minkowski theory [19]. Therefore, the lattice has the topology of a four-dimensional torus.

### Discrete derivatives

On the lattice, it is useful to introduce the covariant backward and forward derivatives

$$\begin{aligned}\nabla_\mu\psi(x) &= \frac{1}{a} [ U_\mu(x)\psi(x+a\hat{\mu}) - \psi(x) ] , \\ \nabla_\mu^*\psi(x) &= \frac{1}{a} [ \psi(x) - U_\mu(x-a\hat{\mu})^{-1}\psi(x-a\hat{\mu}) ] .\end{aligned}$$

To ensure the anti-hermiticity of the lattice Dirac operator, which will be defined in Section 1.5, it is also convenient to define the symmetric covariant derivative

$$\tilde{\nabla}_\mu = \frac{\nabla_\mu + \nabla_\mu^*}{2} .$$

## 1.4 The gauge action

In the continuum theory, the field strength tensor  $F_{\mu\nu}$  can be seen as the flux of the vector potential  $A_\mu$  through a closed path around the point  $x$ . Following this idea, the *plaquette*  $U_{\mu\nu}(x)$  is defined as the shortest non trivial closed loop on the lattice

$$U_{\mu\nu}(x) = U_\mu(x)U_\nu(x+a\hat{\mu})U_\mu^\dagger(x+a\hat{\nu})U_\nu^\dagger(x) . \quad (1.21)$$

From eq. (1.20), the trace of the plaquette is obviously gauge invariant and has the following expansion in terms of the lattice spacing  $a$

$$U_{\mu\nu}(x) = 1 + ig_0a^2F_{\mu\nu} - \frac{1}{2}g_0^2a^4F_{\mu\nu}^2 + \mathcal{O}(a^6) . \quad (1.22)$$

Therefore, the gauge part of the lattice action can be defined by [18]

$$S_G[U_\mu] = \frac{1}{g_0^2} \sum_{x \in \Lambda} \sum_{\mu, \nu} \text{Re Tr} (1 - U_{\mu\nu}(x)) , \quad (1.23)$$

and is known as the Wilson plaquette action. The second term in eq. (1.22) vanishes due to the trace and the real part makes the action real. It is usually written in terms of the parameter  $\beta = 6/g_0^2$  and should not be confused with the  $\beta$  function usually used to define the running of the coupling constant. Finally, using the lattice spacing expansion given by eq. (1.22), we obtain

$$S_G[U_\mu] = \frac{1}{g_0^2} \sum_{x \in \Lambda} \sum_{\mu, \nu} \text{Re Tr} (1 - U_{\mu\nu}(x)) = \frac{a^4}{2} \sum_{x \in \Lambda} \sum_{\mu, \nu} \text{Tr} (F_{\mu\nu}(x)^2) + \mathcal{O}(a^2) ,$$

and the Wilson plaquette action is equivalent to the continuum action given by eq. (1.17) up to discretization errors quadratic in the lattice spacing  $\mathcal{O}(a^2)$ .

## 1.5 The fermionic action

Putting fermions on the lattice is much more difficult and many different actions have been proposed over the years. Each formulation has its own advantages and disadvantages. In the next section, I will introduce the Wilson-Clover formulation mostly used in this work and I will discuss its main properties. Finally, I will briefly present the Twisted mass formulation used in the last chapter of this thesis.

### 1.5.1 Naïve formulation and the doubling problem

On the lattice, the naive discretization of the fermionic part of the action is simply obtained by replacing the covariant derivative by the discrete symmetric covariant derivative  $\tilde{\nabla}_i$  and the continuous integral by a discrete sum over lattice points. For notational convenience, the action is written for one quark flavour:

$$S_F[U_\mu, \psi, \bar{\psi}] = a^4 \sum_{x \in \Lambda} \bar{\psi}(x) \left( \gamma_\mu \tilde{\nabla}_\mu + m \right) \psi(x) = a^4 \sum_{x, y \in \Lambda} \bar{\psi}(x) D(x, y) \psi(y), \quad (1.24)$$

or, explicitly:

$$S_F[U_\mu, \psi, \bar{\psi}] = a^4 \sum_{x \in \Lambda} \left( \bar{\psi}(x) \gamma_\mu U_\mu(x) \psi(x + a\hat{\mu}) - \bar{\psi}(x) \gamma_\mu U_\mu^\dagger(x - a\hat{\mu}) \psi(x - a\hat{\mu}) \right) + ma^4 \sum_{x \in \Lambda} \bar{\psi}(x) \psi(x),$$

where the naive Dirac operator is defined by  $D = \gamma_\mu \tilde{\nabla}_\mu + m$ . However, it is well known that this naive action leads to the so-called fermions doubling problem [20, 21], namely the appearance of non physical degrees of freedom (doublers), even in continuum limit. To trace back this problem, we can compute the propagator of the free quark. In this case, the gauge links are trivial ( $U_\mu = \mathbb{1}$  up to a gauge transformation), and the Dirac operator reads

$$D = \gamma_\mu \partial_\mu + m,$$

where  $\partial_\mu \psi(x) = (1/a)(\psi(x + a\hat{\mu}) - \psi(x))$ . Its Fourier transform is (see Appendix A for notations)

$$\tilde{D}(p) = \frac{i}{a} \sum_{\mu} \gamma_\mu \sin(ap_\mu) + m, \quad (1.25)$$

where  $p_\mu$  belongs to the first Brillouin zone defined by

$$B = \left\{ p_i = \frac{\pi}{L} n_i, \quad i \in [1, 3], \quad p_0 = \frac{\pi}{T} n_0, \quad n_i \in [0, L - 1], \quad n_0 \in [0, T - 1] \right\}.$$

Finally, the propagator, which corresponds to the inverse of the Dirac operator, is given by

$$G(p) = \tilde{D}^{-1}(p) = \frac{-\frac{i}{a} \sum_{\mu} \gamma_\mu \sin(ap_\mu) + m}{\left( \frac{1}{a} \sum_{\mu} \gamma_\mu \sin(ap_\mu) \right)^2 + m^2}.$$

Therefore, at fixed value of  $p_\mu$  and taking the limit  $a \rightarrow 0$  we recover the expected behavior and the propagator has a pole at  $p^2 = -m^2$ . But there are also fifteen other poles in the limit  $a \rightarrow 0$  and  $p_\mu$  finite corresponding to the points

$$p_\mu \in \left[ 0, \frac{\pi}{a} \right], \quad \mu \in [0, 3].$$

This problem is due to the choice of discretization and can be seen as a lattice artifact. It is a consequence of the first order differential equation describing fermions which leads, in the discrete theory, to the sine function. Since in the interacting theory the doublers can interact with each other via quantum loop corrections (in particular the gluons couple to each doublers), it is important to remove them properly. In the next section, we will see how to overcome this difficulty.

### 1.5.2 Wilson Fermions

Many different lattice regularizations are possible and they differ only by terms of order  $\mathcal{O}(a^2)$  which vanish in the continuum limit. In particular, one can add any operator of dimension five to the action without changing its continuum limit. Wilson used this freedom and proposed to add the *Wilson term*, proportional to the discrete Laplace operator [21]

$$a^5 \frac{r}{2} \Delta \psi(x), \quad (1.26)$$

to modify the dispersion relation. The new parameter  $r$  is called the Wilson parameter and is usually set to one. Then, repeating the previous analysis, one obtains

$$\tilde{D}(p) = \frac{i}{a} \sum_{\mu} \gamma_{\mu} \sin(ap_{\mu}) + \frac{1}{a} \sum_{\mu} (1 - \cos(ap_{\mu})) \mathbb{1} + m,$$

which has to be compared with eq. (1.25). When the lattice spacing goes to zero, the doublers acquire a mass  $m + \frac{2\omega}{a}$  where  $\omega$  is the number of components equal to  $\pi/a$ , whereas the mass of the physical fermions is unchanged. The additional mass is of the order of the cut-off and tends to infinity in the continuum limit, therefore the doublers decouple from the theory and can be neglected. This defines the Wilson action

$$S_W[U_{\mu}, \psi, \bar{\psi}] = a^4 \sum_{x \in \Lambda} \bar{\psi}(x) \left\{ \tilde{\nabla}_{\mu} \gamma_{\mu} + m - \frac{ar}{2} \Delta \right\} \psi(x) = a^4 \sum_{x, y \in \Lambda} \bar{\psi}(x) D_W(x, y) \psi(y),$$

where the Wilson Dirac operator is now given by

$$D_W = \frac{1}{2} \{ \gamma_{\mu} (\nabla_{\mu} + \nabla_{\mu}^*) - ar \nabla_{\mu}^* \nabla_{\mu} \} + m. \quad (1.27)$$

More explicitly, it reads

$$S_W[U_{\mu}, \psi, \bar{\psi}] = a^3 \sum_{x \in \Lambda} \bar{\psi}(x) \left\{ \frac{(\gamma_{\mu} - r)}{2} U_{\mu}(x) \psi(x + a\hat{\mu}) - \frac{(\gamma_{\mu} + r)}{2} U_{\mu}^{\dagger}(x - a\hat{\mu}) \psi(x - a\hat{\mu}) \right\} + (am + 4r) \bar{\psi}(x) \psi(x). \quad (1.28)$$

In lattice simulations, it is convenient to define the hopping parameter  $\kappa^{-1} = 2ma + 8r$  as the coupling between neighboring sites. Then, changing the normalization of the fermionic field  $\psi(x) \rightarrow \sqrt{2\kappa/a^3} \psi(x)$ , the action can be written in terms of dimensionless quantities

$$S_W[U_{\mu}, \psi, \bar{\psi}] = \sum_{x \in \Lambda} \kappa \left[ \bar{\psi}(x) (\gamma_{\mu} - r) U_{\mu}(x) \psi(x + a\hat{\mu}) - \bar{\psi}(x + a\hat{\mu}) (\gamma_{\mu} + r) U_{\mu}^{\dagger}(x) \psi(x) \right] + \bar{\psi}(x) \psi(x). \quad (1.29)$$

### 1.5.3 Improvement of the Wilson action

The Wilson plaquette action for the gauge field has quadratic discretization errors in the lattice spacing. On the other hand, as a consequence of the Wilson term introduced to eliminate the doublers, the Wilson action for quarks, given by eq. (1.28), has larger discretization errors proportional to the lattice spacing  $O(a)$ . In the next chapter, I will introduce Monte Carlo algorithms used to evaluate the path integral in lattice simulations. Since the algorithm becomes more and more expensive as one gets closer to the continuum limit, reducing discretization errors is particularly important. The lattice discretization is not unique and one can use this freedom to design *improved* actions with faster convergence rates. Sheikholeslami and Wohlert proposed to add a new dimension five operator [22] to cancel  $O(a)$  effects, this leads to the Wilson-Clover action:

$$S_W^{\text{impr}}[U_\mu, \psi, \bar{\psi}] = S_W[U_\mu, \psi, \bar{\psi}] + \kappa c_{SW} \sum_{x \in \Lambda} \bar{\psi}(x) \frac{i}{2} \sigma_{\mu\nu} \hat{F}_{\mu\nu}(x) \psi(x). \quad (1.30)$$

The additional operator is the Pauli term,  $\sigma_{\mu\nu}$  given in terms of the gamma matrices by

$$\sigma_{\mu\nu} = \frac{i}{2} [\gamma_\mu, \gamma_\nu],$$

and  $\hat{F}_{\mu\nu}$  is the discretized version of the gluon field strength (its normalization differs from the one in the continuum (1.4) by a factor  $ig_0$ ). A convenient regularization is obtained by averaging the four plaquettes lying in the  $(\mu, \nu)$  plane around the point  $x$  (Figure 1.2):

$$\hat{F}_{\mu\nu} = \frac{1}{8a^2} (Q_{\mu\nu} - Q_{\nu\mu}), \quad (1.31)$$

with

$$\begin{aligned} Q_{\mu\nu} = & (U_\mu(x)U_\nu(x+a\hat{\mu})U_\mu^\dagger(x+a\hat{\nu})U_\nu^\dagger(x) \\ & - U_\mu(x)U_\nu^\dagger(x+a\hat{\mu}-a\hat{\nu})U_\mu^\dagger(x-a\hat{\nu})U_\nu(x-a\hat{\nu}) \\ & + U_\nu(x)U_\mu^\dagger(x-a\hat{\mu}+a\hat{\nu})U_\nu^\dagger(x-a\hat{\mu})U_\mu(x-a\hat{\mu}) \\ & - U_\nu^\dagger(x-a\hat{\nu})U_\mu^\dagger(x-a\hat{\mu}-a\hat{\nu})U_\nu(x-a\hat{\mu}-a\hat{\nu})U_\mu(x-a\hat{\mu})) . \end{aligned}$$

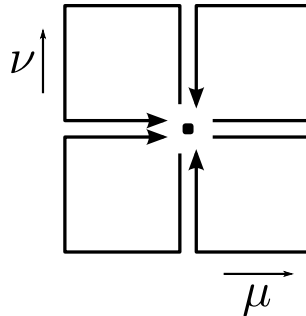


Figure 1.2 – Schematic representation of the discretized field strength operator  $\hat{F}_{\mu\nu}$

At tree level, the  $\mathcal{O}(a)$  improvement is achieved by setting  $c_{\text{SW}} = 1$  but, in the interacting theory,  $c_{\text{SW}}$  depends on the coupling constant  $g_0$  through renormalization. It can be estimated in perturbation theory [22, 23] and has also been computed non-perturbatively for  $N_f = 2$  dynamical quarks [24]; a good approximation is:

$$c_{\text{SW}} = \frac{1 - 0.454g_0^2 - 0.175g_0^4 + 0.012g_0^6 + 0.045g_0^8}{1 - 0.720g_0^2}.$$

Finally, the Wilson-Clover Dirac operator is given by ( $r = 1$ )

$$D_{\text{WC}}(x, y) = \delta_{x,y} + \kappa \sum_{\mu} \{ (\gamma_{\mu} - r) U_{\mu}(x) \delta_{x+\hat{\mu},y} - (\gamma_{\mu} + r) U_{\mu}^{\dagger}(x - a\hat{\mu}) \delta_{x-a\hat{\mu},y} \} \\ + \frac{i}{2} \kappa c_{\text{SW}} \sum_{\mu\nu} \sigma_{\mu\nu} \hat{F}_{\mu\nu}.$$

Higher orders improvements, to cancel terms of order  $a^3$  in the action, have been considered [25] but, due to the huge computational costs, are not implemented in usual simulations.

### 1.5.4 Properties of Wilson Fermions

The Wilson Clover action, thanks to the *Wilson term*, has the correct continuum limit. However, since the *Wilson term* (1.26) is a Dirac scalar, it commutes with  $\gamma_5$  and breaks the chiral symmetry,  $\{D, \gamma_5\} \neq 0$ , even in the massless limit  $m \rightarrow 0$ . Chiral symmetry is only recovered in the continuum limit, when  $a \rightarrow 0$ . A consequence of chiral symmetry breaking, is the presence of an additive mass renormalization term in the action (1.28) which diverges in the continuum limit. The critical value of the hopping parameter ( $\kappa_c$ ) is then defined as the value of  $\kappa$  at which the pion mass vanishes:

$$m = \frac{1}{2a} \left( \frac{1}{\kappa} - \frac{1}{\kappa_c} \right). \quad (1.32)$$

In the free theory  $\kappa_c = \frac{1}{8}$  but when interactions are turned on, its value gets renormalized and has to be computed numerically .

In fact, Nielsen and Ninomiya [26, 27, 28] have analyzed in detail the implementation of the chiral symmetry on the lattice. Their results, known as the Nielsen-Ninomiya no-go theorem, can be summarized as follow: it is impossible to have a chirally invariant, doubler-free, local and translation invariant fermion action on the lattice. Then, at first sight, it seems impossible to have a chirally invariant action without doublers, an important issue when chiral eigenstates play a major role. Nevertheless, there exists a clever way to circumvent this problem: Ginsparg and Wilson proposed an action [29] which violates only weakly the anti-commutation condition  $\{D, \gamma_5\} = 0$  . The major drawback of Ginsparg-Wilson fermions is the high computational cost associated to these simulations compared to the Wilson Clover action.

Finally, the Wilson Clover Dirac operator obeys the following relationship, called  $\gamma_5$ -hermiticity

$$\gamma_5 D_W \gamma_5 = D_W^{\dagger}, \quad (1.33)$$

and will be particularly useful when computing correlations functions on the lattice. As a consequence, the spectrum of the operator  $\gamma_5 D_W$  is either real or composed of complex conjugated pairs of eigenvalues. In particular, the determinant of the Dirac operator is real.

### 1.5.5 Twisted Mass Fermions

Another choice of lattice regularization for the spinor field is the Twisted mass fermion action [30, 31, 32], it will be used in the last chapter of this work.

#### In the continuum

For two mass-degenerate quarks, the fermionic part of the action is given by:

$$S_{\text{TM}}[\chi, \bar{\chi}] = \int d^4x \bar{\chi}(x) (\gamma_\mu D_\mu + m + i\mu\gamma_5\tau^3) \chi(x), \quad (1.34)$$

where  $D_\mu$  is the covariant derivative,  $m$  a bare mass parameter and  $\tau^3$  is a Pauli matrix acting on the SU(2) flavour space. The real parameter  $\mu$  is called the twisted mass and the term  $i\mu\gamma_5\tau^3$  has a non trivial structure in both Dirac space (due to the presence of  $\gamma_5$ ) and in flavour space (due to the Pauli matrix  $\tau^3$ ).

The mass term in equation (1.34) can be written as

$$m + i\mu\gamma_5\tau^3 = M \exp(i\alpha\gamma_5\tau^3),$$

with the so-called polar or invariant mass  $M = \sqrt{m^2 + \mu^2}$  and the twist angle  $\alpha$  defined by  $\tan \alpha = \mu/m$ . Performing an axial transformation on both quark and antiquark fields

$$\psi = \exp(i\alpha\gamma_5\tau^3/2)\chi \quad , \quad \bar{\psi} = \bar{\chi} \exp(i\alpha\gamma_5\tau^3/2), \quad (1.35)$$

one recovers the standard QCD action<sup>2</sup>

$$S_{\text{TM}}[\psi, \bar{\psi}] = \int d^4x \bar{\psi}(x) (\gamma_\mu D_\mu + M) \psi(x). \quad (1.36)$$

Therefore, twisted mass QCD and standard QCD are related by the previous transformation (1.35) and both actions share the same symmetries. The basis  $(\bar{\psi}, \psi)$  where the action has its standard form is called the physical basis whereas the basis  $(\bar{\chi}, \chi)$ , in which lattice simulations are performed, is called the twisted basis. It can be shown that the equivalence between the two formulations is preserved at the quantum level [31].

---

2. We can write

$$\begin{aligned} e^{-i\alpha\gamma_5\tau^3/2} &= \cos(\alpha/2) - i\gamma_5\tau^3 \sin(\alpha/2) \\ e^{-i\alpha\gamma_5\tau^3/2}\gamma_\mu e^{-i\alpha\gamma_5\tau^3/2} &= \gamma_\mu \end{aligned}$$

so that,

$$\begin{aligned} e^{-i\alpha\gamma_5\tau^3/2} (m + i\mu\gamma_5\tau^3) e^{-i\alpha\gamma_5\tau^3/2} &= (m + i\mu\gamma_5\tau^3) e^{-i\alpha\gamma_5\tau^3} \\ &= (m + i\mu\gamma_5\tau^3) (\cos \alpha - i\gamma_5\tau^3 \sin \alpha) \\ &= m \cos \alpha - i\mu\gamma_5\tau^3 \sin \alpha + i\mu\gamma_5\tau^3 \cos \alpha + \mu \sin \alpha \\ &= m(\cos \alpha + \tan \alpha \sin \alpha) \\ &= M \end{aligned}$$

### Lattice formulation

The lattice regularization is obtained from the Wilson regularization with the additional twisted mass term:

$$S_{\text{TM}}[\chi, \bar{\chi}] = a^4 \sum_{x \in \Lambda} \bar{\chi}(x) \left( \tilde{\nabla}_\mu \gamma_\mu - \frac{ar}{2} \Delta + m + i\mu \gamma_5 \tau^3 \right) \chi(x). \quad (1.37)$$

The Wilson term, required to remove the doublers, breaks the axial symmetry and the twisted mass term cannot be removed by a chiral transformation (1.35). Therefore, the equivalence between QCD and twisted mass QCD is only valid in the continuum and the two lattice discretizations are different.

### Properties

The twisted mass formulation has the advantage to automatically remove  $\mathcal{O}(a)$  discretization effects of any physical observable at maximal twist, defined by  $\alpha = \pi/2$  at the classical level. In the interacting theory, the angle  $\alpha$  gets renormalized and has to be tuned numerically. Moreover, in many cases, the renormalization of weak interaction matrix elements is highly simplified.

However, the main drawback of this formulation is the breaking of the flavour symmetry and parity at order  $\mathcal{O}(a^2)$  by the twisted mass term. Of course, these symmetries are restored in the continuum limit but it can complicate the extraction of physical quantities, especially when studying meson spectroscopy.

# Chapter 2

## Computation of observables in lattice QCD

### Contents

---

<b>2.1</b>	<b>Path integrals in Lattice QCD . . . . .</b>	<b>26</b>
<b>2.2</b>	<b>Monte Carlo simulations . . . . .</b>	<b>28</b>
2.2.1	Importance sampling . . . . .	28
2.2.2	Markov Process . . . . .	29
2.2.3	The Hybrid Monte Carlo (HMC) Algorithm . . . . .	30
<b>2.3</b>	<b>The quark propagator . . . . .</b>	<b>32</b>
2.3.1	Definition . . . . .	32
2.3.2	All-to-all propagators . . . . .	33
2.3.3	Time dilution . . . . .	33
2.3.4	Numerical implementation . . . . .	34
<b>2.4</b>	<b>Correlators . . . . .</b>	<b>35</b>
2.4.1	Interpolating operator . . . . .	35
2.4.2	Asymptotic behavior . . . . .	36
2.4.3	Evaluation on the lattice . . . . .	37
<b>2.5</b>	<b>The Generalized Eigenvalues Problem . . . . .</b>	<b>38</b>
<b>2.6</b>	<b>Smearing . . . . .</b>	<b>39</b>
2.6.1	APE smearing . . . . .	39
2.6.2	HYP smearing . . . . .	40
2.6.3	Gaussian smearing . . . . .	41
<b>2.7</b>	<b>Error estimation . . . . .</b>	<b>41</b>
2.7.1	The Jackknife Procedure . . . . .	42
2.7.2	The Gamma method . . . . .	43
<b>2.8</b>	<b>Setting the scale and the continuum limit . . . . .</b>	<b>45</b>
<b>2.9</b>	<b>Discussion of systematic errors . . . . .</b>	<b>46</b>

---

In this chapter, I will explain how observables are computed in Lattice QCD using the Feynman path integral formalism. Here, the lattice spacing  $a$  and the spatial extent  $L$  play respectively the role of ultraviolet (UV) and infrared (IR) regulators leading to a finite number of degrees of freedom. The integration is then performed numerically on a computer. Due to the large number of degrees of freedom, Monte Carlo integration schemes are particularly well suited to this kind of problem and I will describe the Hybrid Monte Carlo algorithm used to generate the gauge configurations analyzed in this work. In practice, a typical lattice QCD simulation is done at some finite lattice spacing  $a$ , in a volume  $V$  and at some unphysical quark mass  $m$ . To recover QCD, it is then necessary to extrapolate the results to the physical point by considering different simulations at various values of the lattice parameters  $a$ ,  $V$  and  $m$ . In particular, I will explain how the continuum limit and chiral extrapolations are performed.

## 2.1 Path integrals in Lattice QCD

In the continuum theory, the euclidean partition function of QCD is given by

$$Z = \int D[U_\mu] D[\psi] D[\bar{\psi}] e^{-(S_G + S_F)} , \quad (2.1)$$

where the field variables  $U_\mu$ ,  $\psi$  and  $\bar{\psi}$  have to be considered as independent.  $S_G$  stands for the gluonic part of the QCD action while  $S_F$  denotes the fermionic part. More generally, in quantum field theory, we are interested in computing expectation values of some observable  $\mathcal{O}$  which depend on both fermionic and gauge fields:

$$\langle \mathcal{O} \rangle = \frac{1}{Z} \int D[U_\mu] D[\psi] D[\bar{\psi}] \mathcal{O}[U, \psi, \bar{\psi}] e^{-(S_G + S_F)} . \quad (2.2)$$

On the lattice, the idea is to regularize the path integral by replacing the continuous integral by a discrete sum over all degrees of freedom and using the discrete action defined in the previous chapter. Since the volume and the lattice spacing are both finite, eq. (2.2) becomes perfectly well defined and the measure in the path integral corresponds to

$$D[U_\mu] = \sum_{x \in \Lambda} \sum_{\mu=1}^4 dU_\mu(x) \quad , \quad D[\psi] = \sum_{x \in \Lambda} \sum_{\alpha, a} d\psi_\alpha^\alpha(x) \quad , \quad D[\bar{\psi}] = \sum_{x \in \Lambda} \sum_{\alpha, a} d\bar{\psi}_\alpha^\alpha(x) ,$$

where  $dU_\mu(x)$  is the Haar measure on the compact  $SU(3)$  group and where  $\alpha$  and  $a$  denote respectively Dirac and color indices.

### Degrees of freedom

There are two complex Grassmann vectors,  $\psi(x)$  and  $\bar{\psi}(x)$ , associated to each site of the lattice. Since each vector component carries one color index, we obtain  $48 \times N_T$  degrees of freedom for each flavour where  $N_T$  is the number of sites. For the gauge field, one link variable is associated to each link of the lattice, and since it carries one Lorentz index and belongs to  $SU(3)$ , we have  $32 \times N_T$  degrees of freedom. A typical size for a lattice is  $N_T = 48^3 \times 96$  and we conclude that the total number of degrees of freedom is of order  $10^9$ . Therefore, stochastic integration methods, like Monte Carlo algorithms are particularly well suited to this kind of very high dimensional integration.

In practice, since it is difficult to implement Grassmann numbers on a computer, we don't directly compute the path integral given by eq. (2.2). Instead, we take advantage of the fact that the fermionic part of the action is quadratic and perform the integration over the fermionic variables formally using Wick contractions. Indeed, writing the fermionic part of the action in terms of the Dirac operator,  $S_F = \sum \bar{\psi} D[U_\mu] \psi$ , we have

$$\int D[\psi] D[\bar{\psi}] e^{-S_F} = \det D, \quad (2.3)$$

$$\int D[\psi] D[\bar{\psi}] \psi_i(y) \bar{\psi}_j(x) e^{-S_F} = - (D^{-1})_{ij} \det D, \quad (2.4)$$

and these formulae can be generalized to the case of any number of fermionic fields. In the case of many flavours, the determinant is the product of  $N_f$  determinants, one for each flavour and with its own mass parameter. Fermion fields are then replaced by a sum over all possible Wick contractions and the result is expressed in terms of the quark propagator of the *interacting* theory. Of course, this quantity is not known analytically and has to be computed separately. In fact, the computation of the quark propagator is often the most expensive part of the simulation (see Section 2.3). Finally, we are left with the gauge field integration:

$$\langle \mathcal{O} \rangle = \frac{1}{Z} \int D[U_\mu] \langle \mathcal{O} \rangle_F [U_\mu] e^{-S_G + \ln \det D}, \quad (2.5)$$

where the fermionic expectation value  $\langle \cdot \rangle_F$  is defined by

$$\langle \mathcal{O} \rangle_F [U_\mu] = \frac{\int D[\psi] D[\bar{\psi}] \mathcal{O}[U_\mu, \psi, \bar{\psi}] e^{-S_F}}{\int D[\psi] D[\bar{\psi}] e^{-S_F}} = \frac{\int D[\psi] D[\bar{\psi}] \mathcal{O}[U_\mu, \psi, \bar{\psi}] e^{-\sum_{xy} \bar{\psi}_y D_{yx} \psi_x}}{\det D},$$

and is expressed in terms of the quark propagator using eqs. (2.3), (2.4) and their generalizations.

The integration over the gauge field is performed via a Monte Carlo algorithm and is the subject of the next section. The idea is to generate an ensemble of  $N_c$  gauge configurations with a probability weight proportional to  $e^{-S_G + \ln \det D}$ , then the expectation value (2.5) is obtained by averaging over gauge configurations:

$$\langle \mathcal{O} \rangle = \frac{1}{N_c} \sum_{i=1}^{N_c} \langle \mathcal{O} \rangle_F [U_\mu^{(i)}]. \quad (2.6)$$

One important issue here is that the fermionic determinant,  $\det D$ , needs to be real and positive to ensure that  $e^{-S_G + \ln \det D}$  can be interpreted as a probability weight. The gamma hermiticity relation (1.33) proves that the determinant is real, but not necessarily positive. One way to solve this problem, with  $N_f = 2$  dynamical fermions, is to assume that up and down quarks are degenerate such that  $\det D = \det D_u \times \det D_d = (\det D_u)^2 > 0$ .

Monte Carlo algorithms are based on stochastic integration methods. Therefore, the previous formula is only an estimator of the true expectation value and the determination of the statistical error, associated to the results, is particularly important and will be discussed in Section 2.7.

**Summary :**

On the lattice, the computation of an observable is done in two steps corresponding basically to the integration over bosons and fermions:

- We first generate  $N_c$  gauge configurations with a probability weight given by  $e^{-S_G + \ln \det D}$ . This has to be done once and for all and the gauge configurations can be used to compute any observables.
- For each gauge configuration, the quark propagator is computed numerically (Section 2.3) and enters the computation via the Wick contractions (eqs. (2.3), (2.4)).

**Pseudofermions**

To generate the gauge configurations, one has to evaluate the fermionic determinant appearing in the probability weight. Due to the large size of this matrix, an exact inversion is not possible with standard algorithms.

A drastic approximation used in the early days of Lattice QCD is to assume that  $\det D = 1$ . This approximation, called the quenched approximation, is equivalent to neglect all fermionic loops. In this case, the theory loses its unitarity and some features of QCD are missing: for example the decay of the  $\rho$  meson into two pions  $\rho \rightarrow \pi\pi$  is no longer possible since it would require the production of a  $q\bar{q}$  pair. The quenched approximation has the obvious advantage of considerably simplifying lattice simulations (since it avoids the computation of the fermionic determinant) but leads to systematic errors of the order of 10% or more depending on the observable which are difficult to evaluate. In particular, masses of hadrons can depend significantly on the hadron used to fix the bare quark mass in the Lagrangian.

To take quark loop effects into account, one can write the fermionic determinant in terms of bosonic variables using the following relation

$$\det D[U] = \int D[\phi^\dagger] D[\phi] e^{-\sum_{x,y} \phi^\dagger(x) D^{-1}(x,y) \phi(y)}, \quad (2.7)$$

where  $\phi$  and  $\phi^\dagger$  are complex scalar fields called *pseudofermions*. In the case of two degenerate dynamical quarks ( $N_f = 2$ ),  $\det D = \det D_u \times \det D_d$ , and the total action which enters the weight of the path integral (2.2) becomes

$$S_{\text{QCD}} = S_G + \sum_{x,y} \phi^\dagger(x) (D^\dagger D)^{-1}(x,y) \phi(y) = S_G + S_{\text{PF}}, \quad (2.8)$$

where  $S_{\text{PF}}$  is the pseudofermion action. Since the determinant is real and positive in  $N_f = 2$  simulations, the inverse matrix  $D^{-1}$  does exist. Of course, the inverse matrix  $D^{-1}$  is also a non-local object but, since  $D$  is a sparse matrix, efficient inversion algorithms exist [33]. They are based on gradient conjugate methods.

## 2.2 Monte Carlo simulations

### 2.2.1 Importance sampling

We would like to evaluate the expectation value (2.5) using a Monte Carlo algorithm. Nevertheless, a naive implementation consisting in generating  $N_c$  gauge configurations

randomly is very inefficient. Indeed, in the path integral, only gauge configurations close to the minimum of the action contribute significantly, the other ones being exponentially suppressed. The solution, called *importance sampling*, is to generate gauge configurations with the probability weight proportional to  $W[\varphi] = e^{-S[\varphi]}$ . Then, an estimator of the expectation value is simply given by the unweighted sum over configurations (2.6). In the next paragraph, I will explain how this can be implemented.

### 2.2.2 Markov Process

In this section, a gauge configuration  $\{U\}$  is a set of matrices  $U_\mu(x) \in \text{SU}(3)$ , one for each link of the lattice. The idea of a Markov process is to start from an initial gauge configuration  $\{U\}_0$  and to successively generate new gauge configurations  $\{U\}_{n+1}$  from the previous  $\{U\}_n$ . This step is called the *updating*. After  $n$  steps, we can define the sequence of gauge configurations, called the *Markov chain*, by

$$W_n = (\{U\}_0, \dots, \{U\}_{n-1}, \{U\}_n),$$

and the associated distribution density  $\rho_n$ . For example, the initial distribution density associated to  $W_0$  is simply given by  $\rho_0 = \delta(\{U\} - \{U\}_0)$ . The aim of the algorithm is to generate gauge configurations in such a way that  $W_n$  tends to the equilibrium density  $\rho_{\text{eq}}$  defined by

$$\rho_{\text{eq}}(\{U\}) = \frac{1}{Z} \det D(U) e^{-S_G[U]}. \quad (2.9)$$

Of course this is rigorously possible only after an infinite number of steps and in actual simulations we have to decide whether or not we are close enough to the equilibrium distribution.

The updating step is a stochastic process which can be characterized by the probability  $P(\{U\} \rightarrow \{U\}')$  to obtain the next configuration  $\{U\}'$  from the previous configuration  $\{U\}$  after one step. This probability is defined for all initial and final gauge configurations and obeys the following property

$$\forall \{U\}, \quad \sum_{\{U\}'} P(\{U\} \rightarrow \{U\}') = 1,$$

which means that, starting from a given gauge configuration  $\{U\}$ , the probability to obtain *any* gauge configuration  $\{U\}'$  is equal to one. In addition we require the following properties:

**Ergodicity :**

$$\forall \{U\}, \quad \forall \{U\}', \quad P(\{U\} \rightarrow \{U\}') > 0, \quad (2.10)$$

which means that every gauge configuration can be reached from any other configuration with a non-zero probability. This property is important to ensure that the starting point of the Markov chain is irrelevant.

**The detailed balance condition**

$$\forall \{U\}, \quad \forall \{U\}', \quad P(\{U\} \rightarrow \{U\}') \rho_{\text{eq}}(\{U\}) = P(\{U\}' \rightarrow \{U\}) \rho_{\text{eq}}(\{U\}'). \quad (2.11)$$

Given these properties, one can prove the following results (actually, the detailed balance is not a necessary but only a sufficient condition):

- The equilibrium distribution is the unique fixed point of the probability transition [34] :

$$\rho_{\text{eq}}(\{U\}') = \sum_{\{U\}} P(\{U\}' \rightarrow \{U\}) \rho_{\text{eq}}(\{U\}) .$$

- Repeating the updating process, the Markov chain density gets closer and closer to the equilibrium distribution:

$$\rho_n \longrightarrow \rho_{\text{eq}} .$$

Of course, in real simulations,  $N_c$  is always finite and the actual density distribution only approaches the equilibrium density. In particular, the first configurations are often highly unlikely and, since the number of configurations is of order  $10^3$ , their weight is not completely negligible when the sum (2.6) is finite, even if their weight would tend to zero in the limit  $N_c \rightarrow \infty$ . To circumvent this problem, we defined the *thermalization* phase as the  $N_{th}$  first updating processes ( $N_{th}$  has to be chosen carefully such that no drift towards the equilibrium expectation value can be seen for the observables in consideration). These gauge configurations are skipped from the final Markov Chain.

Many algorithms used in Lattice QCD fulfill the previous requirements. In the next section I will describe the Hybrid Monte Carlo (HMC) algorithm used to generate the gauge configurations used in this thesis.

### 2.2.3 The Hybrid Monte Carlo (HMC) Algorithm

In the Monte Carlo algorithm, we would like to perform global transformations of the gauge field. First, because local transformations would also require the computation of the full determinant (which is a non-local quantity) and secondly to reduce autocorrelations. However, after a global transformation, the corresponding value of the action can change a lot and the new gauge configuration is unlikely to contribute significantly to the action. Therefore, it would require very small steps in the update algorithm leading to high autocorrelation and a large number of updating. The HMC algorithm [35], presented in this section, solves these problems. It allows for global transformations while maintaining a good efficiency.

As explained in the previous section, the update algorithm used to generate the Markov chain is defined by its transition probability  $P$ . This probability should satisfy the ergodicity and the detailed balance conditions. In our case, the probability is written  $P = P_E P_A$  where:

- $P_E$  is the probability to generate  $\{U\}_{n+1}$  from  $\{U\}_n$  during the update process. It will depend on the details of the algorithm.
- $P_A$  is the acceptance probability to decide whether or not the new gauge configuration is kept. It is chosen such that the detailed balance property is satisfied.

Now, the idea is to interpret the action (2.8) as a potential, associated to a fictitious Hamiltonian, and to add a new set of momenta fields  $\Pi$  which play the role of conjugate variables associated to the gauge field  $U_\mu$ . Gauge links  $U_\mu(x)$  are SU(3) group elements, so we have one su(3) Lie algebra element  $\Pi_\mu(x)$  per site  $x$  and per direction  $\mu$ . Since

the action  $S = S_G + S_F$  does not depend on the momenta, they can be factorized out and do not change the physical results:

$$\begin{aligned} \langle \mathcal{O} \rangle &= \frac{1}{\tilde{Z}} \sum_{x \in \Lambda, \mu} \int D[\Pi_\mu] D[U_\mu] D[\phi] D[\phi^\dagger] \langle \mathcal{O}[U_\mu] \rangle_F e^{-(S_G + S_{PF} + \sum \frac{1}{2} \Pi^2)} \\ &= \frac{1}{\tilde{Z}} \sum_{x \in \Lambda, \mu} \int D[U_\mu] D[\phi] D[\phi^\dagger] \langle \mathcal{O}[U_\mu] \rangle_F e^{-(S_G + S_{PF})}, \end{aligned}$$

where  $\tilde{Z}$  is defined as in (2.1) but now with the total action including the momenta  $\Pi_\mu$ . Then, the total action, including the pseudofermion and momenta fields is:

$$S_{\text{HMC}} = \frac{1}{2} \Pi^2 + S_{\text{QCD}}(U) = \frac{1}{2} \Pi^2 + S_G(U) + \phi^\dagger (D^\dagger(U) D(U))^{-1} \phi. \quad (2.12)$$

This action describes the evolution of a classical system in a 4-dimensional space. The associated time is not related to the physical time but rather to the computer time which labels the gauge configurations. This is called Molecular Dynamics (MD). Quantum fluctuations of the quantum field in 4 dimensions are described by the trajectory of a classical system in a 5 dimensional space-time. The Hamilton-Jacobi equations for this classical system are

$$\begin{cases} \dot{U} = \frac{\delta S_{\text{HMC}}}{\delta \Pi}, \\ \dot{\Pi} = -\frac{\delta S_{\text{HMC}}}{\delta U} = -\frac{\delta S_G}{\delta U} - \phi^\dagger \left( (M^\dagger M)^{-1} \frac{\delta M^\dagger}{\delta U} (M^\dagger)^{-1} + M^{-1} \frac{\delta D}{\delta U} (M^\dagger M)^{-1} \right) \phi \end{cases} \quad (2.13)$$

where the right hand side of the second equation is called the force term and its exact expression depends on the lattice action used in the simulation. The first equation is numerically easy to solve but the second one is much more difficult since it requires the evaluation of the inverse Dirac matrix. Finally, the acceptance probability  $P_A$  is chosen to be

$$P_A(\{U, \Pi\} \rightarrow \{U, \Pi'\}) = \min \left( 1, e^{-S(U', \Pi') + S(U, \Pi)} \right), \quad (2.14)$$

so that, the total probability  $P$  of the Markov process is

$$P(\{U\} \rightarrow \{U'\}) = \int D[\Pi] D[\Pi'] P_M[\Pi] \cdot P_E(\{U, \Pi\} \rightarrow \{U, \Pi'\}) \cdot P_A(\{U, \Pi\} \rightarrow \{U, \Pi'\}) \quad (2.15)$$

where  $P_M \sim \exp(-\frac{1}{2} \sum \Pi^2)$  is a gaussian distribution. One can prove that this probability  $P$  satisfies the detailed balance condition if we also impose that the evolution equations are reversible and area preserving. In the continuum theory, this is always true thanks to Liouville's theorem but not necessarily with integration algorithms where a discrete step size is used. A typical example of algorithm used in simulations is the LeapFrog algorithm.

During the molecular dynamics, the system lies on a hyper surface of constant energy and explores only a subspace of the full phase space  $(\Pi, U)$ . Nevertheless, during this step, the dynamics can produce gauge configurations with very different values for the action  $S_{\text{QCD}}(U)$  associated to the QCD action only. The heat bath step, at the beginning of each MD trajectory, refreshes randomly the momenta of the system and then ensures ergodicity.

An interesting property of this algorithm is that, since the action is a constant of motion during the molecular dynamic, the acceptance rate is theoretically equal to one. But, because of numerical rounding errors during the Leapfrog integration, the acceptance rate is not exactly one but is still very high (errors are of order  $\mathcal{O}(\epsilon^2)$  for a first order integrator and the integration step  $\epsilon$  is usually chosen such that  $P_A \approx 80\%$ ).

### Summary :

The use of an heat-bath algorithm and a molecular dynamics are at the origin of the name *Hybrid* Monte Carlo. The algorithm can finally be summarized as follow:

- At the beginning of each step of the MC, the momenta associated with the fermion fields are generated randomly according to a gaussian distribution via an heat-bath algorithm. Pseudofermion fields are generated in two steps: first, a random field  $\chi$  is generated according to a gaussian distribution and secondly, the pseudofermions are obtained via  $\phi = D\chi$ .
- Then, the gauge fields and momenta are updated using the molecular dynamics evolution eq. (2.13). During this step, the pseudofermion fields are kept constant.
- At the end, the new gauge configuration is accepted with a probability  $P_A$  given by eq. (2.14), this step corrects for the numerical errors introduced by the Leapfrog algorithm. If the configuration is rejected, we restart from the previous state which is included again in the Markov chain.

## 2.3 The quark propagator

### 2.3.1 Definition

Once gauge configurations are generated, the next step is to evaluate the quark propagator appearing in Wick contractions in eq. (2.4). In lattice QCD, the Dirac operator, for a given flavour, is written  $D_{\alpha\beta}^{ab}(y, x)$  where  $(a, \alpha, y)$  and  $(b, \beta, x)$  are respectively the color, spinor and space-time indices associated to the sink and to the source. The size of the matrix is then  $12N \times 12N$  where  $N$  is the total number of sites of the lattice. Finally, the propagator,  $G$ , is defined as the inverse of the Dirac operator:

$$\sum_{y \in \Lambda} D_{\alpha\beta}^{ab}(x, y) G_{\beta\gamma}^{bc}(y, z) = \delta(x, z) \delta_{ac} \delta_{\alpha\gamma} , \quad (2.16)$$

and depends on the lattice action used for the simulation. Since the Dirac operator only involve neighboring points of the lattice, the matrix is sparse and algorithms based on conjugate gradient methods are particularly well suited. Nevertheless, the exact all-to-all inversion, i.e., the solution from each source point to each sink point of the lattice, is impossible with present day computational capabilities (it would requires  $12N \sim 10^8$  inversions for typical lattices). The problem can be simplified by considering the following equation (spinor and color indices are omitted for simplicity):

$$D(x, y)\psi(y) = \delta(x) \quad , \quad \psi(y) = G(y, x)\delta(x) , \quad (2.17)$$

where the solution vector,  $\psi(y)$ , corresponds to the one-to-all solution for a point source placed at the origin  $\delta(x)$ . It would correspond to one row of the full propagator matrix and requires 12 inversions per lattice site. Moreover, the backward propagator can be

obtained from the forward propagator by using the  $\gamma_5$ -hermiticity relation  $G(y, x) = \gamma_5 G(x, y)^\dagger \gamma_5$ .

A drawback of this method is that only a small part of the gauge information is used since we don't exploit the full translational invariance of the propagator (the source is fixed). Since generating gauge configurations is extremely costly, it would be preferable to exploit them to reduce the gauge noise. Moreover, point-to-all propagators are not suited when using non-local interpolating fields.

### 2.3.2 All-to-all propagators

Solutions exist to evaluate all-to-all propagators and are based on stochastic methods [36]. The idea is to use, for each gauge configuration, an ensemble of  $N_s$  stochastic sources satisfying

$$\lim_{N_s \rightarrow \infty} \frac{1}{N_s} \sum_{s=1}^{N_s} \eta_\alpha^a(x)_s [\eta_\beta^b(y)_s]^* = \delta_{\alpha\beta} \delta^{ab} \delta_{x,y}, \quad (2.18)$$

where each component is normalized to one,  $\eta_\alpha^a(x)_{[r]}^* \eta_\alpha^a(x)_{[r]} = 1$  (no summation). This can be implemented using random gaussian numbers on each site of the lattice, for each color and spinor index. Then the Dirac operator is inverted for each source:

$$D(x, y) \psi(y)_s = \eta(x)_s \quad , \quad D_{\alpha\beta}^{ab}(x, y) \psi_\beta^b(y)_s = \eta_\alpha^a(x)_s,$$

where  $\psi_\alpha^a(x)_s$  is the solution vector of size  $12N$ . An unbiased estimator of the propagator is then given by contracting the solution vector with the corresponding source:

$$\psi_\alpha^a(x)_s = G_{\alpha\beta}^{ab}(x, y) \eta_\beta^b(y)_s \quad \Rightarrow \quad G_{\alpha\beta}^{ab}(x, y) = \frac{1}{N_s} \sum_{s=1}^{N_s} \psi_\alpha^a(x)_s \eta_\beta^b(y)_s^*. \quad (2.19)$$

Of course, the number of stochastic sources is always finite and, since the inversion of the Dirac operator is often the most demanding part of the algorithm, it can be quite limited. Then, the condition (2.18) is only approximately fulfilled and the quark propagator obtained by using eq. (2.19) can be very noisy. Indeed, it requires the cancellation of the U(1) noise on the whole lattice whereas the signal decreases exponentially with the space-time separation. Therefore, even if some terms should cancel in average, they can contribute significantly to the variance. An extremely useful tool to reduce the noise is time dilution [36].

### 2.3.3 Time dilution

In general, dilution consists in splitting the source  $\eta$  into several secondary (diluted) sources with vanishing overlap. For example, in time dilution, a secondary source is defined on a single time slice and equal to zero everywhere else. The advantage is that the condition (2.18) is automatically fulfilled for  $t_x \neq t_y$ . Since the time dependence of the quark propagator is known to be large, this leads to a significant variance reduction

$$\eta(\vec{x}, t) = \sum_{\tau} \eta(\vec{x}, t)_{[\tau]} \quad , \quad \eta(\vec{x}, t)_{[\tau]} = 0 \quad \text{unless} \quad t = \tau.$$

The Dirac operator is now inverted on each diluted source and the full propagator is recovered by summing over all secondary sources:

$$G_{\alpha\beta}^{ab}(x, y) = \frac{1}{N_\tau} \sum_\tau \psi_\alpha^a(x)_{[\tau]} \eta_\beta^b(y)_{[\tau]}^*,$$

where, for full-time dilution,  $N_\tau = N_s \times T$ . For example, as shown in ref. [36], on a  $32^3 \times 64$  lattice, the variance will be smaller when using one complete source fully time-diluted rather than 64 sources without dilution. Finally, dilution could also be applied to spinor or color indices. The limit where dilution is applied to all space-time, color and Dirac indices would correspond to the computation of the exact all-to-all propagator.

### 2.3.4 Numerical implementation

In this work, we used the `df1_sap_gcr` inverter from the DD-HMC package [37, 38]. It is based on a conjugate gradient algorithm with Schwarz-preconditioning [39] and low mode deflation [40, 41] which significantly reduces the increase in computational cost as the quark mass is lowered.

#### Krylov Subspace Iteration Methods

The algorithm to compute the quark propagator is based on a conjugate gradient algorithm. This kind of algorithms (Krylov Subspace Iteration Methods) are well suited for large and sparse matrices like the Dirac operator.

#### Spectral decomposition

The low modes of the Dirac operator lead to numerical difficulties when the quark mass is lowered. The idea is to compute exactly the low modes ( $< N_0$ ) of the operator and to treat them separately using the decomposition

$$D^{-1}(x, y) = \sum_{i=1}^{N_0} \frac{1}{\lambda_i} v^{(i)}(x) \otimes v^{(i)}(y)^\dagger + \tilde{D}^{-1}(x, y),$$

where  $(v^{(i)}, \lambda_i)$  are respectively the eigenvectors and eigenvalues. The remaining part of the Dirac operator,  $\tilde{D}^{-1}(x, y)$ , is then better conditioned (since low modes have been suppressed) and easier to invert numerically. The problem comes from the fact that the eigenvalue density increases with the volume making the exact evaluation of the low lying eigenvalues impossible for large lattices. However, as shown in ref. [40], only a small number of the low lying modes needs to be solved exactly to capture the essential physics, such that the method can also be used for large volume.

#### Standard optimizations

Since the square of the Dirac operator only involves even or odd sites separately, one can use the so called even-odd preconditioning. It significantly reduces the condition number of the Dirac operator and leads to an acceleration of the solver. It also reduces the memory space needed to store the fermionic fields.

## 2.4 Correlators

In lattice QCD simulations, we are often interested in the special case of two- or three-point correlation functions. In this section I will explain in more details how the two-point correlation functions can be computed and an example of three-point correlation function will be given in Chapter 4. We will see that two-point correlation functions are useful to extract the energy levels of mesons or some simple matrix elements like decay constants.

### 2.4.1 Interpolating operator

An interpolating operator,  $\mathcal{O}$ , associated to a bound state  $M$ , is an operator with a non-zero overlap with the state of interest. In particular, it must carry the same quantum numbers like parity, spin or flavour numbers. Then, for a scalar field, we have

$$\langle 0|\mathcal{O}(x)|M\rangle = \sqrt{Z}e^{-iP\cdot x},$$

where  $\sqrt{Z} = \langle 0|\hat{\mathcal{O}}|M\rangle$  is the overlap factor associated with the interpolating operator. Similarly, for a vector field

$$\langle 0|\mathcal{O}_\mu(x)|M(\epsilon_\mu)\rangle = \epsilon_\mu\sqrt{Z}e^{-iP\cdot x},$$

where  $\epsilon_\mu$  is the polarization of the field. In practice, the interpolating field couples to every particles with the same quantum numbers and different choices are possible. They lead to different overlap factors  $Z$  and couple differently with the excited states.

The simplest interpolating operator can be constructed from one of the 16 linearly independent combinations of gamma matrices (denoted by  $\Gamma$ ) such that it has the correct quantum numbers (see Table 2.1):

$$\mathcal{O}(x) = \bar{\psi}_1(x)\Gamma\psi_2(x), \quad (2.20)$$

where  $\psi_1$  and  $\psi_2$  may correspond to different flavours. Generally, an interpolating operator for a particle with spatial momentum  $\vec{q}$  is given by

$$\mathcal{O}_{\vec{q}}(t) = \frac{1}{V} \sum_{\vec{x}} e^{-i\vec{q}\cdot\vec{x}} \mathcal{O}(\vec{x}, t).$$

In particular, to compute the mass of a meson, it is convenient to work at vanishing momentum, so we sum over all spatial lattice points. Finally, defining  $\bar{\Gamma} = \gamma_0\Gamma^\dagger\gamma_0$ , we have

$$\mathcal{O}^\dagger(x) = \bar{\psi}_2(x)\bar{\Gamma}\psi_1(x), \quad (2.21)$$

and the meson two-point correlation function at vanishing momentum is

$$C(t) = \langle \mathcal{O}(t)\mathcal{O}^\dagger(0) \rangle = \sum_{\vec{x}, \vec{y}, t'} \langle \mathcal{O}(\vec{x}, t' + t)\mathcal{O}^\dagger(\vec{y}, t') \rangle,$$

where I have used the translational invariance.

	$J^{PC}$	$\Gamma$
Scalar	$0^{++}$	1
	$0^{+-}$	$\gamma_0$
Pseudoscalar	$0^{-+}$	$\gamma_5$
		$\gamma_0\gamma_5$
Vector	$1^{--}$	$\gamma_i$
		$\gamma_0\gamma_i$
Axial	$1^{++}$	$\gamma_5\gamma_i$
Tensor	$1^{+-}$	$\gamma_i\gamma_j$

Table 2.1 – Quantum numbers associated to some local interpolating operators of the form  $\mathcal{O}(x) = \bar{\psi}(x)\Gamma\psi(x)$

### 2.4.2 Asymptotic behavior

In this section, I use the notation  $\hat{\mathcal{O}}$  for the time independent operator in the Schrödinger picture and  $\mathcal{O}(t)$  for the time dependent operator in the Heisenberg picture. Then, using the spectral decomposition

$$\mathbb{1} = \sum_n \int \frac{d^3p_n}{(2\pi)^3 2E_n} |M_n\rangle\langle M_n|,$$

the two-point correlation function becomes

$$C(t) = \langle \mathcal{O}(t)\mathcal{O}^\dagger(0) \rangle = \sum_{n=1}^{\infty} \frac{1}{2E_n} \langle 0|\hat{\mathcal{O}}|M_n\rangle\langle M_n|\hat{\mathcal{O}}^\dagger|0\rangle e^{-E_n t}, \quad (2.22)$$

where  $E_n$  is the energy of the  $n^{\text{th}}$  state of the Hamiltonian and where I used the relativistic normalization of states  $\langle M_n|M_m\rangle = (2E_n)\delta_{nm}$ . In general, due to periodic boundary conditions, the particles can also travel in the other direction. But, in this work, I will mostly study heavy-light mesons where the heavy quark propagates only forward in time (see Section 3.1.6), so I neglect these terms here. In particular, if we note  $M = M_1$  the ground state, then, at sufficiently large time, the correlator has the asymptotic behavior

$$C(t) \xrightarrow{t \rightarrow \infty} \frac{1}{2E_M} \langle 0|\hat{\mathcal{O}}_\Gamma|M\rangle\langle M|\hat{\mathcal{O}}_{\Gamma'}|0\rangle e^{-E_M t}, \quad (2.23)$$

from which we can extract the energy of the ground state and the product of matrix elements  $\langle 0|\hat{\mathcal{O}}_\Gamma|M\rangle\langle M|\hat{\mathcal{O}}_{\Gamma'}|0\rangle$ . Of course, on the lattice, the time  $t$  is always finite and there are contributions of higher excited states which fall off exponentially with time with an exponent proportional to  $E_2 - E_1$ , the energy difference between the first excited state and the ground state.

Since the propagator becomes noisier at large time, it is necessary to reduce the contribution of excited states as much as possible. A first possibility is to choose an

interpolating field with a large overlap with the desired state, this can be achieved by using smearing techniques (Section 2.6). In the next section, I introduce the Generalized Eigenvalue Problem: using many interpolating operators with the same quantum numbers, we will see how the contribution of excited states can be removed in an efficient and systematic way. It will also be particularly useful to extract information about excited states in Chapters 4 and 6.

### 2.4.3 Evaluation on the lattice

On the lattice, the correlation function is estimated via the formula (2.6) and I will now explain in details the procedure in the case of a two-point correlation function. They will be used in Chapters 3, 4 and 6. The correlation function we are interested in is

$$C(t) = \langle \mathcal{O}_\Gamma(t) \mathcal{O}_{\Gamma'}^\dagger(0) \rangle, \quad (2.24)$$

where  $\mathcal{O}_\Gamma$  and  $\mathcal{O}_{\Gamma'}$  are two interpolating operators at vanishing momentum

$$\mathcal{O}_\Gamma(t) = \sum_{\vec{x}} \bar{\psi}_2(x, t) \Gamma \psi_1(x, t) \quad , \quad \mathcal{O}_{\Gamma'}(t) = \sum_{\vec{x}} \bar{\psi}_2(x, t) \Gamma' \psi_1(x, t). \quad (2.25)$$

The correlation function is depicted in Figure 2.1. Then, the fermionic expectation value

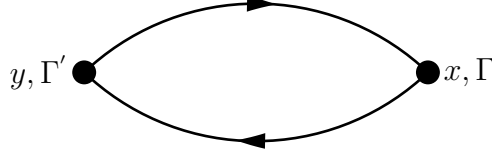


Figure 2.1 – Two-point correlation function

is written in terms of propagators by performing the Wick contractions as explained in Section 2.1. The formula (2.6) gives

$$\begin{aligned} C(t) &= \frac{1}{N_c} \sum_{i=1}^{N_c} \langle \mathcal{O}_\Gamma(t) \mathcal{O}_{\Gamma'}^\dagger(0) \rangle_F \\ &= \frac{1}{N_c} \sum_{i=1}^{N_c} \sum_{x,y} \overbrace{\langle \bar{\psi}_2(x, t) \Gamma \psi_1(x, t) \cdot \bar{\psi}_1(y, 0) \Gamma' \psi_2(y, 0) \rangle_F} \\ &= -\frac{1}{N_c} \sum_{i=1}^{N_c} \sum_{\vec{x}, \vec{y}} \text{Tr} \left[ G_2(y, 0; x, t) \Gamma G_1(x, t; y, 0) \bar{\Gamma}' \right], \end{aligned}$$

where we sum over lattice gauge configurations and take the trace over spinor and color indices. So, for each gauge configuration, we need to compute the quark propagators  $G_1$  and  $G_2$  and then evaluate the trace by performing the correct contractions. The correlation function is finally obtained by averaging over all gauge configurations. In this work, I will always use two degenerate dynamical quarks, therefore the propagator  $G_1$  and  $G_2$  are numerically the same (but formally, they are different, in particular the contractions between  $\bar{\psi}_1$  and  $\psi_2$  must not be considered since only non-singlet flavor interpolating operators are used). Usually, we can also use  $\gamma_5$ -hermiticity to express the

forward Dirac propagator  $G(x; y)$  in terms of the backward Dirac propagator  $G(y; x)$ , namely  $G(x; y) = \gamma_5 G(y; x)^\dagger \gamma_5$  (the Hermitian conjugation refers to spinor space only). In the case of the above two-point correlation function, we obtain

$$C(t) = -\frac{1}{N_c} \sum_{i=1}^{N_c} \sum_{\vec{x}, \vec{y}} \text{Tr} \left[ G(y, 0; x, t) \Gamma \gamma_5 G(y, 0; x, t) \gamma_5 \bar{\Gamma} \right],$$

and only one inversion is needed.

## 2.5 The Generalized Eigenvalues Problem

Using just one interpolating field, extraction of ground state information is often not very precise and the signal gets even worse for the first excited state. Therefore, more sophisticated methods are needed. The idea is to use different interpolating operators, with different overlaps with the excited states, and combine them to create an improved operator with the largest overlap with the ground state. This can be done systematically by solving a Generalized Eigenvalue Problem.

We consider several operators  $\mathcal{O}_i$  with the same quantum numbers, then the correlation matrix is

$$C_{ij}(t) = \langle \mathcal{O}_i(t) \mathcal{O}_j^\dagger(0) \rangle = \sum_{n=1}^{\infty} Z_{ni} Z_{mj}^* e^{-E_n t}, \quad i, j = 1, \dots, N$$

where  $Z_{ni} = \frac{1}{2E_n} \langle 0 | \hat{\mathcal{O}}_i | B_n \rangle$  corresponds to the strength of the overlap between the interpolating field  $\mathcal{O}_i$  and the  $n^{\text{th}}$  excited state. The Generalized Eigenvalue Problem [42] consists in solving the matrix equation

$$C(t) v_n(t, t_0) = \lambda_n(t, t_0) C(t_0) v_n(t, t_0), \quad (2.26)$$

where  $v_n(t, t_0)$  and  $\lambda_n(t, t_0)$  are respectively the generalized eigenvectors and eigenvalues. In the following, we assume that  $t_0 > t/2$ , this condition is necessary to ensure a small contribution of the excited states [42]. From the eigenvalues, we can extract the different energy levels by considering the following estimator

$$E_n^{\text{eff}}(t, t_0) = -\partial_t \log \lambda_n(t, t_0) = \frac{1}{a} \log \frac{\lambda_n(t, t_0)}{\lambda_n(t+a, t_0)} = E_n + \mathcal{O}(e^{-\Delta E_{N+1, n} t}), \quad (2.27)$$

where  $E_n$  is the exact energy of the  $n^{\text{th}}$  state and  $\Delta E_{N+1, n} = E_{N+1} - E_n$  is the energy difference between the  $n^{\text{th}}$  and  $(N+1)^{\text{th}}$  states. This formula has to be compared with the case where only one interpolating field is used, in this case the suppression factor is only  $\mathcal{O}(\exp(-(E_2 - E_1)t))$ . It is then advantageous to have a large basis of interpolating fields. However, the GEVP tends to be unstable when large basis are used, mainly if the interpolating fields are not sufficiently different. In practice, in this work, the choice  $N = 3 - 5$  seems optimal.

From the eigenvectors, we can also build improved interpolating operators having the optimized overlap with the desired states, reducing the contamination from higher excited states. First, we define:

$$\hat{Q}_n^{\text{eff}}(t, t_0) = R_n(t, t_0) \left( \hat{\mathcal{O}}, v_n(t, t_0) \right)^\dagger, \quad (2.28)$$

where  $R_n$  is a normalization coefficient given by

$$R_n(t, t_0) = (v_n(t, t_0), C(t)v_n(t, t_0))^{-1/2} \left( \frac{\lambda_n(t_0 + a, t_0)}{\lambda_n(t_0 + 2a, t_0)} \right)^{t/(2a)}, \quad (2.29)$$

and where  $(a, b) = a_i^* b_i$  is the inner product over eigenvector indices. Then, this operator can be used as an effective creation operator, namely we have

$$e^{-Ht} \left( \hat{Q}_n^{\text{eff}}(t, t_0) \right)^\dagger |0\rangle = |n\rangle + \mathcal{O}(e^{-\Delta E_{N+1, n} t_0}) \quad \text{at fixed } t - t_0. \quad (2.30)$$

Again, the magnitude of the contamination from higher excited states is small and decreases when increasing the value of  $t_0$ .

We can now apply these results in the case of a matrix element of the form  $\mathcal{M}_n = \langle 0 | \hat{P} | n \rangle$  to obtain:

$$\mathcal{M}_n^{\text{eff}} = \langle 0 | \hat{P} e^{-Ht} \left( \hat{Q}_n^{\text{eff}}(t, t_0) \right)^\dagger | 0 \rangle = \langle P(t) (Q_n^{\text{eff}}(t, t_0))^\dagger \rangle = \mathcal{M}_n + \mathcal{O}(e^{-\Delta E_{N+1, n} t_0}). \quad (2.31)$$

Using eq. (2.28), we can express this estimator in terms of eigenvalues and eigenvectors:

$$\mathcal{M}_n^{\text{eff}}(t, t_0) = R_n(t, t_0) \left( \tilde{C}(t), v_n(t, t_0) \right), \quad (2.32)$$

where  $\tilde{C}_i(t) = \langle P(t) \mathcal{O}_i^\dagger(0) \rangle$ .

## 2.6 Smearing

Another technique used to improve the quality of the signal is called smearing. It is a transformation where each gauge link variable  $U_\mu(x)$  is replaced by an average of the gauge link variables along certain paths connecting the endpoints of the original link. In particular, it reduces the short distance fluctuations of the quantum field without affecting its IR structure: indeed, the smearing transformation consists in adding irrelevant operators and their contributions vanish in the continuum limit. It is extremely useful to reduce the gauge noise of observables and many different algorithms exist. In this work, we will use two of them: the APE and the HYP smearings.

Smearing can also be used on the fermionic field to increase the overlap of an interpolating operator with the ground state. In particular, in this work, the different operators used in the Generalized Eigenvalue Problem basis will usually correspond to different levels of Gaussian smearing applied to some local operator.

### 2.6.1 APE smearing

The APE smearing was introduced by the APE Collaboration [43], the idea is to replace each link variable  $U_\mu(x)$  by a weighted average of this link and the surrounded staples

$$\tilde{U}_\mu(x) = (1 - \alpha)U_\mu(x) + \frac{\alpha}{6} \sum_{\nu \neq \mu} C_{\mu\nu}(x), \quad (2.33)$$

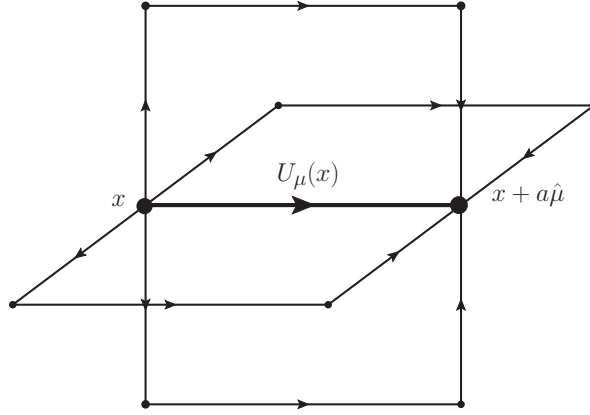


Figure 2.2 – Illustration of the four staples in an hyperplan containing the original link  $U_\mu(x)$ . The last two staples lie out of this hyperplan.

where the staples  $C_{\mu\nu}(x)$  correspond to the six shortest paths starting from the point  $x$  and ending at the point  $x + a\hat{\mu}$  (see Figure 2.2). The transformation (2.33) does not belong to  $SU(3)$  and the new link variable has to be projected back to  $SU(3)$ :

$$U_\mu^{\text{APE}}(x) = \text{Proj}_{SU(3)} \tilde{U}_\mu(x). \quad (2.34)$$

Finally, this smearing procedure can be iterated several times.

## 2.6.2 HYP smearing

The HYP smearing (hypercubic smearing) [44] can be seen as a generalization of the APE smearing where fat links are now constructed from links which lie in hypercubes containing the original link. The smoothing procedure is done in three steps with coefficients  $(\alpha_1, \alpha_2, \alpha_3)$ . In this work, it will be applied to the time-links of heavy-light correlation functions, in this case one has

$$U_0^{\text{HYP}}(x) = \text{Proj}_{SU(3)} \left[ (1 - \alpha_1)U_0(x) + \frac{\alpha_1}{6} \sum_{\pm i \neq 0} \tilde{V}_{i;0}(x) \tilde{V}_{0;i}(x + \hat{i}) \tilde{V}_{i;0}^\dagger(x + \hat{0}) \right],$$

where the decorated links  $\tilde{V}_{\mu,\nu}(x)$  are defined by

$$\tilde{V}_{\mu,\nu}(x) = \text{Proj}_{SU(3)} \left[ (1 - \alpha_2)U_\mu(x) + \frac{\alpha_2}{4} \sum_{\pm \rho \neq \nu, \mu} \bar{V}_{\rho;\nu,\mu}(x) \bar{V}_{\mu;\rho,\nu}(x + \hat{\rho}) \bar{V}_{\rho;\nu,\mu}^\dagger(x + \hat{\mu}) \right],$$

and finally the decorated links  $\bar{V}_{\mu,\nu}(x)$  is defined by

$$\bar{V}_{\mu;\nu,\rho}(x) = \text{Proj}_{SU(3)} \left[ (1 - \alpha_3)U_\mu(x) + \frac{\alpha_3}{2} \sum_{\pm \eta \neq \rho, \nu, \mu} U_\eta(x) U_\mu(x + \hat{\eta}) U_\eta^\dagger(x + \hat{\mu}) \right].$$

The optimal choice obtained in ref. [44] corresponds to the HYP1 action and is given by  $\vec{\alpha}_{\text{HYP1}} = (0.75, 0.6, 0.3)$ . Another choice proposed in ref. [45] after minimizing the noise to signal ratio is called HYP2 and is given by  $\vec{\alpha}_{\text{HYP2}} = (1.0, 1.0, 0.5)$ .

### 2.6.3 Gaussian smearing

While APE and HYP smearings are applied to the gauge field and used to reduce the noise coming from short distance fluctuations, the Gaussian Smearing [46] is applied to the fermionic field and is defined by

$$\psi^{(k)}(x) = (1 + \kappa_G \Delta)^{n_k} \psi(x), \quad (2.35)$$

where  $\Delta$  is the 3-d Laplace operator defined in Appendix A,  $n_k$  is the number of steps, and  $\kappa_G$  is the coupling strength of the nearest neighbors in space directions. Gaussian smearing is often combined with gauge link smearing where the Laplace operator is itself constructed from fat links. Intuitively, starting from a local source, the transformation (2.35) leads to a non local source with a gaussian distribution, the radius of the source  $r_k = 2a\sqrt{\kappa_G n_k}$  increases with the number of iterations. Since mesons are extended objects, the smeared interpolating field  $\psi^{(k)}$  is expected to have a better overlap with the ground state level as depicted in Figure 2.3.

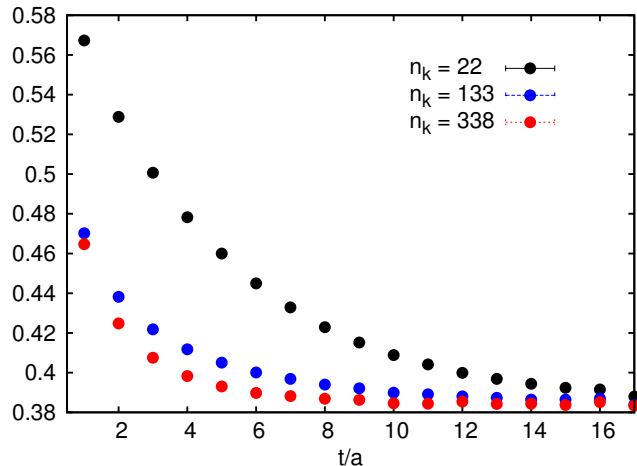


Figure 2.3 – Effective mass  $m^{\text{eff}}(t) = \log(C(t)/C(t+a))$  using heavy-light two-point correlation functions for the  $B$  meson computed with different levels of smearing. Here  $\kappa_G = 0.1$  and  $n_k = (33, 133, 338)$ .

## 2.7 Error estimation

In a Monte Carlo simulation, the Markov chain has a finite size (typically of the order of  $10^4$ ) and the same configurations are used to compute different observables which are therefore correlated. Moreover, since the Markov Process generates the new gauge configuration from the previous one, it also introduces autocorrelation. We would like to estimate the statistical error associated to an observable computed on the lattice (using eq. (2.6)) taking into account all correlations. I will briefly discuss two techniques used in this work. The first one is the Jackknife method, and is based on re-sampling methods. The second is the Gamma Method [47] where one tries to estimate the full autocorrelation matrix. Systematic errors are not considered here and will be the subject of the next section.

In Lattice QCD, the primary observables are usually correlation functions. We label a set of  $P$  primary observables (with  $N$  measurements for each) by:

$$\{\alpha_p^n \mid p = 0 \cdots P ; n = 1 \cdots N\}. \quad (2.36)$$

### 2.7.1 The Jackknife Procedure

The Jackknife procedure was originally introduced by Quenouille for bias reduction. Later Tukey noticed that the same technique turns out to be useful to estimate the variance. It has the advantage to be easily implemented and also very fast. For a review see [48].

#### Mean value estimate

The mean value  $\hat{\alpha}$  of a primary observable is given by the following unbiased estimator

$$\bar{\alpha}_p = \frac{1}{N} \sum_{i=1}^N \alpha_p^i. \quad (2.37)$$

Then, for each secondary observable  $f$ , function of the primary observables  $\alpha_p$ , an estimator of the true mean  $\hat{f} = f(\hat{\alpha})$  is given by

$$\bar{f} = f(\bar{\alpha}_p). \quad (2.38)$$

However, this estimator has generally a bias of order  $1/N$  which can be corrected by the Jackknife procedure (formula (2.42)). However, since the statistical errors in the Monte Carlo simulation are of order  $1/\sqrt{N}$ , this bias can usually be safely neglected.

To estimate the variance, one would naively use the following formula:

$$\sigma^2(f) = \frac{1}{N(N-1)} \sum_{i=1}^N (f(\alpha_p^i) - \bar{f})^2, \quad (2.39)$$

but  $f(\alpha_p^i)$  is generally a spread distribution,  $\langle f(\alpha_p^i) \rangle \neq \hat{f}$ , and the previous formula fails. Moreover it does not take into account autocorrelations. The blocking procedure described in the next section will address the second issue and the Jackknife resampling method will propose a solution to the first one.

#### Blocking

We divide our  $N$  measurements into  $N_B$  blocks including  $B$  consecutive measurements ( $N = N_B \times B$ ). The block average  $\beta_p^b$  of the primary observables  $p$  is then

$$\beta_p^b = \frac{1}{B} \sum_{i=1}^B \alpha_p^{i+(b-1)B}, \quad b = 1, \dots, N_B. \quad (2.40)$$

If the block size is chosen to be larger than the autocorrelation time ( $N \gg B \gg \tau$ ), the block variables can be considered as *independent* new variables characterized by their mean  $\bar{\beta}_p^b$  and their variance. But, obviously, the mean and the variance are invariant under such blocking transformation. Therefore, the statistical error on the primary observables  $\alpha_p$  could be estimated via the naive estimator (2.39) using the block variables  $\beta_p^b$ . The problem appears when non-linear functions of the primary observables are considered since  $\langle f(\beta_p^b) \rangle \neq \hat{f}$ . In this case, the Jackknife procedure can be used.

### Jackknife samples

The *Jackknife samples* (bins) are defined by

$$J_p^b = \frac{1}{N-B} \left( \sum_{i=1}^N \alpha_p^i - \sum_{i=1}^B \alpha_p^{i+(b-1)N} \right) = \frac{1}{N-B} (N\bar{\alpha}_p - B\beta_p^b), \quad (2.41)$$

and correspond to the full sample where the block  $b$  has been deleted. Consequently, each jackknife block contains most of the information (especially when  $B = 1$ , the one-deleted Jackknife) and are clearly not independent.

From the Jackknife sample, the bias of order  $1/N$  in (2.38) can be corrected by considering

$$\bar{f}_J = \bar{f} - (N_B - 1) (\bar{f}_0 - \bar{f}) \quad , \quad \bar{f}_0 = \frac{1}{N_B} \sum_{n=1}^{N_B} f(J_p^b). \quad (2.42)$$

### Error estimate

Finally, an unbiased estimator of the variance for a secondary variable is given by the Jackknife variance (see ref. [49] for a proof),

$$\sigma_J^2(f) = \frac{N_B - 1}{N_B} \sum_{b=1}^{N_B} (f(J_p^b) - \bar{f}_0)^2, \quad (2.43)$$

where the pre-factor  $\frac{N_B-1}{N_B}$  corrects the fact that our variables are not independent but correspond to a resampling of the original one. In eq. (2.43) the mean estimate  $\bar{f}$  could also be used instead of  $\bar{f}_0$ . In practice, to check the reliability of the result, we can check that the result does not depend on the block size  $B$  which should be chosen larger than the autocorrelation time. Finally, using the Jackknife procedure to propagate errors has the advantage to take into account cross-correlations automatically, contrary to the standard propagation of errors where they must be added explicitly.

## 2.7.2 The Gamma method

The  $\Gamma$ -method is described in details in ref. [47] and I just recall the main formulae. The central point is the estimation of the full autocorrelation matrix

$$\Gamma_{nm}(t) = \frac{1}{N-t} \sum_{i=1}^{N-t} (\alpha_n^i - \bar{\alpha}_n) (\alpha_m^{i+t} - \bar{\alpha}_m), \quad (2.44)$$

for times  $t \ll N$ , in terms of the primary observables  $\alpha_n$ . To estimate the error associated to a secondary observable  $f$ , which depends on the primary observables  $\alpha_n$ , we first evaluate the projected autocorrelation function defined by

$$\Gamma_f(t) = \sum_{n,m} f_n f_m \Gamma_{nm}(t) \quad , \quad f_n = \frac{\partial f}{\partial \alpha_n}(\bar{\alpha}_n), \quad (2.45)$$

where  $f_n$  is the partial derivative of  $f$  with respect to  $\alpha_n$  and evaluated at the central value  $\bar{\alpha}_n$ . In practice, the derivatives are computed numerically. In particular,  $\Gamma_f(0)$

corresponds to the variance of  $f$  neglecting the autocorrelation. Finally, we can define the integrated autocorrelation time by

$$\tau_{\text{int},f}(W) = \frac{1}{2} + \sum_{t=1}^W \rho_f(t) \quad , \quad \rho_f(t) = \frac{\Gamma_f(t)}{\Gamma_f(0)} \quad , \quad (2.46)$$

where  $W$  is a cutoff (*summation window*) needed due to the finite size of the Markov chain. Furthermore, since the noise of the autocorrelation function is roughly constant in time, the signal is dominated by noise at large time. The statistical error of the observable  $f$  from  $N$  measurements is finally given by

$$\sigma_{\Gamma,f}^2 = \frac{\Gamma_f(0)}{N} \times 2 \tau_{\text{int},f}(W) \quad . \quad (2.47)$$

In the case where autocorrelation is absent, we have  $\tau_{\text{int},f} = 1/2$  and one recovers the expected estimator for the variance. The value of the cutoff  $W$  should be large enough so that the remaining part in eq. (2.46) is indeed small, but not too large to include only terms with negligible noise. In ref. [47], the author proposed an automatic procedure for searching the window  $W$  and a typical example is given in Figure 2.4. However, neglecting the tail of the autocorrelation function leads to an underestimation of  $\tau_{\text{int}}$  and, therefore, of the statistical error.

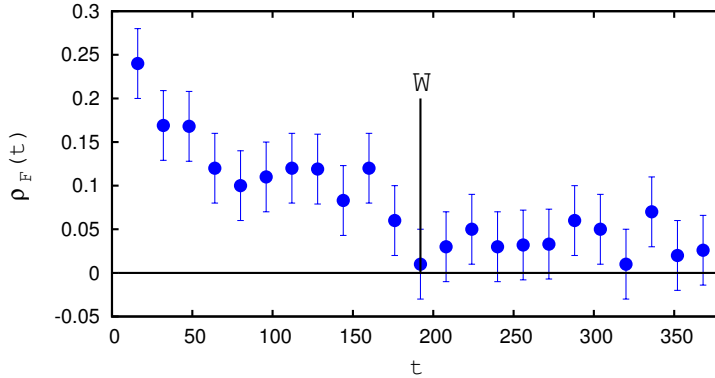


Figure 2.4 – Typical example for the determination of the windows.

Therefore, an improved estimator for  $\tau_{\text{int},f}$  was proposed in ref. [50] which takes into account the tail of the autocorrelation matrix. This critical slowing down is due to the presence of slow modes in the Monte Carlo transition matrix and the associated characteristic time,  $\tau_{\text{exp}}$ , depends on the algorithm. Each observable couples differently to these slow modes and, when this coupling is small, the tail of the autocorrelation function is difficult to estimate. In the aforementioned reference, the author gives an upper bound for the neglected part in eq. (2.46) which corresponds to  $\tau_{\text{exp}} \rho_f(W)$  and then can be used to obtain a more conservative estimate of the error. Since the topological charge is particularly sensitive to the slow modes, it is one of the most popular quantities used to estimate  $\tau_{\text{exp}}$ .

Once  $\tau_{\text{exp}}$  is approximately known, the idea is to choose a second window  $W_u$ , where the signal differs significantly from zero, and to estimate the remaining part in eq. (2.46) by  $\rho_f(t) \approx \rho(W_u) e^{-(t-W_u)/\tau_{\text{exp}}}$  for  $t > W_u$ . Then, one obtains

$$\tau_{\text{int},f}^{(2)}(W_u) = \tau_{\text{int},f}(W_u) + \tau_{\text{exp}} \rho(W_u) \quad , \quad (2.48)$$

where the first part is computed explicitly in the region where it is rather well determined by using eq. (2.46) and the second part is an estimation of the contribution of the tail. The statistical error is now given by

$$\sigma_{\Gamma,f}^2 = \frac{\Gamma_f(0)}{N} \times 2 \tau_{\text{int},f}^{(2)}(W_u). \quad (2.49)$$

An illustration of the window procedure is given in Figure 2.5.

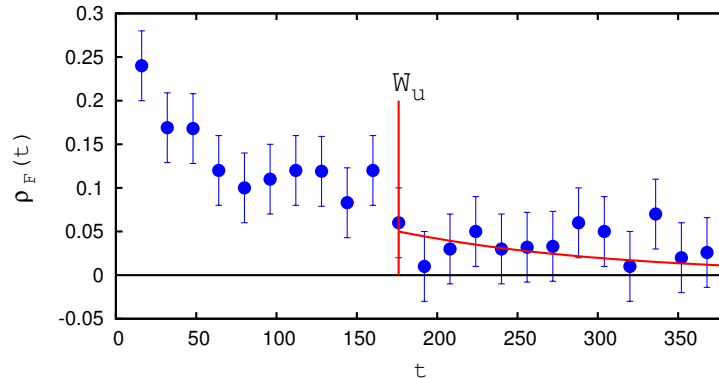


Figure 2.5 – Improved estimator for the integrated autocorrelation time.

## 2.8 Setting the scale and the continuum limit

In the first chapter, the action was formulated in terms of dimensionless quantities parametrized by the bare coupling constant  $g_0$  and the bare quark masses  $m_i$  (or, equivalently, by  $\beta$  and the hopping parameters  $\kappa_i$ ). In the case of  $N_f = 2$  simulations, where only two degenerate dynamical quarks are considered, we are left with two free parameters ( $\beta, \kappa$ ). The first one sets the global scale of the simulation and the second one is used to tune the quark mass.

### Setting the scale

Any observable is obtained in lattice units and, to compare the result with experiment, it is convenient to convert it in physical units. This step, called setting the scale, consists in computing the lattice spacing in physical units by imposing one observable, computed on the lattice, to match its physical value. Setting the scale and adjusting the quark masses is a coupled problem. Therefore, to set the scale one usually chooses a physical observable  $\mathcal{A}$  which depends weakly on the quark masses so that the two steps can be considered as independent. The scale is then obtained by imposing the condition<sup>1</sup>

$$a[\text{MeV}^{-1}] = \frac{(a\mathcal{A})_{\text{lat}}}{\mathcal{A}_{\text{exp}}[\text{MeV}]},$$

where  $(a\mathcal{A})_{\text{lat}}$  is the value of the observable computed on the lattice and  $\mathcal{A}_{\text{exp}}$  is its physical value in MeV. Typical observables are the omega baryon mass [51], or the pion and kaon decay constants  $f_\pi, f_K$  [52]. The observable should be chosen with care: beside the fact that it should not depend too much on the quark masses, it should also be easily

1. The conversion factor between fm and MeV is  $1 \text{ fm}^{-1} = 197.327 \text{ MeV}$

computed on the lattice with a small statistical error to allow for a precise estimation. The systematic errors should also be well under control: in particular, the mass of the  $\rho$  meson is not an optimal choice since it corresponds to a resonance. Finally, the error on the scale will affect all quantities expressed in physical units but also the continuum and chiral extrapolations (see Section 2.9).

The quark masses are determined in a second step. In this work, up and down quarks are assumed to be degenerate and their mass can be set by computing just one observable, like the pion mass. First, the pion mass is computed in lattice units  $(am_\pi)_{\text{lat}}$ , then the result is converted in physical units using the previous estimation of the lattice spacing:

$$m_\pi[\text{MeV}] = \frac{(am_\pi)_{\text{lat}}}{a[\text{MeV}^{-1}]} .$$

There is an ambiguity in setting the scale at finite lattice spacing due to discretization errors, but this ambiguity should vanish in the continuum limit and does not affect the results extrapolated to  $a \rightarrow 0$ . Nevertheless, since we work with  $N_f = 2$  dynamical quarks, an ambiguity arises from the choice of observables used to match the theory with experiment.

### The continuum limit

Lattice QCD offers a natural regularization of the theory both in the infrared (IR) and in the ultraviolet (UV) regimes (via the lattice spacing  $a$  and the spatial extent  $L$  of the lattice). To compare the results with experiment, we would like to remove both cut-offs. Neglecting volume effects, this is performed by taking the limit  $a \rightarrow 0$  at fixed physical volume (corresponding to larger and larger lattice resolutions  $L/a$ ).

## 2.9 Discussion of systematic errors

A typical lattice simulation is performed in a physical volume of a few fermi ( $L \sim 3$  fm) and at lattice spacing of the order  $a \sim 0.06$  fm corresponding to lattice resolutions  $L/a \sim 50$ . In this work, we also work at unphysical quark masses where the pion mass lies in the range [190 – 450] MeV. Therefore, many systematic errors have to be considered.

### Discretization effects

Due to the finite lattice spacing  $a$ , one expects discretization errors linear in the lattice spacing. However, improved actions and operators can be used to cancel  $\mathcal{O}(a)$  artifacts. In the case of Wilson fermions, this is done by adding the Clover term (1.30) in the action and higher-dimensional counterterms to the currents of interest. The theory is then called  $\mathcal{O}(a)$ -improved and the first corrections for on-shell quantities are quadratic in the lattice spacing. To evaluate discretization errors, we can perform several simulations, at different values of the lattice spacing  $a$ , and then extrapolate to the continuum limit. To keep the physical volume  $V$  constant, the lattice resolution  $L/a$  has to be increased and the numerical cost of the simulations grows. Therefore,  $\mathcal{O}(a)$ -improvement can help to reduce the range over which the lattice spacing should vary.

### Volume effects

This source of systematic errors is due to the finite size of the lattice: due to periodic boundary conditions, virtual pions can travel around the lattice. The associated corrections  $\mathcal{O}(e^{-m_\pi L})$  were computed in ref. [53] and decrease exponentially with the volume. The CLS ensembles used in this work fulfill the criterion  $Lm_\pi > 4$  and volume effects are expected to be very small. Therefore, we will not perform any infinite volume extrapolation.

### Dynamical quarks

Evaluating the quark propagator on the lattice becomes more and more difficult as the pion mass gets closer to its physical value. Therefore, many lattice simulations are performed at non-physical quark masses. To estimate the associated systematic error, different simulations at several quark masses are performed and the results are extrapolated to the chiral limit using fit formulae inspired from chiral perturbation theory [54, 55]. A second source of systematic errors comes from the fact that only two dynamical quarks are used in the simulations (quark loops with  $c$ ,  $s$ ,  $b$  and  $t$  quarks are neglected) and the associated error is more difficult to estimate.



# Chapter 3

## Computation of the $b$ -quark mass and $B$ -meson decay constant with $N_f = 2$ dynamical quarks

### Contents

---

<b>Introduction</b> . . . . .	<b>51</b>
<b>3.1 The Heavy Quark Effective Theory</b> . . . . .	<b>52</b>
3.1.1 The need for an Effective Field Theory . . . . .	53
3.1.2 The physical picture . . . . .	53
3.1.3 Derivation of the effective Lagrangian . . . . .	54
3.1.4 Symmetries . . . . .	56
3.1.5 Spectroscopy . . . . .	56
3.1.6 Regularization on the lattice . . . . .	57
<b>3.2 Correlations functions in the framework of HQET</b> . . . . .	<b>58</b>
<b>3.3 Matching with QCD</b> . . . . .	<b>59</b>
3.3.1 Non-perturbative renormalization : motivations . . . . .	59
3.3.2 The general idea . . . . .	60
3.3.3 The matching . . . . .	60
3.3.4 Heavy quark mass dependence . . . . .	61
3.3.5 Conclusion . . . . .	62
<b>3.4 The axial current and <math>\mathcal{O}(a)</math> improvement</b> . . . . .	<b>62</b>
3.4.1 Definition in QCD . . . . .	62
3.4.2 Definition in HQET . . . . .	63
<b>3.5 Computation of <math>m_B</math> and <math>f_B</math> in HQET at order <math>1/m</math></b> . . . . .	<b>64</b>
<b>3.6 The Generalized Eigenvalue Problem</b> . . . . .	<b>66</b>
3.6.1 The $1/m$ expansion . . . . .	66
3.6.2 Expression of the mass . . . . .	67
3.6.3 Expression of the decay constant . . . . .	67
<b>3.7 Simulation parameters</b> . . . . .	<b>69</b>
3.7.1 Lattice ensembles . . . . .	69
3.7.2 Interpolating operators . . . . .	69
3.7.3 Error estimation . . . . .	70

<b>3.8</b>	<b>Determination of the RGI b-quark mass <math>M_b</math></b>	<b>70</b>
<b>3.9</b>	<b>Conversion to the <math>\overline{MS}</math> scheme</b>	<b>73</b>
3.9.1	Discussion	75
<b>3.10</b>	<b>Computation of the B meson decay constants <math>f_B</math> and <math>f_{B_s}</math></b>	<b>77</b>
3.10.1	Interpolation of the HQET parameters	77
3.10.2	Matrix elements	77
3.10.3	Continuum extrapolation	79
3.10.4	Discussion	80
3.10.5	Phenomenology	81
<b>Conclusion</b>		<b>83</b>

---

## Introduction

The  $B$ -physics sector is particularly relevant for many tests of the Standard Model and the search of New Physics, especially since the experimental accuracy has increased thanks to the LHCb experiment. For example, the  $b$ -quark mass, besides being one of the fundamental parameters of the Standard Model, enters as an input parameter in various decay rates which yield useful constraints for the Cabibbo-Kobayashi-Maskawa (CKM) matrix which parametrizes flavour-changing quark transitions and can probe the presence of new physics by testing the unitarity of the matrix. In particular, a major part of the error in the determination of  $V_{ub}$  from inclusive decays comes from the error on  $m_b$ . The  $b$ -quark mass also enters the prediction of the cross section for the Higgs decay,  $H \rightarrow b\bar{b}$ , which is the largest branching ratio for a SM-like Higgs. Due to the non-perturbative nature of the strong interaction, a lattice computation of the  $b$ -quark mass, from first principles, is an important component for high-precision tests of the Standard Model. Indeed, the value cited in the PDG is dominated by results obtained via perturbative QCD.

The  $B_{(s)}$  meson decay constant, which parametrizes the matrix element of the axial current  $A_\mu = \bar{b}\gamma_\mu\gamma_5q$  via  $\langle 0|A_\mu|B_{(s)}(p)\rangle = ip_\mu f_{B_{(s)}}$  also enters, as an input parameter, many leptonic decays used to constrain new physics. Indeed, low energy processes and rare events can be sensitive probes to new physics beyond the standard model since new particles could appear as virtual particles in loop or via new couplings at tree level. In particular, the branching ratio  $\mathcal{B}(B \rightarrow \tau\nu_\tau)$  [56, 57] can be used to predict the CKM matrix element  $V_{ub}$  using the  $B$ -meson decay constant as an input parameter. Using the results of the PDG the value turns out to be slightly different, but compatible at one sigma, compared to the other exclusive determination from  $B \rightarrow \pi\ell\nu$  [58, 59] which uses the  $B \rightarrow \pi$  form factors, also partially computed on the lattice. Therefore, any improvement in the non-perturbative computation of hadronic matrix elements would be useful for a better understanding of the experimental results and to decide whether this discrepancy is due to an experimental problem, a hint of new physics or an underestimate of the uncertainty on the decay constant  $f_B$  governing that decay. In the strange sector, the branching ratio  $\mathcal{B}(B_s^0 \rightarrow \mu^+\mu^-)$  has recently been measured at the LHC [60, 61] and is in excellent agreement with the Standard Model prediction [62, 63] which depends on the decay constant  $f_{B_s}$ .

The main difficulty when dealing with heavy-light mesons on the lattice, is the presence of many different energy scales. In lattice simulations, the lattice spacing should be small compared to the Compton wavelength of the heavy quark ( $\lambda_b \sim 1/m_b$ ) whereas a large volume is necessary to have small volume effects. Therefore, with present day computational facilities, the  $B$  meson cannot be directly simulated on the lattice. To overcome this problem, many different approaches have been proposed. One possibility is to simulate the  $B$  meson at smaller  $b$  quark mass and then extrapolate the results to the physical mass. The static limit of HQET can then be used to constraint the fit in the large mass limit. This strategy is the one followed by the ETM Collaboration [64, 65, 66, 67]. In this work, we take advantage of the fact that, due to its large mass, the  $b$ -quark is well described by the Heavy Quark Effective field Theory (HQET) where irrelevant degrees of freedom, at energies above the hadronization scale, have been integrated out.

HQET is an effective theory which consists in a systematic expansion of the QCD Lagrangian and correlation functions in  $1/m_h$  where  $m_h$  is the mass of the heavy quark. At first order, the effective Lagrangian is parametrized by a small number of parameters which are determined by matching the effective theory with QCD. Once the parameters of the effective theory are known, they can be used to predict the value of some observables like the  $B$ -meson decay constant. On the lattice, due to the appearance of power divergences, already in the static limit, a perturbative matching is not reliable. The solution proposed by the ALPHA Collaboration is based on a non-perturbative matching [68] of HQET and QCD in finite volume at static and first order in  $1/m_h$ . On the QCD side of the lattice simulations, the bare quark mass is an input parameter which is not known a priori due to renormalization effects. Therefore, this matching has been performed at different values of the heavy quark mass which parametrizes all quantities. By imposing that the  $B$  meson mass computed using the effective theory, and extrapolated to the physical point, should correspond to its physical mass, one can obtain the physical value of  $b$ -quark mass by interpolating the results. All the steps are performed using the renormalization group invariant (RGI) quark mass and the results are finally converted to the  $\overline{\text{MS}}$  scheme where a comparison with literature can be done. Finally we can interpolate the HQET parameters at the physical  $b$ -quark mass and use them to compute other interesting observables like the mass splitting between the pseudoscalar  $B$  and vector  $B^*$  mesons or the value of the  $B$  meson decay constant  $f_B$ .

This work is based on ten CLS (Coordinated Lattice Simulations) ensembles [69] with two dynamical quarks at three different lattice spacings and pion masses in the range [190 – 450] MeV to allow for a precise continuum and chiral extrapolations. All steps are performed non-perturbatively and perturbation theory only enters at the end of the computation of the  $b$ -quark mass to convert our results in the more familiar  $\overline{\text{MS}}$  scheme. In particular, the matching of the effective theory with QCD, previously done by the ALPHA Collaboration with gauge configurations produced in the Schrödinger Functional setup, has been performed non-perturbatively.

In the first sections, I will introduce the Heavy Quark Effective Theory (HQET) and summarize the main steps of the non-perturbative matching. Then, I will present the computation of the HQET matrix elements needed to extract the mass of the  $b$ -quark and the  $B$  meson decay constant on the lattice. In particular, I will explain how the Generalized Eigenvalue Problem can be combined with the  $1/m_h$  expansion to reduce higher excited states contamination to masses and matrix elements. Then, I will present the results on the computation of the  $b$ -quark mass and discuss in detail the error analysis. Finally, after the interpolation of the HQET parameters to  $m_b$ , I will present the results on the computation of the  $B$  and  $B_s$  meson decay constants and discuss the phenomenological implications.

### 3.1 The Heavy Quark Effective Theory

The Heavy Quark Effective Theory (HQET) [70, 71, 72, 73, 74] has proven to be an extraordinary tool for studying heavy flavour physics. It consists in an expansion of the QCD Lagrangian in inverse powers of the heavy quark mass. In the static limit, where  $m \rightarrow \infty$ , a new symmetry, the spin-flavour symmetry, appears and provides some new physical insight. Moreover, in the case of the  $b$ -quark, we will see that numerical results

indicate a fast convergence of the  $1/m$  expansion. Finally, from a numerical point of view, HQET highly simplifies the computation of the heavy quark propagator.

### 3.1.1 The need for an Effective Field Theory

The major difficulty in  $B$ -physics lies in the many different scales that have to be treated simultaneously on the lattice. In particular, the mass of the light quarks ( $u$  and  $d$ ) is of the order of the MeV, much below the characteristic scale of QCD  $\Lambda \approx 200$  MeV, whereas the mass of the  $b$ -quark is approximately 4.2 GeV in the  $\overline{\text{MS}}$  scheme. Lattice QCD offers a natural regularization of QCD with ultraviolet (UV) and infrared (IR) cutoffs respectively given by the lattice spacing  $a$  and the size of the box  $L$ . On one hand, if we want to control discretization effects due to the large mass of the  $b$ -quark, we need a sufficiently small lattice spacing  $a \ll m_B^{-1}$ . On the other hand, the typical contribution of volume effects is of order  $\mathcal{O}(e^{-m_\pi L})$  [75] which lead to the following constraints:

$$L^{-1} \ll m_\pi, \dots, m_B \ll a^{-1}. \quad (3.1)$$

We conclude that, for  $Lm_\pi > 4$  and  $am_B < 1/2$ , lattice resolutions bigger than 80 are needed, but beyond present day computational resources. A possibility would be to work at unphysical heavy quark masses (with masses between the charm and the bottom quarks where the constraint  $m_B \ll a^{-1}$  can be relaxed) and then extrapolate the results to the physical mass. It is, to some extent, the path followed by the ETM Collaboration [64]. A second possibility, developed by the ALPHA Collaboration, is to use an Effective Field Theory.

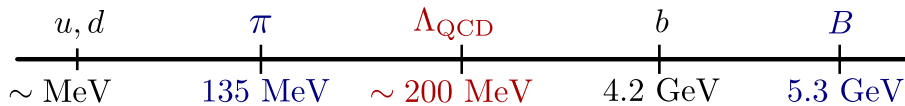


Figure 3.1 – An illustration of the relevant mass scales in lattice simulations with a  $B$  meson

### 3.1.2 The physical picture

The basic idea of an effective field theory is to disentangle the relevant degrees of freedom, in the energy sector of interest, from the other ones which involve processes at higher energy scale. Once they have been isolated, one can formulate a new Lagrangian which captures the essential physics but where irrelevant degrees of freedom no longer appear. Usually, integrating out the heavy degrees of freedom inevitably leads to non-local interactions (in particular, due to virtual particles exchange, like heavy-heavy quark-antiquark pairs production, which occur at very short distances). Therefore, a second step is needed where these non-local interactions are expressed in terms of local one through an operator product expansion (OPE) in terms of a small parameter ( $\Lambda/m_b$  in our case). At first order, the new Lagrangian is expected to be easier to deal with and higher-order corrections can be added systematically. The derivation of the HQET Lagrangian following these steps was done in ref. [76]. In the next section, I will present a less rigorous, but simpler, approach to get the physical insight.

In the case of heavy-light mesons, the heavy quark, bound in a heavy meson, is almost on-shell and moves at the same velocity than the meson. Since the hadron has

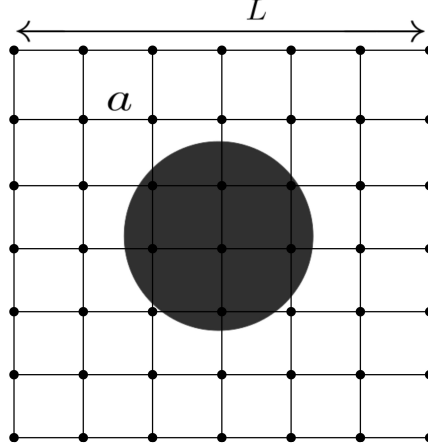


Figure 3.2 – Schematic picture of the  $B$  meson on the lattice. The size of the box  $L$  should be large enough to have small volume effects and the lattice spacing small enough to reduce discretization errors.

a size of order  $R \sim 1$  fm and due to the uncertainty principle, the typical momentum transfer is small  $p \sim R^{-1} \sim \Lambda_{\text{QCD}}$ . Therefore, in the reference frame of the hadron, the heavy quark is almost static and the light degrees of freedom are associated with the light antiquark and gluons which exchange momenta of order  $\Lambda_{\text{QCD}}$  with the heavy quark.

### 3.1.3 Derivation of the effective Lagrangian

I now present a short derivation of the HQET Lagrangian in Minkowski space-time, including first order corrections. The first step is to isolate the relevant degrees of freedom. Since the heavy quark is almost on-shell, the spinor can be decomposed into its heavy and light components:

$$\psi(x) = P_+ \psi(x) + P_- \psi(x) = \varphi(x) + \chi(x), \quad (3.2)$$

where  $P_+$  and  $P_-$  are projectors given by

$$P_{\pm} = \frac{1 \pm \not{v}}{2},$$

where  $v$  is the velocity of the heavy hadron and where the projectors  $P_{\pm}$  satisfy the following constraints:  $P_{\pm}^2 = P_{\pm}$ ,  $P_{\pm} P_{\mp} = 0$  and  $P_+ + P_- = 1$ . Indeed, for an on-shell quark and in the limit of infinite mass, we have exactly  $P_+ \psi(x) = \psi(x)$  and, in the limit of large but finite mass,  $P_+ \psi(x) = \mathcal{O}(1)$  and  $P_- \psi = \mathcal{O}(1/m_b)$ . In terms of these new degrees of freedom, the heavy part of the QCD Lagrangian reads

$$\begin{aligned} \mathcal{L} &= \bar{\psi}(x) (i\not{D} - m_b) \psi(x) \\ &= \bar{\varphi}(x) (iv \cdot D - m_b) \varphi(x) - \bar{\chi}(x) (iv \cdot D + m_b) \chi(x) + \bar{\varphi}(x) i\not{D}_{\perp} \chi(x) + \bar{\chi}(x) i\not{D}_{\perp} \varphi(x) \end{aligned}$$

with the decomposition

$$\not{D} = \not{v} (v \cdot D) + \not{D}_{\perp},$$

where I have used  $\{\not{D}_{\perp}, \not{v}\} = 0$  which is a consequence of  $\{\not{D}, \not{v}\} = 2v \cdot D$ . Finally, light quarks are still described by the usual QCD Lagrangian (1.2).

The main contribution to the time dependence comes from the classical phase factor  $im_b t$ . To eliminate this spurious dependence, one can go one step further by writing the momentum of the heavy quark  $p_b^\mu = (m_b + k^0, \mathbf{k})$  where the constant phase factor  $im_b t$  has been factorized out:

$$\varphi(x) = e^{-im_b(v \cdot x)} \psi_h(x) \quad , \quad \chi(x) = e^{-im_b(v \cdot x)} \psi_H(x) . \quad (3.3)$$

In this step, quarks and antiquarks are treated differently. In particular, for an antiquark, we would have written

$$\varphi(x) = e^{im_b(v \cdot x)} \psi_h(x) \quad , \quad \chi(x) = e^{im_b(v \cdot x)} \psi_H(x) ,$$

and the next steps are the same with the substitution  $v \leftrightarrow -v$ . In particular, the field  $\psi_h$  in eq. (3.3) creates a heavy quark and the field  $\bar{\psi}_h$  annihilates a heavy quark, but does not create an antiquark. Pair productions of heavy quarks are forbidden since they involve momenta of order  $m_b \gg \Lambda_{\text{QCD}}$ . Using the new fields  $\psi_h$  and  $\psi_H$ , the Lagrangian becomes

$$\begin{aligned} \mathcal{L} = & \bar{\psi}_h(x) (iv \cdot D) \psi_h(x) - \bar{\psi}_H(x) (iv \cdot D + 2m_b) \psi_H(x) + \bar{\psi}_h(x) i \not{D}_\perp \psi_H(x) \\ & + \bar{\psi}_H(x) i \not{D}_\perp \psi_h(x) , \end{aligned}$$

where the heavy component  $\psi_H$  has a mass  $2m_b$  and where the small component  $\psi_h$  is massless. The HQET Lagrangian could be obtained by integrating out explicitly the heavy field  $\psi_H$  as done in ref. [76], or we can express the heavy field  $\psi_H$  in terms of the light field  $\psi_h$  using the Dirac equation:

$$\begin{cases} (iv \cdot D + 2m_b) \psi_H = i \not{D}_\perp \psi_h \\ -iv \cdot D \psi_h = i \not{D}_\perp \psi_H \end{cases} ,$$

and

$$\mathcal{L} = \bar{\psi}_h (iv \cdot D) \psi_h + \bar{\psi}_h i \not{D}_\perp \frac{1}{2m_b + iv \cdot D} i \not{D}_\perp \psi_h . \quad (3.4)$$

The price to pay, when expressing the Lagrangian in terms of the light degrees of freedom, is the appearance of non-local terms. They can be removed by expanding the second term of eq. (3.4) with respect to  $\Lambda_{\text{QCD}}/m_b$ :

$$\frac{1}{2m_b + iv \cdot D} = \frac{1}{2m_b} \sum_{n=0}^{\infty} \left( -\frac{iv \cdot D}{2m_b} \right)^n .$$

At order  $\Lambda_{\text{QCD}}/m$ , we are left with

$$\frac{1}{2m_b} \bar{\psi}_h i \not{D}_\perp i \not{D}_\perp \psi_h = \frac{1}{2m_b} \bar{\psi}_h (iD_\perp)^2 \psi_h + \frac{1}{2m_b} \bar{\psi}_h \left( \frac{g}{2} \sigma_{\mu\nu} F^{\mu\nu} \right) \psi_h ,$$

where  $F^{\mu\nu}$  is the gluonic field strength appearing in (1.4),  $\sigma_{\mu\nu} = (i/2)[\gamma_\mu, \gamma_\nu]$  and where I used the relation  $[D^\mu, D^\nu] = -igF^{\mu\nu}$  (1.4). Finally, the HQET Lagrangians at static and  $1/m$  orders are respectively given by

$$\mathcal{L}_{\text{HQET}}^{\text{stat}} = \bar{\psi}_h i(v \cdot D) \psi_h \quad , \quad \mathcal{L}_{\text{HQET}}^{1/m} = \mathcal{L}_{\text{HQET}}^{\text{stat}} - \omega_{\text{spin}} \mathcal{O}_{\text{spin}} - \omega_{\text{kin}} \mathcal{O}_{\text{kin}} ,$$

where

$$\mathcal{O}_{\text{spin}} = -\bar{\psi}_h(x) \frac{g}{2} \sigma_{\mu\nu} F^{\mu\nu} \psi_h(x) \quad , \quad \mathcal{O}_{\text{kin}} = \bar{\psi}_h(x) (D_\perp)^2 \psi_h(x) .$$

At the classical level, we have  $\omega_{\text{spin}} = \omega_{\text{kin}} = \frac{1}{2m_b}$ . Since, at the end, we are interested in the Euclidean formulation of the theory in the reference frame where the heavy quark is at rest, I give the corresponding results (without changing the notations for simplicity)

$$\mathcal{L}_{\text{HQET}}^{\text{stat}} = \bar{\psi}_h D_0 \psi_h, \quad (3.5)$$

$$\mathcal{L}_{\text{HQET}}^{1/m} = \mathcal{L}_{\text{HQET}}^{\text{stat}} - \omega_{\text{spin}} \mathcal{O}_{\text{spin}} - \omega_{\text{kin}} \mathcal{O}_{\text{kin}}, \quad (3.6)$$

where the kinetic and spin operators now read

$$\mathcal{O}_{\text{spin}} = \bar{\psi}_h(x) g \sigma \cdot \mathbf{B} \psi_h(x), \quad \mathcal{O}_{\text{kin}} = \bar{\psi}_h(x) \mathbf{D}^2 \psi_h(x), \quad (3.7)$$

with  $\sigma \cdot \mathbf{B} = \sigma_{ij} F_{ij} / (2i)$ . Truncation errors in the Lagrangian (3.6) are of order  $\mathcal{O}(\Lambda_{\text{QCD}}^2 / m_b^2)$ .

### 3.1.4 Symmetries

We can now discuss the symmetries of the HQET Lagrangian. In the static limit, the Lagrangian (3.5) does not depend on the mass of the heavy quark. Moreover, since there is no Dirac matrix, the spin of the heavy quark remains unchanged during interactions and decouples from the light degrees of freedom. This is the heavy-quark spin-flavour symmetry [71]: in the limit of infinite mass, the strong interaction becomes independent of the mass and spin of the heavy quark. Therefore, mesons can be classified according to the quantum numbers associated to the light degrees of freedom, like their angular momentum  $j$  or parity  $P$ . In particular, for each value of  $j$ , there are two degenerate states with total angular momentum  $J = j \pm 1/2$ . In the case of the  $B$ -meson, the state within the fundamental doublet  $j^P = (1/2)^-$ , corresponds to the pseudoscalar  $B$  ( $J = 0$ ) and vector  $B^*$  ( $J = 1$ ) mesons.

At order  $1/m$ , there are two additional operators in the Lagrangian (3.6). The first one,  $\mathcal{O}_{\text{kin}}$ , corresponds to the kinetic energy associated to the light degrees of freedom. The second one,  $\mathcal{O}_{\text{spin}}$ , has a non-trivial Dirac structure and describes the interactions between the heavy quark spin and gluons. In particular, it breaks the mass degeneracy between the pseudoscalar ( $B$ ) and vector mesons ( $B^*$ ) belonging to the same  $j = 1/2$  doublet.

### 3.1.5 Spectroscopy

The mass of the  $B$  ( $J^P = 0^-$ ) and  $B^*$  ( $J^P = 1^-$ ) mesons in the Heavy Quark Effective theory are respectively given by [77]

$$m_B = m_b + \bar{\Lambda} - \frac{\lambda_1}{2m_b} - \frac{3\lambda_2}{2m_b} \quad (3.8)$$

$$m_{B^*} = m_b + \bar{\Lambda} - \frac{\lambda_1}{2m_b} + \frac{\lambda_2}{2m_b} \quad (3.9)$$

where the parameter  $\bar{\Lambda}$  measures the contribution to the mass carried by the light degrees of freedom and is independent of the heavy quark mass. In particular,  $\bar{\Lambda}$  has the same value for all particles within the same spin-flavour multiplet like the  $B$ ,  $B^*$ ,  $D$  and  $D^*$  states. In particular, the masses of the  $D$  and  $D^*$  mesons, in the static limit, are obtained by using the same equations after the substitution  $m_b \leftrightarrow m_c$ . Finally, the

parameters  $\lambda_1$  and  $\lambda_2$  correspond to HQET matrix elements with operator insertions  $\mathcal{O}_{\text{kin}}$  and  $\mathcal{O}_{\text{spin}}$  respectively.

From eqs. (3.8), (3.9) the mass splitting between the pseudoscalar  $B$  and the vector  $B^*$  mesons is given by the spin term  $m_{B^*} - m_B = \frac{2\lambda_2}{m_b}$ . The experimental value quoted in the PDG [2] is

$$m_{B^*} - m_B = 45.78 \pm 0.35 \text{ MeV} , \quad (3.10)$$

and is indeed small compared to the mass of the meson, in agreement with the  $1/m_b$  expansion. Moreover, we have

$$m_{B^*}^2 - m_B^2 = (m_{B^*} + m_B)(m_{B^*} - m_B) = 4\lambda_2 + \mathcal{O}(\Lambda_{\text{QCD}}/m_b) , \quad (3.11)$$

which is independent of the mass of the heavy quark when first order corrections are neglected. This result is also in good agreement with the experimental data

$$m_{B^*}^2 - m_B^2 \approx 0.48 \text{ GeV}^2 \quad , \quad m_{D^*}^2 - m_D^2 \approx 0.55 \text{ GeV}^2 \quad (3.12)$$

### 3.1.6 Regularization on the lattice

In this section, I give the lattice regularization of the HQET Lagrangian. On the lattice, we choose to work in the reference frame of the  $B$ -meson where the  $b$ -quark is static. The light quark is still described by the QCD Lagrangian discussed in Chapter 1.

#### Static Lagrangian

In the reference frame of the  $B$ -meson, where the heavy quark is at rest, the static HQET Lagrangian (3.5) reads

$$\mathcal{L}_{\text{HQET}}^{\text{stat}} = \bar{\psi}_h(x) D_0 \psi_h(x) . \quad (3.13)$$

On the lattice, we associate two Grassmann-valued spinor fields  $\bar{\psi}_h$  et  $\psi_h$  to each site of the lattice and subject to the constraints

$$P_+ \psi_h = \psi_h \quad , \quad \bar{\psi}_h P_+ = \bar{\psi}_h .$$

Then, by replacing the covariant derivative by the lattice backward covariant derivative  $\nabla_0^* \psi(x) = (1/a)[\psi(x) - U_0^\dagger(x - a\hat{0})\psi(x - a\hat{0})]$ , we obtain the Eichten-Hill [70] action

$$S = a^4 \sum_x \bar{\psi}_h(x) \nabla_0^* \psi_h(x) , \quad (3.14)$$

which describes a static heavy quark (for an anti-quark,  $P_+$  should be replaced by  $P_-$  and the backward covariant derivative by the forward covariant derivative). The choice of the backward derivative prevents the presence of doublers and one can show that discretization effects are of order  $\mathcal{O}(a^2)$  [78]. This lattice action also preserves all the continuum heavy quark symmetries discussed in the previous subsection. In practice, other actions can be used which differ only by the choice of the lattice derivative:

$$\nabla_W^* \psi(x) = \frac{1}{a} \left( \psi(x) - W_0^\dagger(x - a\hat{0})\psi(x - a\hat{0}) \right) , \quad (3.15)$$

where  $W_0$  is a time-like parallel transporter equivalent to  $U_0$  up to terms of order  $\mathcal{O}(a^2)$ . Fat links  $W_0$  are essential to reduce the exponential growth of the noise-to-signal ratio due to the linear divergence in the binding energy  $E^{\text{stat}}$  [79]. In this work, two different smearings HYP1 and HYP2 (see Section 2.6.2) will be used [45].

### The static propagator

The heavy quark propagator  $G_h$  is solution of the following equation:

$$D_0 G_h(x, y) = \delta(x, y) P_+,$$

and can be computed analytically in terms of the gauge link variables, avoiding the need of costly matrix inversions. Explicitly, we have

$$G_h(x, y) = \theta(x_0 - y_0) \delta^{(3)}(\vec{x} - \vec{y}) \mathcal{P}(y, x)^\dagger P_+, \quad (3.16)$$

where  $\mathcal{P}(y, x)$  is the Wilson line from  $x$  to  $y$ :

$$\mathcal{P}(x, x) = 1 \quad , \quad \mathcal{P}(x, x + R\hat{\mu}) = W(x, \mu) W(x + a\hat{\mu}, \mu) \dots W(x + a(R-1)\hat{\mu}, \mu) \quad , \quad R > 0.$$

From the spatial  $\delta$  function and  $\theta$  function, it is clear that the heavy quark propagates only (forward) in time.

### The $1/m$ corrections

When including  $1/m$  corrections, we need a lattice regularization of the operators  $\mathcal{O}_{\text{kin}}$  and  $\mathcal{O}_{\text{spin}}$  discussed in the previous section. The first one is simply obtained by using the 3D lattice Laplace operator  $\mathbf{D}^2$  (Appendix A.9). For the spin operator  $\mathcal{O}_{\text{spin}}$ , one can use the discretized version of  $\sigma \cdot \mathbf{B} = \frac{1}{2i} \sigma_{ij} \hat{F}^{ij}$  where  $\sigma_{ij}$  is given in Appendix A and  $\hat{F}^{ij}$  is the lattice field strength tensor given by eq. (1.31) :

$$\mathcal{O}_{\text{spin}} = \bar{\psi}_h(x) \sigma \cdot \mathbf{B} \psi_h(x) \quad , \quad \mathcal{O}_{\text{kin}} = \bar{\psi}_h(x) \mathbf{D}^2 \psi_h(x), \quad (3.17)$$

the coupling  $g$  does not appear in  $\mathcal{O}_{\text{spin}}$  compared to eq. (3.7), due to the different normalization of the field strength on the lattice (1.31).

## 3.2 Correlations functions in the framework of HQET

At order  $1/m$ , the Lagrangian contains two dimension five operators,  $\mathcal{O}_{\text{kin}}$  and  $\mathcal{O}_{\text{spin}}$ , and the path integral based on the Lagrangian (3.6) is not renormalizable. In particular, the continuum limit of the corresponding theory (NRQCD [80] [81]) does not exist. Therefore, to use NRQCD, one has to choose a sufficiently small lattice spacing to have controllable discretization effects but, since the lattice spacing also acts like a cut-off, it should satisfy the condition  $am_B > \mathcal{O}(1)$  where NRQCD is expected to work. In this window, one can then use improved lattice actions by adding new terms to the Lagrangian to reduce discretization effects. Another disadvantage of NRQCD is that the matching with QCD is done only perturbatively.

To solve these problems, the HQET path integral is obtained by expanding the action in  $1/m$ . The  $1/m$  terms in the Lagrangian are then treated as operator insertions and the expectation value of any observable  $\mathcal{A}$  is given by

$$\begin{aligned} \langle \mathcal{A} \rangle &= \frac{1}{Z} \int \mathcal{D}\phi \mathcal{A} e^{-a^4 \sum_x [\mathcal{L}_{\text{light}}(x) + \mathcal{L}_{\text{HQET}}^{\text{stat}}(x) - \omega_{\text{spin}} \mathcal{O}_{\text{spin}}(x) - \omega_{\text{kin}} \mathcal{O}_{\text{kin}}(x)]} \\ &\approx \frac{1}{Z} \int \mathcal{D}\phi \mathcal{A} \left( 1 + a^4 \sum_x \omega_{\text{spin}} \mathcal{O}_{\text{spin}}(x) + \omega_{\text{kin}} \mathcal{O}_{\text{kin}}(x) \right) e^{-a^4 \sum_x [\mathcal{L}_{\text{light}}(x) + \mathcal{L}_{\text{HQET}}^{\text{stat}}(x)]} \\ &\approx \langle \mathcal{A} \rangle_{\text{stat}} + \omega_{\text{kin}} a^4 \sum_x \langle \mathcal{A} \mathcal{O}_{\text{kin}}(x) \rangle_{\text{stat}} + \omega_{\text{spin}} a^4 \sum_x \langle \mathcal{A} \mathcal{O}_{\text{spin}}(x) \rangle_{\text{stat}}, \end{aligned}$$

where the path integral weight  $\langle \cdots \rangle_{\text{stat}}$  is always given by the static part of the HQET Lagrangian. Here,  $\mathcal{L}_{\text{light}}$  denotes the light part of the action (*up* and *down* quarks) and  $\mathcal{D}\phi$  is a short-notation for the path integral measure. In the following we will write

$$\begin{aligned} \langle \mathcal{A} \rangle &= \langle \mathcal{A} \rangle_{\text{stat}} + \omega_{\text{kin}} a^4 \sum_x \langle \mathcal{A} \mathcal{O}_{\text{kin}}(x) \rangle_{\text{stat}} + \omega_{\text{spin}} a^4 \sum_x \langle \mathcal{A} \mathcal{O}_{\text{spin}}(x) \rangle_{\text{stat}} \\ &= \langle \mathcal{A} \rangle_{\text{stat}} + \omega_{\text{kin}} \langle \mathcal{A} \rangle_{\text{kin}} + \omega_{\text{spin}} \langle \mathcal{A} \rangle_{\text{spin}} . \end{aligned} \quad (3.18)$$

### $\mathcal{O}(a)$ improvement and $1/m$ expansion

It should be noted that  $\mathcal{O}(a)$  improvement of the action, in the path integral weight, is crucial when considering HQET beyond the static order. Indeed, on the lattice, we cannot disentangle the contributions coming from the  $1/m$ -expansion and the one coming from the  $a$ -expansion since an operator can mix with all other operators with the same or lower dimension allowed by lattice symmetries. The static Lagrangian is already  $\mathcal{O}(a)$  improved and  $\mathcal{O}(a)$  improvement of  $\mathcal{L}_{\text{light}}$  has been discussed in Section 1.5.3. At order  $1/m$  we cannot exclude corrections linear in the lattice spacing and the first corrections are then of order  $\mathcal{O}(a^2, a/m_b)$ .

## 3.3 Matching with QCD

In Section 3.1.3, we have derived the HQET Lagrangian and obtained the classical values of the HQET parameters:  $\omega_{\text{kin}} = \omega_{\text{spin}} = 1/m_b$ . In the quantum field theory, they receive quantum corrections and the parameters have to be renormalized (to include loop effects like, for example, heavy-particle exchange). Consequently the HQET parameters depend on both heavy quark mass and the lattice spacing (through the coupling constant). The relations between the couplings in HQET and QCD are imposed by the requirement that the two theories describe the same physics, and are called matching conditions.

### 3.3.1 Non-perturbative renormalization : motivations

When discussing the renormalization of the HQET Lagrangian, a mass counter term  $\delta m$  should be added even if it is set to zero in the classical action (3.13). Indeed, this counter term is necessary to cancel a linear divergence in the self-energy of the static quark [70], due to the mixing of  $\bar{\psi}_h(x) D_0 \psi_h(x)$  with the scalar density  $\bar{\psi}_h(x) \psi_h(x)$ . In practice,  $\delta m$  is set to zero on the lattice action and its effect is absorbed in the redefinition of the  $b$ -quark mass which now contains a linear divergence:  $m_{\text{bare}} = m_b + \delta m$  (here,  $m_b$  is the mass appearing in the phase factor in eq. (3.3)). This linear divergence has been computed to two loops in perturbation theory in refs. [82, 83]. At order  $1/m$  new divergences appear, in particular the kinetic term

$$\mathcal{O}_{\text{kin}} = \bar{\psi}_h(x) \mathbf{D}^2 \psi_h(x) ,$$

can mix with the operators  $\bar{\psi}_h(x) D_0 \psi_h(x)$  and  $\bar{\psi}_h(x) \psi_h(x)$  leading respectively to linear and quadratic divergences [84].

Because of these divergences, the total uncertainty is difficult to estimate as long as the renormalization is carried out perturbatively [84]. The strategy followed by the ALPHA collaboration is to renormalize the theory non-perturbatively [85, 86, 87, 88].

### 3.3.2 The general idea

At order  $1/m$ , five parameters  $\omega_i$  are needed to compute the mass and the decay constant of the  $B$  meson

$$\omega_i = \left( m_{\text{bare}}, \log(Z_A^{\text{HQET}}), c_A^{(1)}, \omega_{\text{kin}}, \omega_{\text{spin}} \right), \quad i \in [1..5] \quad (3.19)$$

where  $m_{\text{bare}}$ ,  $\omega_{\text{kin}}$  and  $\omega_{\text{spin}}$  directly enter through the Lagrangian density (3.6). The parameter  $Z_A^{\text{HQET}}$  is the renormalization factor of the axial current and  $c_A^{(1)}$  is a coefficient appearing in the  $1/m$  expansion of the axial current [89]. They will be introduced in more details in the next section. We would like to compute these parameters at different lattice spacings for the computation of hadronic observables. In principle, we could compute five observables in the effective field theory and match them with experimental results, but proceeding this way would reduce significantly the predictive power of the effective theory. Instead, the idea is to compute five observables in both QCD and HQET and then to impose the following matching conditions

$$\Phi_i^{\text{QCD}} = \Phi_i^{\text{HQET}}(\omega_j), \quad i \in [1, \dots, 5], \quad (3.20)$$

to determine the HQET parameters. To simplify the analysis, the five observables should have a simple (linear) dependence on the HQET parameters  $\omega_i$ . Finally, at static order, there are only two parameters:

$$\omega_i^{\text{stat}} = \left( m_{\text{bare}}^{\text{stat}}, \log(Z_A^{\text{stat}}) \right), \quad i \in [1, 2]. \quad (3.21)$$

### 3.3.3 The matching

The matching of HQET and QCD at order  $1/m$  was performed by the ALPHA collaboration in ref. [68]. The five observables, defined in the Schrödinger functional scheme [90], are written

$$\Phi_i^{\text{HQET}}(L, a) = \eta_i(L, a) + \alpha_{ij}(L, a)\omega_j(a), \quad (3.22)$$

where  $\eta_i(L, a)$  and  $\alpha_{ij}(L, a)$  are correlation functions computed in HQET. Taking the continuum limit  $\Phi_i^{\text{QCD}}(L_1, 0) = \lim_{a \rightarrow 0} \Phi_i^{\text{QCD}}(L_1, a)$  and imposing the matching conditions (3.20), the HQET parameters  $\omega_i(a)$  can be obtained at different given lattice spacings  $a$ . However, the matching of HQET and QCD has to be done with the following constraints:

- the lattice spacing  $a$  should be small enough,  $a^{-1} \gg m_b$ , to have controllable discretization effects in QCD simulations with a relativistic  $b$ -quark.
- the volume  $V = L^3$  has to be large enough to allow for a precise  $1/m$  expansion in HQET  $m_b \gg L^{-1}$ .
- the lattice resolution should satisfy the constraint  $L/a = \mathcal{O}(10)$  imposed by present day computer limitations.

To fulfill these constraints, we conclude that the matching has to be done in a small volume  $L \approx 0.4$  fm where the lattice spacing lie in the range (0.025 fm to 0.05 fm). But these lattice spacings are too small for lattice simulations with a  $B$  meson in a large volume and with reasonable resolutions (namely  $a \in [0.05 - 0.08$  fm]). Consequently,

an intermediate step is needed to obtain the values of the HQET parameters at larger lattice spacing.

The technique, described in details in ref. [88] and schematized in Figure 3.3, is based on the computation of step-scaling functions which relate the observables  $\Phi_i^{\text{HQET}}(L, a)$  at different volumes  $L_1$  and  $L_2 = 2L_1$ . First, the correlation functions  $\eta_i(L, a)$  and  $\alpha_{ij}(L, a)$  are computed in the two different volumes but with the same lattice spacings  $a$  (so that the HQET parameters  $\omega_j(a)$  are the same). Then, using different lattice spacings in the range (0.025 fm to 0.05 fm) we can extrapolate the step scaling functions to the continuum limit and obtain  $\Phi_i^{\text{QCD}}(L_2, a = 0)$ . Finally, in the larger volume  $L_2$ , we can compute the correlation functions  $\eta_i(L_2, a)$  and  $\alpha_{ij}(L_2, a)$  at larger lattice spacings and obtain  $\omega_j(a)$  by matching  $\Phi_i^{\text{HQET}}(L_2, a)$  with  $\Phi_i^{\text{QCD}}(L_2, a = 0)$  using eq. (3.22).

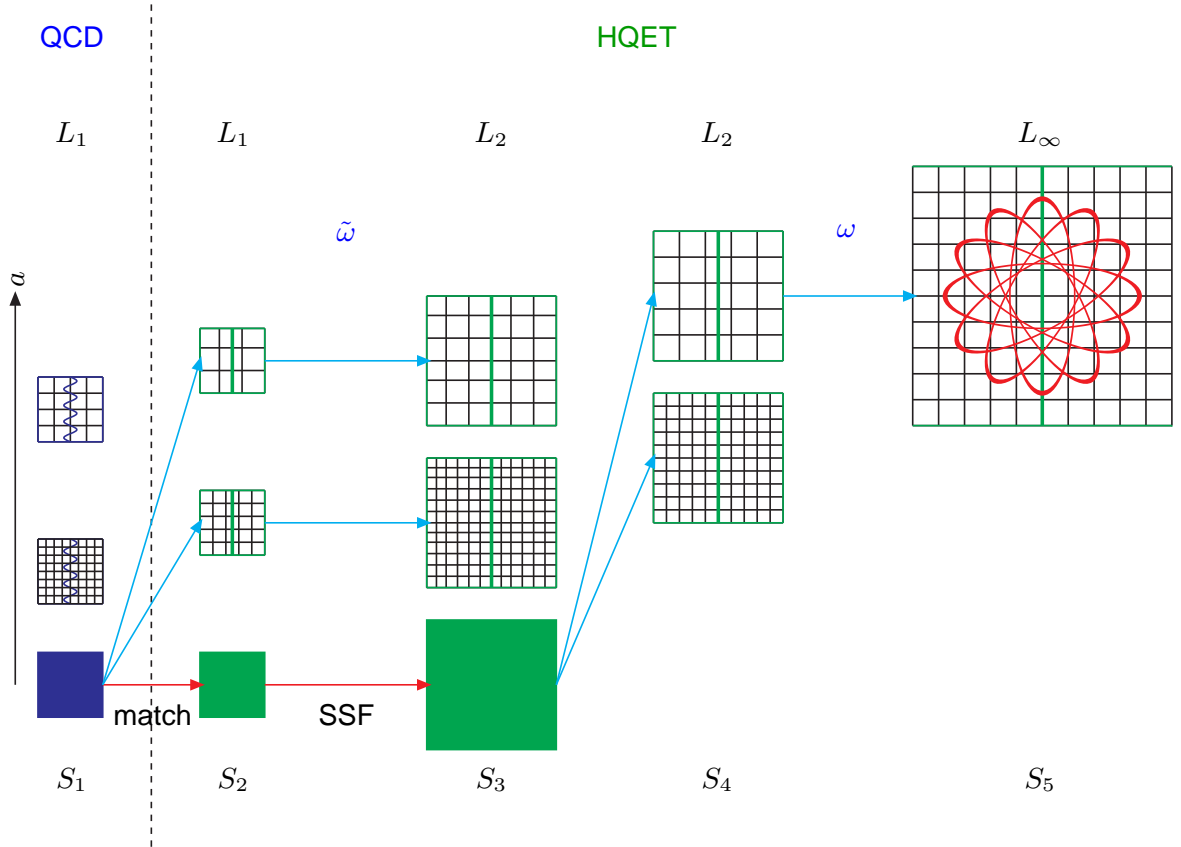


Figure 3.3 – Sketch of the strategy for the matching of QCD and HQET. Figure taken from [88].

### 3.3.4 Heavy quark mass dependence

As explained in the beginning of this section, the HQET parameters depend, in addition to the lattice spacing, on the heavy quark mass. Therefore, the matching was performed at several value of the  $b$ -quark mass  $m_b$ . In HQET, the mass of the  $b$  quark is parametrized by the dimensionless quantity  $z = L_1 M$  where  $L_1 \approx 0.4$  fm is a fixed volume defined by  $\bar{g}^2(L_1/2) = 2.989$  [68] ( $g$  is the strong coupling in the Schrödinger

functional scheme) and  $M$  is the Renormalization Group Invariant mass (RGI). The HQET parameters  $\omega(z, a)$  depend on both the lattice spacing  $a$  and the heavy quark mass  $z$  where  $z$  takes the following values

$$z = 4, 6, 7, 9, 11, 13, 15, 18, 21,$$

which correspond to a RGI mass  $M$  in the range from 2 GeV to 10 GeV which includes the physical mass. In QCD simulations, with two dynamical light quarks ( $N_f = 2$ ) and one heavy quenched quark, the relation between  $M$  and the bare quark mass  $m_{q,h}$  appearing in the Lagrangian is known non-perturbatively [68]. Since the relation will be useful when discussing the errors on the  $b$  quark mass, I give the explicit formula:

$$M = h(L)Z_m(g_0, L/a)(1 + b_m(g_0)am_{q,h})m_{q,h} + \mathcal{O}(a^2), \quad (3.23)$$

where  $h(L) = M/\overline{m}^{\text{SF}}(\mu)$  is the regularization independent ratio of the RGI heavy quark mass and the running quark mass  $\overline{m}^{\text{SF}}$  in the Schrödinger functional scheme. It has been computed by the ALPHA collaboration [91] and  $h(L) = 1.521(14)$  at the scale  $\mu = 1/L_0 = 2/L_1$ . Finally, the factor  $Z_m$  is a combination of renormalization coefficients (see the previous reference for the details), the parameter  $b_m(g_0)$  is an improvement coefficient and the relation between the hopping parameter  $\kappa_h$  and the bare quark mass  $m_{q,h}$  is given by eq. (1.32).

### 3.3.5 Conclusion

At the end of this procedure, the values of the HQET parameters are known at different values of the lattice spacing, different heavy quark masses and for the two static actions HYP1 and HYP2. Moreover, two independent matchings were performed for the static and  $1/m$  theories [68]. Indeed, it is important to notice that, due to operator mixing, static and  $1/m$  results cannot be compared by simply neglecting the kinematic and spin terms. In particular, the kinetic term diverges quadratically and does not have a continuum limit.

## 3.4 The axial current and $\mathcal{O}(a)$ improvement

### 3.4.1 Definition in QCD

To study the  $B$  meson on the lattice, we introduce the heavy-light axial current. In QCD, it is defined by  $A_\mu(x) = Z_A \overline{\psi}_h(x) \gamma_\mu \gamma_5 \psi_l(x)$  where  $\psi_h(x)$  and  $\psi_l(x)$  are respectively associated to the heavy and light quarks and  $Z_A$  is the renormalization constant, determined from the chiral Ward identities [92]. The correlation function for the time component reads

$$C_{AA}^{\text{QCD}}(t) = a^3 \sum_{\vec{x}} \langle A_0(x) A_0^\dagger(0) \rangle. \quad (3.24)$$

Inserting the spectral decomposition, one obtains

$$C_{AA}^{\text{QCD}}(t) = \frac{1}{2} \sum_n \langle 0 | \hat{A}_0 | B_n \rangle \langle B_n | \hat{A}_0^\dagger | 0 \rangle e^{-m_{B_n} t}, \quad (3.25)$$

where I used the non-relativistic normalization of states  $\langle B_n | B_n \rangle = 2V$  and where  $|B_n\rangle$  corresponds to the  $n^{\text{th}}$  state of the Hamiltonian with zero spatial momentum (states

with non-zero spatial momentum are absent due to the sum over lattice sites). From eq. (3.25), we conclude that the mass and the decay constant of the  $B$  meson are encoded in this correlator

$$\begin{cases} am_B = -\lim_{t \rightarrow \infty} \frac{\partial_0 + \partial_0^*}{2} \log C_{AA}^{\text{QCD}}(t) \\ a^{3/2} f_B \sqrt{\frac{m_B}{2}} = \lim_{t \rightarrow \infty} \left( e^{m_B x_0} C_{AA}^{\text{QCD}}(t) \right)^{1/2} \end{cases}, \quad (3.26)$$

where the discrete derivatives are defined in Appendix A and the decay constant, which parametrizes the matrix element of the axial current, is defined by

$$\langle 0 | A_0 | B(\vec{p} = 0) \rangle = \sqrt{m_B} f_B.$$

Using the relativistic normalization, one would obtain the usual definition of the decay constant,  $\langle 0 | A_\mu | B(p) \rangle_{\text{rel}} = p_\mu f_B$ .

### 3.4.2 Definition in HQET

In HQET, the renormalized and  $\mathcal{O}(a)$ -improved axial current is [78]

$$A_0^{\text{HQET}} = Z_A^{\text{HQET}} (1 + b_A^{\text{stat}} am_q) \left( A_0^{\text{stat}} + ac_A^{(1)} \delta A_0^{(1)} + ac_A^{(2)} \delta A_0^{(2)} \right), \quad (3.27)$$

with

$$\delta A_0^{(1)}(x) = \psi_l(x) \gamma_5 \gamma_i \tilde{\nabla} \psi_h(x) \quad , \quad \delta A_0^{(2)}(x) = -\frac{\partial_i + \partial_i^*}{2} A_i^{\text{stat}}(x), \quad (3.28)$$

where  $Z_A^{\text{HQET}}$  and  $c_A^{(1)}$  are the HQET parameters introduced in the previous section. Since  $\delta A_0^{(2)}$  does not contribute to correlation functions at vanishing spatial momentum, this term will not be considered in the following. In particular,  $Z_A^{\text{HQET}}$  is the renormalization factor of the heavy-light axial current in the effective theory. Since a mass-independent renormalization scheme is used for the matching procedure described in the previous section (dynamical light quarks were tuned to be massless), the renormalized axial current must be multiplied by the improvement factor  $(1 + b_A^{\text{stat}} m_q)$  to ensure that the renormalized current with massive light quarks is still  $\mathcal{O}(a)$  improved [93]. Here,  $m_q$  denotes the subtracted light quark mass given by  $m_q = m_0 - m_c$  where  $m_0$  is the bare light quark mass and  $m_c$  is the critical mass (the point where the PCAC mass vanishes). The improvement coefficient  $b_A^{\text{stat}}$  has been computed to 1-loop in perturbation theory [94]. Finally, at static order,  $c_A^{(1)} = c_A^{\text{stat}}$  is purely an improvement coefficient, but at order  $1/m$ , the coefficient  $c_A^{(1)}$  comes from the  $1/m$  expansion of the axial current and has to be determined non-perturbatively. The values of the improvement coefficients  $b_A^{\text{stat}}$  and  $c_A^{\text{stat}}$  are given in Table 3.1 for different values of the coupling constant  $g_0$ .

Similarly to the previous section, the correlation function now reads

$$C_{AA}(t) = e^{-m_{\text{bare}} x_0} a^3 \sum_x \left\langle A_0^{\text{HQET}}(x) A_0^{\text{HQET}}(0)^\dagger \right\rangle, \quad (3.29)$$

where the mass shift  $m_{\text{bare}}$  has been explicitly written. As explained before, at the classical level it corresponds to the heavy quark mass but, in the quantized theory,

$\beta = 6/g_0^2$	$\kappa_c(g_0^2)$	$c_A^{\text{stat}}(g_0^2)$		$b_A^{\text{stat}}(g_0^2)$	
		HYP1	HYP2	HYP1	HYP2
5.2	0.1360546	0.0033461	0.0597692	0.6045384	0.6638461
5.3	0.1364572	0.0032830	0.0586415	0.6025660	0.6607547
5.5	0.1367749	0.0031636	0.0565090	0.5988363	0.6549090

Table 3.1 – Numerical values of the critical parameter  $\kappa_c(g_0^2)$  [52] and of the improvement coefficients  $b_A^{\text{stat}}$  and  $c_A^{\text{stat}}$  from 1-loop perturbation theory [94].

it compensates for a power divergence. Finally, using the decomposition (3.18) for the computation of an expectation value in HQET, we arrive at the following  $1/m$  expansion

$$C_{AA}(t) = e^{-m_{\text{bare}}t} \left( Z_A^{\text{HQET}} \right)^2 (1 + b_A^{\text{stat}} am_q)^2 \left[ C_{AA}^{\text{stat}}(t) + c_A^{(1)} (C_{A\delta A}^{\text{stat}}(t) + C_{\delta AA}^{\text{stat}}(t)) \right. \\ \left. + \omega_{\text{kin}} C_{AA}^{\text{kin}}(t) + \omega_{\text{spin}} C_{AA}^{\text{spin}}(t) \right] \quad (3.30)$$

with

$$C_{AA}^{\text{stat}}(t) = \sum_{\vec{x}, y, z} \langle A_0(y_0 + t, \vec{x}) A_0^*(y) \rangle_{\text{stat}}, \quad (3.31)$$

$$C_{\delta AA}^{\text{stat}}(t) = \sum_{\vec{x}, y, z} \langle \delta A_0(y_0 + t, \vec{x}) A_0^*(y) \rangle_{\text{stat}}, \quad (3.32)$$

$$C_{AA}^{\text{kin/spin}}(t) = \sum_{\vec{x}, y, z} \langle A_0(y_0 + t, \vec{x}) A_0^*(y) \mathcal{O}_{\text{kin/spin}}(z) \rangle_{\text{stat}}. \quad (3.33)$$

In the next section, I will explain how the  $B$  meson mass and decay constant can be computed from this correlation function. Then, in Section 3.6, I will use the Generalized Eigenvalue Problem to obtain improved estimators, where higher excited states contamination has been further suppressed.

## 3.5 Computation of $m_B$ and $f_B$ in HQET at order $1/m$

### The $B$ meson mass

Using eqs. (3.26), (3.30), and considering  $1/m$  terms as small parameters, the mass of the  $B$ -meson is now given by

$$m_B = - \lim_{t \rightarrow \infty} \frac{\partial_0 + \partial_0^*}{2} \log C_{AA}(t) = m_{\text{bare}} + E^{\text{stat}} + \omega_{\text{kin}} E^{\text{kin}} + \omega_{\text{spin}} E^{\text{spin}}, \quad (3.34)$$

where the HQET matrix elements  $E^{\text{stat}}$ ,  $E^{\text{kin}}$  and  $E^{\text{spin}}$  are defined by

$$E^{\text{stat}} = - \lim_{t \rightarrow \infty} \frac{\partial_0 + \partial_0^*}{2} \log C_{AA}^{\text{stat}}(t), \quad (3.35)$$

$$E_y = - \lim_{t \rightarrow \infty} \frac{\partial_0 + \partial_0^*}{2} \frac{C_{AA}^{\text{kin}}(t)}{C_{AA}^{\text{stat}}(t)}, \quad y \in [\text{kin}, \text{spin}]. \quad (3.36)$$

The term  $C_{A\delta A}$  does not contribute to the mass since the ratio  $C_{A\delta A}^{\text{stat}}/C_{AA}^{\text{stat}}$  tends towards a constant. In the static limit, the mass is obtained by replacing the HQET parameter  $m_{\text{bare}}$  by its static value  $m_{\text{bare}}^{\text{stat}}$  and ignoring  $1/m$  corrections

$$m_B^{\text{stat}} = - \lim_{t \rightarrow \infty} \frac{\partial_0 + \partial_0^*}{2} \log C_{AA}(t) = m_{\text{bare}}^{\text{stat}} + E^{\text{stat}}. \quad (3.37)$$

Using the spectral decomposition and the non-relativistic normalization of states  $\langle B|B \rangle = 2L^3$ ,  $E^{\text{stat}}$ ,  $E^{\text{kin}}$  and  $E^{\text{spin}}$  can be expressed in terms of matrix elements. Indeed, the static correlation function can be written

$$C_{AA}^{\text{stat}}(t) = a^3 \sum_{\vec{x}} \langle A_0(x) A_0^\dagger(0) \rangle_{\text{stat}} = \frac{1}{2} \sum_n \langle 0|A_0|B_n \rangle_{\text{stat}} \langle B_n|A_0^\dagger|0 \rangle_{\text{stat}} e^{-E_n^{\text{stat}} t},$$

and the kinetic term

$$\begin{aligned} C_{AA}^{\text{kin}}(x_0) &= a^7 \sum_{\vec{x}, y} \langle A_0(x) A_0^*(0) \mathcal{O}_{\text{kin}}(y) \rangle_{\text{stat}} \\ &= \frac{a}{4} \sum_{y_0 \leq x_0} \sum_{n, m} \underbrace{\langle 0|A_0|B_n \rangle_{\text{stat}} \langle B_n|\mathcal{O}_{\text{kin}}(0)|B_m \rangle_{\text{stat}} \langle B_m|A_0^*|0 \rangle_{\text{stat}}}_{\alpha_{nm}} e^{-E_n(x_0 - y_0) - E_m y_0} \\ &= \frac{ax_0}{4} \sum_n \alpha_{nn} e^{-E_n x_0} - \frac{1}{4} \sum_{n \neq m} \alpha_{nm} a \frac{e^{-E_n(x_0+1)} - e^{-E_m(x_0+1)}}{e^{-E_n} - e^{-E_m}} \\ &= \frac{ax_0}{4} \sum_n \alpha_{nn} e^{-E_n x_0} - \frac{1}{4} \sum_{n \neq m} (\alpha_{nm} + \alpha_{mn}) a \frac{e^{-E_n(x_0+1)}}{e^{-E_n} - e^{-E_m}}. \end{aligned}$$

Therefore, we obtain

$$\begin{aligned} R_{AA}^{\text{kin}}(x_0) &= \frac{C_{AA}^{\text{kin}}(x_0)}{C_{AA}^{\text{stat}}(x_0)} = \frac{ax_0}{2} \langle B|\mathcal{O}_{\text{kin}}(0)|B \rangle \\ &\quad - \frac{1}{2} \sum_{m>1} (\alpha_{1m} + \alpha_{m1}) a \frac{e^{-E_1}}{e^{-E_1} - e^{-E_m}} + \mathcal{O}(x_0 e^{-(E_2 - E_1)x_0}), \end{aligned}$$

and similarly for  $R_{AA}^{\text{spin}}$ . Consequently, from eq. (3.36), we found

$$E_{\text{kin}} = -\frac{1}{2} \langle B|\mathcal{O}_{\text{kin}}(0)|B \rangle_{\text{stat}}, \quad E_{\text{spin}} = -\frac{1}{2} \langle B|\mathcal{O}_{\text{spin}}(0)|B \rangle_{\text{stat}}. \quad (3.38)$$

### The mass splitting

In Section 3.1.5, we have computed the mass splitting between the pseudoscalar  $B$  and vector  $B^*$  mesons in terms of the HQET parameter  $\lambda_2$ . From the previous formulae and the results in ref. [77], we found

$$E^{\text{spin}} = -3\lambda_2 \quad \Rightarrow \quad \Delta m_B = 4\lambda_2 = -\frac{4}{3} \omega_{\text{spin}} E^{\text{spin}}. \quad (3.39)$$

Then, the mass splitting is simply given in terms of the matrix element  $E^{\text{spin}}$  and the HQET parameter  $\omega_{\text{spin}}$ . It is useful to recall that, contrary to the kinetic term, the spin term indeed has a continuum limit.

### The $B$ -meson decay constant

Similarly, using eqs. (3.26), (3.30) the decay constants at static and  $1/m$  orders are respectively given by

$$a^{3/2} f_B^{\text{stat}} \sqrt{\frac{m_B}{2}} = \lim_{t \rightarrow \infty} \left\{ Z_A^{\text{stat}} (1 + b_A^{\text{stat}} a m_q) \left( e^{E^{\text{stat}} t} C_{AA}^{\text{stat}}(t) \right)^{1/2} \left[ 1 + \frac{1}{2} c_A^{\text{stat}} \frac{C_{AA}^{\text{dA}}(t)}{C_{AA}^{\text{stat}}(t)} \right] \right\} \quad (3.40)$$

and

$$a^{3/2} f_B \sqrt{\frac{m_B}{2}} = \lim_{t \rightarrow \infty} \left\{ Z_A^{\text{HQET}} (1 + b_A^{\text{stat}} a m_q) \left( e^{E^{\text{stat}} t} C_{AA}^{\text{stat}}(t) \right)^{1/2} \left[ 1 + \frac{1}{2} \omega_{\text{kin}} \left( t E^{\text{kin}} + \frac{C_{AA}^{\text{kin}}(t)}{C_{AA}^{\text{stat}}(t)} \right) + \frac{1}{2} \omega_{\text{spin}} \left( t E^{\text{spin}} + \frac{C_{AA}^{\text{spin}}(t)}{C_{AA}^{\text{stat}} t} \right) + \frac{1}{2} c_A^{(1)} \frac{C_{AA}^{\text{dA}}(t)}{C_{AA}^{\text{stat}}(t)} \right] \right\} \quad (3.41)$$

## 3.6 The Generalized Eigenvalue Problem

The mass and the decay constant of the  $B$  meson are respectively given by eqs. (3.34), (3.41). They are expressed in terms of a single correlation function and valid at large time where the excited states contribution can be safely neglected. As discussed in Section 2.5, the GEVP can be used to reduce the contamination from excited states and improve the quality of the signal in simulations. In this section, I will give improved estimators for the quantities  $E_{\text{stat}}$ ,  $E_{\text{kin}}$ ,  $E_{\text{spin}}$ ,  $f_B^{\text{stat}}$ ,  $f_B^{\text{spin}}$  and  $f_B^{\text{kin}}$ . The actual choice of the interpolating operator basis will be discussed in the following section.

### 3.6.1 The $1/m$ expansion

We would like to combine the  $1/m$  expansion of HQET with the Generalized Eigenvalue Problem. The solution, proposed in ref. [42], is to treat  $1/m$  corrections as small perturbations

$$C(t) = C^{\text{stat}}(t) + \omega_{1/m} C^{1/m}(t), \quad (3.42)$$

where  $\omega_{1/m}$  is a short-notation for  $\omega_{\text{kin}}$  and  $\omega_{\text{spin}}$ . Similarly, the eigenvalues and eigenvector are decomposed into static and  $1/m$  corrections

$$\lambda_n(t, t_0) = \lambda_n^{\text{stat}}(t, t_0) + \omega_{1/m} \lambda_n^{1/m}(t, t_0), \quad (3.43)$$

$$v_n(t, t_0) = v_n^{\text{stat}}(t, t_0) + \omega_{1/m} v_n^{1/m}(t, t_0). \quad (3.44)$$

Inserting eqs. (3.42), (3.43) and (3.44) in the Generalized Eigenvalue Problem

$$C(t) v_n(t, t_0) = \lambda_n(t, t_0) C(t_0) v_n(t, t_0), \quad (3.45)$$

and considering only the lowest order, we obtain

$$C^{\text{stat}}(t) v_n^{\text{stat}}(t, t_0) = \lambda_n^{\text{stat}}(t, t_0) C^{\text{stat}}(t_0) v_n^{\text{stat}}(t, t_0). \quad (3.46)$$

The solutions of this equation are the static eigenvalues  $\lambda_n^{\text{stat}}(t, t_0)$  and eigenvectors  $v_n^{\text{stat}}(t, t_0)$  which are chosen to be normalized such that  $(v_n^{\text{stat}}(t, t_0), C^{\text{stat}}(t) v_n^{\text{stat}}(t, t_0)) = \delta_{nm}$ . Then, since  $1/m$  corrections are treated in the framework of perturbation theory,

they can be expressed in terms of the static solutions. At first order, the solutions of eq. (3.45) read

$$\frac{\lambda_n^{1/m}(t, t_0)}{\lambda_n^{\text{stat}}(t, t_0)} = (v_n^{\text{stat}}(t, t_0), [C^{1/m}(t)/\lambda_n^{\text{stat}}(t, t_0) - C^{1/m}(t_0)] v_n^{\text{stat}}(t, t_0)) , \quad (3.47)$$

$$v^{1/m}(t, t_0) = \sum_{k=1, k \neq n}^N \frac{(v_k^{\text{stat}}, [C^{1/m}(t) - \lambda_n^{\text{stat}}(t, t_0)C^{1/m}(t_0)] v_n^{\text{stat}})}{\lambda_n^{\text{stat}}(t, t_0) - \lambda_k^{\text{stat}}(t, t_0)} v_k^{\text{stat}}(t, t_0) . \quad (3.48)$$

This formula can now be used to obtain the expressions of  $E^{\text{stat}}$ ,  $E^{\text{kin}}$ ,  $E^{\text{spin}}$ ,  $f_B^{\text{stat}}$ ,  $f_B^{\text{spin}}$  and  $f_B^{\text{kin}}$  in terms of the eigenvalues and eigenvectors.

### 3.6.2 Expression of the mass

Using the results of Section 2.5, the mass of the  $n^{\text{th}}$  state can be extracted by considering the large time behavior of the following effective energy

$$E_n^{\text{eff}}(t, t_0) = a^{-1} \log \frac{\lambda_n(t, t_0)}{\lambda_n(t+1, t_0)} = E_n + \mathcal{O}(e^{-\Delta E_{N+1, n} t}) , \quad (3.49)$$

up to small corrections when the condition  $t_0 > t/2$  is satisfied. Expanding this equation in  $\omega^{1/m}$  and using the eigenvalue decomposition (3.43) we arrive at

$$E_n^{\text{eff}}(t, t_0) = E_n^{\text{eff,stat}}(t, t_0) + \omega^{1/m} E_n^{\text{eff,1/m}}(t, t_0) , \quad (3.50)$$

with

$$E_n^{\text{eff,stat}} = a^{-1} \log \frac{\lambda_n^{\text{stat}}(t, t_0)}{\lambda_n^{\text{stat}}(t+1, t_0)} = E_n^{\text{stat}} + \mathcal{O}(e^{-\Delta E_{N+1, n}^{\text{stat}} t}) , \quad (3.51)$$

$$E_n^{\text{eff,1/m}} = \frac{\lambda_n^{1/m}(t, t_0)}{\lambda_n^{\text{stat}}(t, t_0)} - \frac{\lambda_n^{1/m}(t+1, t_0)}{\lambda_n^{\text{stat}}(t+1, t_0)} = E_n^{1/m} + \mathcal{O}(t \Delta E_{N+1, n}^{1/m} e^{-\Delta E_{N+1, n}^{\text{stat}} t}) , \quad (3.52)$$

where  $1/m$  stands for kin or spin and where the  $1/m$  corrections for the eigenvalues are given by eq. (3.47) and are expressed in terms of the static quantities according to eq. (3.47). These improved estimators for  $E_n^{\text{eff,stat}}$  and  $E_n^{\text{eff,1/m}}$  can be used to compute the mass of the  $B$  meson through

$$m_B = m_{\text{bare}} + E^{\text{stat}} + \omega_{\text{kin}} E^{\text{kin}} + \omega_{\text{spin}} E^{\text{spin}} , \quad (3.53)$$

or, in the static limit

$$m_B^{\text{stat}} = m_{\text{bare}}^{\text{stat}} + E^{\text{stat}} . \quad (3.54)$$

### 3.6.3 Expression of the decay constant

In QCD, using the Generalized Eigenvalue Problem, the (generalized) decay constant is given by

$$f_B^{(n)} \sqrt{\frac{m_{B_n}}{2}} = Z_A^{\text{HQET}} (1 + b_A^{\text{stat}} m_q) \times p_n ,$$

where  $m_{B_n}$  is the mass of the  $n^{\text{th}}$  state and  $p_n$  is extracted from the effective matrix element (see eq. (2.32))

$$p_n^{\text{eff}}(t, t_0) = R_n(t, t_0) \times (v_n(t, t_0), C_L(t)) \xrightarrow[t \rightarrow +\infty]{} \langle 0 | \hat{A}_0 | B_n \rangle , \quad (3.55)$$

where

$$(C_L(t))_i = \sum_{x,\vec{y}} \langle A_0^{\text{stat}}(x_0 + t, \vec{y}) O_i^*(x) \rangle_{\text{stat}}. \quad (3.56)$$

In the effective theory, following the same path of reasoning and using the same notions as in Section 2.5, the  $1/m$  expansion reads

$$p_n^{\text{eff}}(t, t_0) = p_n^{\text{eff,stat}}(t, t_0) \left( 1 + \omega^{1/m} p_n^{\text{eff,1/m}}(t, t_0) + c_A^{(1)} p_n^{\text{eff,dA}}(t, t_0) \right), \quad (3.57)$$

where the last term comes from the  $\mathcal{O}(a)$  improvement of the axial current and where the matrix elements  $p_n^{\text{eff,stat}}$ ,  $p_n^{\text{eff,dA}}$  and  $p_n^{\text{eff,1/m}}$  are expressed in terms of eigenvectors and eigenvalues:

$$p_n^{\text{eff,stat}} = R_n^{\text{stat}}(t, t_0) (v_n^{\text{stat}}(t, t_0), C_L^{\text{stat}}(t)), \quad (3.58)$$

$$p_n^{\text{eff,dA}} = R_n^{\text{stat}}(t, t_0) (v_n^{\text{stat}}(t, t_0), C_{\delta A}(t)), \quad (3.59)$$

$$p_n^{\text{eff,1/m}} = \frac{R_n^{1/m}(t, t_0)}{R_n^{\text{stat}}(t, t_0)} + \frac{(v_n^{\text{stat}}(t, t_0), C_L^{1/m}(t))}{(v_n^{\text{stat}}(t, t_0), C_L^{\text{stat}}(t))} + \frac{(v_n^{1/m}(t, t_0), C_L^{\text{stat}}(t))}{(v_n^{\text{stat}}(t, t_0), C_L^{\text{stat}}(t))}, \quad (3.60)$$

where, similarly to  $C_L(t)$ , the correlator  $C_{\delta A}(t)$  is given by

$$(C_{\delta A}(t))_i = \sum_{x,\vec{y}} \langle \delta A_0^{(1)}(x_0 + t, \vec{y}) O_i^*(x) \rangle_{\text{stat}}, \quad (3.61)$$

where  $\delta A_0^{(1)}$  is the improvement term discussed in Section 3.4.2, and

$$R_n^{\text{stat}} = (v_n^{\text{stat}}(t, t_0), C(t) v_n^{\text{stat}}(t, t_0))^{-1/2} \left( \frac{\lambda_n^{\text{stat}}(t_0 + a, t_0)}{\lambda_n^{\text{stat}}(t_0 + 2a, t_0)} \right)^{t/(2a)}$$

$$\frac{R_n^{1/m}}{R_n^{\text{stat}}} = -\frac{1}{2} \frac{(v_n^{\text{stat}}(t, t_0), C^{1/m}(t) v_n^{\text{stat}}(t, t_0))}{(v_n^{\text{stat}}(t, t_0), C^{\text{stat}}(t) v_n^{\text{stat}}(t, t_0))} + \frac{t}{2a} \left( \frac{\lambda_n^{1/m}(t_0 + a, t_0)}{\lambda_n^{\text{stat}}(t_0 + a, t_0)} - \frac{\lambda_n^{1/m}(t_0 + 2a, t_0)}{\lambda_n^{\text{stat}}(t_0 + 2a, t_0)} \right).$$

The asymptotic behavior of the matrix elements (3.58), (3.59) and (3.60) is known:

$$p_n^{\text{eff,stat}} = p_n^{\text{stat}} + \gamma_{n,N}^{\text{stat}} e^{-(E_{N+1}^{\text{stat}} - E_n^{\text{stat}})t_0}, \quad (3.62)$$

$$p_n^{\text{eff,dA}} = p_n^{\text{dA}} + \gamma_{n,N}^{\text{dA}} e^{-(E_{N+1}^{\text{stat}} - E_n^{\text{stat}})t_0}, \quad (3.63)$$

$$p_n^{\text{eff,1/m}} = p_n^{1/m} + \left[ \gamma_{n,N}^{1/m} - \frac{\gamma_{n,N}^{1/m}}{p_n^{\text{stat}}} t_0 (E_{N+1}^{1/m} - E_n^{1/m}) \right] e^{-(E_{N+1}^{\text{stat}} - E_n^{\text{stat}})t_0}, \quad (3.64)$$

where the condition  $t_0 > t/2$  is assumed. Therefore, the excited states contribution is exponentially suppressed by a factor  $\mathcal{O}(\exp(-(E_{N+1} - E_n)t_0))$ . Finally, to consistently truncate the expansion at order  $1/m$ , we rather compute the logarithm of the decay constant

$$\log \left( a^{3/2} f_B \sqrt{\frac{m_B}{2}} \right) = \log(Z_A^{\text{HQET}}) + b_A^{\text{stat}} m_q + \log(p^{\text{stat}}) + \omega_{\text{kin}} p^{\text{kin}} + \omega_{\text{spin}} p^{\text{spin}} + a c_A^{(1)} p^{\text{dA}} \quad (3.65)$$

or, in the static approximation

$$\log \left( a^{3/2} f_B^{\text{stat}} \sqrt{\frac{m_B}{2}} \right) = \log(Z_A^{\text{stat}}) + b_A^{\text{stat}} m_q + \log(p^{\text{stat}}) + a c_A^{\text{stat}} p^{\text{dA}}, \quad (3.66)$$

where, for simplicity, I use the notation  $p_1^X = p^X$  for the ground state matrix elements.

CLS	$\beta$	$a$ (fm)	$L/a$	$\kappa$	$\kappa_s$	$m_\pi$ (MeV)	$m_\pi L$	# cfigs	$\frac{\text{\#cfigs}}{\tau_{\text{exp}}}$
A4	5.2	0.0749(9)	32	0.13590	0.13528	386(5)	4.7	1012	122
A5			32	0.13594	0.13528	333(4)	4.0	1001	164
B6			48	0.13597	0.13524	283(4)	5.2	636	52
E5	5.3	0.0651(6)	32	0.13625	0.13578	441(4)	4.7	1000	120
F6			48	0.13635	0.13574	314(3)	5.0	500	30
F7			48	0.13638	0.13573	269(3)	4.3	602	36
G8			64	0.13642	×	194(2)	4.1	410	17
N5	5.5	0.0482(6)	48	0.13660	0.13626	444(4)	5.2	477	4.2
N6			48	0.13667	0.13625	341(3)	4.0	950	38
O7			64	0.13671	0.13624	269(2)	4.2	980	20

Table 3.2 – Details of the CLS ensembles used: bare coupling  $\beta = 6/g_0^2$ , lattice spacing  $a$ , spatial extent  $L$  in lattice units ( $T = 2L$ ), pion mass  $m_\pi$ ,  $m_\pi L$ , number of configurations employed, and number of configurations employed normalized in units of the exponential autocorrelation time  $\tau_{\text{exp}}$  as estimated in ref. [50]. Additionally, we specify the CLS label id and the Gaussian smearing parameters  $n_G$  used to build different interpolating fields as described in the text.

## 3.7 Simulation parameters

### 3.7.1 Lattice ensembles

Our measurements are carried out on a subset of the CLS (Coordinated Lattice Simulations) ensembles, which have been generated using either the DD-HMC [39, 38, 41, 37] or the MP-HMC [95] algorithm, using the Wilson plaquette action [18] and  $N_f = 2$  flavours of non-perturbatively  $\mathcal{O}(a)$  improved Wilson quarks [22, 96]. Parameters of the lattice simulations are collected in Table 3.2. In order to suppress finite-size effects, we consider only ensembles satisfying  $m_\pi L > 4.0$ . The light valence quark masses are equal to the sea quark mass, and the (quenched)  $b$ -quark is treated by HQET.

The value of the lattice spacing in physical units for each value of  $\beta = 5.2, 5.3, 5.5$  has been computed in references [97, 52] via the kaon decay constant  $f_K = 155$  MeV. The authors also computed the values of  $m_\pi$  and  $f_\pi$  which will enter the chiral extrapolations.

### 3.7.2 Interpolating operators

The basis of interpolating operators correspond to three different levels of gaussian smearing, as explained in Section 2.6.3, with a triply (spatially) APE smeared covariant Laplacian

$$\mathcal{O}_k(x_0) = \sum_{\vec{x}} \bar{\psi}_h(x) \gamma_0 \gamma_5 \psi_l^{(k)}(x) \quad , \quad \psi_l^{(k)}(x) = (1 + \kappa_G a^2 \Delta)^{n_k} \psi_l(x) \quad , \quad (3.67)$$

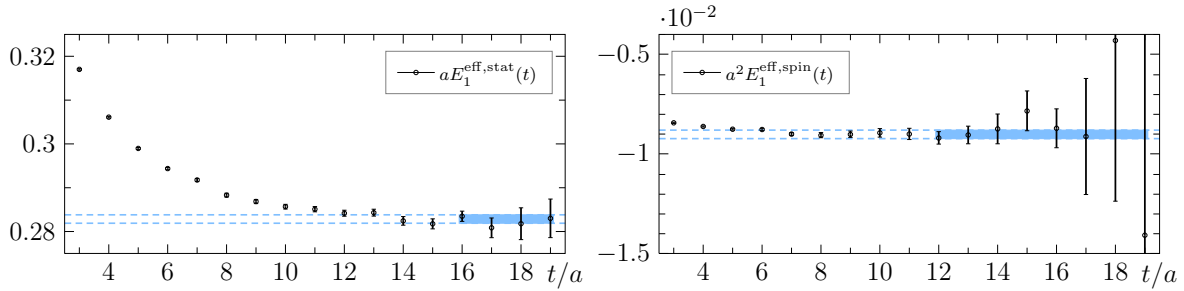


Figure 3.4 – Illustration of typical plateaus for the ground state static energy (left panel) and the  $\mathcal{O}(1/m_b)$  chromomagnetic energy (right); the CLS ensemble shown here is N6 ( $a = 0.048$  fm,  $m_\pi = 340$  MeV).

we choose  $\kappa_G = 0.1$  and the number of smearing iterations  $n_k$  has been chosen such that the physical radii of the wave functions are the same at each lattice spacing ( $r_i \approx 0.2, 0.3, 0.7$  fm):

$$\begin{aligned} \beta = 5.2 & : n_G \in \{15, 60, 155\}, \\ \beta = 5.3 & : n_G \in \{22, 90, 225\}, \\ \beta = 5.5 & : n_G \in \{33, 135, 338\}. \end{aligned}$$

### 3.7.3 Error estimation

To estimate the statistical error in a reliable way, we used the method described in Section 2.7 and took into account the contribution of the tails of the autocorrelation function, due to the coupling of our observables to the slow modes of the Markov chain. The value of  $\tau_{\text{exp}}$  has been computed via the topological charge and its values are summarized in Table 3.2. Finally, the propagation of these effects through the continuum-extrapolated result at the physical pion mass is carried out by iterating the formulae of Section 2.7 where all correlations are taken into account. In particular, the results of fits to the data are considered as functions  $f$  of the original data. Nevertheless, the weights in the fits are precomputed and then kept fixed such that  $f$  does not depend on the weights. Finally, whenever the contribution of the tails of the autocorrelation is small, I have checked that the errors are compatible with the jackknife analysis.

## 3.8 Determination of the RGI $b$ -quark mass $M_b$

As explained in the introduction, the strategy is to compute the mass of the  $B$ -meson for different values of the heavy quark mass, parametrized by  $z = L_1 M$ . The mass dependence is encoded in the HQET parameters through the matching with QCD. After extrapolating our result to the continuum and chiral limit, we can impose the constraint  $m_B(z = z_b) = m_B^{\text{phys}}$  to obtain the physical value of the heavy quark mass  $z_b = L_1 M_b$  where  $M_b$  is the renormalization group invariant (RGI)  $b$ -quark mass. As a final step, we will convert this result in the more familiar  $\overline{\text{MS}}$  scheme to obtain  $\overline{m}_b^{\overline{\text{MS}}}(\overline{m}_b^{\overline{\text{MS}}})$ .

The first step is to compute the HQET matrix elements  $E^{\text{stat}}$ ,  $E^{\text{kin}}$  and  $E^{\text{spin}}$  from the Generalized Eigenvalue Problem using eqs. (3.51), (3.52). In these formulae, we choose

the convention  $t_0 = t - 1$  to have a good control over excited states. In extracting our estimates for the ground state energies  $E_1^{\text{stat, kin, spin}}$  from the GEVP, the time intervals  $[t_{\min}, t_{\max}]$  over which we fit the plateaus are chosen so as

$$r(t_{\min}) = \frac{|A(t_{\min}) - A(t_{\min} - \delta)|}{\sqrt{\sigma^2(t_{\min}) + \sigma^2(t_{\min} - \delta)}} \leq 3, \quad (3.68)$$

where  $A$  is the plateau average,  $\sigma$  is the statistical error,  $\delta = 2/(E_{N+1}^{\text{stat}} - E_1^{\text{stat}}) \sim 0.3$  fm, and  $t_{\max}$  is fixed to  $\sim 0.9$  fm. This will assure that our selection criterion  $\sigma_{\text{sys}} \leq \sigma/3$  is satisfied [98], where  $\sigma_{\text{sys}} \propto \exp[-(E_{N+1} - E_1)t_{\min}]$ . An illustration of two typical plateaus of  $E_1^{\text{stat}}$  and  $E_1^{\text{spin}}$  is shown in Figure 3.4.

Then, using eq. (3.53), we compute the  $B$ -meson mass for each ensemble, each heavy quark mass  $z$  and each lattice discretizations HYP1 and HYP2. Then, using the NLO formula from HMchPT [99] and the fact that the action and the correlation functions are  $\mathcal{O}(a)$  improved, we use the following chiral and continuum extrapolation formula

$$m_{B,\delta}(z, y, a) = B(z) + C(y - y^{\text{exp}}) - \frac{3\hat{g}^2}{16\pi} \left( \frac{m_\pi^3}{f_\pi^2} - \frac{(m_\pi^{\text{exp}})^3}{(f_\pi^{\text{exp}})^2} \right) + D_\delta a^2, \quad (3.69)$$

where  $y = m_\pi^2/(8\pi^2 f_\pi^2)$ ,  $\hat{g} = 0.489(32)$  is the  $B^*B\pi$  coupling recently determined in ref. [100] and  $f_\pi^{\text{exp}} = 130.4$  MeV is the pion decay constant. The subscript  $\delta$  corresponds to the lattice discretization of the heavy quark:  $\delta = 1$  for HYP1 and  $\delta = 2$  for HYP2. Finally, the previous formula can be recast in the more convenient form

$$m_{B,\delta}^{\text{sub}}(z, y, a) = m_{B,\delta}(z, y, a) + \frac{3\hat{g}^2}{16\pi} \left( \frac{m_\pi^3}{f_\pi^2} - \frac{(m_\pi^{\text{exp}})^3}{(f_\pi^{\text{exp}})^2} \right) = B(z) + C(y - y^{\text{exp}}) + D_\delta a^2. \quad (3.70)$$

The results are shown in Figure 3.5. From the right plot, we conclude that the  $B$  meson mass depends almost linearly on  $z$  and the values of the fit parameter  $B(z)$ , for  $z$  around the physical  $b$ -quark mass, are summarized in Table 3.3.

Using a quadratic interpolation of  $m_B(z, m_\pi^{\text{exp}}, 0)$  we determine the value  $z_b$  by imposing the condition

$$m_B(z_b, m_\pi^{\text{exp}}, 0) = m_B^{\text{exp}}, \quad (3.71)$$

where  $m_B^{\text{exp}} = 5279.5$  MeV [2] is the physical mass. We obtain

$$z_b = 13.25(22)(13)_z, \quad (3.72)$$

where the first error includes the statistical error, the error coming from the HQET parameters and the error coming from the scale setting. The second error originates from the uncertainty in the parameters  $h(L_0) = M/\bar{m}^{\text{SF}}(L_0)$  used to tune the heavy quark mass during the matching between QCD and HQET (see eq. (3.23)). In particular, this error introduces a systematic shift between the value of  $z$  and the RGI quark mass  $M$ . The associated error can be estimated using the relation

$$z_b = \left[ \frac{z_b}{h(L_0)} \right] \times h(L_0),$$

where  $[\cdot]$  has to be taken at its central value and  $h(L_0) = 1.521(14)$  [68]. Finally, the RGI quark mass is given by

$$M_b = z_b \times \frac{f_K}{[L_1 f_K]}, \quad (3.73)$$

id	$y$	$z = 11$		$z = 13$		$z = 15$	
		HYP1	HYP2	HYP1	HYP2	HYP1	HYP2
A4	0.0771(14)	4434(62)	4454(62)	5024(70)	5042(70)	5597(78)	5613(78)
A5	0.0624(13)	4419(62)	4440(62)	5010(70)	5028(70)	5583(78)	5600(78)
B6	0.0484(9)	4398(62)	4420(62)	4988(70)	5008(70)	5562(78)	5579(78)
E5	0.0926(15)	4474(59)	4492(59)	5069(66)	5084(66)	5646(73)	5661(73)
F6	0.0562(9)	4436(59)	4452(58)	5031(66)	5046(66)	5609(73)	5622(73)
F7	0.0449(7)	4431(58)	4444(58)	5026(65)	5037(65)	5603(73)	5613(73)
G8	0.0260(5)	4415(59)	4434(59)	5010(66)	5027(66)	5589(73)	5603(73)
N5	0.0940(24)	4586(57)	4594(57)	5193(64)	5200(63)	5783(71)	5789(70)
N6	0.0662(10)	4563(57)	4568(56)	5169(63)	5174(63)	5759(70)	5763(70)
O7	0.0447(7)	4539(56)	4555(56)	5147(63)	5161(63)	5737(69)	5750(70)
$B(z)$		4610(57)		5207(63)		5787(69)	

Table 3.3 – Raw data of  $m_{B,\delta}(z, m_\pi, a)$  in MeV for all ensembles (id),  $z$  and HYP actions considered in this work. In the last row we report  $B(z) \equiv m_{B,\delta}^{\text{sub}}(z, m_\pi^{\text{exp}}, 0)$  for the  $z$  that were used in the quadratic interpolation to fix  $z_b$  using eq. (3.71).

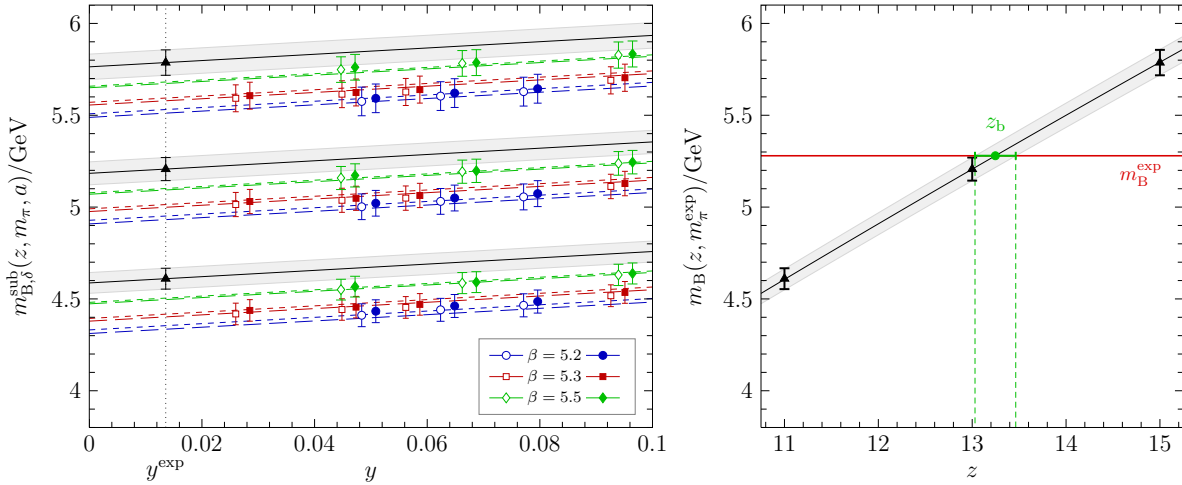


Figure 3.5 – (Left) Chiral and continuum extrapolation of  $m_{B,\delta}^{\text{sub}}(z, y, a)$  for the  $z$  used in the determination of  $z_b$ . Open/filled symbols refer to HYP1/HYP2 data points as do long/short dashed curves, respectively. (Right) Interpolation to  $z_b$  by imposing eq. (3.71).

where  $f_K = 155$  MeV is the physical value of the kaon decay constant. The quantity  $L_1 f_K$  has been computed in ref. [52] and their result reads

$$L_1 f_K = \lim_{a \rightarrow 0} [L_1/a] [a f_K] = 0.312(8), \quad (3.74)$$

so that

$$M_b = 6.58(16)(6)_z \text{ GeV}. \quad (3.75)$$

This is our results for the renormalization group invariant (RGI) mass of the  $b$ -quark with two dynamical quarks. In the next section, I will convert this result into the  $\overline{\text{MS}}$  scheme.

### Discretization effects

To extrapolate our result to the continuum (eq. (3.69)) we used a fit quadratic in the lattice spacing. This is because the theory is  $\mathcal{O}(a)$  improved and lattice artifacts linear in  $a$  have been removed. Nevertheless, as explained in Section 3.2,  $\mathcal{O}(a/m_b)$  terms remain and have been neglected so far. Nevertheless, we have checked that adding a term  $F_\delta \cdot (a/m_b)$  to eq. (3.69) does not change significantly the results. In particular, the  $\chi^2$  does not change and the fitting parameter  $B(z)|_{z=13}$  changes to 5227(79) MeV leading to  $z_b = 13.18(27)(13)$ , in agreement with our previous value.

## 3.9 Conversion to the $\overline{\text{MS}}$ scheme

In this section, I convert the RGI quark mass of the previous section into the  $\overline{\text{MS}}$  scheme and start with a brief introduction of the Renormalization Group Invariant (RGI) mass and of the Lambda parameter which will be useful in the discussion. In QCD, the  $\beta$  and  $\tau$  functions describe respectively the running of the renormalized coupling constant  $\bar{g}$  and of the renormalized mass  $\bar{m}_b$  and are perfectly defined beyond perturbation theory. In this section, I work in the  $\overline{\text{MS}}$  scheme and the  $\beta$  and  $\tau$  functions are defined by the equations

$$\mu \frac{d\bar{g}}{d\mu} = \beta(\bar{g}) \quad , \quad \mu \frac{d\bar{m}_b}{d\mu} = \tau(\bar{g})\bar{m}_b . \quad (3.76)$$

In the perturbative regime, their expansions in the running coupling read

$$\beta(\bar{g}) = -b_0\bar{g}^3 - b_1\bar{g}^5 - b_2\bar{g}^7 - \dots \quad , \quad \tau(\bar{g}) = -d_0\bar{g}^2 - d_1\bar{g}^4 - \dots ,$$

where the parameters  $b_0$ ,  $b_1$  and  $d_0$  are scheme independent (for mass independent schemes [10]) but depend on the number of active quarks,  $N_f$ . These functions are known up to 4-loop in perturbation theory [101, 102] and their values are summarized in Appendix D. The  $\Lambda$  and  $M_b$  parameters are defined via the equations

$$\Lambda = \mu (b_0\bar{g}^2(\mu))^{-b_1/2b_0^2} \exp\left(-\frac{1}{2b_0\bar{g}^2(\mu)}\right) \times \exp\left\{-\int_0^{\bar{g}(\mu)} dx \left[\frac{1}{\beta(x)} + \frac{1}{b_0x^3} - \frac{b_1}{b_0^2x}\right]\right\} , \quad (3.77)$$

$$M_b = \bar{m}_b(\mu) (2b_0\bar{g}^2(\mu))^{-d_0/2b_0} \times \exp\left\{-\int_0^{\bar{g}(\mu)} dx \left[\frac{\tau(x)}{\beta(x)} - \frac{d_0}{b_0x}\right]\right\} , \quad (3.78)$$

and have the particularity to be renormalization group invariant (RGI). It means that they are scale independent and satisfy the renormalization group equation

$$\frac{dP}{d\mu} = 0 \Leftrightarrow \left(\mu \frac{\partial}{\partial \mu} + \beta(\bar{g}) \frac{\partial}{\partial \bar{g}} + \tau(\bar{g})\bar{m} \frac{\partial}{\partial \bar{m}}\right) P(\bar{g}(\mu), \bar{m}(\mu), \mu) = 0 , \quad (3.79)$$

where  $P = M_b, \Lambda$ . The mass  $M_b$  is also scheme independent, contrary to  $\Lambda$  which differs in the  $\overline{\text{MS}}$  and in the Schrödinger Functional scheme. Nevertheless, the relation between different schemes is exactly determined by a one-loop computation (Appendix D).

**Determination of  $\overline{m}_b^{\overline{\text{MS}}}(\overline{m}_b^{\overline{\text{MS}}})$** 

Taking the ratio of eqs. (3.77), (3.78), we obtain :

$$\frac{M_b}{\Lambda_{\overline{\text{MS}}}} = \frac{\overline{m}(\mu)}{\mu} f(\overline{g}(\mu)), \quad (3.80)$$

where  $f$  is a function of the renormalized coupling  $\overline{g}$  only. Choosing the renormalization scale  $\mu = \mu^*$  where  $\mu^*$  is defined via the relation  $m(\mu^*) = \mu^*$ , the previous eq. (3.80) implicitly defines  $g^* = g(\mu^*)$  via

$$f(g^*) = \frac{M_b}{\Lambda_{\overline{\text{MS}}}}.$$

Then, eq. (3.78) can be used to write

$$\overline{m}_b^{\overline{\text{MS}}}(\overline{m}_b^{\overline{\text{MS}}}) = M_b \times \rho \left( r_b = \frac{M_b}{\Lambda_{\overline{\text{MS}}}} \right), \quad (3.81)$$

where  $\rho$  is given by

$$\rho(y) = (2b_0 g^{*2})^{d_0/2b_0} \times \exp \left\{ \int_0^{g^*} dx \left[ \frac{\tau(x)}{\beta(x)} - \frac{d_0}{b_0 x} \right] \right\},$$

and  $g^*$  is implicitly given by  $y = f(g^*)$ . I have computed the function  $\rho$  numerically at 4-loops with  $N_f = 2$  active quarks: a very good approximation (with a relative error smaller than  $10^{-4}$ ) is given by

$$\rho(y) = 0.6400 - 0.00426 \times (y - 21) + 0.00015 \times (y - 21)^2, \quad y \in [20, 22].$$

The  $\Lambda$  parameter in eq. (3.81) has been computed non-perturbatively by the ALPHA collaboration for  $N_f = 2$  dynamical quarks in the Schrödinger functional scheme [52] and the result reads  $L_1 \Lambda_{\text{SF}} = 0.264(15)$  where the length scale  $L_1$  originates from the non-perturbative finite-volume matching used for the matching of the HQET parameters. Therefore,  $M_b$  and  $r_b$  are computed according to

$$M_b = \frac{z_b f_K}{[L_1 f_K]}, \quad r_b = \frac{z_b}{[L_1 \Lambda_{\text{SF}}]} \times \frac{\Lambda_{\text{SF}}}{\Lambda_{\overline{\text{MS}}}},$$

where the ratio between  $\Lambda_{\text{SF}}$  and  $\Lambda_{\overline{\text{MS}}}$  used to convert the results in the  $\overline{\text{MS}}$  scheme is known and given in Appendix D. Finally, I obtain

$$\overline{m}_b^{\overline{\text{MS}}}(\overline{m}_b^{\overline{\text{MS}}}) = 4.212(96)(26) \text{ GeV}, \quad (3.82)$$

where, as before, the first error is statistical and the second error comes from the uncertainties associated with the non-perturbative running of the quark mass (via  $M_b$ ) and of the coupling constant (via  $L_1 \Lambda_{\text{SF}}$ ) in the Schrödinger functional scheme. I now explain how this second error is estimated. The uncertainties associated with  $L_1 \Lambda_{\text{SF}}$  and  $M_b$  are encoded in the dimensionless functions  $k(L_0)$  and  $h(L_0)$  defined by

$$k(L_0) = 2 \cdot [\Lambda_{\text{SF}} L_1] \cdot \frac{\Lambda_{\overline{\text{MS}}}}{\Lambda_{\text{SF}}}, \quad h(L_0) = M/\overline{m}^{\text{SF}}(L_0), \quad L_0 = L_1/2.$$

Since  $h(L_0)$  and  $k(L_0)$  have been computed using the same lattice ensembles, they are correlated and their covariance matrix is

$$\text{Cov}(h(L_0), k(L_0)) = \begin{pmatrix} 1.99 & -0.67 \\ -0.67 & 0.49 \end{pmatrix} 10^{-4}.$$

Therefore, to take the correlations into account,  $r_b$  and  $M_b$  should be written in terms of  $h(L_0)$  and  $k(L_0)$ :

$$M_b = [\overline{m}_b^{\text{SF}}] \times h(L_0) \quad , \quad r_b = \frac{M_b}{\Lambda_{\overline{\text{MS}}}} = [L_0 \overline{m}_{\text{SF}}] \times \frac{h(L_0)}{k(L_0)},$$

where  $[ \cdot ]$  has to be taken at its central value. Finally, the uncertainty arising from the perturbative running in the  $\overline{\text{MS}}$  scheme is negligible: adding the recently computed 5-loop term in the mass anomalous dimension [103] does not change the numbers at the one per mille level.

### Determination of $\overline{m}_b(\mu = 2 \text{ GeV})$ and $\overline{m}_b(\mu = 4 \text{ GeV})$

The evaluations of  $\overline{m}_b(\mu)$  with some fixed  $\mu$  are performed analogously. From eqs. (3.77), (3.78) we can write

$$\overline{m}(\mu) = M_b \times F[\overline{g}(\mu)] = M_b \times \rho_\mu \left( u_b = \frac{\mu}{\Lambda_{\overline{\text{MS}}}} \right),$$

where the function  $\rho_\mu$ , which depends on the scale  $\mu$ , is computed numerically at 4-loops with  $N_f = 2$ . I obtain

$$\rho_{2\text{GeV}}(y) = 1.12072 - 0.090008 \times y + 0.00479475 \times y^2 \quad , \quad y \in [5.5 - 7],$$

$$\rho_{4\text{GeV}}(y) = 0.845697 - 0.0229766 \times y + 0.000570605 \times y^2 \quad , \quad y \in [11.5 - 13.5],$$

with a relative error smaller than  $10^{-4}$ . Finally, we found

$$\overline{m}_b(4 \text{ GeV}) = 4.25(12) \text{ GeV}, \quad (3.83)$$

$$\overline{m}_b(2 \text{ GeV}) = 4.88(14) \text{ GeV}. \quad (3.84)$$

As before, to evaluate the error coming from the non-perturbative running, I express  $u_b$  and  $M_b$  in terms of the correlated variables  $h(L_0)$  and  $k(L_0)$ :

$$u_b = \frac{\mu}{\Lambda_{\overline{\text{MS}}}} = \frac{[L_0 \mu]}{k(L_0)} \quad , \quad M_b = \left[ \frac{M_b}{h(L_0)} \right] \times h(L_0),$$

where  $[ \cdot ]$  numbers have to be evaluated at their central values.

### 3.9.1 Discussion

Our result  $M_b = 6.58(16)(6)_z \text{ GeV}$ , or  $\overline{m}_b^{\overline{\text{MS}}}(\overline{m}_b^{\overline{\text{MS}}}) = 4.21(17) \text{ GeV}$ , is in agreement with the value obtained by the ETM Collaboration in ref. [64]:  $\overline{m}_b^{\overline{\text{MS}}}(\overline{m}_b^{\overline{\text{MS}}}) = 4.29(12) \text{ GeV}$ . They also used two dynamical quarks ( $N_f = 2$ ), but a completely different approach to treat the heavy quark. Our result is also compatible with the value cited in the PDG [2]. Finally, I discuss the error budget on  $z_b$ : 60% of the total error comes from the HQET parameters and 20% comes from the relativistic  $Z_A$  needed in the scale setting via the kaon decay constant and only 17% comes from the hadronic matrix elements computed in HQET.

$N_f$	Ref.	$M_b$	$\Lambda_{\overline{\text{MS}}}^{(N_f)}$ (MeV)	$\overline{m}_b^{\overline{\text{MS}}}(\overline{m}_b^{\overline{\text{MS}}})$	$\overline{m}_b(4 \text{ GeV})$	$\overline{m}_b(2 \text{ GeV})$
0	[87]	6.76(9)	238(19)	4.35(5)	4.39(6)	4.87(8)
2	This work [1]	6.58(17)	314(19)	4.21(11)	4.25(12)	4.88(14)
5	PDG [2]	7.50(8)	212(8)	4.18(3)	4.215(36)	4.912(45)

Table 3.4 – Masses of the  $b$ -quark in GeV in theories with different quark flavour numbers  $N_f$  and for different schemes/scales as well as  $\Lambda_{\overline{\text{MS}}}$  and the RGI mass  $M$ .

### Running of the quark mass

The mass of the  $b$ -quark computed in this work corresponds to the mass in the theory with two dynamical quarks ( $u$  and  $d$ ), assumed to be degenerate, and one heavy quenched quark ( $b$ ). Therefore, the running of the previous section in the  $\overline{\text{MS}}$  scheme is always performed with  $N_f = 2$  active quarks. In particular, the value of the  $\Lambda$  parameter [52] used in eq. (3.77), and the heavy quark mass renormalization [91] in the QCD side of the matching (see eq. (3.23)), correspond to the same theory with  $N_f = 2$ .

Of course, this effective theory is only an approximation of the full theory where all quarks are dynamical. Therefore, as explained in Section 2.8, there is an ambiguity in the scale setting since the contribution of heavier quarks (not taken into account in the sea) can be different depending on the quantity used to set the scale. In particular, different choices of observables can lead to slightly different results. In this work, because the matching with experiment is done at low energy (the scale is set via the kaon decay constant [52] and the mass of the  $B$  meson in physical units depends on this scale) the approximation of QCD by the effective theory is expected to be better at these energies. The results in Table 3.4 are in agreement with this statement. At all scales  $\mu$  between 2 GeV and  $\mu = m_b$ , the mass of the  $b$ -quark is weakly dependent on  $N_f$  and this dependence is no longer detectable at the lowest scale 2 GeV. Below this scale, the validity of the perturbative running is questionable and we did not performed it.

On the other hand, the pair  $(M_b, \Lambda)$  depends significantly on  $N_f$ . The parameters  $M_b$  and  $\Lambda$  are integration constants for the renormalization group equations (3.76). Since the perturbative coefficients of the  $\beta$  and  $\tau$  functions depend on  $N_f$ , the quantities  $M_b$  and  $\Lambda$  also inevitably depend on  $N_f$ . In the  $\overline{\text{MS}}$  scheme,  $M_b$  and  $\Lambda$  also depend on the number of active quarks: when the renormalization scale passes through a quark mass, matching conditions have to be taken into account in the running given by equations 3.76.

### Comparison with the static limit

We have performed the same analysis in the static limit. Again, it is important to notice that the HQET parameters are different at the static and  $1/m$  orders since they corresponds to independent matching. In particular, the continuum limit of the combination  $\omega_{\text{kin}} E^{\text{kin}} + \omega_{\text{spin}} E^{\text{spin}}$  does not exist and the divergent contribution is absorbed in the coefficient  $m_{\text{bare}}$  so that  $m_{\text{bare}} \neq m_{\text{bare}}^{\text{stat}}$ . Our results are

$$z_b^{\text{stat}} = 13.24(21)(13)_z \quad , \quad M_b^{\text{stat}} = 6.57(17) \text{ GeV} \quad , \quad (3.85)$$

which give, after conversion into the  $\overline{\text{MS}}$  scheme:

$$\left[ \overline{m_b^{\text{MS}}}(\overline{m_b^{\text{MS}}}) \right]^{\text{stat}} = 4.21(11) \text{ GeV} . \quad (3.86)$$

We conclude that the result obtained in the static limit is very similar and that the  $1/m_b$  expansion is very precise in this case. Then, we expect that  $1/m_b^2$  corrections are very small compared to the present accuracy. Finally, it should be noticed that the difference between static and  $1/m_b$  orders is known precisely: we have computed

$$z_b^{1/m} = z_b - z_b^{\text{stat}} = -0.008(51) . \quad (3.87)$$

## 3.10 Computation of the $\mathbf{B}$ meson decay constants $\mathbf{f_B}$ and $\mathbf{f_{B_s}}$

In this section, I present the results on the computation of the  $B$  meson decay constant  $f_B$  with two dynamical quarks at static and first order in HQET. We have also computed the strange  $B$  meson decay constant  $f_{B_s}$  and the ratio  $f_{B_s}/f_B$ . The later has the advantage to eliminate many systematic errors like the conversion in physical unit or the renormalization factor of the axial current.

### 3.10.1 Interpolation of the HQET parameters

The HQET parameters have been computed at different values of the heavy quark mass, parametrized by the parameter  $z$ , and the physical value  $z_b$  was determined in the previous section by imposing the mass of the heavy-light  $B$  meson to coincide with its experimental value. Therefore, the HQET parameters can be interpolated at the physical  $b$ -quark mass  $z_b = z_b^{\text{phys}}$  and used to make predictions. Since the mass dependence of the HQET parameters is rather smooth, and since  $z_b$  is close to the point  $z = 13$ , we choose a quadratic polynomial in the range  $z = 11 - 15$ . The results are given in Table 3.5 and some typical examples of interpolations are depicted in Figure 3.6.

### 3.10.2 Matrix elements

For the computation of the strange  $B_s$  meson decay constant  $f_{B_s}$ , the hopping parameter  $\kappa_s$  for the strange quark has been determined in ref. [52]. The values of  $\kappa_s$  for each ensemble are summarized in Table 3.2.

The matrix elements given by eqs. (3.58), (3.59) and (3.60) are computed using the results of the Generalized Eigenvalue Problem with the convention  $t_0 = t - 1$ . Similarly to the previous section, the plateaus are chosen such that  $r(t_{\min}) \leq 3$  where  $r$  is defined in eq. (3.68). Some typical plateaus are given in Figure 3.7. The error analysis is performed using the Gamma-procedure discussed in Section 2.7.

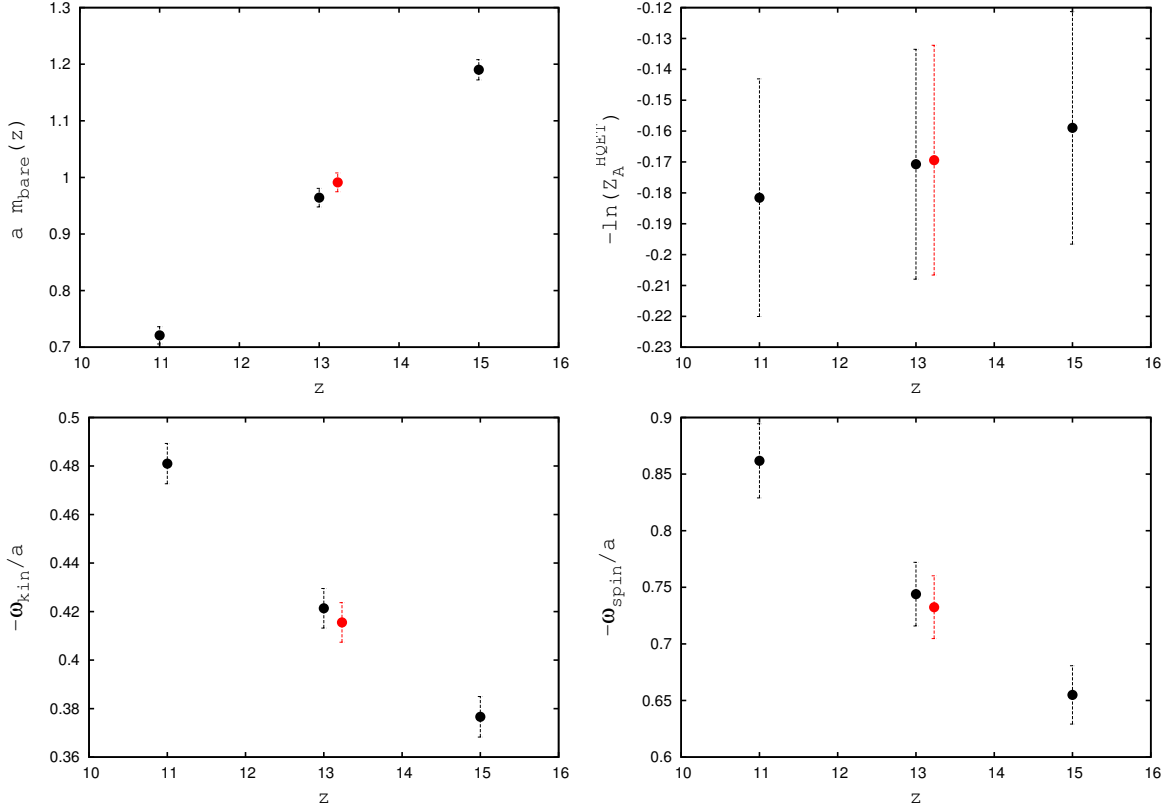


Figure 3.6 – Interpolation of the HQET parameters at the physical  $b$ -quark mass  $z_b^{\text{phys}} = 13.24(25)$  for the HYP1 action at  $\beta = 5.3$ . From the upper left side to the lower right side:  $\omega_1 = am_{\text{bare}}$ ,  $\omega_2 = -\ln(Z_A^{\text{stat}})$ ,  $\omega_4 = \omega_{\text{kin}}/a$  and  $\omega_5 = \omega_{\text{spin}}/a$ .

	$\beta = 5.5$		$\beta = 5.3$		$\beta = 5.2$	
	HYP1	HYP2	HYP1	HYP2	HYP1	HYP2
$am_{\text{bare}}^{\text{stat}}$	0.969(10)	1.000(10)	1.317(13)	1.350(13)	1.520(15)	1.554(15)
$-\ln(Z_A^{\text{stat}})$	0.271(5)	0.181(5)	0.283(5)	0.177(5)	0.291(6)	0.177(6)
$am_{\text{bare}}$	0.594(16)	0.606(16)	0.993(18)	1.014(18)	1.214(19)	1.239(19)
$-\ln(Z_A^{\text{HQET}})$	0.156(42)	0.163(36)	0.169(37)	0.146(32)	0.169(35)	0.136(31)
$-c_A^{\text{HQET}}/a$	0.07(12)	0.67(12)	0.00(10)	0.55(10)	0.01(9)	0.54(9)
$\omega_{\text{kin}}/a$	0.520(13)	0.525(13)	0.415(10)	0.419(10)	0.378(9)	0.380(9)
$\omega_{\text{spin}}/a$	0.949(40)	1.090(46)	0.731(31)	0.883(37)	0.655(27)	0.812(33)

Table 3.5 – HQET parameters at the physical point  $\omega_i(z = z_b)$ . The parameters are given for  $z_b$  determined such that  $m_B = 5279.5$  MeV [1], which corresponds to  $z_b^{\text{stat}} = 13.24(25)$  at static order, and to  $z_b = 13.25(26)$  for HQET expanded to  $\mathcal{O}(1/m)$ . The bare coupling is  $g_0^2 = 6/\beta$ .

id	$y$	$f_B$ [MeV]		$f_{B_s}$ [MeV]		$f_{B_s}/f_B$	
		HYP1	HYP2	HYP1	HYP2	HYP1	HYP2
A4	0.0771(14)	212(9)	210(10)	227(8)	227(8)	1.071(28)	1.084(23)
A5	0.0624(13)	206(7)	204(7)	226(6)	224(6)	1.096(20)	1.100(19)
B6	0.0484(9)	198(8)	195(7)	224(8)	223(7)	1.127(36)	1.144(32)
E5	0.0926(15)	215(7)	213(8)	232(8)	231(9)	1.077(28)	1.086(25)
F6	0.0562(9)	203(8)	201(8)	228(7)	228(7)	1.120(48)	1.138(39)
F7	0.0449(7)	201(6)	200(6)	222(6)	223(7)	1.103(26)	1.119(24)
G8	0.0260(5)	190(8)	190(8)	–	–	–	–
N5	0.0940(24)	222(16)	221(15)	–	–	–	–
N6	0.0662(10)	205(14)	205(15)	229(15)	231(15)	1.115(50)	1.126(46)
O7	0.0447(7)	199(14)	194(14)	–	228(14)	–	1.178(85)
LO	$y^{\text{exp}}, a = 0$	188(12)		225(13)		1.184(60)	
NLO	$y^{\text{exp}}, a = 0$	186(12)		–		1.203(61)	

Table 3.6 – Raw data for  $f_B$ ,  $f_{B_s}$  and their ratio  $f_{B_s}/f_B$ , using HQET parameters at the physical point  $\omega_i(z = z_b)$ , with  $z_b = 13.25$  as determined in ref. [1]. The last two rows summarize our results of a combined chiral and continuum extrapolation using either the LO or the NLO fit ansatz (3.88) for each individual observable.

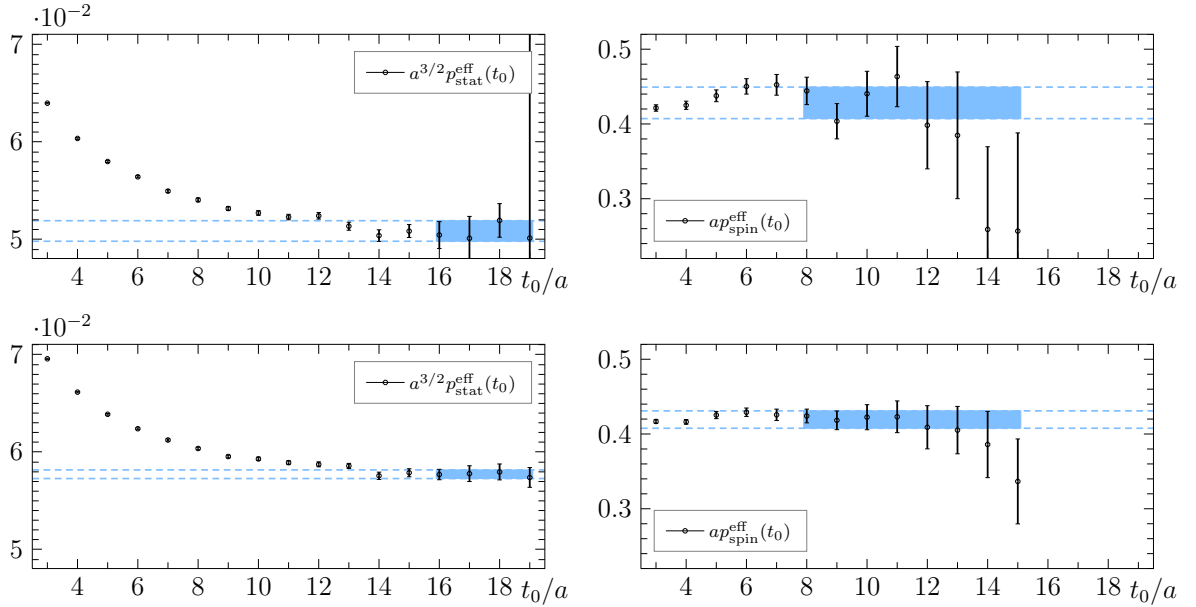


Figure 3.7 – Typical plateau averages after applying the GEVP analysis to data obtained on the  $N_f = 2$  CLS ensemble N6 ( $a = 0.048$  fm,  $m_\pi = 340$  MeV). The two plots on top correspond to the  $B$ -meson matrix elements  $p_{\text{stat}}^{\text{eff}}$  (left) and  $p_{\text{spin}}^{\text{eff}}$  (right) and the two lower plots correspond to the  $B_s$ -meson matrix elements  $p_{\text{stat}}^{\text{eff}}$  (left) and  $p_{\text{spin}}^{\text{eff}}$  (right)

### 3.10.3 Continuum extrapolation

The decay constant can be computed using the previous matrix elements and the interpolated HQET parameters according to eq. (3.65). The results for each CLS ensem-

ble and each heavy quark action are summarized in Table 3.6 and Table 3.7. Finally, to perform the continuum and chiral extrapolation, we used formulae from Heavy Meson Chiral Perturbation Theory (HM $\chi$ PT)

$$\begin{aligned} f_B^\delta(y, a) \sqrt{\frac{m_B}{2}} &= A \left[ 1 - \frac{3}{4} \frac{1 + 3\hat{g}^2}{2} (y \log(y) - y^{\text{exp}} \log(y^{\text{exp}})) \right] + C (y - y^{\text{exp}}) + D^\delta a^2, \\ f_{B_s}^\delta(y, a) \sqrt{\frac{m_{B_s}}{2}} &= A_s + C_s (y - y^{\text{exp}}) + D_s^\delta a^2, \end{aligned} \quad (3.88)$$

where the parameter  $y$  is still defined by  $y = m_\pi^2/8\pi^2 f_\pi^2$  and  $y^{\text{exp}}$  corresponds to the value of  $y$  at the physical point  $f_\pi = 130.4$  MeV and  $m_\pi = 134.98$  MeV. The two actions HYP1 and HYP2 for the heavy quark, which correspond to different cutoff effects, are parametrized by  $\delta$ . Finally, the  $B_{(s)}$  meson masses are taken at their physical values  $m_B = 5279.5$  MeV and  $m_{B_s} = 5366.3$  MeV. We decided to treat  $f_{B_s}$  as a dependent observable, to be derived from the ratio  $f_{B_s}/f_B$ . Indeed, this ratio has reduced systematic errors. In particular, the error on the lattice spacing, which enters via the factor  $a^{3/2}$  in eq. (3.41) cancels similarly to the axial current renormalization factor  $Z_A^{\text{HQET}}$ . Our final results read

$$f_B = 186(13)(2)_\chi \text{ MeV} \quad , \quad f_{B_s}/f_B = 1.203(62)(19)_\chi .$$

where the first error is statistical and include the error on the lattice spacing and the uncertainty from the HQET parameters. The second systematic error accounts for the discrepancy between the NLO HM $\chi$ PT fit ansatz and the LO fit ansatz where logarithms are neglected. The NLO extrapolation is shown in Figure 3.8 where the result of the LO extrapolation is also plotted. Finally, the strange  $B$ -meson decay constant  $f_{B_s}$  becomes

$$f_{B_s} = 224(14)(2)_\chi \text{ MeV} .$$

Similarly to the case of the  $b$ -quark mass, we also tried a continuum extrapolation with a term linear in the lattice spacing. Indeed, at first order in the HQET expansion, discretization effects proportional to  $\mathcal{O}(a/m_h)$  still remain. We do not observe any significant change within our error.

### 3.10.4 Discussion

In order to have an estimate of the  $\mathcal{O}(1/m_h)$  corrections, we perform the analysis at static order in HQET. We use the same fit formulae as in equations (3.88), but the decay constants are now computed using the static HQET parameters. The results are summarized in Table 3.7 and we obtain

$$f_B^{\text{stat}} = 190(5)(2)_\chi \text{ MeV} \quad , \quad f_{B_s}^{\text{stat}}/f_B^{\text{stat}} = 1.189(24)(30)_\chi \quad , \quad f_{B_s}^{\text{stat}} = 226(6)(9)_\chi \text{ MeV} .$$

Therefore, as for the  $b$ -quark mass, first order corrections are small and the  $1/m_h$  expansion is expected to be accurate. We can also compare our results with the previous estimation of  $f_{B_s}$  by the ALPHA Collaboration in the quenched approximation [104]. The scale  $r_0$  [105] was employed to convert the result in physical units and their result, for two values of  $r_0$ , read

$$f_{B_s}^{N_f=0} = 216(5) \text{ MeV} \quad (r_0 = 0.5 \text{ fm}) \quad , \quad f_{B_s}^{N_f=0} = 252(7) \text{ MeV} \quad (r_0 = 0.45 \text{ fm}) .$$

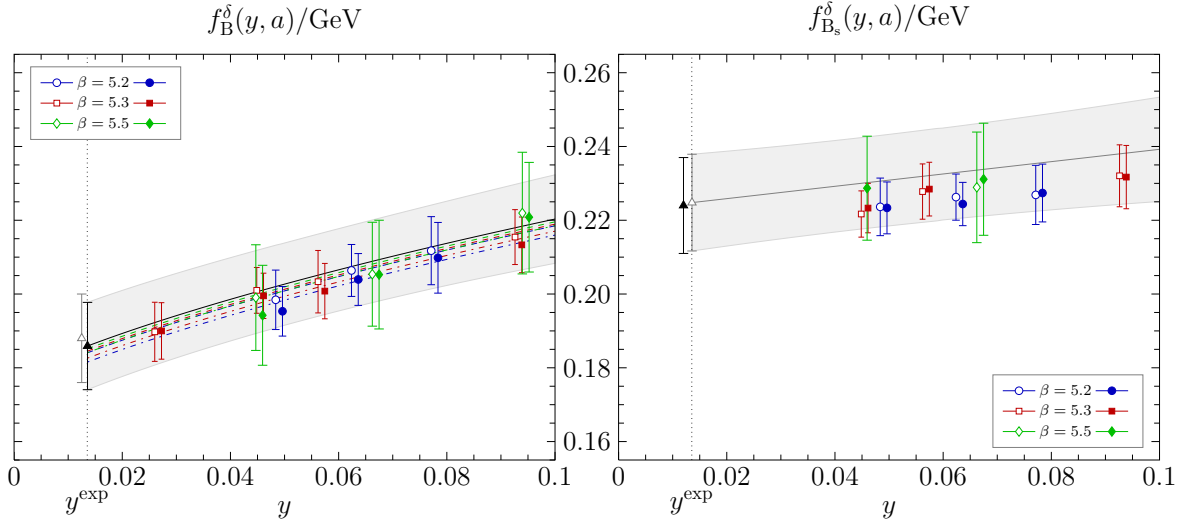


Figure 3.8 – Extrapolation of the  $B$  (left panel) and  $B_s$  (right panel) meson decay constant to the physical point. On the left, the extrapolation using  $\text{HM}\chi\text{PT}$  at NLO (filled triangle) is compared to a linear one (open triangle), in order to extract the systematic error from truncating  $\text{HM}\chi\text{PT}$  at NLO. For  $f_{B_s}$  only a LO formula is known and shown. As a comparison we also add our final result, the continuum value of  $f_{B_s} = [f_{B_s}/f_B]f_B$ . All data points are listed in Table 3.6.

Since the true value of  $r_0$  is expected to lie in the range  $[0.45 - 0.5]$  fm, our results are in agreement with the quenched value and no  $N_f$  dependence can be stated at this level of precision.

Finally, we can compare our results with other published data. One lattice simulation with two dynamical quarks is cited by the Flavour Lattice Averaging Group (FLAG) [106] and has been updated since [64]. The authors obtained the results  $f_B = 189(8)$  MeV,  $f_{B_s} = 228(8)$  MeV and  $f_{B_s}/f_B = 1.206(24)$  which are compatible with ours. Moreover, averaging both  $N_f = 2$  results produces numbers which are consistent with the estimate from  $N_f = 2 + 1$  computations quoted by the FLAG [107, 108, 109].

### 3.10.5 Phenomenology

The decay constants of the  $B$  and  $B_s$  mesons enter the determination of the CKM matrix elements via the leptonic decays  $B^- \rightarrow \tau^- \bar{\nu}_\tau$  and  $B_s \rightarrow \mu^+ \mu^-$ . The corresponding branching ratios are

$$\mathcal{B}(B^- \rightarrow \tau^- \bar{\nu}_\tau) = \frac{G_F^2 |V_{ub}|^2}{8\pi} \tau_B f_B^2 m_B m_\tau^2 \times \left(1 - \frac{m_\tau^2}{m_B^2}\right)^2, \quad (3.89)$$

$$\mathcal{B}(B_s \rightarrow \mu^+ \mu^-) = \frac{G_F^2}{\pi} \left[ \frac{\alpha_{em}(m_Z)}{4\pi \sin^2 \theta_W} \right]^2 \tau_{B_s} f_{B_s}^2 m_{B_s} m_\mu^2 \sqrt{1 - \frac{4m_\mu^2}{m_{B_s}^2}} |V_{tb}^* V_{ts}|^2 Y^2. \quad (3.90)$$

where  $Y \equiv Y(x_{tW}, x_{Ht}, \alpha_s)$  include QCD corrections as well as the leading electroweak corrections [62]. Here,  $x_{tW} = m_t^2/m_W^2$  and  $x_{Ht} = m_H^2/m_t^2$  where  $m_t$  is the top quark mass in the  $\overline{\text{MS}}$  scheme,  $m_W = 80.385$  GeV is the mass of the  $W$  boson and  $m_H = 125$  GeV is the mass of the Higgs boson.

id	$y$	$f_B^{\text{stat}}$ [MeV]		$f_{B_s}^{\text{stat}}$ [MeV]		$f_{B_s}^{\text{stat}}/f_B^{\text{stat}}$	
		HYP1	HYP2	HYP1	HYP2	HYP1	HYP2
A4	0.0771(14)	240(4)	228(4)	264(5)	250(4)	1.101(9)	1.096(7)
A5	0.0624(13)	235(4)	223(4)	265(5)	249(4)	1.128(6)	1.117(5)
B6	0.0484(9)	224(5)	213(4)	259(4)	244(4)	1.154(20)	1.143(15)
E5	0.0926(15)	240(4)	231(4)	263(4)	252(4)	1.092(10)	1.090(8)
F6	0.0562(9)	224(5)	214(4)	257(4)	245(4)	1.149(18)	1.148(16)
F7	0.0449(7)	219(4)	210(3)	252(4)	241(4)	1.152(10)	1.144(10)
G8	0.0260(5)	212(4)	205(4)	–	–	–	–
N5	0.0940(24)	241(6)	236(6)	–	–	–	–
N6	0.0662(10)	225(7)	217(5)	254(4)	245(4)	1.129(24)	1.133(18)
O7	0.0447(7)	217(9)	208(7)	–	244(6)	–	1.172(39)
LO	$y^{\text{exp}}, a = 0$	192.5(52)		234.1(48)		1.219(25)	
NLO	$y^{\text{exp}}, a = 0$	190.3(51)		–		1.189(24)	

Table 3.7 – Raw data for  $f_B^{\text{stat}}$ ,  $f_{B_s}^{\text{stat}}$  and their ratio  $f_{B_s}^{\text{stat}}/f_B^{\text{stat}}$ , using static HQET parameters at the physical point  $\omega_i^{\text{stat}}(z = z_b^{\text{stat}})$ , with  $z_b^{\text{stat}} = 13.24$  as determined in ref. [1]. The last two rows summarize our results for a combined chiral and continuum extrapolation using either the LO or NLO fit ansatz (3.88) for each individual observable.

The branching ratio  $\mathcal{B}(B \rightarrow \tau\nu_\tau)$  has been measured by the Belle and BaBar collaborations. Using as inputs the experimental value  $\mathcal{B}(B \rightarrow \tau\nu_\tau)_{\text{exp}} = 1.05(25) \times 10^{-4}$  quoted by the PDG [2, 110, 111, 112, 57] and our estimate of  $f_B$ , we get

$$|V_{ub}| = 4.15(29)_{f_B}(48)_B \times 10^{-3}, \quad (3.91)$$

where the errors come from  $f_B$  and the branching ratio respectively. This result can be compared with the other exclusive determinations from  $B \rightarrow \pi\ell\nu$ , which use, as an input, the  $B \rightarrow \pi$  form factor computed on the lattice. The PDG quotes  $|V_{ub}| = 3.23(31) \times 10^{-3}$  and the main contribution to the uncertainty comes from the lattice input. Therefore, the two results differ by roughly  $1.5 \sigma$  and further improvement on the lattice results could help to clarify the situation. Finally, we can also compare this result with the inclusive determination of the CKM matrix element  $\overline{B} \rightarrow X_u \ell \bar{\nu}_\ell$  from which we obtain  $|V_{ub}| = 4.41(15)_{\text{exp}} \binom{+15}{-17} \times 10^{-3}$  (see Figure 3.9).

In the strange sector, using the recent combination of experimental measurements at LHC, namely  $\mathcal{B}(B_s \rightarrow \mu^+\mu^-) = (2.9 \pm 0.7) \times 10^{-9}$  [60, 61, 113], together with our determination of  $f_{B_s}$ , and all input parameters of (3.90) set as in ref. [62], we obtain

$$|V_{tb}^* V_{ts}| = 3.89(24)_{f_{B_s}}(47)_B \times 10^{-2}. \quad (3.92)$$

The number is in good agreement with the extraction from global fits, which is mostly constrained by  $B_s^0 - \overline{B}_s^0$  mixing.

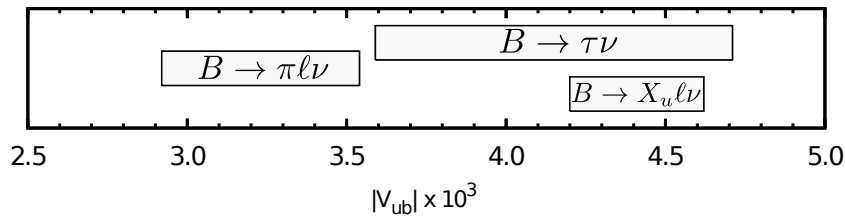


Figure 3.9 – Different determinations of the CKM matrix element  $V_{ub}$ . The exclusive determination  $B \rightarrow \tau \nu$  use our estimate of the decay constant  $f_B$  and  $B \rightarrow \pi \ell \nu$  use the form factor  $B \rightarrow \pi$  as a lattice input [2].

## Conclusion

In this chapter, I have reported about the determination of the  $b$ -quark mass and  $B$  meson decay constant from first principle lattice QCD with two dynamical quarks. Present day computer resources don't allow to directly simulate dynamical  $b$  quarks on the lattice and I have presented how to overcome this difficulty. Namely, we have used the Heavy Quark Effective Theory on the lattice, at first order in the inverse quark mass  $1/m_b$ , and the matching and renormalization were performed non-perturbatively. This approach has the advantage to avoid all perturbative errors. The effective theory depends on five parameters which have to be computed by matching the effective theory with QCD. Performing this matching at different values of the  $b$  quark mass, the HQET parameters inherit this mass dependence and the physical mass of the  $b$ -quark is then obtained by imposing the mass of the  $B$  meson, computed in HQET, to correspond to its physical value.

Perturbative results only enter in the final step of the computation when we convert our RGI quark mass in the  $\overline{\text{MS}}$  scheme for comparison with other results; we found

$$\overline{m}_b^{\overline{\text{MS}}}(\overline{m}_b^{\overline{\text{MS}}}) = 4.21(11) \text{ GeV}.$$

Systematic errors are also well under control. In particular, the Generalized Eigenvalue Problem was used to reduce the contamination of excited states and a continuum and chiral extrapolations were performed. Finally, our result is in good agreement with other lattice results at  $N_f = 2$ : the ETM collaboration recently obtain a similar error [64] but with a completely different approach. Therefore, it is an important cross-check of the result cited in the PDG [2] (see Table 3.4). Finally, the error budget indicates that a competitive results could be obtain in the near future.

Once the interpolation of the HQET parameters at the physical  $b$ -quark mass has been performed, the effective theory can be used to compute other observables. In this work, we focused on the decay constants  $f_B$  and  $f_{B_s}$  which are useful for phenomenology. After the continuum and the chiral extrapolations, our results read

$$f_B = 186(13)(2)_\chi \text{ MeV} \quad , \quad f_{B_s}/f_B = 1.203(62)(19)_\chi \quad , \quad f_{B_s} = 224(14)(2)_\chi \text{ MeV}$$

and are compatible with other lattice determinations. Comparing our results with the static order of HQET, we conclude that  $1/m_h$  corrections turn out be very small  $\lesssim 2.5\%$ . Moreover, the HQET parameters contribute to 15% of the total error and the

determination of the  $\omega_i$  could be further improved with today's machines. Finally, I have presented the phenomenological results concerning the determination of the CKM matrix elements from leptonic decays and the lattice contribution of the total error.

In the future, the HQET parameters, interpolated at the physical  $b$ -quark, could be used to compute other interesting observables, like the scalar  $B_0^*$  meson decay constant. The latter can be used to gain some insight concerning the precision of phenomenological application of HM $\chi$ PT, in particular concerning the relevance of the contribution of the  $J^P = (0^+, 1^-)$  doublet states in chiral loops [114, 115].

# Chapter 4

## On the $B^{*'} \rightarrow B\pi$ transition

### Contents

---

<b>Introduction</b> . . . . .	<b>86</b>
<b>4.1 Heavy Meson Chiral Lagrangians</b> . . . . .	<b>87</b>
4.1.1 Spectroscopy . . . . .	87
4.1.2 Chiral perturbation theory . . . . .	90
4.1.3 The CCWZ formalism . . . . .	91
<b>4.2 The <math>g_{B^{*'}B\pi}</math> coupling</b> . . . . .	<b>94</b>
4.2.1 Definition . . . . .	94
4.2.2 The coupling in $\text{HM}\chi\text{PT}$ . . . . .	94
4.2.3 Pion LSZ reduction . . . . .	95
<b>4.3 Computation on the Lattice</b> . . . . .	<b>97</b>
4.3.1 Estimators . . . . .	97
4.3.2 Two- and three-point correlation functions . . . . .	99
<b>4.4 Simulation parameters</b> . . . . .	<b>101</b>
<b>4.5 Lattice results</b> . . . . .	<b>102</b>
<b>4.6 Decay thresholds</b> . . . . .	<b>105</b>
<b>4.7 Diagonal couplings <math>g_{11}</math> and <math>g_{22}</math></b> . . . . .	<b>105</b>
<b>Conclusion</b> . . . . .	<b>107</b>

---

## Introduction

In the previous chapter, I have introduced the Heavy Quark Effective Theory (HQET), discretized on the lattice, to simulate the  $b$ -quark. On the contrary, light quarks interactions are well described by chiral perturbation field theory which corresponds to the limit of vanishing quark mass in QCD. In this chapter, the  $B$  meson will be studied in the framework of the Heavy Meson Chiral Lagrangians where both HQET and the chiral perturbation theory are used together. We will see that, at lowest order in the inverse heavy quark mass and power of pion momentum, only three coupling constants, usually denoted  $\hat{g}$ ,  $\tilde{g}$  and  $h$  are necessary to parametrize the effective Lagrangian for lowest positive and negative parity states. The coupling constant  $\hat{g}$  has been studied intensively on the lattice [116, 117, 118, 119]. However, very little is known about the coupling between the ground state  $B$  meson and its radial excitation  $B^{*'}$ .

Questions have been raised recently on the poor handling of excited states in the analyses of experimental data and their comparison with theoretical predictions, particularly in the case of heavy-light  $B$  and  $D$  mesons. For instance, it has been advocated that the  $\sim 3\sigma$  discrepancy observed between exclusive and inclusive estimates of the CKM matrix element  $V_{cb}$  might be reduced if the transition  $B \rightarrow D'$  were large. This attractive hypothesis implies a suppression of the  $B \rightarrow D^{(*)}$  hadronic form factors, as a study in the OPE formalism suggests [124]. On the other hand, it has been argued that the light-cone sum rule determination of the  $g_{D^*D\pi}$  coupling, which parametrizes the  $D^* \rightarrow D\pi$  decay, likely fails to reproduce the experimental measurement unless one explicitly includes the contribution from the first radial excited  $D^{(*)'}$  state on the hadronic side of the three-point Borel sum rule [125]. Comparison with sum rules is of particular importance because the heavy mass dependence of  $\hat{g}_Q \equiv \frac{g_{H^*H\pi}f_\pi}{2\sqrt{m_H m_{H^*}}}$  deduced from recent lattice simulations [117, 118, 100, 121, 122, 126] and experiment [120] seems

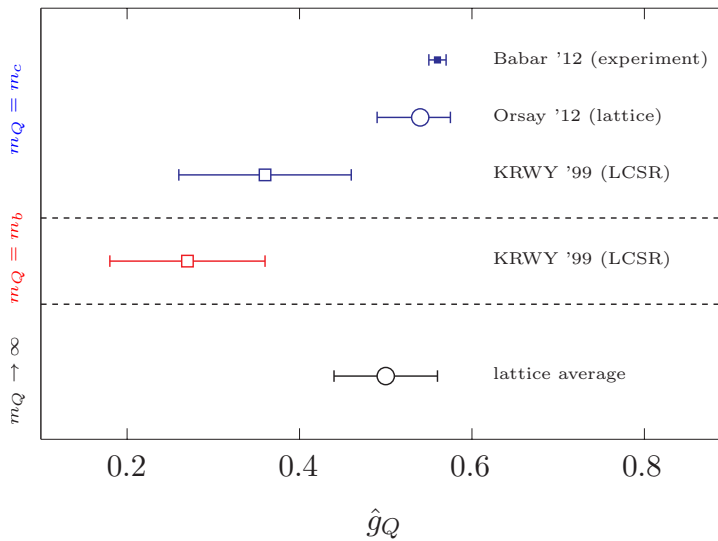


Figure 4.1 – Experimental measurement [120], lattice computations [117, 118, 100, 121, 122] and sum rules estimates [123] of  $\hat{g}_c$ ,  $\hat{g}_b$  and  $\hat{g} \equiv \hat{g}_\infty$ . We have performed a weighted average of recent  $\hat{g}$  lattice results at  $N_f = 2$  with respect to the error quoted in [117, 118, 100, 121].

much weaker than expected from analytical methods [123], as shown in Figure 4.1.

The Generalized Eigenvalue Problem (GEVP) allows to deal with excited states of mesons [127], especially to extract the spectrum [128, 98, 129, 130]. Similar techniques can now be applied to three-point correlation functions to perhaps illuminate the phenomenological issues discussed above. In this chapter, I will report on the lattice computation of the coupling  $g_{12} \equiv \langle B^{*'} | \mathcal{A}_i | B \rangle$  in the static limit of HQET, where  $\mathcal{A}_i$  is the axial vector bilinear of light quarks and  $B^{*'}$  is polarized along the  $i$ th direction ref. [131]. As a by-product of our work, I will also present the computation of the diagonal couplings  $g_{11} \equiv \langle B^* | \mathcal{A}_i | B \rangle$  and  $g_{22} \equiv \langle B^{*'} | \mathcal{A}_i | B' \rangle$ .

The Heavy Quark Symmetry at leading order in HQET is well suited for our qualitative study. As the spectra of excited  $B$  and  $B^*$  mesons are degenerate, it is enough to solve a single Generalized Eigenvalue Problem while degrees of freedom  $\sim m_b$ , that are somehow irrelevant for the dynamics of the cloud of light quarks and gluons that governs the process we examine, are integrated out. The plan of this chapter is the following: first, I discuss the spectroscopy of  $B$  mesons and summarize the main results, then I introduce the Heavy Meson Chiral Lagrangians and in particular the  $g_{B^{*'}B\pi}$  coupling. I will explain how this coupling can be computed on the lattice using three-point correlation functions and the GEVP. Finally, I will present our results and see how it can solve the aforementioned issues.

## 4.1 Heavy Meson Chiral Lagrangians

In the previous chapter, by integrating out the heavy degrees of freedom, which were irrelevant at the energy scale we were interested in, we obtained a simpler formulation which does not depend on the complicated structure of the complete theory. In particular, from a numerical point of view, the heavy quark propagator becomes much easier to evaluate since it does not rely on the costly inversion of the Dirac operator. Another very successful example of effective theory for QCD is the chiral perturbation theory (ChPT) to describe the dynamics of light quarks. In this case, the expansion parameter is the momentum exchanged in a given process,  $p^2$ . In this section, I explain how HQET and ChPT can be used together to describe Heavy-light mesons. The up, down and strange quarks, with masses below the QCD scale  $\Lambda_{QCD} \approx 200$  MeV, are considered as light, while the other quarks are considered as heavy and will be treated in the framework of HQET.

### 4.1.1 Spectroscopy

The spectroscopy of heavy-light mesons is simplified by the heavy quark symmetry since, in the limit of infinite mass, the spin  $\vec{S}_Q$  of the heavy quark decouples from the light degrees of freedom. Therefore,  $\vec{S}_Q$  is conserved independently from the total angular momentum of the light degrees of freedom  $\vec{j}_l$ , characterized by its spin  $\vec{S}_l$  and its orbital momentum  $\vec{L}$ :

$$J = j_l \pm \frac{1}{2} \quad \text{with} \quad \vec{j}_l = \vec{S}_l + \vec{L}.$$

In the case of  $B$  mesons, the spin of the light quark is  $S_l = \frac{1}{2}$ , and the two lightest states correspond to  $L = 0$  for the ground state pseudoscalar  $B(J^P = 0^-)$  meson and

$L$	$j_l^P$	$J^P$	state	$m$ (MeV)	dom. decay	Rad. excitation
0	$(1/2)^-$	$0^-$	$B$	$5279.58 \pm 0.17$ [2]	$B\gamma$	$B'$
		$1^-$	$B^*$	$5325.2 \pm 0.4$ [2]		$B^{*'}$
1	$(1/2)^+$	$0^+$	$B_0^*$	(text bellow)	$B\pi$ (s-wave)	
		$1^+$	$B_1^*$	(text bellow)	$B^*\pi$ (s-wave)	
1	$(3/2)^+$	$1^+$	$B_1$	(text bellow)	$B^*\pi$ (d-wave)	
		$2^+$	$B_2^*$	(text bellow)	$B^{(*)}\pi$ (d-wave)	

Table 4.1 – Quantum numbers of the ground state  $B$  meson and its excitations. The theory predicts the existence of two broad ( $B_0^*$  and  $B_1^*$ ) and two narrow ( $B_1$  and  $B_2^*$ ) bound states with  $j_l^P = (1/2)^+$  and  $j_l^P = (3/2)^+$ . The last two columns correspond to the dominant decay mode and the radial excitations respectively.

the vector  $B^*(J^P = 1^-)$  meson. Four orbitally excited states correspond to  $L = 1$  and are usually denoted by  $B^{**}$ . They split into one narrow doublet with  $j_l^P = (1/2)^+$  and one broad doublet with  $j_l^P = (3/2)^+$ , similar to the fine structure of the hydrogen atom in quantum mechanics. The splitting inside each doublet arises from the coupling with the spin of the heavy quark and would correspond to the hyperfine structure of the hydrogen atom. Finally, the radial excitations have the same orbital-parity quantum numbers and are denoted by a prime. The results are summarized in Table 4.1.

Contrary to charmed mesons, the  $B$  meson spectrum is still poorly known and the spectroscopy has not been fully established yet. Only the ground state  $J^P = 0^-$  and the excited state  $J^P = 1^-$  are referenced in the PDG with masses respectively given by  $m_{B^0} = 5279.58 \pm 0.17$  MeV and  $m_{B^*} = 5325.2 \pm 0.4$  MeV (see Table 4.1). With the last results of the LHCb Collaboration, the two narrow states ( $B_1$  and  $B_2^*$ ) are now quite well measured but the broad states ( $B_0^*$  and  $B_1^*$ ) have not been precisely measured yet. Moreover, even from the theoretical point of view, it is not clear whether the two narrow  $B^{**}$  states should be heavier or not than the two broad states. A summary of the experimental results is illustrated in Figure 4.2.

### Pseudoscalar $B$ and vector $B^*$ mesons

The pseudoscalar  $B$  meson is the lightest meson containing a  $b$ -quark. The mass difference between the vector ( $B^*$ ) and the pseudoscalar ( $B$ ) mesons has been discussed in the previous chapter. Due to the small mass difference, smaller than the pion mass, only electromagnetic decays are allowed and these mesons are stable via the strong interaction.

### Orbitally excited states $B^{**}$

Since the members of the  $j_l^P = (3/2)^+$  doublet decay in d-waves, these states are expected to be narrow; on the contrary, the members of the  $j_l^P = (1/2)^+$  decay in s-waves and are expected to be broad. Concerning the spectrum, the OPAL [132], ALEPH [133, 134] and DELPHI [135] Collaborations report on the first measurements of the

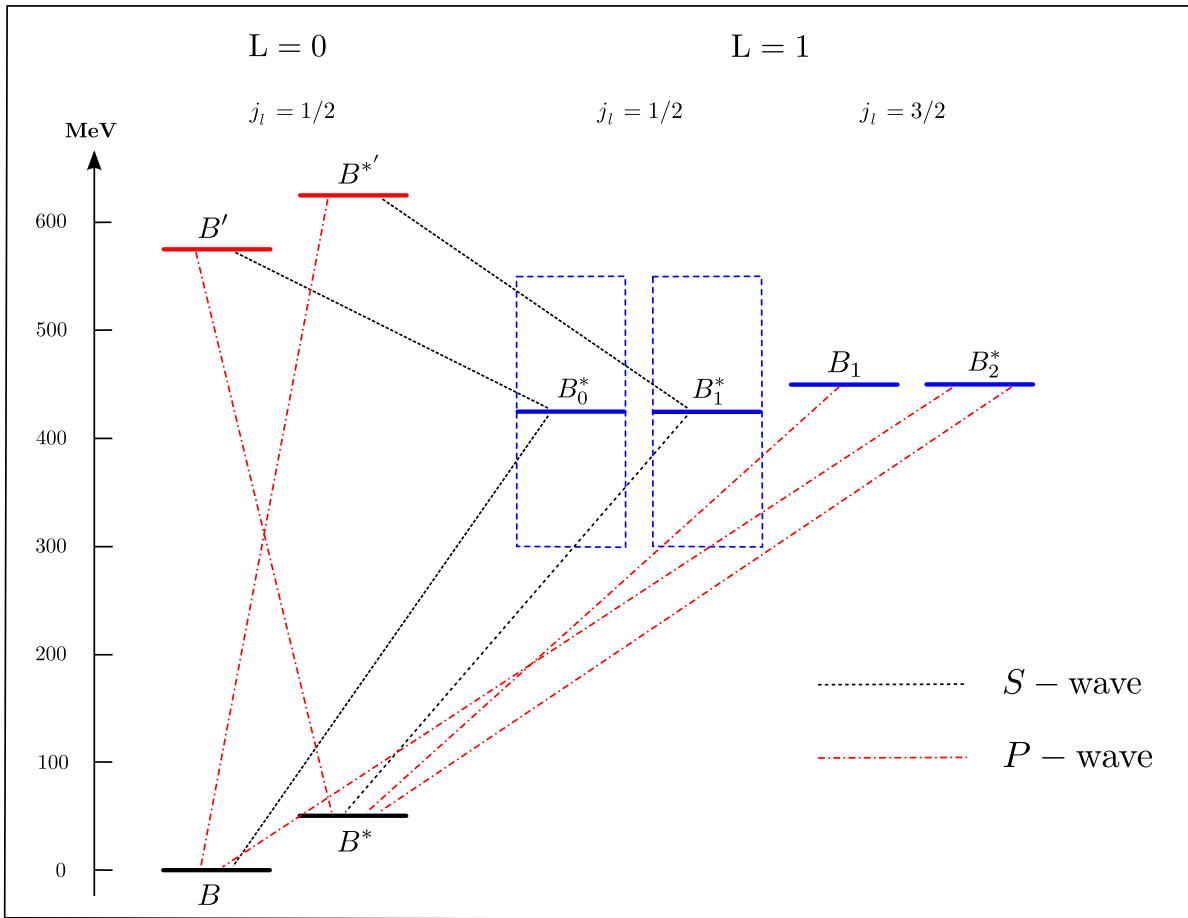


Figure 4.2 – Spectrum of the B mesons. Only the strong decays via pion in s- and p-waves are shown. The decay of the vector  $B^*$  meson with the emission of a pion is not allowed experimentally since  $m_{B^*} - m_B < m_\pi$ .

two narrow radially excited  $B$  mesons at LEP in 1995. The DELPHI Collaboration also reports on the detection of a signal compatible with the first radial excitation of the  $B$  meson [136, 137] and, in 2003, after a new analysis on the data sample they succeed to separate the two  $B^{**}$  narrow states ( $B_1^0$  and  $B_2^{*0}$ ) [138]. In 1999, the L3 collaboration also reports on the measurements of the orbitally excited  $B^{**}$  at LEP [139] and on the presence of a state, in the region 5.9 – 6.0 GeV, which could be associated to the radial excitation  $B'$ .

In 2007 and 2009, the CDF [140, 141] and D0 [142, 143] Collaborations measured the  $B^{**}$  states at the Tevatron collider. Finally, in 2013, the CDF Collaboration updated their results to take into account the full data sample [144] and also succeed to measure the non-neutral  $B^{**}$  mesons.

More recently, the LHCb Collaboration [145] has presented precise measurements of the two narrow orbital excitations of the  $B$  meson. For the  $B_1$  meson they found

$$m_{B_1^0} = 5724.1(1.7)_{\text{stat}}(2.0)_{\text{syst}}(0.5)_{\text{syst}} \text{ MeV},$$

$$m_{B_1^+} = 5726.3(1.9)_{\text{stat}}(3.0)_{\text{syst}}(0.5)_{\text{syst}} \text{ MeV},$$

and for the  $B_2^*$  meson

$$\begin{aligned} m_{B_2^{*0}} &= 5738.6(1.2)_{\text{stat}}(1.2)_{\text{syst}}(0.3)_{\text{syst}} \text{ MeV} , \\ m_{B_2^{*+}} &= 5739.0(3.3)_{\text{stat}}(1.6)_{\text{syst}}(0.3)_{\text{syst}} \text{ MeV} . \end{aligned}$$

### Radially excited states

According to quark models and lattice simulations [146, 147, 148], the first radial excitation of the pseudoscalar  $B$  meson should lie in the range 5.8 – 6.0 GeV (a value compatible with the results presented in this chapter) and can decay strongly. Recent results from the LHCb and CDF Collaborations present first hints of a radially excited state. The CDF Collaboration [144] reports on the presence of a new resonance with a mass  $m_{B(5970)^0} = 5978(5)_{\text{stat}}(12)_{\text{syst}}$  MeV and  $m_{B(5970)^+} = 5961(5)_{\text{stat}}(12)_{\text{syst}}$  MeV which could be interpreted as the radial excitation of the  $B$  meson.

### 4.1.2 Chiral perturbation theory

The massless QCD Lagrangian is invariant under the symmetry group  $SU(N)_V \otimes SU(N)_A \otimes U(1) \otimes U(1)_A$  and the axial symmetry associated to  $U(1)_A$  is broken at the quantum level by the axial anomaly [11, 12]. The symmetry associated to the  $U(1)$  group is simply the baryon conservation number. Under the action of the group  $SU(N)_V$  a meson is transformed into another meson with the same parity but a different isospin (isospin rotation). On the contrary, the group  $SU(N)_A$  mixes mesons with opposite parity. For example, in the case of the pion, if we note  $\theta_V$  and  $\theta_A$  the two rotation angles associated with the groups  $SU(2)_V$  and  $SU(2)_A$ , we have

$$\vec{\pi} \xrightarrow{SU(3)_V} \vec{\pi} + \vec{\theta}_V \times \vec{\pi} \quad , \quad \vec{\pi} \xrightarrow{SU(3)_A} \vec{\pi} + \vec{\theta}_A \sigma .$$

The axial symmetry predicts an exact degeneracy between states of opposite parity, which is not realized in the physical spectrum. Indeed the mass of the  $\rho$  meson is  $m_\rho = 770$  MeV whereas the mass of the  $a_1$  is  $m_{a_1} = 1260$  MeV. Therefore, we are forced to conclude that the group  $SU(N)_A$  is broken. Of course, chiral symmetry is explicitly broken by quark masses in the QCD Lagrangian but, since they are small ( $m_{u,d} < 10$  MeV), we would expect the mass difference to be also small compared to the masses themselves. This apparent contradiction can be solved by assuming the spontaneous breaking of chiral symmetry.

Therefore, we assume that the QCD vacuum is not invariant under the action of the group  $SU(N)_A$  and that the symmetry is broken by the presence of the chiral condensate  $\langle \bar{q}q \rangle \neq 0$ . According to the Goldstone theorem, we predict the existence of  $N^2 - 1$  Goldstone bosons corresponding to the number of broken generators or, in other words, to the number of generators which allow to switch from one degenerate vacuum to another. In the case of two light quarks ( $N = 2$ ), they can be identified with the three lightest mesons: the pions. When the strange quark is introduced, the kaon and the eta mesons are also considered as (pseudo) Goldstone bosons. Experimentally, their masses are not exactly zero due to the small mass terms in the QCD Lagrangian.

In the next paragraphs, I introduce an effective Lagrangian which takes into account both the chiral symmetry for light quarks and the heavy quark symmetry introduced in the previous chapter for heavy quarks. This has been studied for the first time in refs. [149, 150, 151].

### 4.1.3 The CCWZ formalism

The CCWZ formalism worked out by Callan, Coleman, Wess and Zumino [152, 153] can be used to construct the most general effective Lagrangian which is consistent with the  $SU(N)_R \otimes SU(N)_L/SU(N)_V$  spontaneous symmetry breaking pattern. The idea is that, at low energy, the symmetries of the fundamental Lagrangian should be conserved but are not necessarily linearly realized since heavy degrees of freedom have been integrated out. To simplify the notations, I will write  $G = SU(N)_R \otimes SU(N)_L$  the group which leaves the Lagrangian invariant and  $H = SU(N)_V$  the unbroken subgroup. The most general transformation of the group  $G$  can be written as

$$\psi \rightarrow \psi' = \left[ \exp \left( iT_a \theta_R^a \frac{1 + \gamma_5}{2} \right) \exp \left( iT_a \theta_L^a \frac{1 - \gamma_5}{2} \right) \right] \psi, \quad (4.1)$$

where  $\psi = (u, d, s)^T$  is an  $SU(N)$  vector and where  $\vec{\theta}_L$  and  $\vec{\theta}_R$  parametrize the  $SU(N)_L$  and  $SU(N)_R$  rotations respectively. The previous transformation can be written in terms of  $\vec{\theta}_V = (\vec{\theta}_L + \vec{\theta}_R)/2$  and  $\vec{\theta}_A = (\vec{\theta}_R - \vec{\theta}_L)/2$ :

$$\psi \rightarrow \psi' = \exp(iT_A \theta_A^a \gamma_5) \exp(iT_a \theta_V^a) \psi. \quad (4.2)$$

The generators of the unbroken subgroup  $H$  are written  $T_a \mathbb{1}$  and the Goldstone bosons are associated to the broken generators,  $T_a \gamma_5$ , and therefore belong to  $G \setminus H$ .

In QCD, the  $SU(N)_R \otimes SU(N)_L$  symmetry is only approximate because quarks are massive. However, the mass of the light quarks are small compared to the QCD scale  $\Lambda_{\text{QCD}}$  such that the pseudo-Goldstone bosons are also light. Therefore, they can be used as the light degrees of freedom of the effective theory. The first step consists in factorizing out the Goldstone bosons,  $\varphi(x)$ , from the field  $\psi(x)$  by performing a local symmetry transformation. Of course, the Lagrangian is not invariant under local transformations of the symmetry group  $G$ , and the parameters of this transformation, encoded in  $\gamma(x)$ , depend on the position  $x$

$$\psi(x) = e^{i\gamma_5 \varphi(x)} \tilde{\psi}(x) = \gamma(x) \tilde{\psi}(x). \quad (4.3)$$

Since a global transformation of the group  $G$  leaves the Lagrangian invariant, the different terms appearing in the effective Lagrangian will always contain at least one derivative of the Goldstone field (or, equivalently, with terms proportional to the momentum of the Goldstone). If not, the effective Lagrangian would depend on the Goldstone bosons when they are constant. This momentum will be used as the small parameter expansion of the effective theory and, at first order, the Lagrangian contains only terms with the minimal number of derivatives whereas higher order corrections can be added systematically. Since the Lagrangian is a functional of the fields and their derivatives, it is interesting to study the influence of the eq. (4.3) on derivatives. One immediately finds

$$\partial \psi(x) = \gamma(x) \left( \partial \tilde{\psi}(x) + \gamma^{-1}(x) \partial \gamma(x) \tilde{\psi}(x) \right). \quad (4.4)$$

Since  $\gamma \in G$ , its derivative can be written as the group element  $\gamma$  time a linear combination of the group generators  $T_a \mathbb{1}$  and  $T_a \gamma_5$ . Therefore, the term  $\gamma^{-1}(x) \partial_\mu \gamma(x)$  can be written as

$$\gamma^{-1}(x) \partial_\mu \gamma(x) = \sum_a \mathcal{A}_\mu^a(x) \gamma_5 T^a + \sum_a \mathcal{V}_\mu^a(x) T^a. \quad (4.5)$$

The fields  $\mathcal{A}_\mu(x)$  and  $\mathcal{V}_\mu(x)$  are defined by the previous equation and depend on  $\gamma(x)$ . In particular, if we define  $\xi(x) = \exp(i\varphi(x))$ , the previous equation can be written in matrix form

$$\begin{pmatrix} \xi & 0 \\ 0 & \xi^\dagger \end{pmatrix} \begin{pmatrix} \partial_\mu \xi^\dagger & 0 \\ 0 & \partial_\mu \xi \end{pmatrix} = \begin{pmatrix} \mathcal{V}_\mu - \mathcal{A}_\mu & 0 \\ 0 & \mathcal{V}_\mu + \mathcal{A}_\mu \end{pmatrix}, \quad (4.6)$$

and one obtains

$$\mathcal{A}_\mu = \frac{1}{2} (\xi^\dagger \partial_\mu \xi - \xi \partial_\mu \xi^\dagger), \quad (4.7)$$

$$\mathcal{V}_\mu = \frac{1}{2} (\xi^\dagger \partial_\mu \xi + \xi \partial_\mu \xi^\dagger), \quad (4.8)$$

where the two fields  $\mathcal{A}_\mu(x)$  and  $\mathcal{V}_\mu(x)$  are expressed in terms of the Goldstone fields and their derivatives. The most general Lagrangian is then written in terms of the fields  $\xi(x)$ ,  $\mathcal{A}_\mu(x)$  and  $\mathcal{V}_\mu(x)$ . We will see how the symmetries of QCD constrain the effective field theory by studying how these fields transform under the action of the group  $G$ .

Under an arbitrary element of the group  $G$ , the field  $\psi$  transforms according to eq. (4.1). In terms of the Goldstone field  $\varphi(x)$ , it reads

$$\underbrace{e^{iT_a \theta_R^a \frac{1+\gamma_5}{2}} e^{iT_a \theta_L^a \frac{1-\gamma_5}{2}}}_{g \in G} \underbrace{e^{i\gamma_5 \varphi(x)}}_{\gamma(x)} = \underbrace{e^{i\gamma_5 \varphi'(x)}}_{\gamma'(x)} \underbrace{e^{iT_a \theta^a(\varphi(x))}}_{U \in H}, \quad (4.9)$$

where the important point is that  $U$  generally depends on the Goldstone field:  $\theta$  is a function of  $\theta_R$ ,  $\theta_L$  and  $\varphi$ . Following [154], we can introduce

$$R = \exp(iT_a \theta_R^a), \quad L = \exp(iT_a \theta_L^a), \quad (4.10)$$

then, from eq. (4.9) and projecting on right and left chiralities with  $P_\pm = \frac{1 \pm \gamma_5}{2}$ , we obtain

$$L e^{-i\varphi(x)} = e^{-i\varphi'(x)} U(x), \quad (4.11)$$

$$R e^{i\varphi(x)} = e^{i\varphi'(x)} U(x), \quad (4.12)$$

so that the Goldstone field  $\xi(x) = e^{i\varphi(x)}$  transforms as

$$\xi(x) \rightarrow R \xi(x) U^\dagger(x) = U(x) \xi(x) L^\dagger.$$

It is also convenient to define  $\Sigma(x) = \xi(x)^2$  such that  $\Sigma(x) \rightarrow R \Sigma(x) L^\dagger$ . Under the action of the group  $SU(N)_V$ , the field  $\mathcal{A}_\mu$  transforms according to  $\mathcal{A}_\mu \rightarrow U \mathcal{A}_\mu U^\dagger$  and the field  $\mathcal{V}_\mu$  according to  $\mathcal{V}_\mu \rightarrow U \mathcal{V}_\mu U^\dagger + U \partial_\mu U^\dagger$  and therefore can be used to define a covariant derivative

$$\mathcal{D}_\mu = \partial_\mu + \mathcal{V}_\mu, \quad (4.13)$$

Finally, the Goldstone bosons are usually parametrized by

$$\Sigma(x) = \xi^2(x) = \exp\left(\frac{2i}{f_\pi} \mathcal{M}\right) \in SU(N), \quad (4.14)$$

where, for  $N = 3$ , the hermitian traceless matrix  $\mathcal{M}$  is given by

$$\mathcal{M} = \begin{pmatrix} \sqrt{\frac{1}{2}}\pi^0 + \sqrt{\frac{1}{6}}\eta & \pi^+ & K^+ \\ \pi^- & -\sqrt{\frac{1}{2}}\pi^0 + \sqrt{\frac{1}{6}}\eta & K^0 \\ K^- & \bar{K}^0 & -\sqrt{\frac{2}{3}}\eta \end{pmatrix}.$$

To conclude, the CCWZ formalism provides a systematic way to construct an effective Lagrangian for a spontaneously broken symmetry: it is the most general Lagrangian built from the fields  $\xi(x)$ ,  $\mathcal{A}_\mu(x)$  and with the covariant derivative  $\mathcal{D}_\mu$ . At lowest order in the pion momentum (minimal number of partial derivatives), it is

$$\mathcal{L}_{\text{light}} = \frac{f_\pi^2}{8} \text{Tr} (\partial_\mu \Sigma \partial^\mu \Sigma^\dagger) , \quad (4.15)$$

where the trace is taken over the SU(3) group. The pre-factor is chosen such that the kinetic term has the correct normalization. This Lagrangian can be expanded in terms of the Goldstone fields using eq. (4.14) and higher-order corrections originate from chiral symmetry breaking terms but will not be considered here [154].

### Heavy-light meson fields

The second step consists in introducing matter fields which couple to the light sector via the fields  $\mathcal{A}_\mu$  and  $\mathcal{V}_\mu$  defined in the previous paragraph. Following the notations of refs. [155, 156], the heavy-light pseudoscalar  $M(0^-)$  and vector  $M^*(1^-)$  mesons of negative parity are represented by the field  $H_a$  where the latin index  $a$  corresponds to the flavor of the light quark ( $M = Qq_a$ ,  $a = 1, 2, 3$ ) [149]:

$$H_a = \frac{1 + \not{\psi}}{2} [P_a^{\mu*} \gamma_\mu - P_a \gamma_5] , \quad \bar{H} = [P_a^{\mu*} \gamma_\mu + P_a^\dagger \gamma_5] \frac{1 + \not{\psi}}{2} ,$$

and  $P$ ,  $P_\mu^*$  are field operators which destroy respectively pseudoscalar and vector heavy-light mesons. They obey the following normalization conditions

$$\langle 0|P|M\rangle = \sqrt{m_M} \quad , \quad \langle 0|P_\mu^*|M^*\rangle = \sqrt{m_M} \epsilon_\mu .$$

Under a heavy quark spin transformation  $S \in \text{SU}(2)$ , the field  $H_a$  transforms as  $H_a \rightarrow SH_a$  and under chiral  $\text{SU}(N)_L \otimes \text{SU}(N)_V$  transformations as  $H_a \rightarrow H_b U_{ba}^\dagger$ . Similarly, we have  $\bar{H}_a \rightarrow \bar{H}_a S^{-1}$  and  $\bar{H}_a \rightarrow U_{ab} \bar{H}_b$ .

The Lagrangian should be invariant under the Heavy Quark Symmetry discussed in the previous chapter and couple to the Goldstone field via the fields  $\mathcal{A}_\mu$  and  $\mathcal{V}_\mu$ . The most general Lagrangian for negative parity states satisfying these conditions, in the static limit of HQET, is [149, 157, 151]

$$\mathcal{L}_{\text{heavy}}^- = ig \langle H_b \gamma_\mu \gamma_5 \mathcal{A}_{ba}^\mu \bar{H}_a \rangle + i \langle H_b v^\mu \mathcal{D}_{\mu ba} \bar{H}_a \rangle , \quad (4.16)$$

where the trace  $\langle \dots \rangle$  is taken over  $4 \times 4$  matrices and where  $a, b$  are SU(3) indices associated to the light quark.

The positive parity states can be introduced in a similar way. In this work, only states belonging to the doublet  $(0^+, 1^+)$  will be considered and they are represented by the field

$$S = \frac{1 + \not{\psi}}{2} [D_1^\mu \gamma_\mu \gamma_5 - D_0] ,$$

where  $D_1^\mu$  and  $D_0$  are field operators which destroy  $B_1^*$  and  $B_0^*$  mesons. The associated Lagrangian reads

$$\mathcal{L}_{\text{heavy}}^+ = i\tilde{g} \langle S_b \gamma_\mu \gamma_5 \mathcal{A}_{ba}^\mu \bar{S}_a \rangle + i \langle S_b v^\mu \mathcal{D}_{\mu ba} \bar{S}_a \rangle . \quad (4.17)$$

Finally, the part of the Lagrangian which mixes states of opposite parity is given by

$$\mathcal{L}_{\text{mix}} = ih \langle S_b \gamma_\mu \gamma_5 \mathcal{A}_{ba}^\mu \bar{H}_a \rangle . \quad (4.18)$$

## Heavy Chiral Lagrangian

We can now combine the chiral symmetry and the heavy quark symmetry to obtain the Heavy Meson Chiral Lagrangian at first order in the pion momentum and in the static limit of HQET, it reads

$$\begin{aligned}
\mathcal{L} = & \frac{f_\pi^2}{8} \partial^\mu \Sigma_{ab} \partial_\mu \Sigma_{ba}^\dagger && \text{(Goldstone bosons)} \\
& + ig \langle H_b \gamma_\mu \gamma_5 \mathcal{A}_{ba}^\mu \bar{H}_a \rangle + i \langle H_b v^\mu \mathcal{D}_{\mu ba} \bar{H}_a \rangle && \text{(negative parity states)} \\
& + i\tilde{g} \langle S_b \gamma_\mu \gamma_5 \mathcal{A}_{ba}^\mu \bar{S}_a \rangle + i \langle S_b v^\mu \mathcal{D}_{\mu ba} \bar{S}_a \rangle && \text{(positive parity states)} \\
& + ih \langle S_b \gamma_\mu \gamma_5 \mathcal{A}_{ba}^\mu \bar{H}_a \rangle. && \text{(4.19)}
\end{aligned}$$

The first part contains the kinetic term for the Goldstone bosons and  $f_\pi = 130.4$  MeV is the pion decay constant. The second, fourth and sixth terms describe interactions between heavy-light mesons with an odd number of pions. The third and fifth terms of the Lagrangian contain the kinematic terms of the heavy-light mesons and interactions with an even number of pions. Finally, this Lagrangian is parametrized by three coupling constants,  $g$ ,  $\tilde{g}$  and  $h$ , which can be extracted from the lattice. They are particularly useful since this Lagrangian is used to extrapolate lattice results to the chiral limit.

## 4.2 The $g_{B^{*'}B\pi}$ coupling

I now present the first lattice estimate of the hadronic coupling  $g_{12}$  which parametrizes the strong decay of a radially excited  $B^{*'}$  meson into the ground state  $B$  meson. First, I introduce the  $g_{B^{*'}B\pi}$  coupling and explain how it can be computed on the lattice using the Generalized Eigenvalue Problem. Then, I present our results and discuss their phenomenological implications.

### 4.2.1 Definition

Similarly to the  $g_{B^*B\pi}$  coupling [116, 117, 118], the  $g_{B^{*'}B\pi}$  parametrizes the  $B^{*'}$   $\rightarrow$   $B\pi$  decay and is defined via the following on-shell matrix element

$$\langle B^-(p') \pi^+(q) | B^{*0'}(p) \rangle = -g_{B^{*'}B\pi} q_\mu \epsilon^\mu(p), \quad (4.20)$$

where  $\epsilon^\mu$  is the polarization of the  $B^{*'}$  meson and where we used the relativistic normalization of states

$$\langle B(p) | B(p') \rangle = 2p^0 (2\pi)^3 \delta^{(3)}(\mathbf{p} - \mathbf{p}').$$

In our isospin convention, the coupling corresponds to  $g_{B^{*'}B\pi} = g_{B^{*0'}B^-\pi^+}$  but can be easily related to other isospin conventions

$$g_{B^{*'}B\pi} = -g_{B^{*-'}\bar{B}^0\pi^-} = \sqrt{2} g_{B^{*0'}B^0\pi^0} = -\sqrt{2} g_{B^{*+'}B^+\pi^0}.$$

### 4.2.2 The coupling in HM $\chi$ PT

The matrix element we are interested in is encoded in the second term of the Heavy Chiral Lagrangian (4.19) which describes the interaction of  $j_l^P = (1/2)^-$  heavy mesons

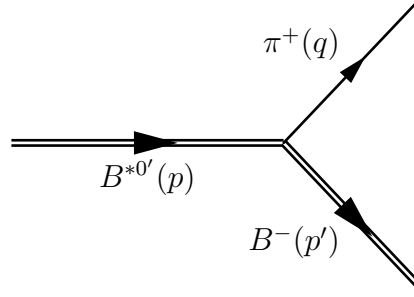


Figure 4.3 – Definition of the  $g_{B^*B\pi}$  coupling. The radially excited  $B^{*'}$  vector meson decays into a pseudoscalar  $B$  meson and a pion.

with an odd number of pions. I will present the result in the case of the  $g_{B^*B\pi}$  coupling, but the derivation for the  $g_{B^*B\pi}$  coupling is exactly the same. Explicitly, keeping only the lowest order terms in the momentum of the pion, we have

$$\begin{aligned}
 ig \langle H_b \gamma_\mu \gamma_5 \mathcal{A}_{ba}^\mu \bar{H}_a \rangle &= ig \langle \frac{1+\psi}{2} [P_\mu^* \gamma^\mu - P \gamma_5]_b \gamma_\mu \gamma_5 \mathcal{A}_{\mu ba} [P_\mu^\dagger \gamma^\mu + P^\dagger \gamma_5]_a \frac{1+\psi}{2} \rangle \\
 &= ig \langle \frac{1+\psi}{2} P_{\mu b}^* \gamma^\mu \gamma_\mu \gamma_5 \mathcal{A}_{\mu ba} P_a^\dagger \gamma_5 \rangle + \text{other terms} \\
 &= 4ig \langle \frac{1+\psi}{2} P_{\mu b}^* \gamma_5 \frac{i}{f_\pi} \partial_\mu \mathcal{M}_{ba} P_a^\dagger \gamma_5 \rangle + \text{other terms} \\
 &= -\frac{2g}{f_\pi} \langle P_{\mu b}^* \partial_\mu \mathcal{M}_{ba} P_a^\dagger \rangle + \text{other terms}
 \end{aligned}$$

where “other terms” include other interactions and higher order-terms in the pion momentum. Finally, we obtain the following Feynman rule

$$-\frac{2\sqrt{M_H M_{H^*}}}{f} g q \cdot \epsilon.$$

Therefore, at tree level in the HM $\chi$ PT Lagrangian, the matrix element reads

$$\langle B^0(p) \pi^+(q) | B^{*+}(p') \rangle = -\frac{2\sqrt{m_B m_{B^*}}}{f_\pi} g q_\mu \epsilon^\mu(p') (2\pi)^4 \delta^{(4)}(p' - p - q),$$

and

$$g_{B^*B\pi} = \frac{2\sqrt{m_B m_{B^*}}}{f_\pi} g.$$

This formula is valid in the limit of infinite mass and gets corrections of order  $1/m_b$ .

### 4.2.3 Pion LSZ reduction

The LSZ reduction formula can be used to express the previous  $S$  matrix element in terms of form factors which can be evaluated on the lattice.

$$\begin{aligned}
 \langle B^0(p) \pi^+(q) | B^{*+}(p') \rangle &\xrightarrow{\text{on-shell pion}} i \int d^4x e^{iqx} (\square + m_\pi^2) \langle B^0(p) | \pi(x) | B^{*+}(p') \rangle \\
 &= i (m_\pi^2 - q^2) \int d^4x e^{iqx} \langle B^0(p) | \pi(x) | B^{*+}(p') \rangle
 \end{aligned}$$

Then, using the PCAC relation

$$\pi(x) = \frac{1}{m_\pi^2 f_\pi} \partial^\mu A_\mu(x),$$

where  $A_\mu(x)$  is the light-light axial current and  $f_\pi$  is the pion decay constant, we obtain

$$\begin{aligned} \langle B^0(p)\pi^+(q)|B^{*+}(p') \rangle &\xrightarrow{\text{on-shell pion}} i \frac{m_\pi^2 - q^2}{f_\pi m_\pi^2} \int d^4x e^{iqx} \langle B^0(p) | \partial_\mu A^\mu(x) | B^{*+}(p') \rangle \\ &= q^\mu \frac{m_\pi^2 - q^2}{f_\pi m_\pi^2} \int d^4x e^{iqx} \langle B^0(p) | A^\mu(x) | B^{*+}(p') \rangle \\ &= q^\mu \frac{m_\pi^2 - q^2}{f_\pi m_\pi^2} \int d^4x e^{iqx} \langle B^0(p) | e^{iP \cdot x} A^\mu(0) e^{-iP \cdot x} | B^{*+}(p') \rangle \\ &= q^\mu \frac{m_\pi^2 - q^2}{f_\pi m_\pi^2} (2\pi)^4 \delta^{(4)}(q + p - p') \langle B^0(p) | A^\mu(0) | B^{*+}(p') \rangle. \end{aligned}$$

We conclude that, close to the pole at  $q^2 = m_\pi^2$ , the  $g_{B^{*'}B\pi}$  coupling is given by

$$g_{B^{*'}B\pi}(q^2) \times (\epsilon \cdot q) = -q^\mu \frac{m_\pi^2 - q^2}{f_\pi m_\pi^2} \langle B^0(p) | A_\mu(0) | B^{*'+}(p+q) \rangle. \quad (4.21)$$

### Parametrization of the transition amplitude

The transition amplitude of interest is parametrized by three form factors as

$$\begin{aligned} \langle B^0(p) | A^\mu | B^{*'+}(p', \epsilon^\lambda) \rangle &= 2m_{B^{*'}} A_0(q^2) \frac{\epsilon^\lambda \cdot q}{q^2} q^\mu + (m_B + m_{B^{*'}}) A_1(q^2) \left( \epsilon^{\lambda\mu} - \frac{\epsilon^\lambda \cdot q}{q^2} q^\mu \right) \\ &\quad + A_2(q^2) \frac{\epsilon^\lambda \cdot q}{m_B + m_{B^{*'}}} \left[ (p_B + p_{B^{*'}})^\mu + \frac{m_B^2 - m_{B^{*'}}^2}{q^2} q^\mu \right], \end{aligned} \quad (4.22)$$

where  $q = p' - p$  is the transfer momentum. In the zero recoil kinematic configuration which corresponds to  $\vec{p} = \vec{p}' = \vec{0}$ , one has  $q_{\text{max}}^2 = (m_{B^{*'}} - m_B)^2$  and we are left with the form factor  $A_1$ :

$$\langle B^0(p) | A^i | B^{*'+}(p', \epsilon^\lambda) \rangle = (m_B + m_{B^{*'}}) A_1(q_{\text{max}}^2) \epsilon^{\lambda i}. \quad (4.23)$$

Then, taking the non relativistic normalization of states,  $|H\rangle = \sqrt{2m_H} |H\rangle_{\text{HQET}}$ , we arrive at

$$\langle B^0(p) | A^i | B^{*'+}(p', \epsilon^\lambda) \rangle_{\text{HQET}} = \frac{m_B + m_{B^{*'}}}{2\sqrt{m_B m_{B^{*'}}}} A_1(q_{\text{max}}^2) \epsilon^{\lambda i}. \quad (4.24)$$

Finally, choosing the quantization axis along the  $z$  direction and the polarization vector  $\epsilon^\mu(0) = (0, 0, 0, 1)$  we get

$$\langle B^0(p) | A^3 | B^{*'+}(p', \epsilon^\lambda) \rangle_{\text{HQET}} = A_1(q_{\text{max}}^2) \equiv g_{12}, \quad (4.25)$$

where the result is valid in the static limit. In the next section, I will explain how this form factor, called  $g_{12}$ , can be extracted on the lattice using three-point correlation function.

### Relation to the $g_{B^*B\pi}$ coupling

I now discuss the relationship between the form factor  $A_1(q_{\max}^2)$  and the  $g_{B^*B\pi}$  coupling. Taking the divergence  $q_\mu A^\mu$  of the transition amplitude (4.22), the second and third terms vanish and we obtain

$$\langle B^0(p) | q_\mu A^\mu | B^{*+}(p', \epsilon^\lambda) \rangle = 2m_{B^*} A_0(q^2) \epsilon^\lambda \cdot q, \quad (4.26)$$

so that, from eq. (4.21)

$$g_{B^*B\pi} \underset{q^2 \rightarrow m_\pi^2}{=} -2m_{B^*} A_0(q^2) \frac{m_\pi^2 - q^2}{f_\pi m_\pi^2}.$$

Since the form factor  $A_0$  has a pole at the pion mass, the extrapolation to  $q^2 = m_\pi^2$  is not easy. However, since the parametrization of the transition amplitude contains an unphysical pole at  $q^2 = 0$ , the form factors have to obey the following condition

$$2m_{B^*} A_0(0) = (m_B + m_{B^*}) A_1(0) + (m_B - m_{B^*}) A_2(0),$$

which can be used to express  $A_0$  in terms of the two form factors  $A_1$  and  $A_2$ . If, in addition, we assume a small  $q^2$  dependence of the form factors then we arrive at

$$g_{B^*B\pi} \approx -\frac{(m_B + m_{B^*})}{f_\pi} A_1(0) - \frac{(m_B - m_{B^*})}{f_\pi} A_2(0). \quad (4.27)$$

Therefore, on the lattice, we don't directly compute the coupling constant  $g_{B^*B\pi}$  but rather the form factor  $A_1$  at  $q^2 = q_{\max}^2$ . To obtain the coupling constant, a first step would be to compute the distribution in  $r$  of the axial density, namely

$$f_A(\vec{r}) \equiv \langle B^* | [\bar{\psi}_l \gamma^i \gamma^5 \psi_l](\vec{r}) | B \rangle \quad , \quad A_1(0) = 4\pi \int_0^\infty r^2 f_A(r) e^{i\vec{q}\cdot\vec{r}} dr, \quad (4.28)$$

where  $r$  is the distance between the heavy quark line and the current insertion (see Figure 4.4), to extrapolate the form factor  $A_1$  at  $q^2 = m_\pi^2$ . A similar extrapolation has been carried out in ref. [158] where the authors computed the radial distribution of the vector, axial and scalar density for the form factors of the heavy-light mesons, but not with radially excited states. Finally, the contribution of the form factor  $A_2$  is expected to be less important due to the mass difference appearing in eq. (4.27). In particular, in the case of the  $g_{B^*B\pi}$  coupling, the contribution of this form factor vanishes in the static limit of HQET since  $m_B = m_{B^*}$  and in our case,

$$\frac{m_B - m_{B^*}}{m_B + m_{B^*}} \sim 4\%.$$

## 4.3 Computation on the Lattice

### 4.3.1 Estimators

In this section, I explain how the matrix element (4.25) can be extracted on the lattice using the Generalized Eigenvalue Problem. The two-point correlation functions associated to the pseudoscalar  $B$  and vector  $B^*$  mesons are

$$C_P^{(2)}(t) = \langle P(t) P^\dagger(0) \rangle \quad , \quad C_V^{(2)}(t) = \frac{1}{3} \sum_{k=1}^3 \langle V_k(t) V_k^\dagger(0) \rangle,$$

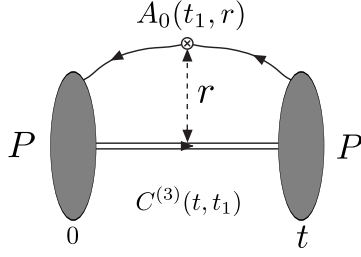


Figure 4.4 – Three-point correlation for the computation of the distribution in  $r$  of the axial density  $f_A(\vec{r})$ .

where  $P(x) = \bar{\psi}_h(x)\gamma_5\psi_l(x)$  and  $V_k(x) = \bar{\psi}_h(x)\gamma_k\psi_l(x)$  are respectively the heavy-light pseudoscalar and vector currents. Here,  $\psi_h$  refers to the heavy quark and  $\psi_l$  to the light quark. Thanks to the Heavy Quark Symmetry, the two-point correlation functions are equal and only one of them has to be computed (therefore, the subscript  $P$  or  $V$  will be dropped in the following). We will also need the following three-point correlation function

$$C^{(3)}(t, t_1) = \frac{1}{3} \sum_{k=1}^3 \langle V_k(t)A_k(t_1)P^\dagger(0) \rangle, \quad (4.29)$$

where  $A_\mu(x) = Z_A \bar{\psi}_l(x)\gamma_\mu\gamma_5\psi_l(x)$  is the light to light axial current and the normalization factor  $Z_A$  has been computed non-perturbatively by the ALPHA collaboration [159, 52].

We can now use the results of the GEVP introduced in Section 2.5 to compute efficiently the matrix element  $\langle B|A_i(0)|B_i^{*'} \rangle$ . The basis of interpolating operators  $\mathcal{O}^{(i)}(t)$  is based on different levels of Gaussian smearing and the details of the parameters are given in Section 4.4. The associated two and three-point correlation matrices are written

$$\begin{aligned} C_{ij}^{(2)}(t) &= \langle \mathcal{O}^{(i)}(t)\mathcal{O}^{(j)\dagger}(0) \rangle, \\ C_{ij}^{(3)}(t, t_1) &= \langle V_k^{(i)}(t)A_k(t_1)P^{(j)\dagger}(0) \rangle. \end{aligned}$$

First we solve the GEVP for the two-point correlation functions

$$C^{(2)}(t)v_n(t, t_0) = \lambda_n(t, t_0)C^{(2)}(t_0)v_n(t, t_0), \quad (4.30)$$

then, we use the eigenvectors, the eigenvalues and eq. (2.30) to obtain the following estimator:

$$\begin{aligned} \langle B_n|A_i(0)|B_{m,i}^{*'} \rangle &= \langle 0|\widehat{Q}_n^{\text{eff}}(t-t_1, t_0)e^{-H(t-t_1, t_0)}\widehat{A}_i e^{-Ht_1} \left( \widehat{Q}_m^{\text{eff}}(t_1, t_0) \right)^\dagger |0 \rangle \\ &= R_n(t-t_1, t_0)R_m(t_1, t_0) (v_n(t-t_1, t_0), C^{(3)}(t, t_1)v_n(t_1, t_0)) \\ &= \mathcal{M}_{nm}^{\text{GEVP}} \end{aligned}$$

where, as before,  $(\cdot, \cdot)$  is the inner product over eigenvector indices. When the convention  $t_0 = t-1$  is used, I do not write explicitly the dependence on  $t_0$  of the eigenvalues and eigenvectors and they are simply written  $\lambda_n(t)$  and  $v_n(t)$ . Finally, with  $t_2 = t-t_1$ , we obtain:

$$\mathcal{M}_{mn}^{\text{GEVP}}(t_2, t_1) = \frac{(v_m(t_2), C^{(3)}(t_1+t_2, t_1)v_n(t_1)) \lambda_m(t_2+1)^{-t_2/2} \lambda_n(t_1+1)^{-t_1/2}}{(v_m(t_2), C^{(2)}(t_2)v_m(t_2))^{1/2} (v_n(t_1), C^{(2)}(t_1)v_n(t_1))^{1/2}}, \quad (4.31)$$

and one can show that the rate of convergence is given by [160]

$$\mathcal{M}_{mn}^{\text{GEVP}} = \mathcal{M}_{mn} + \mathcal{O}\left(e^{-\Delta_{N+1,m}t_2}, e^{-\Delta_{N+1,n}t_1}\right),$$

where  $\mathcal{M}_{mn} = \langle B_n | A_i(0) | B_m^* \rangle$  and  $B_n$  is the  $n^{\text{th}}$  excited state ( $n = 1$  corresponds to the ground state). In this work, we choose the particular value  $t_1 = t_2$  to obtain the best convergence rate. In ref. [160], the authors also proposed an improved estimator obtained by summing over the insertion time  $t_1$ :

$$\mathcal{M}_{mn}^{\text{sGEVP}}(t, t_0) = -\partial_t \left( \frac{(v_m(t, t_0), [K(t, t_0)/\lambda_n(t, t_0) - K(t_0, t_0)] v_n(t, t_0))}{(v_m(t, t_0), C(t_0)v_m(t, t_0))^{1/2} (v_n(t, t_0), C(t_0)v_n(t, t_0))^{1/2}} e^{\Sigma_{mn}(t_0, t_0)t_0/2} \right) \quad (4.32)$$

where

$$\Sigma_{mn}(t, t_0) = E_n(t, t_0) - E_m(t, t_0),$$

is the difference of energy between the  $m^{\text{th}}$  and  $n^{\text{th}}$  states and

$$K_{ij}(t, t_0) = \sum_{t_1} e^{-(t-t_1)\Sigma(t, t_0)} C_{ij}^{(3)}(t, t_1),$$

is the summed three-point correlation function. The advantage of this estimator is that the new rate of convergence is

$$\begin{aligned} \mathcal{M}_{mn}^{\text{sGEVP}} &= \mathcal{M}_{mn} + \mathcal{O}\left(t e^{-\Delta_{N+1,n}t}\right) & n > m \\ &= \mathcal{M}_{mn} + \mathcal{O}\left(e^{-\Delta_{N+1,m}t}\right) & n < m \end{aligned}$$

where  $t = t_1 + t_2$ . A proof of this result is given in Appendix B where I have calculated the time dependence of the corrections at first order in  $\epsilon$  using the following decomposition

$$C^{(2)}(t) = C_0^{(2)}(t) + \epsilon C_1^{(2)}(t) = \sum_{n=1}^N \psi_{ni} \psi_{nj} e^{-E_n t} + \sum_{n=N+1}^{\infty} \psi_{ni} \psi_{nj} e^{-E_n t}.$$

Finally, the sign of the eigenvectors has been fixed by imposing the positivity of the ‘decay constant’

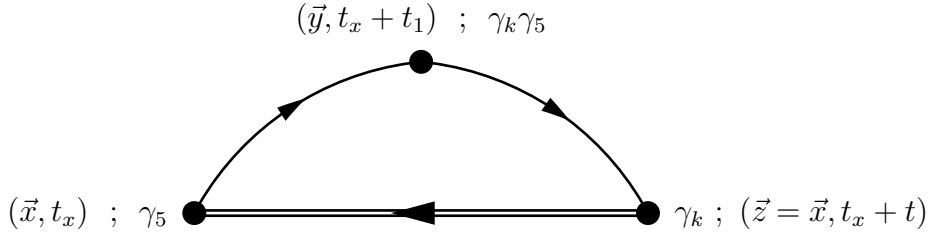
$$f_{B_n} \equiv \langle B_n | A_0 | 0 \rangle = \frac{\sum_i C_{L,i}^{(2)}(t) v_{n,i}(t, t_0) \lambda_n(t_0 + 1, t_0)^{-t/2}}{\sqrt{(v_n(t, t_0), C^{(2)}(t) v_n(t, t_0))}},$$

where the two-point correlation function  $C_L^{(2)}$  is defined similarly to eq. (3.56).

### 4.3.2 Two- and three-point correlation functions

To compute the two-point and three-point correlation functions, we use interpolating fields for static-light mesons of the so-called Gaussian smeared-form [46]

$$O_i(x_0) = \sum_{\vec{x}} \mathcal{O}(x) = \sum_{\vec{x}} \bar{\psi}_h(x) \Gamma(1 + \kappa_G a^2 \Delta)^{n_i} \psi_l(x) = \sum_{\vec{x}} \bar{\psi}_h(x) \Gamma \psi_l^{(i)}(x),$$

Figure 4.5 – Three-point correlation function  $C^{(3)}(t, t_1)$ .

where  $\kappa_G = 0.1$  is a hopping parameter,  $n_i$  is the number of applications of the operator  $(1 + \kappa_G a^2 \Delta)$ , and  $\Delta$  the gauge-covariant 3-D Laplacian constructed from three-times APE-blocked links [43].  $n_i$  is chosen such that the radius  $r_i \equiv 2a\sqrt{\kappa_G n_i}$  of the “wave-function” is smaller than 0.6 fm.

To compute the three-point correlation function on the lattice, we first perform the Wick contractions in the fermionic expectation value according to eq. (2.6). Since we work at zero spatial momentum, we sum over all spatial lattice points. In the following there is no summation over  $k$  but, at the end, we average the result over  $k = 1, 2, 3$ :

$$\begin{aligned} C^{(3)}(t, t_1) &= \frac{1}{V^3} \sum_{\vec{x}, \vec{y}, \vec{z}} \sum_{t_x} Z_A \langle V_k(\vec{z}, t + t_x) A_k(\vec{y}, t_1 + t_x) P^\dagger(\vec{x}, t_x) \rangle \\ &= \frac{1}{V^3} \sum_{\vec{x}, \vec{y}, \vec{z}} \sum_{t_x} Z_A \langle \overbrace{\psi_h(z) \gamma_k \psi_l(z) \cdot \psi_l(y) \gamma_k \gamma_5 \psi_l(y) \cdot \psi_l(x) \gamma_5 \psi_h(x)} \rangle \\ &= -\frac{1}{V^3} \sum_{\vec{x}, \vec{y}, \vec{z}} \sum_{t_x} Z_A \text{Tr} [G_h(x; z) \gamma_k G_l(z; y) \gamma_k \gamma_5 G_l(y, x) \gamma_5], \end{aligned}$$

where only one Wick contraction is considered among the light quarks. Indeed, one light quark-antiquark pair corresponds to the up quark and the other one to the down quark, therefore the quark propagators are formally different even if numerically they are the same (the quark masses are degenerate). The result is illustrated in Figure 4.5. We can now use the  $\gamma_5$ -hermiticity of the light propagator, namely  $G_l(x, y) = \gamma_5 G_l^\dagger(y, x) \gamma_5$ , to have both light propagators starting at the same space-time point. The heavy quark propagator is also replaced by its explicit form, given by eq. (3.16). Finally, we arrive at

$$C^{(3)}(t, t_1) = -\frac{1}{V^3} \sum_{\vec{x}, \vec{y}, \vec{z}} \sum_{t_x} Z_A \text{Tr} \left[ \delta(\vec{x} - \vec{z}) \mathcal{P}(z, x)^\dagger P_+ \gamma_k G_l(z; y) \gamma_k G_l^\dagger(x, y) \right].$$

The light quark propagator is evaluated by using stochastic sources with full time dilution as explained in Section 2.3 and the  $N_s$  diluted sources are labeled by the index  $s$ . We place one stochastic source  $\eta_s$  in  $y$  and perform two inversions, one with the source  $\eta_s(y)$  and one with the source  $\gamma_i \eta_s(y)$ . The solution vectors are respectively  $\psi_s$  and  $\tilde{\psi}_s$ :

$$\psi_s(x) = \sum_y G_l(x, y) \eta_s(y) \quad , \quad \tilde{\psi}_s(x) = \sum_y G_l(x, y) \gamma_k \eta_s(y).$$

Then, using the properties of the stochastic sources of Section 2.3, we obtain

$$\frac{1}{N_s} \sum_s \psi_s(z) \tilde{\psi}_s^\dagger(x) = \frac{1}{N_s} \sum_s \sum_{\vec{y}_1, \vec{y}_2} G_l(z, y_1) \eta_s(y_1) \eta_s(y_2)^\dagger \gamma_k G_l(x, y_2)^\dagger = \sum_{\vec{y}} G_l(z, y) \gamma_k G_l(x, y)^\dagger.$$

and finally, the three-point correlation function is

$$C^{(3)}(t, t_1) = -\frac{1}{N_s} \sum_s \frac{1}{V^2} \sum_{\vec{x}} Z_A \text{Tr} \left[ \left( P_+ \mathcal{P}(\vec{x}, t + t_x; \vec{x}, t_x) \tilde{\psi}_s(\vec{x}, t_x) \right)^\dagger (\gamma_k \psi_s(\vec{x}, t + t_x)) \right].$$

In practice, we use a single full-diluted source on each gauge configuration (therefore, there is one secondary source per time slice and  $s \in [1, T]$ ), except on the CLS ensemble E5g where we have four stochastic sources for each gauge configuration. The two-point correlation function

$$C^{(2)}(t) = \left\langle \frac{1}{V^2} \sum_{\vec{y}, \vec{x}} P(y) P^\dagger(x) \right\rangle \Big|_{y_0=x_0+t},$$

is computed similarly and we obtain:

$$\begin{aligned} C^{(2)}(t) &= -\frac{1}{V^2} \sum_{\vec{y}, \vec{x}} \overbrace{\psi_h(x) \gamma_5 \psi_l(x) \psi_l(y) \gamma_5 \psi_h(y)} \\ &= \frac{1}{V^2} \sum_{\vec{y}, \vec{x}} \text{Tr} [G_h(y, x) \gamma_5 G_l(x, y) \gamma_5] \\ &= \frac{1}{N_s} \sum_s \frac{1}{V} \sum_{\vec{x}} \text{Tr} \left[ (\mathcal{P}(x, y) P_+ \gamma_5 \eta_s(y))^\dagger (\gamma_5 \psi_s(x)) \right]. \end{aligned} \quad (4.33)$$

## 4.4 Simulation parameters

In this work, we used a subset of the CLS ensembles used for the computation of the  $b$ -quark mass. These simulations use non-perturbatively  $\mathcal{O}(a)$ -improved  $N_f = 2$  Wilson-Clover action, the plaquette gauge action and the HYP2 discretization for the static quark action. The parameters of the ensembles used in this work are collected in Table 4.2. Three lattice spacings ( $0.05 \text{ fm} \lesssim a \lesssim 0.08 \text{ fm}$ ) are considered with pion masses in the range  $[310, 440] \text{ MeV}$ . Finally, the statistical error is estimated from the jackknife procedure introduced in Section 2.7.

CLS	$\beta$	$L^3 \times T$	$\kappa$	$a$ (fm)	$m_\pi$ (MeV)	# cfgs
A5	5.2	$32^3 \times 64$	0.13594	0.075	330	500
E5g	5.3	$32^3 \times 64$	0.13625	0.065	440	500
F6		$48^3 \times 96$	0.13635		310	600
N6	5.5	$48^3 \times 96$	0.13667	0.048	340	400

Table 4.2 – Parameters of the simulations: the bare coupling  $\beta = 6/g_0^2$ , the resolution of the lattice, the hopping parameter  $\kappa$ , the lattice spacing  $a$  in physical units, the pion mass and the number of gauge configurations.

## 4.5 Lattice results

To reduce the statistical uncertainty in the ratio (4.32), we have taken the asymptotic value of the energy splittings  $\Sigma_{mn}^\infty = E_n - E_m$  and an example of plateau for  $\Sigma_{12}^\infty$  is shown in Figure 4.6.

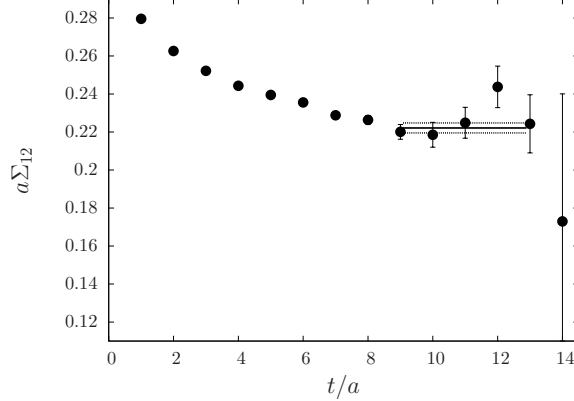


Figure 4.6 – Plateau of  $\Sigma_{12}(t) = E_2^{\text{eff}}(t) - E_1^{\text{eff}}(t)$  for the CLS ensemble E5g.

In Figure 4.7, I also plot the effective energy given by eq. (2.27) for the different energy levels obtained by solving the GEVP. The fact that a good signal is observed even for the second excited state indicates that the second energy level, corresponding to the  $B^{*'}$  meson, is correctly extracted from the GEVP.

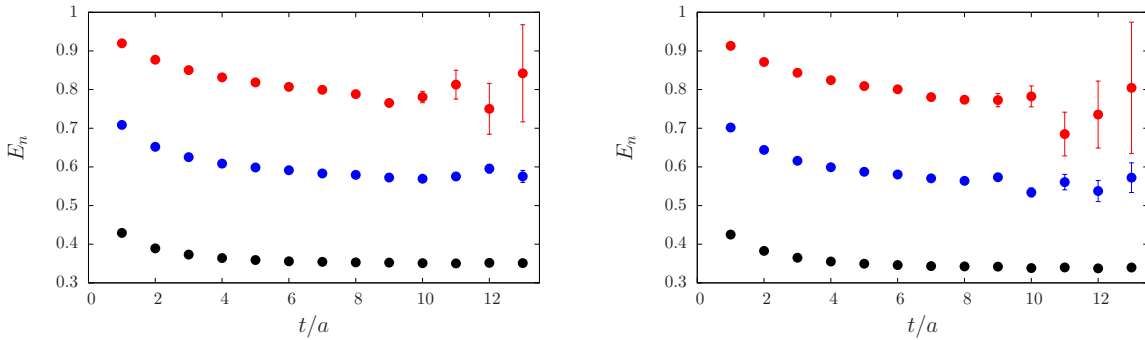


Figure 4.7 – Effective energy for the first three levels using the GEVP. On the left for the ensemble E5g and on the right for the ensemble F6.

The results for  $\Sigma_{12}^\infty$  on each lattice ensemble are given in Table 4.3. The error we quote includes the discrepancy between plateaus that we extract for different time ranges

$$[t_{\min}, t_{\max}] \quad , \quad [t_{\min} \pm 0.2 r_0, t_{\max} \pm 0.2 r_0]$$

where the Sommer scale  $r_0$  [105] is about 0.5 fm [52].

We have solved both  $3 \times 3$  and  $4 \times 4$  GEVP systems and checked the stability of the results when the local operator is included, as shown in Figure 4.8. Hereafter we will present results for a  $3 \times 3$  matrix of correlators with values of  $r_i \equiv$

$\{0.19 \text{ fm}, 0.39 \text{ fm}, 0.62 \text{ fm}\}$ . To check the dependence on  $t_0$ , to which the higher excited states contribution is sensitive, we have both fixed it at a small value (typically,  $t_0 = 2a$ ) and let it vary as  $t - a$ . Though the uncertainty is a bit larger, we have confirmed the

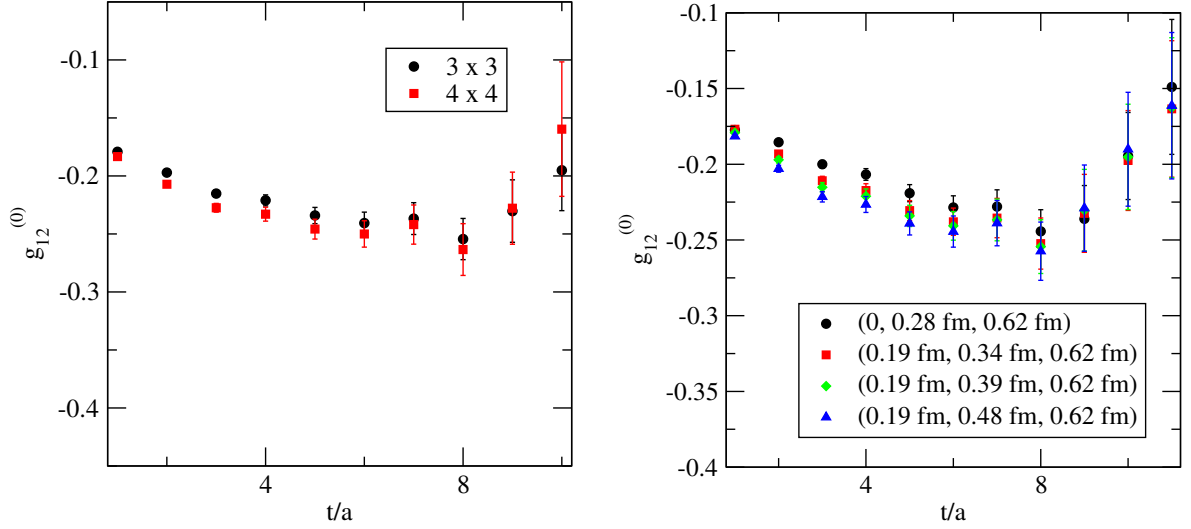


Figure 4.8 – Dependence of bare  $g_{12}$  on the size of the GEVP (left) and on the radius of wave functions (right) for the CLS ensemble E5g.

finding of [160] that using sGEVP (4.32) seems beneficial compared to the standard GEVP approach (4.31) to more strongly suppress contamination from higher excited states in the hadronic matrix element we measure. As illustrated in Figure 4.9, plateaus obtained from the GEVP and sGEVP are compatible:  $-0.25(1)$  for GEVP and  $-0.23(2)$  for sGEVP, with one additional point in the plateau of the sGEVP. Therefore, in the following we give results using the sGEVP only.

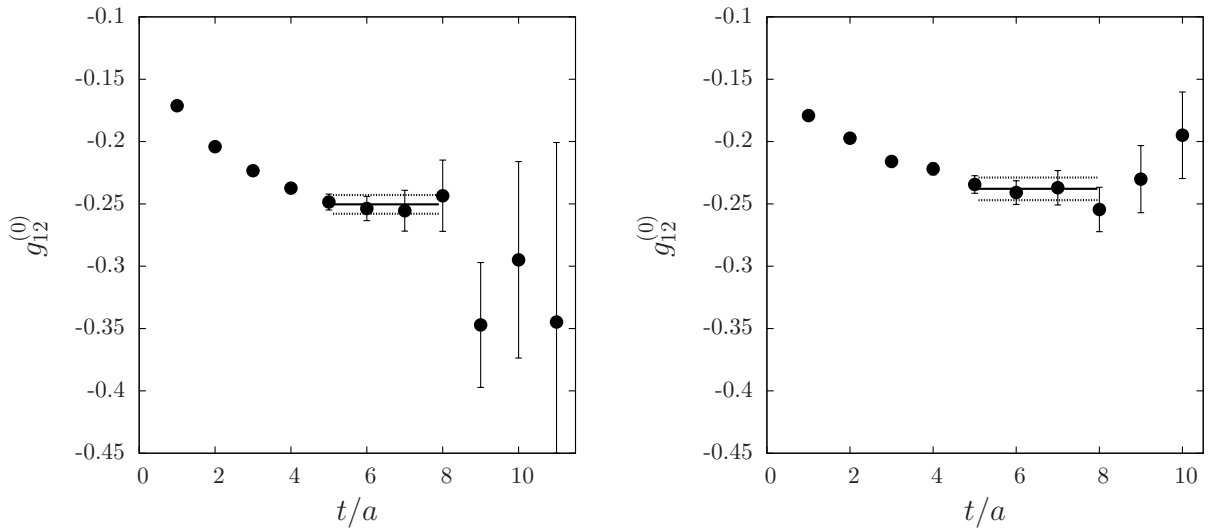


Figure 4.9 – Plateaus of bare  $g_{12}$  extracted by GEVP (left) and sGEVP (right) for the CLS ensemble E5g.

After applying a non-perturbative procedure to renormalize the axial light-light current [159, 52], we are ready to extrapolate to the continuum limit. Inspired by Heavy Meson Chiral Perturbation Theory at leading order [151, 154] and thanks to the  $\mathcal{O}(a)$  improvement of the three-point correlation functions, we apply two fit forms:

$$g_{12}(a, m_\pi) = C_0 + C_1 (a/a_{\beta=5.3})^2 + C_2 (m_\pi/m_\pi^{\text{exp}})^2, \quad (4.34)$$

$$g_{12}(a, m_\pi) = C'_0 + C'_1 (a/a_{\beta=5.3})^2. \quad (4.35)$$

We show in Figure 4.10 the continuum extrapolation (4.34) of  $g_{12}$ . We observe quite large cut-off effects ( $\sim 30\%$  at  $\beta = 5.3$ ), it is thus crucial to have several lattice spacings. We obtain finally, using (4.34) as the best estimate of the central value,

$$g_{12} = -0.17(3)(2), \quad (4.36)$$

where the first error is statistical, and the second error corresponds to the chiral uncertainty that we evaluate from the discrepancy between (4.34) and (4.35). We collect in Table 4.3 the value of  $g_{12}$  at each lattice point and the fit parameters for (4.34) and (4.35) are given in Table 4.4.

	A5	E5g	F6	N6
$a\Sigma_{12}^\infty$	0.255(8)	0.222(8)	0.216(12)	0.173(7)
$g_{12}$	-0.245(29)	-0.186(8)	-0.207(15)	-0.181(12)

Table 4.3 – Values of the mass splitting  $a\Sigma_{12}^\infty$  in lattice units and the coupling  $g_{12}$  for the different ensembles

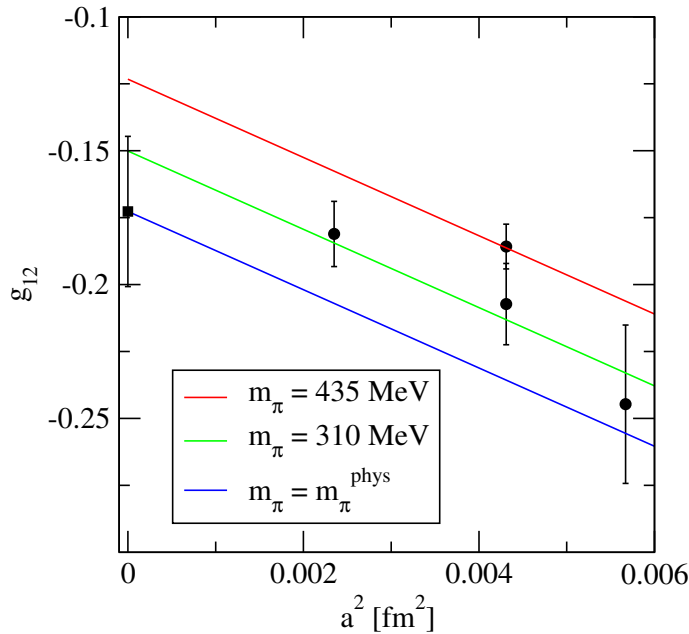


Figure 4.10 – Continuum and chiral extrapolation of  $g_{12}$ .

	fit (4.34)	fit (4.35)
$C_0$	-0.178(29)	-0.155(26)
$C_1$	-14.6(7.3)	-9.2(6.6)
$C_2$	0.29(16)	×

Table 4.4 – Fit parameters of eqs. (4.34), (4.35).

## 4.6 Decay thresholds

In simulations with light dynamical quarks, the onset of multi-hadron thresholds due to the emission of pions must be considered when examining excited  $B$  meson properties. Such thresholds significantly complicate the extraction of hadron-to-hadron matrix elements from the two- and three-point correlation functions considered here. In this section, we study the possibility of such strong decays on our lattices. Since parity and angular momentum are conserved, we have:

$$P_{B^{*'}} = P_H \times P_\pi \times (-1)^L \quad , \quad J_{B^{*'}} = L + J_H + S_\pi \quad ,$$

where  $P$  is the parity of the state. Since  $P_\pi = -1$ ,  $S_\pi = 0$ ,  $P_{B^{*'}} = -1$  and  $J_{B^{*'}} = 1$  the above relations become

$$\begin{aligned} 1 &= P_H \times (-1)^L \quad , \\ 1 &= L + J_H \quad , \end{aligned}$$

and we are left with only two possibilities. Either  $L = 0$ , then  $P_H = 1$  and  $J_H = 1$ , and the state corresponds to  $H = B_1^*$ . Either  $L = 1$ , then  $P_H = -1$  and  $J_H = 0$  which corresponds to the state  $H = B$ .

### Decay $B^{*'} \rightarrow B_1^* \pi$

The threshold for this decay is  $m_{B^{*'}} = m_{B_1^*} + m_\pi$  and, according to the results listed in Table 4.3, we have  $230 \text{ MeV} \leq \Sigma_{12} - m_\pi \leq 360 \text{ MeV}$ . If we assume that  $400 \text{ MeV} \lesssim m_{B_1^*} - m_B \lesssim 500 \text{ MeV}$  in the pion mass range  $[310, 440] \text{ MeV}$ , (as has been found in a recent lattice study of the static light meson spectrum [161]), we conclude that our analysis is safe from these threshold effects. These statements are also in good agreement with our result for the scalar  $B_0^*$  meson presented in the next chapter. Indeed, in the static limit of HQET, the mesons  $B_1^*$  and  $B_0^*$  are degenerate.

### Decay $B^{*'} \rightarrow B(\vec{p})\pi(-\vec{p})$

Since the heavy quark is static, this decay is not possible in our simulations.

## 4.7 Diagonal couplings $g_{11}$ and $g_{22}$

With our data, we can also extract the diagonal couplings  $g_{11}$  and  $g_{22}$ . In particular  $g_{11}$  is related to the  $g_{B^*B\pi}$  coupling in the Heavy Chiral Lagrangian (4.19) and represents the hadronic matrix element of the light axial current between the meson states

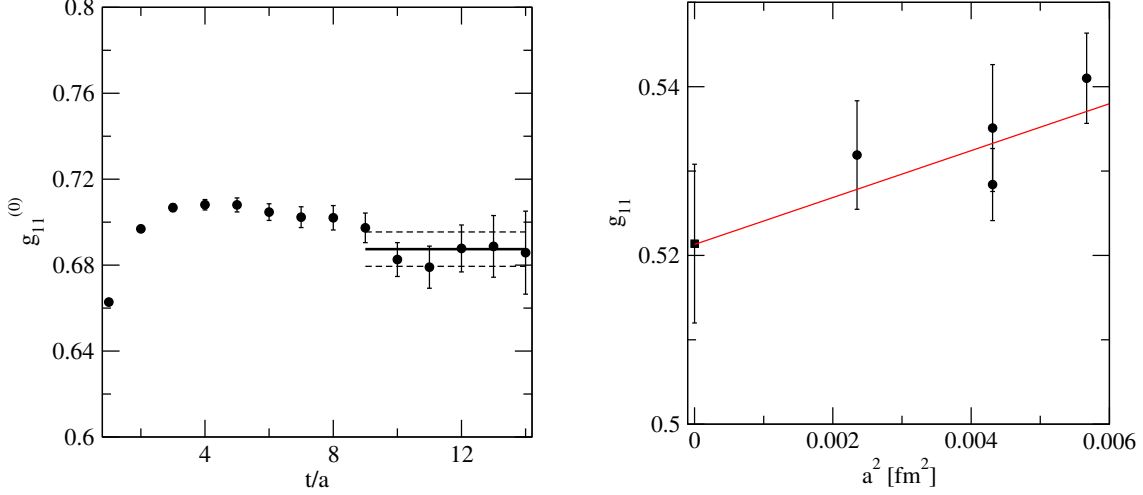


Figure 4.11 – Plateau of bare  $g_{11}$  for the CLS ensemble E5g (left) and its extrapolation to the continuum and chiral limit (right).

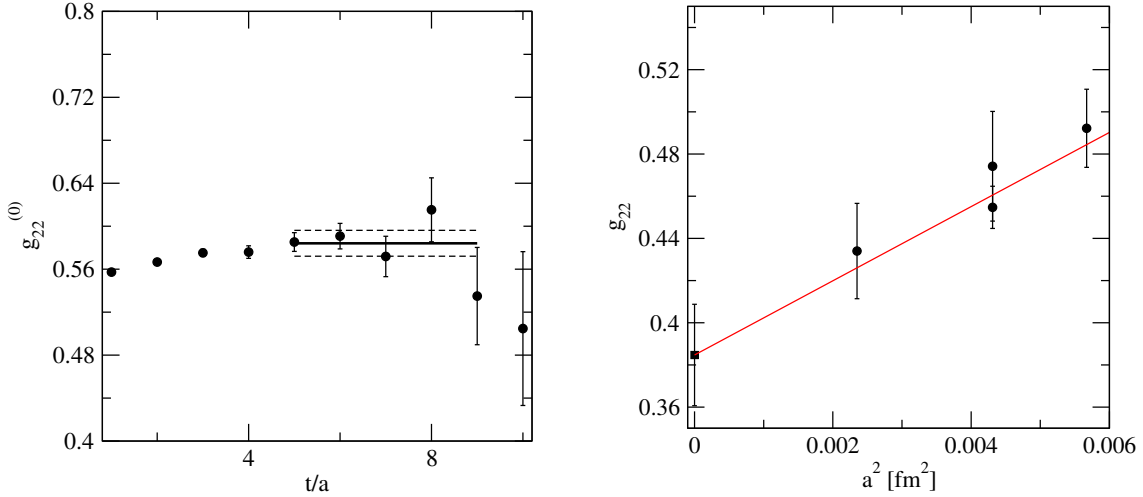


Figure 4.12 – Plateau of bare  $g_{22}$  for the CLS ensemble E5g (left) and its extrapolation to the continuum and chiral limit (right).

belonging to the doublet  $J^P = (0^-, 1^-)$ . Indeed, in the symmetric case and in the static limit of HQET, the contribution from the factor  $A_2$  in eq. (4.27) vanishes thanks to the mass degeneracy. Moreover, in the symmetric case, where  $n = m$ , the estimators given by eqs. (4.31), (4.32) become

$$\mathcal{M}_{nn}^{\text{GEVP}}(t_2, t_1) = \frac{(v_n(t_2), C^{(3)}(t_1 + t_2, t_1)v_n(t_1))}{(v_n(t_2), C^{(2)}(t_1 + t_2)v_n(t_2))}, \quad (4.37)$$

$$\mathcal{M}_{nn}^{\text{sGEVP}}(t, t_0) = -\partial_t \left( \frac{(v_n(t, t_0), [K(t, t_0)/\lambda_n(t, t_0) - K(t_0, t_0)]v_n(t, t_0))}{(v_n(t, t_0), C(t_0)v_n(t, t_0))} \right). \quad (4.38)$$

We show in Figure 4.11 a typical plateau of the bare coupling  $g_{11}$  and the extrapolation to the continuum and chiral limit. That extrapolation is smooth, with a negligible dependence on  $m_\pi$ , and we obtain from the fit form (4.34)

$$g_{11} = 0.52(2), \quad (4.39)$$

CLS	$g_{11}$	$g_{22}$
A5	0.541(5)	0.492(19)
E5g	0.535(8)	0.455(10)
F6	0.528(4)	0.474(26)
N6	0.532(6)	0.434(23)
physical point	0.516(12)(5)(10)	0.385(24)(28)

Table 4.5 – Value of  $g_{11}$  and  $g_{22}$  at the lattice points and at the physical point. The third error on  $g_{11}$  is an estimate of the effects of higher excited states.

this result is in excellent agreement with a computation by the ALPHA Collaboration focused on that quantity [100]. We have added an error of 2% due to higher excited states which is estimated from plateaus at early times with a range ending at  $\sim r_0$ . Following the same strategy, we show in Figure 4.12 a typical plateau of the bare coupling  $g_{22}$  and the extrapolation to the continuum and chiral limit, once again quite smooth, with an almost absent dependence on the sea quark mass. We obtain from the fit form (4.35)

$$g_{22} = 0.38(4). \quad (4.40)$$

Remarkably, the “diagonal” couplings  $g_{11}$  and  $g_{22}$  are significantly larger than the off-diagonal one  $g_{12}$ . This suggests that neglecting the contribution from  $B'$  mesons to the three-point light-cone sum rule used to obtain  $g_{B^*B\pi}$  introduces uncontrolled systematics. Note that the decay constant  $f_{B^*}$  itself is large compared to  $f_B$  [162, 104]. For completeness we have collected in Table 4.5 the values of  $g_{11}$  and  $g_{22}$  at each lattice point and at the physical point and the fit parameters of (4.34) and (4.35) are given in Table 4.6.

	$g_{11}$		$g_{22}$	
	fit (4.34)	fit (4.35)	fit (4.34)	fit (4.35)
$C_0$	0.515(13)	0.521(9)	0.416(27)	0.385(24)
$C_1$	0.012(9)	0.012(9)	0.074(25)	0.076(26)
$C_2$	0.0011(15)	×	-0.0033(33)	×

Table 4.6 – Fit parameters of eqs. (4.34) and (4.35)

## Conclusion

We have performed a first estimate of the axial form factor  $A_1(q_{\max}^2) \equiv g_{12}$  parameterizing at zero recoil the decay  $B^{*'} \rightarrow B$  in the static limit of HQET from  $N_f = 2$

lattice simulations. Four lattice ensembles at three lattice spacings and pion masses in the range [310–440] MeV were used to perform the continuum and chiral extrapolation. Assuming the positivity of decay constants  $f_B$  and  $f_{B^{*'}}$ , we have obtained a *negative* value for this form factor. It is almost three times smaller than the  $g_{11}$  coupling: we obtain  $g_{12} = -0.17(4)$  while  $g_{11} = 0.52(2)$ . Moreover we find  $g_{22} = 0.38(4)$ , which is not strongly suppressed with respect to  $g_{11}$ . Our work is a first hint of confirmation of the statement made in ref. [125] to explain the small value of  $g_{D^*D\pi}$  computed analytically when compared to experiment. This computation using light-cone Borel sum rules may have been too naive. Following ref. [158], a next step in our general study of excited static-light meson states would be the measurement of  $A_1(0)$  by computing the distribution in  $r$  of the axial density  $f_A(r) \equiv \langle B^{*'} | \bar{\psi}_l [\gamma^i \gamma^5 \psi_l](r) | B \rangle$  from which we can obtain  $A_1(0) = 4\pi \int_0^\infty r^2 f_A(r) e^{i\vec{q}\cdot\vec{r}} dr$  (see the discussion in Section 4.2.3).

# Chapter 5

## Computation of the soft pion coupling $h$

### Contents

---

<b>Introduction</b> . . . . .	<b>110</b>
<b>5.1 Strategy</b> . . . . .	<b>111</b>
5.1.1 Definition of the coupling . . . . .	111
5.1.2 Relation between continuum and lattice observables . . . . .	111
5.1.3 Extraction of $ax$ . . . . .	112
<b>5.2 Lattice setup</b> . . . . .	<b>114</b>
5.2.1 The interpolating operators basis . . . . .	115
5.2.2 Wick contractions . . . . .	116
5.2.3 Lattice computation . . . . .	118
<b>5.3 Signal analysis</b> . . . . .	<b>120</b>
5.3.1 Correlation functions . . . . .	120
5.3.2 One-end trick . . . . .	121
<b>5.4 Results</b> . . . . .	<b>122</b>
5.4.1 Contribution from <i>Box</i> and <i>Cross</i> diagrams . . . . .	122
5.4.2 Contribution from the mismatch $\Delta = m_{B_0^*} - E_{B\pi} \neq 0$ . . . . .	122
5.4.3 Extrapolations . . . . .	123
<b>5.5 Discussions</b> . . . . .	<b>126</b>
<b>Conclusion</b> . . . . .	<b>127</b>

---

## Introduction

In this chapter, I present the results on the computation of the soft pion coupling  $h$  which parametrizes the  $B_0^* \rightarrow B\pi$  hadronic transition in the Heavy Meson Chiral Lagrangian (4.19).

On the lattice, the inversion of the Dirac operator (1.27) gets more and more difficult as the light quark mass becomes small. Therefore, most simulations are performed at unphysical light quark masses and the results are extrapolated using fit formulae inspired by chiral perturbation theory. In the case of heavy-light mesons, one can use the Heavy Meson Chiral Perturbation Theory discussed in the previous chapter. In particular, the coupling  $g$  represents the hadronic matrix element between mesons belonging to the negative parity doublet  $J^P = (0^-, 1^-)$  and appears in chiral loops like the one depicted in Figure 5.1. Such terms were already used for the extrapolation of the  $B$  meson decay constant in Chapter 3. However, on the lattice, since the pion mass is not so small compared to the mass difference between the scalar and pseudoscalar  $B$  mesons, similar chiral loops including positive parity states  $J^P = (0^+, 1^+)$  should also be considered. Therefore, the knowledge of  $h$  is important, especially since this coupling is larger than  $g$  [115]. Finally, there is a third kind of diagrams that should also be considered, they involve the  $J^P = (0^+, 1^+)$  states and the corresponding coupling is denoted by  $\tilde{g}$ , however this coupling is relatively small [115].

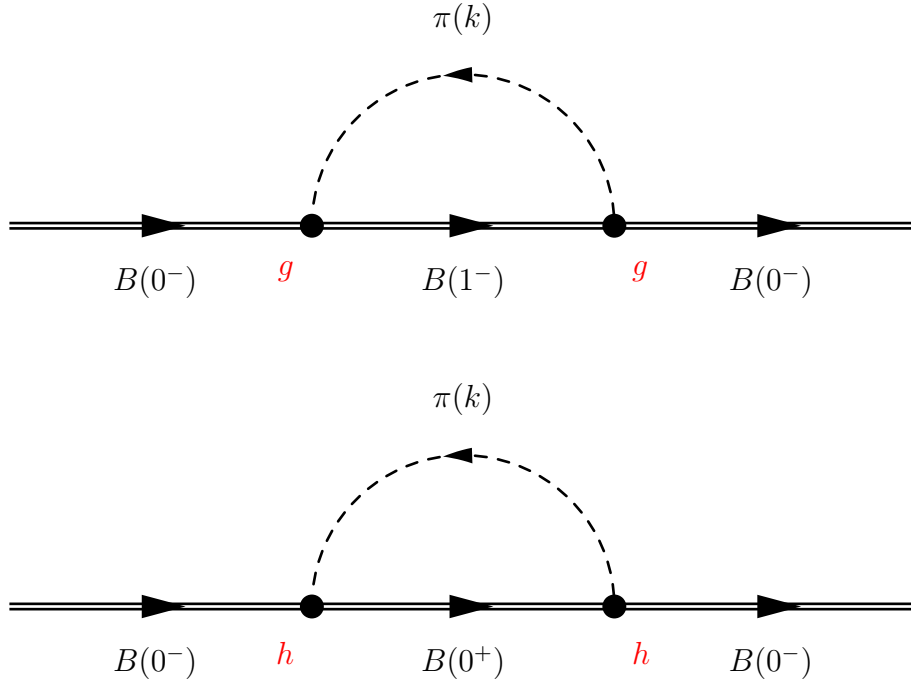


Figure 5.1 – Chiral loop diagrams contributing to the self-energy of the heavy meson. Double lines correspond to heavy meson propagators and dashed lines correspond to pion propagators. Each vertex is proportional to the effective coupling  $g$  or  $h$ .

The general method to deal with resonance states and strong decays on the lattice has been developed in refs. [163, 164]. The strategy is to compute the spectrum in the considered channel ( $J^P = 0^+$  in our case) and to compare it with the expected results for free particles. Indeed, due to the finite size of the lattice, asymptotic states do not exist and the two particles interact with each other. However, the energy shifts between the

interacting case and the free case, and due to interactions in finite volume, are related to the scattering phase shift in infinite volume, itself related to the mass and the width of the unstable particle. This procedure has been successfully applied in the case of light resonances like the  $\rho$  meson and, more recently, in the case of the  $D$  meson [165] but, due to the high numerical cost of the method, only one lattice ensemble was considered. In this work, we follow an alternative approach proposed in ref. [166] to compute the coupling constant associated with the hadronic transition  $B_0^* \rightarrow B\pi$  when we are near threshold.

## 5.1 Strategy

The computation of the effective coupling  $h$  could be performed similarly to  $g_{12}$  in the previous chapter. This strategy has been followed in ref. [115] where the authors have evaluated the corresponding three-point correlation functions and constructed ratios which converge to the corresponding matrix element. However, since the coupling relates two heavy-light mesons that are not degenerate in mass, one obtains the form factor at  $q_{\max}^2 = (m_{B_0^*} - m_B)^2$  and the result has to be extrapolated to the kinematical limit  $q^2 \rightarrow 0$ . This can be done by analyzing the radial distribution in  $r$  of the axial density as explained in the previous chapter (see eq. (4.28)). Here, we follow a different approach based on the computation of two-point correlation functions.

### 5.1.1 Definition of the coupling

The effective coupling  $h$  in the Heavy Meson Chiral Lagrangian (4.19) can be related to the coupling constant  $g_{B_0^*B\pi}$  which parametrizes the hadronic transition  $B_0^* \rightarrow B\pi$ . The computation is similar to the one presented in Section 4.2.2 and, in the static limit, we obtain

$$g_{B_0^*B\pi} = \langle \pi^\pm(q) B(p') | B_0^*(p) \rangle = \sqrt{m_B m_{B_0^*}} \frac{m_{B_0^*}^2 - m_B^2}{m_{B_0^*}} \frac{h}{f_\pi}, \quad (5.1)$$

where  $f_\pi = 130$  MeV is the pion decay constant.

### 5.1.2 Relation between continuum and lattice observables

In the next section, I will explain how the matrix element  $x = \langle B_0^* | B\pi \rangle$  can be extracted from the lattice by studying the mixing of hadronic states using two-point correlation functions. This matrix element is related to the coupling  $g_{B_0^*B\pi}$  through eq. (5.1) but the proportionality factor depends on the normalization of states. To obtain this normalization factor on the lattice, the authors in ref. [167] proposed to use the Fermi golden rule.

#### In the continuum

In the continuum theory, the two-body differential decay rate is given by

$$d\Gamma(B_0^* \rightarrow B\pi) = \frac{1}{2m_{B_0^*}} \left( \prod_{i=1}^2 \frac{d^3 p_i}{(2\pi)^3} \frac{1}{2E_i} \right) | \mathcal{A}(B_0^* \rightarrow B\pi) |^2 (2\pi)^4 \delta^{(4)}(p_{B_0^*} - p_B - p_\pi),$$

where  $\mathcal{A}$  is the S-matrix amplitude associated with the process  $B_0^* \rightarrow B\pi$  and  $p_i$  are the 4-momentum of the particles. In the center of mass frame, assuming the amplitude  $\mathcal{A}$  is independent of the exchanged momentum, we can perform the integration over the phase space to obtain

$$\Gamma(B_0^* \rightarrow B\pi) = \frac{|\vec{k}|}{8\pi m_{B_0^*}^2} g_{B_0^* B\pi}^2, \quad (5.2)$$

where

$$|\vec{k}| = \frac{\sqrt{\left(m_{B_0^*}^2 - (m_B + m_\pi)^2\right) \left(m_{B_0^*}^2 - (m_B - m_\pi)^2\right)}}{2m_{B_0^*}}, \quad (5.3)$$

is the momentum of the particles in the center of mass frame.

### On the lattice

On the lattice, the Fermi golden rule reads

$$\Gamma(B_0^* \rightarrow B\pi) = (2\pi)x^2\rho,$$

where  $x = \langle B_0^* | B\pi \rangle$  and  $\rho$  is the density of states, corresponding to the number of final states with a pion of momentum  $k$ :

$$\rho = \frac{L^3 k E_\pi}{2\pi^2}.$$

Finally, the proportionality factor between the transition rate and the matrix element  $ax$  computed on the lattice is given by

$$\frac{\Gamma(B_0^* \rightarrow B\pi)}{k} = \frac{1}{\pi} \left(\frac{L}{a}\right)^3 (aE_\pi) \times (ax)^2, \quad (5.4)$$

where  $aE_\pi$  is the pion mass computed on the lattice. Therefore, if  $ax$  is known on the lattice, we can use eqs. (5.4), (5.2) to obtain the coupling  $g_{B_0^* B\pi}$ , itself related to  $h$  via eq. (5.1). In the next section, I explain how  $ax$  is computed on the lattice.

### 5.1.3 Extraction of $ax$

The two lightest states with quantum numbers  $J^P = 0^+$  are the scalar  $B$  meson and the two-body state  $B(\vec{0})\pi(\vec{0})$  where the pion has relative momentum zero. Due to the finite extent of the lattice, the momenta of the particles take only discrete values  $\vec{p} = \frac{2\pi}{L}\vec{n}$  where  $\vec{n} \in \mathbb{Z}$  and the spectrum above threshold is not continuous. In practice, this spectrum is also far from being continuous: in the case of the CLS ensemble E5g which corresponds to a volume of  $\sim 2$  fm (Table 5.1), the first two-pion states have energies  $E_\pi(\vec{p} = \vec{0}) = m_\pi = 440$  MeV and  $E_\pi(p = \frac{2\pi}{L}) = \sqrt{m_\pi^2 + \vec{p}^2} \approx 740$  MeV respectively.

I follow the ideas presented in ref. [168] and in refs. [169, 167]. Assuming for the moment that the states are normalized to one and inserting the spectral decomposition

in the two-point correlation function, we obtain

$$\begin{aligned}
C_{B_0^*-B\pi}(t) &= \sum_{t_1} \langle 0 | \mathcal{O}^{B_0^*} | B_0^* \rangle x \langle B\pi | \mathcal{O}^{B\pi} | 0 \rangle e^{-m_{B_0^*} t_1} e^{-E_{B\pi}(t-t_1)} \\
&+ \sum_{t_1, t_2, t_3} \langle 0 | \mathcal{O}^{B_0^*} | B_0^* \rangle x^3 \langle B\pi | \mathcal{O}^{B\pi} | 0 \rangle e^{-m_{B_0^*} t_1} e^{-E_{B\pi}(t_2-t_1)} e^{-m_{B_0^*}(t_3-t_2)} e^{-E_{B\pi}(t-t_3)} \\
&+ \mathcal{O}(x^5) + \text{excited states}
\end{aligned} \tag{5.5}$$

where the contribution from excited states has been neglected and will be discussed later. Higher order terms,  $\mathcal{O}(x^5)$ , corresponding to multiple interactions, have also been neglected. I will show that  $x \ll 1$  in our simulations so that this assumption is indeed perfectly correct within our level of precision. Finally, in the case of degenerate states ( $m_{B_0^*} \approx E_{B\pi}$ ), the previous equation becomes

$$C_{B_0^*-B\pi}(t) = \langle 0 | \mathcal{O}^{B_0^*} | B_0^* \rangle x \langle B\pi | \mathcal{O}^{B\pi} | 0 \rangle \times t e^{-m_{B_0^*} t}. \tag{5.6}$$

Therefore, one can extract the matrix element  $ax$  by analyzing the asymptotic behavior of the ratio  $R(t)$  defined by

$$R(t) = \frac{C_{B_0^*-B\pi}(t)}{(C_{B_0^*-B_0^*}(t) C_{B\pi-B\pi}(t))^{1/2}} \approx xt, \tag{5.7}$$

where  $C_{B_0^*-B_0^*}(t)$  and  $C_{B\pi-B\pi}(t)$  are two-point correlation functions constructed with the interpolating operators  $\mathcal{O}^{B_0^*}$  and  $\mathcal{O}^{B\pi}$  respectively. When the energy of the two eigenstates are not exactly the same, the result depends on the mass difference  $\Delta = m_{B_0^*} - E_{B\pi}$ . For the linear term in  $x$ , the time dependence can be computed explicitly and one obtains the same formula after the following substitution

$$t \longrightarrow \frac{2}{\Delta} \sinh\left(\frac{\Delta}{2} t\right) = t + \frac{\Delta^2 t^3}{24} + \mathcal{O}(\Delta^4). \tag{5.8}$$

I will show in Section 5.4.2 that these corrections are very small with our lattice ensembles thanks to the smallness of the mass difference  $\Delta$ .

### Excited states

So far, the contribution from excited states has been completely neglected. However, as stressed in ref. [168], their contribution should be carefully studied. Neglecting multiple interactions as in eq. (5.6), but considering the excited states contribution, we obtain

$$C_{B_0^*-B\pi}(t) = \sum_{nm} \sum_{t_1} \langle 0 | \mathcal{O}^{B_0^*} | X_n \rangle x_{nm} \langle X_m | \mathcal{O}^{B\pi} | 0 \rangle e^{-E_n t_1} e^{-E_m(t-t_1)},$$

where  $x_{nm} = \langle X_n | X_m \rangle$ . Here,  $X_1 = B_0^*$ ,  $X_2 = B\pi$  and  $X_n$ ,  $n > 2$  correspond to higher excited states sorted in ascending order of energy. Clearly, since the time insertion  $t_1$  is implicitly summed over (contrary to the three-point correlation function studied in the previous chapter, there is no explicit dependence on  $t_1$ ), the contribution from the excited states cannot be disentangled from the ground state contribution if we are far from threshold.

To simplify the discussion, let us assume that  $E = m_{B_0^*} = E_{B\pi}$ , a good approximation in our case. Then, the contribution of an excited state, with energy  $E_3$ , has the form (here, I assume that this state has a non-negligible overlap with  $\mathcal{O}^{B_0^*}$ , the symmetric case corresponding to a non-negligible overlap with  $\mathcal{O}^{B\pi}$  is similar):

$$\begin{aligned} & \sum_{t_1} \langle 0 | \mathcal{O}^{B_0^*} | X_3 \rangle x_{32} \langle B\pi | \mathcal{O}^{B\pi} | 0 \rangle e^{-E_3 t_1} e^{-E(t-t_1)} \\ &= \langle 0 | \mathcal{O}^{B_0^*} | X_3 \rangle x_{32} \langle B\pi | \mathcal{O}^{B\pi} | 0 \rangle e^{-Et} \sum_{t_1} e^{(E_3-E)t_1} \\ &= \langle 0 | \mathcal{O}^{B_0^*} | B_0^* \rangle x \langle B\pi | \mathcal{O}^{B\pi} | 0 \rangle e^{-Et} \times \frac{\langle 0 | \mathcal{O}^{B_0^*} | X_3 \rangle x_{32}}{\langle 0 | \mathcal{O}^{B_0^*} | B_0^* \rangle x} \sum_{t_1} e^{(E_3-E)t_1}, \end{aligned}$$

where, in the last line, I have factorized out the ground state contribution. Since  $E_3 > E$ , the last sum over  $t_1$  converges rapidly to a constant. Therefore, comparing this result with the one obtained in eq. (5.6), we see that excited states contributions to  $C_{B_0^*-B\pi}(t)$  are suppressed by a factor  $t$  (to be compared with the usual exponential suppression in the general case, see eq. (2.22)). So, taking excited states into account, we get

$$R(t) = \frac{C_{B_0^*-B\pi}(t)}{(C_{B_0^*-B_0^*}(t)C_{B\pi-B\pi}(t))^{1/2}} \approx A + xt, \quad (5.9)$$

plus corrections which decrease exponentially with time.

### Generalized Eigenvalue Problem (GEVP)

The Generalized Eigenvalue Problem discussed in Section 2.5 can help to reduce the contamination from excited states by reducing their overlap factor with the interpolating operators  $\mathcal{O}^{B_0^*}$  and  $\mathcal{O}^{B\pi}$ . In this case, the estimator is given by

$$R^{\text{GEVP}}(t) = \frac{(v_{B_0^*}(t), C_{B_0^*-B\pi}(t), v_{B\pi}(t))}{\sqrt{(v_{B_0^*}(t), C_{B_0^*-B_0^*}(t), v_{B_0^*}(t)) \times (v_{B\pi}(t), C_{B\pi-B\pi}(t), v_{B\pi}(t))}}, \quad (5.10)$$

where the eigenvectors are computed using the best combination of interpolating operators. At large times, where the excited states contribution is small, the discrete derivative

$$x^{\text{eff}}(t) = \partial_t R^{\text{GEVP}}(t) = \frac{R^{\text{GEVP}}(t+a) - R^{\text{GEVP}}(t)}{a},$$

should converge to a plateau.

## 5.2 Lattice setup

Similarly to the previous chapter, we use a subset of the CLS ensembles presented in Chapter 3. From the experimental results summarized in Section 4.1.1, the mass difference between the ground state  $B$  meson and the scalar  $B_0^*$  meson is expected to be of the order of  $\sim 400$  MeV. Therefore, since our pion masses lie in the range  $[280 - 440]$  MeV, we are near threshold and the method presented in the previous section is perfectly suited.

CLS	$\beta$	$L^3 \times T$	$\kappa$	$a$ (fm)	$m_\pi$ (MeV)	# cfgs
B6	5.2	$48^3 \times 96$	0.13597	0.075	280	250
E5	5.3	$32^3 \times 64$	0.13625	0.065	440	450
F6		$48^3 \times 96$	0.13635		310	300
N6	5.5	$48^3 \times 96$	0.13667	0.048	340	250

Table 5.1 – Simulations parameters: the bare coupling constant  $\beta = 6/g_0^2$ , spatial extent in lattice units  $L$  (with  $T = 2L$ ), hopping parameter  $\kappa$ , lattice spacing  $a$  in physical units, pion mass  $m_\pi$  and number of configurations.

The quark-antiquark interpolating operators have the same quantum numbers as the  $B(\vec{0})\pi(\vec{0})$  system but couple only weakly to this state. Therefore, I have also considered meson-meson interpolating operators which are expected to have a better overlap with the two particle states. In our case, for isospin  $I = 1/2$ , they are formally given by

$$\mathcal{O}^{B\pi} = \left| \frac{1}{2}, \frac{1}{2} \right\rangle = \sqrt{\frac{2}{3}} \pi^+(0) B^-(0) - \sqrt{\frac{1}{3}} \pi^0(0) \bar{B}^0(0),$$

with

$$\begin{aligned} \bar{B}^0 &= \bar{d}b = \left| \frac{1}{2}, +\frac{1}{2} \right\rangle & \pi^+ &= \bar{d}u = |1, 1\rangle, \\ B^- &= \bar{u}b = \left| \frac{1}{2}, -\frac{1}{2} \right\rangle & \pi^0 &= \frac{1}{\sqrt{2}}(\bar{u}u - \bar{d}d) = |1, 0\rangle. \end{aligned}$$

### 5.2.1 The interpolating operators basis

The quark-antiquark interpolating operators correspond to

$$\mathcal{O}_{\Gamma,n}^B(t) = \frac{1}{V} \sum_{\vec{x}} \left[ \bar{d}^{(n)}(x) \Gamma b(x) \right] = \frac{1}{V} \sum_{\vec{x}} \bar{\psi}_l^{(n)}(x) \Gamma \psi_h(x),$$

where  $\Gamma$  is chosen such that  $\mathcal{O}_{\Gamma,n}^B$  has the quantum numbers  $J^P = 0^+$  for the scalar meson and  $J^P = 0^-$  for the pseudoscalar meson, and are listed in Table 5.2.  $\psi_l^{(n)}$  corresponds to the light field  $\psi_l$  after  $R_n$  iterations of Gaussian smearing

$$\psi_l^{(n)}(x) = (1 + \kappa_G a^2 \Delta)^{R_n} \psi_l(x).$$

I have implemented two different kinds of operators: the local operators where  $\Gamma = \gamma_0$  or  $\Gamma = \gamma_5$  and the non-local operators where  $\Gamma = \gamma_i \overleftarrow{\nabla}_i^s$  or  $\Gamma = \gamma_i \gamma_0 \gamma_5 \overleftarrow{\nabla}_i^s$  where  $\overleftarrow{\nabla}_i^s$  is the symmetrized covariant derivative applied on the light quark. Finally, writing  $\bar{\Gamma} = \gamma_0 \Gamma^\dagger \gamma_0$ , one obtains

$$\mathcal{O}_{\Gamma,n}^{B\dagger}(t) = \frac{1}{V} \sum_{\vec{x}} \bar{\psi}_h(x) \bar{\Gamma} \psi_l^{(n)}(x).$$

In the case of meson-meson interpolating operators, I have only considered local interpolating fields with gaussian smearing applied to the light field. Therefore, with  $\Gamma = \gamma_5$ , I obtain

$$\mathcal{O}_{\Gamma,n}^{B\pi} = \frac{1}{V^2} \sum_{\vec{x}_i} \sqrt{\frac{2}{3}} [\bar{d}(x_1)\Gamma u(x_1)] [\bar{u}^{(n)}(x_2)\Gamma b(x_2)] - \sqrt{\frac{1}{6}} [\bar{u}(x_1)\Gamma u(x_1) - \bar{d}(x_1)\Gamma d(x_1)] \times [\bar{d}^{(n)}(x_2)\Gamma b(x_2)] ,$$

and

$$\mathcal{O}_{\Gamma,n}^{B\pi^\dagger} = \frac{1}{V^2} \sum_{\vec{x}_i} \sqrt{\frac{2}{3}} [\bar{b}(x_2)\bar{\Gamma} u^{(n)}(x_2)] [\bar{u}(x_1)\bar{\Gamma} d(x_1)] - \sqrt{\frac{1}{6}} [\bar{b}(x_2)\bar{\Gamma} d^{(n)}(x_2)] [\bar{u}(x_1)\bar{\Gamma} u(x_1) - \bar{d}(x_1)\bar{\Gamma} d(x_1)] .$$

$J^P$	Local			Non local		
$0^-$	$\Gamma = \gamma_5$	$\Gamma^\dagger = \Gamma$	$\bar{\Gamma} = -\Gamma$	$\Gamma = \gamma_i \gamma_0 \gamma_5 \overleftarrow{\nabla}_i^s$	$\Gamma^\dagger = -\bar{\Gamma}$	$\bar{\Gamma} = -\bar{\Gamma}$
$0^+$	$\Gamma = \gamma_0$	$\Gamma^\dagger = \Gamma$	$\bar{\Gamma} = \Gamma$	$\Gamma = \gamma_i \overleftarrow{\nabla}_i^s$	$\Gamma^\dagger = \bar{\Gamma}$	$\bar{\Gamma} = -\bar{\Gamma}$

Table 5.2 – Local and non-local interpolating operators used in this chapter for the pseudoscalar and scalar  $B$  meson.

## 5.2.2 Wick contractions

### • $B - B$ correlation functions

Correlation functions with quark-antiquark interpolating operators are computed for both scalar and pseudoscalar quantum numbers. They are given by

$$C_{B-B}^{nm}(t) = \langle \mathcal{O}_{\Gamma_1,n}^B(t) \mathcal{O}_{\Gamma_2,m}^B(0)^\dagger \rangle = -\frac{1}{V^2} \sum_{\vec{x},\vec{y}} \text{Tr} [G_l^{mn}(y,x) \Gamma_1 G_h(x,y) \bar{\Gamma}_2] \quad (5.11)$$

and correspond to the diagram depicted in Figure 5.2.

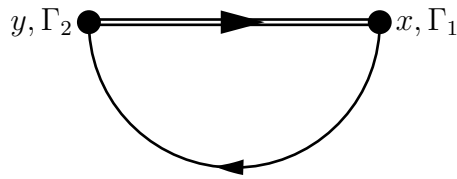


Figure 5.2 – Diagram corresponding to the two-point correlation function  $C_{B-B}^{nm}(t)$ .

- $B\pi - B\pi$  correlation functions

In this case, only local operators are considered and we obtain ( $\Gamma = \gamma_5$ ):

$$\begin{aligned} \langle \mathcal{O}_{\Gamma,n}^{B\pi}(t) \mathcal{O}_{\Gamma,m}^{B\pi}(0)^\dagger \rangle &= \frac{2}{3V^4} \sum_{\vec{x}_i, \vec{y}_i} \langle [\bar{d}(x_1) \Gamma u(x_1)] [\bar{u}^{(n)}(x_2) \Gamma b(x_2)] [\bar{b}(y_2) \bar{\Gamma} u^{(m)}(y_2)] [\bar{u}(y_1) \bar{\Gamma} d(y_1)] \rangle \\ &+ \frac{1}{6V^4} \sum_{\vec{x}_i, \vec{y}_i} [\bar{u}(x_1) \Gamma u(x_1) - \bar{d}(x_1) \Gamma d(x_1)] [\bar{d}^{(n)}(x_2) \Gamma b(x_2)] [\bar{b}(y_2) \bar{\Gamma} d^{(m)}(y_2)] [\bar{u}(y_1) \bar{\Gamma} u(y_1) \\ &\hspace{20em} - \bar{d}(y_1) \bar{\Gamma} d(y_1)] \\ &- \frac{1}{3V^4} \sum_{\vec{x}_i, \vec{y}_i} [\bar{d}(x_1) \Gamma u(x_1)] [\bar{u}^{(n)}(x_2) \Gamma b(x_2)] [\bar{b}(y_2) \bar{\Gamma} d^{(m)}(y_2)] [\bar{u}(y_1) \bar{\Gamma} u(y_1) - \bar{d}(y_1) \bar{\Gamma} d(y_1)] \\ &- \frac{1}{3V^4} \sum_{\vec{x}_i, \vec{y}_i} [\bar{u}(x_1) \Gamma u(x_1) - \bar{d}(x_1) \Gamma d(x_1)] [\bar{d}^{(n)}(x_2) \Gamma b(x_2)] [\bar{b}(y_2) \bar{\Gamma} u^{(m)}(y_2)] [\bar{u}(y_1) \bar{\Gamma} d(y_1)] \end{aligned}$$

where the details of the Wick contractions are given in Appendix C. The result reads

$$C_{B\pi-B\pi}^{mm}(t) = \frac{\alpha}{V^4} \sum_{\vec{x}_i, \vec{y}_i} \text{Tr} [G_l(y_1, x_1) \Gamma G_l(x_1, y_1) \bar{\Gamma}] \text{Tr} [G_h(y_2, x_2) \Gamma G_l^{nm}(x_2, y_2) \bar{\Gamma}] \quad (5.12)$$

$$+ \frac{\beta}{V^4} \sum_{\vec{x}_i, \vec{y}_i} \text{Tr} [G_l(y_1, x_1) \Gamma G_l^{0n}(x_1, x_2) \Gamma G_h(x_2, y_2) \bar{\Gamma} G_l^{m0}(y_2, y_1) \bar{\Gamma}] \quad (5.13)$$

$$+ \frac{\gamma}{V^4} \sum_{\vec{x}_i, \vec{y}_i} \text{Tr} [G_l^{0n}(y_1, x_2) \Gamma G_h(x_2, y_2) \bar{\Gamma} G_l^{m0}(y_2, x_1) \Gamma G_l(x_1, y_1) \bar{\Gamma}] \quad (5.14)$$

where  $\alpha = 1$ ,  $\beta = -3/2$  and  $\gamma = 1/2$ . They are associated with the *direct*, *box* and *cross* diagrams depicted in Figure 5.3.

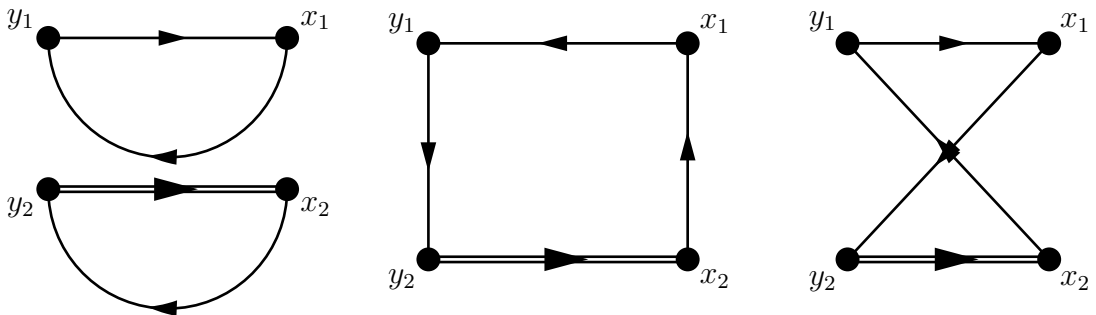


Figure 5.3 – Direct, box and cross diagrams for the  $C_{B\pi-B\pi}^{mm}(t)$  correlation functions.

- $B\pi - B_0^*$  et  $B_0^* - B\pi$  correlation functions

Finally, we need to compute the crossed correlation functions with both quark-antiquark and meson-meson interpolating operators (Figure 5.4). Here  $\Gamma_1 = \gamma_5$  has the quantum numbers of the pseudoscalar meson and  $\Gamma_2$  has the quantum numbers of

the scalar meson:

$$\begin{aligned} \langle \mathcal{O}_{\Gamma_1, n}^{B\pi}(t) \mathcal{O}_{\Gamma_2, m}^{B_0^* \dagger}(0) \rangle &= \sqrt{\frac{2}{3}} \frac{1}{V^3} \sum_{\vec{x}_i, \vec{y}} \langle [\bar{d}(x_1) \Gamma_1 u(x_1)] [\bar{u}^{(n)}(x_2) \Gamma_1 b(x_2)] [\bar{b}(y) \bar{\Gamma}_2 d^{(m)}(y)] \rangle \\ &\quad - \sqrt{\frac{1}{6}} \frac{1}{V^3} \sum_{\vec{x}_i, \vec{y}} [\bar{u}(x_1) \Gamma_1 u(x_1) - \bar{d}(x_1) \Gamma_1 d(x_1)] [\bar{d}^{(n)}(x_2) \Gamma_1 b(x_2)] [\bar{b}(y) \bar{\Gamma}_2 d^{(m)}(y)] \end{aligned}$$

and the result of the Wick contractions reads

$$C_{B\pi-B_0^*}^{nm}(t) = -\frac{1}{V^3} \sqrt{\frac{3}{2}} \sum_{\vec{x}_i, \vec{y}} \text{Tr} [G_l^{m0}(y, x_1) \Gamma_1 G_l^{0n}(x_1, x_2) \Gamma_1 G_h(x_2, y) \bar{\Gamma}_2] . \quad (5.15)$$

Similarly, the correlation function  $C_{B_0^*-B\pi}^{nm}(t)$  is given by

$$\begin{aligned} \langle \mathcal{O}_{\Gamma_2, n}^{B_0^*}(t) \mathcal{O}_{\Gamma_1, m}^{B\pi \dagger}(0) \rangle &= \sqrt{\frac{2}{3}} \frac{1}{V^3} \sum_{\vec{y}_i, \vec{x}} \langle [\bar{d}^{(n)}(x) \Gamma_2 b(x)] [\bar{b}(y_2) \bar{\Gamma}_1 u^{(m)}(y_2)] [\bar{u}(y_1) \bar{\Gamma}_1 d(y_1)] \rangle \\ &\quad - \sqrt{\frac{1}{6}} \frac{1}{V^3} \sum_{\vec{y}_i, \vec{x}} [\bar{d}^{(n)}(x) \Gamma_2 b(x)] [\bar{b}(y_2) \bar{\Gamma}_1 d^{(m)}(y_2)] [\bar{u}(y_1) \bar{\Gamma}_1 u(y_1) - \bar{d}(y_1) \bar{\Gamma}_1 d(y_1)] \end{aligned}$$

and, after performing the Wick contractions, we get

$$C_{B_0^*-B\pi}^{nm}(t) = -\frac{1}{V^3} \sqrt{\frac{3}{2}} \sum_{\vec{y}_i, \vec{x}} \text{Tr} [G_l^{m0}(y_2, y_1) \bar{\Gamma}_1 G_l^{0n}(y_1, x) \Gamma_2 G_h(x, y_2) \bar{\Gamma}_1] . \quad (5.16)$$

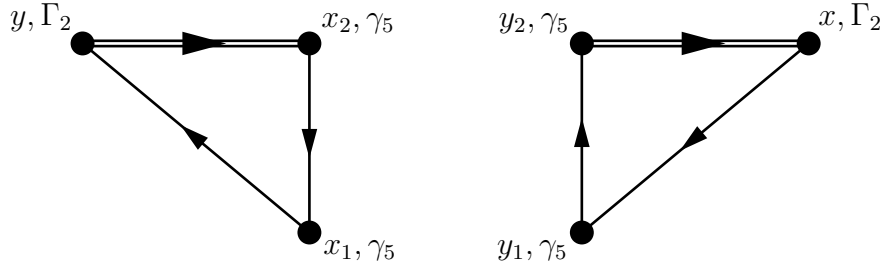


Figure 5.4 – Triangle diagrams for the  $C_{B\pi-B_0^*}^{nm}(t)$  and  $C_{B_0^*-B\pi}^{nm}(t)$  correlation functions.

### 5.2.3 Lattice computation

The light quark propagator is evaluated by using stochastic sources with full-time dilution as explained in Section 2.3 and the solution vector, corresponding to the source  $\eta$ , is denoted  $\psi_\eta$ . The heavy quark propagator in the static limit is given by eq. (3.16) and is trivial to evaluate since no matrix inversion is required.

The two-point correlation functions for the  $B$  meson, with quark-antiquark interpolating operators, are given by

$$\begin{aligned} C_{B-B}^{nm}(t) &= -\frac{1}{V^2} \sum_{\vec{x}, \vec{y}} \text{Tr} [G_l^{mn}(y, x) \Gamma_1 G_h(x, y) \bar{\Gamma}_2] \delta(t + t_y - t_x) \\ &= \pm \frac{1}{V N_s} \sum_{\vec{x}, s} \text{Tr} \left[ (P_+ \mathcal{P}(y, x) \Gamma_1 \eta^{(n)}(x))^\dagger (\Gamma_2 \psi_\eta^{(m)}(y)) \right] \Big|_{\vec{x}=\vec{y}} \delta(t + t_y - t_x), \end{aligned}$$

where the trace is taken over Dirac and color indices. The global sign  $\pm$  depends on the choice of the interpolating operator and the results are summarized in Table 5.3.

$J^P$	loc-loc	loc-der	der-loc	der-der
$0^-$	+	+	-	-
$0^+$	-	+	-	+

Table 5.3 – Global sign of the two-point correlation functions  $C_{B-B}^{nm}(t)$ . The abbreviations loc and der correspond to local and derivative interpolating operators respectively.

The correlation functions with meson-meson interpolating operators require at least two inversions of the Dirac operator. The solution vector  $\psi_\eta$  is multiplied by the matrix  $\gamma_5$  and used as a secondary source, the new solution is denoted  $\psi_{\bar{\eta}}$

$$\psi_{\bar{\eta}}(x) = \sum_{\vec{y}_1} G_l(x, y_1) \gamma_5 \psi_\eta(y_1) = \sum_{\vec{y}_1, \vec{x}_1} G_l(x, y_1) \gamma_5 G_l(y_1, x_1) \eta(x_1).$$

Therefore,  $\psi_{\bar{\eta}}(y_2)$  is an estimator of the product of two propagators  $G_l(y_2, y_1) \gamma_5 G_l(y_1, x_1)$ . Using the  $\gamma_5$ -hermiticity of the propagator,  $G_l(x, y) = \gamma_5 G_l^\dagger(y, x) \gamma_5$ , we find

$$\begin{aligned} C_{\text{box}}^{mm}(t) &= \frac{1}{V^4} \sum_{\vec{x}_i, \vec{y}_i} \text{Tr} [G_h(x_2, y_2) \gamma_5 G_l^{m0}(y_2, y_1) \gamma_5 G_l(y_1, x_1) \gamma_5 G_l^{0n}(x_1, x_2) \gamma_5] \delta(t + t_y - t_x) \\ &= \frac{1}{V^4} \sum_{\vec{x}_i, \vec{y}_i} \text{Tr} [G_h(x_2, y_2) \gamma_5 G_l^{m0}(y_2, y_1) \gamma_5 G_l(y_1, x_1) G_l^{m0}(x_2, x_1)^\dagger] \delta(t + t_y - t_x) \\ &= \frac{1}{V^4 N_s} \sum_{\vec{x}_2, \vec{y}_2, s} \text{Tr} [G_h(x_2, y_2) \gamma_5 \psi_{\bar{\eta}}^{(m)}(y_2) \psi_\eta^{(n)\dagger}(x_2)] \delta(t + t_y - t_x) \\ &= \frac{1}{V^3 N_s} \sum_{\vec{x}_2, s} \text{Tr} \left[ \left( P_+ \mathcal{P}(y_2, x_2) \psi_\eta^{(n)}(x_2) \right)^\dagger \left( \gamma_5 \psi_{\bar{\eta}}^{(m)}(y_2) \right) \right] \Big|_{\vec{x}_2 = \vec{y}_2} \delta(t + t_y - t_x), \end{aligned} \quad (5.17)$$

and for the *cross* diagram

$$\begin{aligned} C_{\text{cross}}^{mm}(t) &= \frac{1}{V^4} \sum_{x_i} \text{Tr} [G_h(x_2, y_2) \gamma_5 G_l^{m0}(y_2, x_1) \gamma_5 G_l(x_1, y_1) \gamma_5 G_l^{0n}(y_1, x_2) \gamma_5] \delta(t + t_y - t_x) \\ &= \frac{1}{V^4} \sum_{\vec{x}_i, \vec{y}_i} \text{Tr} [G_h(x_2, y_2) \gamma_5 G_l^{m0}(y_2, x_1) (G_l^{n0}(x_2, y_1) \gamma_5 G_l(y_1, x_1))^\dagger] \delta(t + t_y - t_x) \\ &= \frac{1}{V^4 N_s} \sum_{\vec{x}_2, \vec{y}_2, s} \text{Tr} [G_h(x_2, y_2) \gamma_5 \psi_{\bar{\eta}}^{(m)}(y_2) \psi_\eta^{(n)\dagger}(x_2)] \delta(t + t_y - t_x) \\ &= \frac{1}{V^3 N_s} \sum_{\vec{x}_2, s} \text{Tr} \left[ \left( P_+ \mathcal{P}(y_2, x_2) \psi_\eta^{(n)}(x_2) \right)^\dagger \left( \gamma_5 \psi_{\bar{\eta}}^{(m)}(y_2) \right) \right] \Big|_{\vec{x}_2 = \vec{y}_2} \delta(t + t_y - t_x). \end{aligned} \quad (5.18)$$

The box and cross diagrams are much more expensive to compute numerically since they require a second inversion of the Dirac operator for each intermediate time.

Finally, we have to consider the case where one interpolating operator ( $\Gamma_1 = \gamma_5$ ) is a quark-antiquark operator and the other one is a meson-meson operator ( $\Gamma_2$ )

$$\begin{aligned} C_{B\pi^*-B_0^*}^{mm}(t) &= -\sqrt{\frac{3}{2}} \frac{1}{V^3} \sum_{\vec{x}_i, \vec{y}} \text{Tr} [G_h(x_2, y) \bar{\Gamma}_2 G_l^{m0}(y, x_1) \gamma_5 G_l^{0n}(x_1, x_2) \gamma_5] \delta(t + t_y - t_x) \\ &= \pm \sqrt{\frac{3}{2}} \frac{1}{V^2 N_s} \sum_{\vec{x}_2, s} \text{Tr} \left[ (P_+ \mathcal{P}(y, x_2) \psi_\eta^{(n)}(x_2))^\dagger (\Gamma_2 \psi_\eta^{(m)}(y)) \right] \Big|_{\vec{x}_2 = \vec{y}} \delta(t + t_y - t_x), \end{aligned}$$

where the minus or plus signs correspond to local and derivative interpolating operators respectively. Similarly, for the second diagram, we obtain

$$\begin{aligned} C_{B_0^*-B\pi}^{mm}(t) &= -\sqrt{\frac{3}{2}} \frac{1}{V^3} \sum_{\vec{x}, \vec{y}_i} \text{Tr} [G_h(x, y_2) \gamma_5 G_l^{m0}(y_2, y_1) \gamma_5 G_l^{0n}(y_1, x) \Gamma_2] \delta(t + t_y - t_x) \\ &= \pm \sqrt{\frac{3}{2}} \frac{1}{V^2 N_s} \sum_{\vec{x}, s} \text{Tr} \left[ (P_- \mathcal{P}(y_2, x) \Gamma_2^\dagger \psi_\eta^{(n)}(x))^\dagger (\psi_\eta^{(m)}(y_2)) \right] \Big|_{\vec{x} = \vec{y}_2} \delta(t + t_y - t_x), \end{aligned} \quad (5.19)$$

and in this case, the minus (plus) sign corresponds to local (derivative) interpolating operators. To keep the same notation as before (the stochastic source in  $x$ ), I write

$$C_{B_0^*-B\pi}^{mm}(t) = +\sqrt{\frac{3}{2}} \frac{1}{V^2 N_s} \sum_{\vec{z}, \vec{x}_2, s} \text{Tr} \left[ (P_- \mathcal{P}(x_2, z) \Gamma_2 \psi_\eta^{(n)}(z))^\dagger (\psi_\eta^{(m)}(x_2)) \right] \Big|_{\vec{x}_2 = \vec{z}} \delta(t + t_x - t_z).$$

For these correlation functions, I have also tested an other estimator where the first solution vector  $\psi_\eta(x)$  is used as a secondary source. The solution is then denoted  $\psi_{\tilde{\eta}}$  and we find

$$\begin{aligned} C_{B_0^*-B\pi}^{mm}(t) &= -\sqrt{\frac{3}{2}} \frac{1}{V^3} \sum_{\vec{x}, \vec{y}_i} \text{Tr} [G_h(x, y_2) \gamma_5 G_l^{m0}(y_2, y_1) \gamma_5 G_l^{0n}(y_1, x) \Gamma_2] \delta(t + t_y - t_x) \\ &= -\sqrt{\frac{3}{2}} \frac{1}{V^3 N_s} \sum_{\vec{x}, \vec{y}_2, s} \text{Tr} [G_h(x, y_2) \gamma_5 \psi_{\tilde{\eta}}^{(m)}(y_2) \eta^{(n)\dagger}(x) \Gamma_2] \delta(t + t_y - t_x) \\ &= -\sqrt{\frac{3}{2}} \frac{1}{V^2 N_s} \sum_{\vec{x}, s} \text{Tr} \left[ (P_+ \mathcal{P}(y_2, x) \Gamma_2 \eta^{(n)}(x))^\dagger (\gamma_5 \psi_{\tilde{\eta}}^{(m)}(y_2)) \right] \Big|_{\vec{x} = \vec{y}_2} \delta(t + t_y - t_x). \end{aligned} \quad (5.20)$$

In the next section, I discuss which method offers the best results.

## 5.3 Signal analysis

### 5.3.1 Correlation functions

In Figure 5.5, I plot the evolution of the statistical errors for the correlation functions  $C_{B_0^*-B\pi}(t)$  for local and derivative interpolating operators. The statistical error is rather independent of the number of smearing iterations.

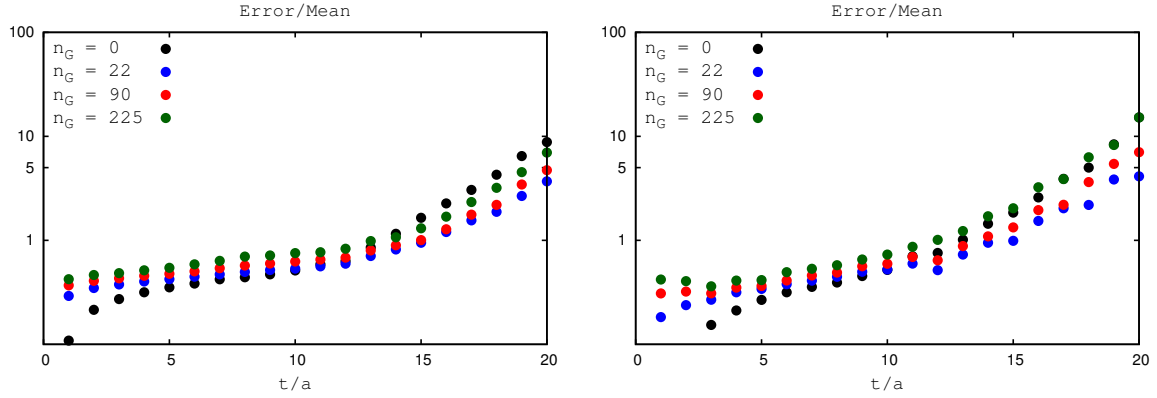


Figure 5.5 – The right (left) plot shows the evolution of the statistical error for  $C_{B_0^* - B\pi}(t)$  in percent for local (derivative) interpolating operators and for the different levels of smearing. The results correspond to the lattice ensemble E5g.

### 5.3.2 One-end trick

As explained in the previous section, the correlation function  $C_{B_0^* - B\pi}(t)$  has been computed using two different methods. In the first method, I perform only one source inversion and use the  $\gamma_5$ -hermiticity of the propagator to evaluate the two light-quark propagators (see eq. (5.19)). In the second method, I use the first solution vector as a secondary source and perform a second inversion of the Dirac operator to evaluate the product of the two quark propagators (see eq. (5.20)). In Figure 5.6, I compare the growth of the statistical error with time for both methods. The first method is clearly the optimal choice with our sources and statistics, therefore I will only use this one in the next sections.

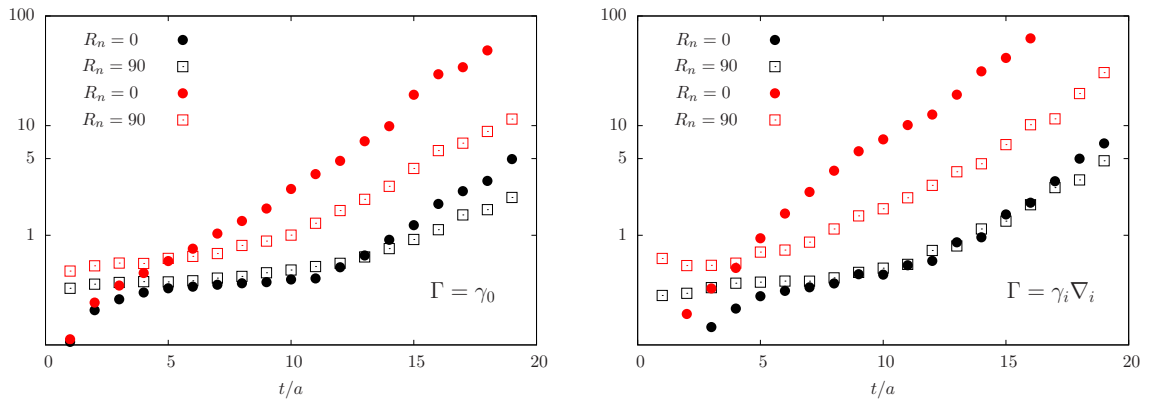


Figure 5.6 – Comparison of the statistical error (in percent) for the correlation functions  $C_{B_0^* - B\pi}(t)$  for the two different methods explained in the text (HYP1 action). The black points correspond to the one-end-trick and the red one to the double inversion of the lattice Dirac operator. On the left, for local interpolating operators. On the right, for derivative interpolating operators. The results correspond to the lattice ensemble E5g.

## 5.4 Results

### 5.4.1 Contribution from *Box* and *Cross* diagrams

In the case of the ensemble E5g, we have also computed the box and cross diagrams respectively given by eqs. (5.17), (5.18). As can be seen from Figure 5.7, their contributions are rather small compared to the direct one.

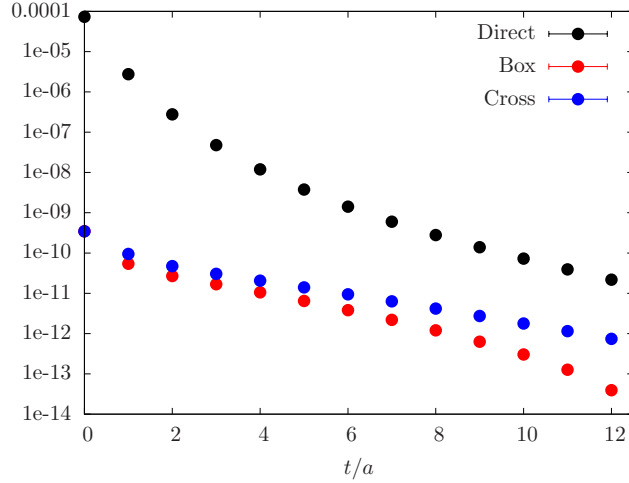


Figure 5.7 – Contributions from direct, cross and box diagrams to the two-point correlation function. The direct diagram in black gives the dominant contribution.

Neglecting the box and cross diagrams, I obtain  $ax = 0.0241(10)$  and  $h = 0.84(5)$  for the HYP1 action. When they are taken into account, I find  $ax = 0.0228(10)$  and  $h = 0.78(5)$ . Therefore the two results are compatible within our errors and the computation of these diagrams does not seem necessary at our level of precision.

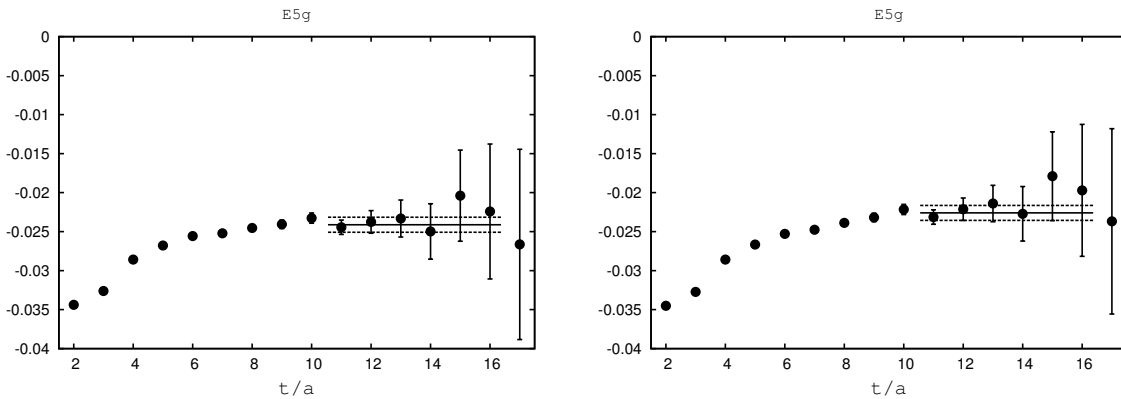


Figure 5.8 – Values of  $x^{\text{eff}}(t)$ . On the left: neglecting the box and cross diagrams, on the right: taking into account the box and cross diagrams.

### 5.4.2 Contribution from the mismatch $\Delta = m_{B_0^*} - E_{B\pi} \neq 0$

I have computed the mass difference between the scalar and the pseudoscalar mesons on our lattice ensemble. The results are summarized in Table 5.4. In all cases, the

quantity  $a\Delta = am_{B_0^*} - aE_{B\pi}$  is very small and the corrections in eq. (5.8), proportional to  $\Delta^2 t^3$ , are negligible. Indeed, we have

$$\frac{3t^2\Delta^2}{24} \ll 1 \quad \text{for } t \in [0 - 20],$$

and the deviation from a constant cannot be seen within our error bars. It should be stressed that, on the lattice, we don't have directly access to the mass of the resonance and a more careful study should be done. Nevertheless, the deviations are expected to be small and should not change the conclusion. The linear behavior of the triangle diagram for ensemble E5g and N6 is depicted in Figure 5.9.

CLS	HYP	$am_{B_0^*} - am_B$	$am_\pi$	$a\Delta$
B6	HYP1	0.143(4)	0.1073(7)	0.036(4)
	HYP2	0.141(4)	0.1073(7)	0.034(4)
E5	HYP1	0.133(6)	0.1454(5)	-0.012(6)
	HYP2	0.133(6)	0.1454(5)	-0.012(6)
F6	HYP1	0.130(8)	0.1036(5)	0.026(8)
	HYP2	0.129(3)	0.1036(5)	0.025(3)
N6	HYP1	0.094(3)	0.0837(4)	0.010(3)
	HYP2	0.092(3)	0.0837(4)	0.008(3)

Table 5.4 – Mass splitting,  $a\Delta = am_{B_0^*} - aE_{B\pi}$ , between the scalar  $B_0^*$  meson and the two particles state  $B(\vec{0})\pi(\vec{0})$  for each CLS ensemble.

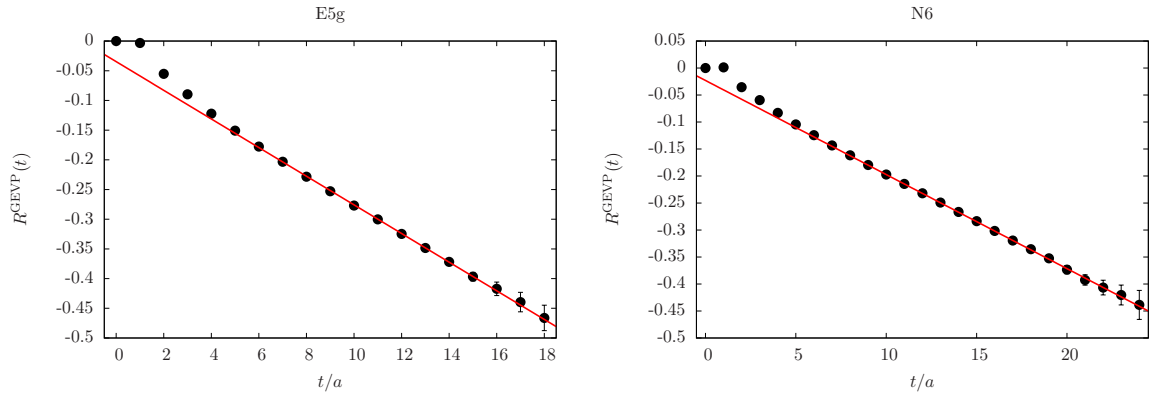


Figure 5.9 – Evolution of  $R^{\text{GEVP}}(t)$  with  $t/a$  for the CLS ensembles E5g and N6 (black dots). The red line corresponds to a linear fit where the excited states contribution is negligible.

### 5.4.3 Extrapolations

The value of  $h$ , computed using the strategy described in Section 5.1 for each ensemble, are given in Table 5.5 and the plateaus for  $x^{\text{eff}}(t)$  are plotted in Figure 5.10.

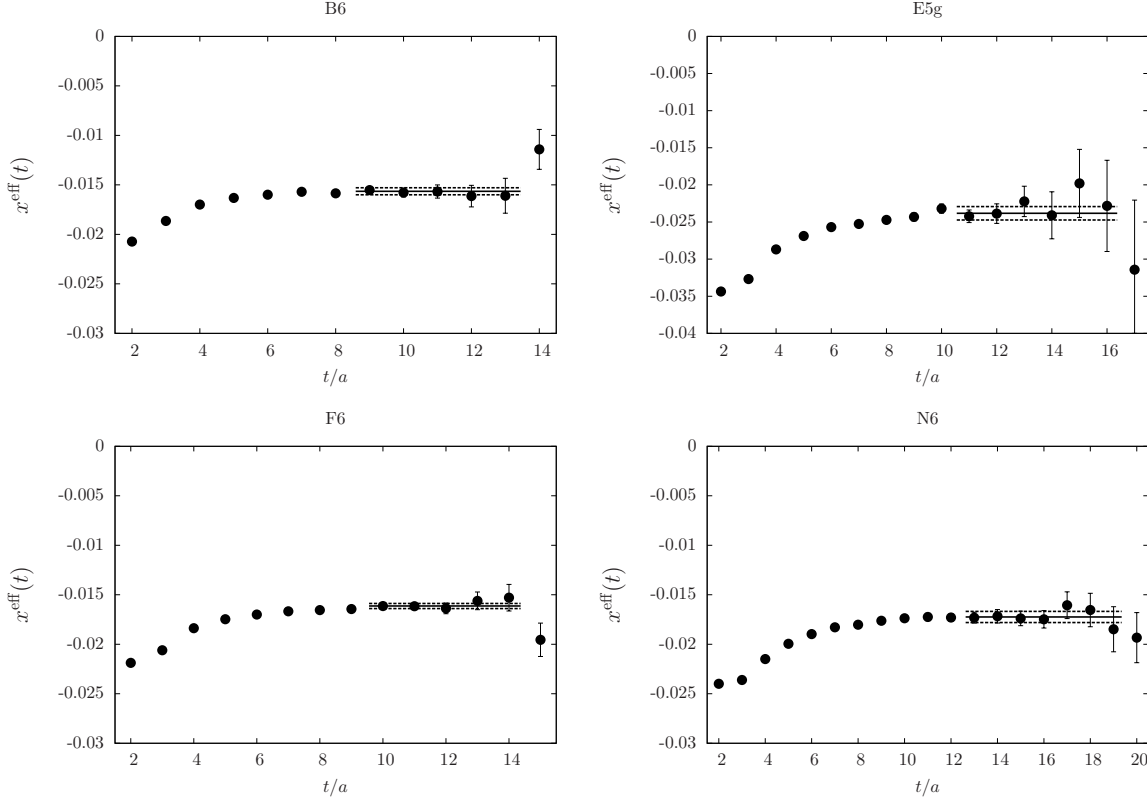


Figure 5.10 – Plateaus for  $x^{\text{eff}}(t)$  obtained by using eq. (5.10) for each ensemble (HYP1 action). From the upper left to the lower right: B6, E5, F6 and N6. I used  $t_0 = 5$  for  $t > t_0$  and  $t_0 = t - 1$  elsewhere.

The values obtained by using HYP1 and HYP2 actions are perfectly compatible and no dependence on the heavy quark discretization can be stated. Moreover, the data show clear plateaus and thus, to the accuracy of our results, the excited states contribution is small. Since there is no clear dependence on the lattice spacing, I used three different formulae for the chiral extrapolation

$$h = h_0, \quad (5.21)$$

$$h = h_0 + C (m_\pi^2 - (m_\pi^{\text{exp}})^2), \quad (5.22)$$

$$h = h_0 \left[ 1 - \frac{3\hat{g}^2 + 3\tilde{g}^2 + 2\tilde{g}\hat{g}}{(4\pi f_\pi)^2} \left( m_\pi^2 \log(m_\pi^2) - (m_\pi^{\text{exp}})^2 \log((m_\pi^{\text{exp}})^2) \right) \right] + C (m_\pi^2 - (m_\pi^{\text{exp}})^2), \quad (5.23)$$

where, in the third formula, I take into account the first order corrections in chiral perturbation theory computed in ref. [170] and where  $\hat{g} = 0.489(32)$  is the  $B^*B\pi$  coupling determined in ref. [100],  $\tilde{g} = -0.19(2)(1)$  is the  $B_1^*B_0^*\pi$  coupling [115] and  $f_\pi = 130.4$  MeV is the pion decay constant. The quark mass dependence is very small and the influence of the chiral logarithms does not change our result significantly. Our final result is

$$h_0 = 0.86(4)(2), \quad (5.24)$$

where the first error is statistical and the second error corresponds to the uncertainty that we evaluate from the discrepancy between the fit formulae (5.21) and (5.22). The

CLS	HYP	$ax$	$h$
B6	HYP1	-0.0156(4)	0.86(4)
	HYP2	-0.0156(4)	0.86(4)
E5	HYP1	-0.0241(10)	0.84(5)
	HYP2	-0.0238(9)	0.83(5)
F6	HYP1	-0.0159(3)	0.86(3)
	HYP2	-0.0161(3)	0.87(3)
N6	HYP1	-0.0174(6)	0.85(4)
	HYP2	-0.0172(6)	0.85(3)

Table 5.5 – Raw data for  $ax$  and  $h$  for each CLS ensemble and heavy quark action HYPi.

chiral extrapolation is shown in Figure 5.11 and the fit parameters are collected in Table 5.6.

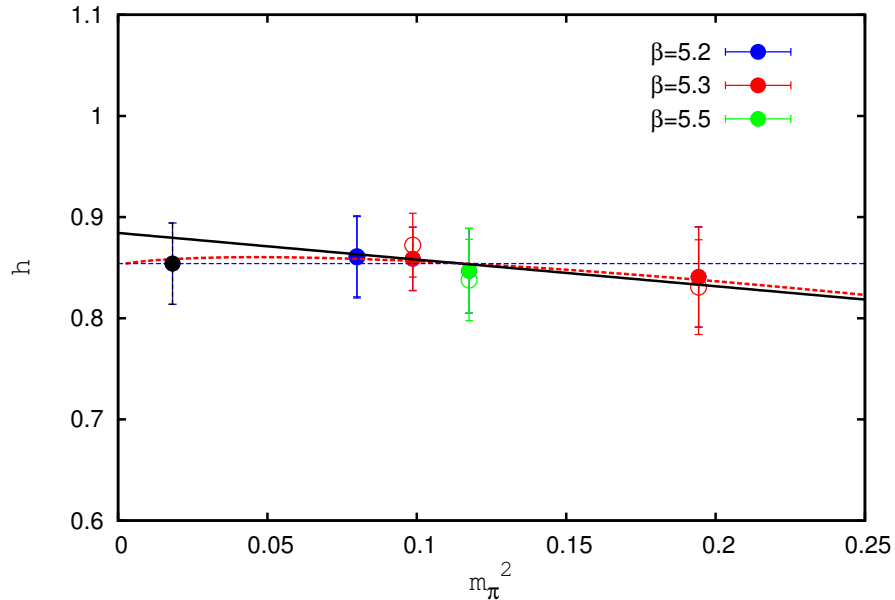


Figure 5.11 – Chiral extrapolation of the effective coupling  $h$ . The dashed blue line corresponds to the constant fit (5.21), the black line corresponds to the linear fit formula (5.22) and the dashed red line corresponds to the fit formula (5.23) with the expression derived in  $\text{HM}\chi\text{PT}$ . Plain and empty circle correspond respectively to HYP1 and HYP2 discretizations.

Rigorously, in the fit formulae (5.23), we have neglected the contribution from the heavy-light states of opposite parity computed in ref. [170]. They have been studied

	fit (5.21)	fit (5.22)	fit (5.23)
$h_0$	0.85(3)	0.88(4)	0.86(4)
$C$ (GeV $^{-2}$ )	$\times$	-0.26(30)	-0.35(33)

Table 5.6 – Fit parameters of eqs. (5.21), (5.22).

in ref. [115]. Neglecting them corresponds to the assumption  $m_\pi \ll \Delta = m_{B_0^*} - m_B$ . Since, for our lattice ensembles, the pion mass lies in the range [280 – 440] MeV and the mass difference between the scalar  $B$  meson and the ground state  $B$  meson is of the order of  $\Delta \sim 400$  MeV, the contribution from positive parity states cannot be neglected. Therefore, we also tried the fit formula

$$h = h_0 \left[ 1 - \frac{3\widehat{g}^2 + 3\widetilde{g}^2 + 2\widehat{g}\widetilde{g}}{4(4\pi f_\pi)^2} \left( m_\pi^2 \log(m_\pi^2) - (m_\pi^{\text{exp}})^2 \log((m_\pi^{\text{exp}})^2) \right) - \frac{h^2}{(4\pi f)^2} \left( \frac{m_\pi^2}{2\Delta^2} m_\pi^2 \log(m_\pi^2) - \frac{(m_\pi^{\text{exp}})^2}{2(\Delta^{\text{exp}})^2} (m_\pi^{\text{exp}})^2 \log((m_\pi^{\text{exp}})^2) \right) \right] + C (m_\pi^2 - (m_\pi^{\text{exp}})^2), \quad (5.25)$$

where the couplings  $\widehat{g}$  and  $\widetilde{g}$  are fixed to the previous values and the mass difference  $\Delta$  is given in Table 5.4. The result is

$$h_0 = 0.87(4), \quad (5.26)$$

and is also perfectly compatible with our previous result (5.24).

## 5.5 Discussions

In refs. [168, 169], the authors proposed an independent method to evaluate the coupling  $h$ . Indeed, one can show that the connected contribution to the correlation function  $C_{B_0^*-B\pi}(t)$ , which include box (5.17) and cross (5.18) diagrams, has the following behavior

$$\widetilde{R}(t) = \frac{(v_{B\pi}(t), C_{\text{connected}}(t), v_{B\pi}(t))}{(v_{B\pi}(t), C_{B\pi-B\pi}(t), v_{B\pi}(t))} = B + \frac{1}{2}x^2t^2 + \mathcal{O}(t), \quad (5.27)$$

where

$$C_{\text{connected}}(t) = -\frac{3}{2}C_{\text{box}}(t) + \frac{1}{2}C_{\text{cross}}(t).$$

These diagrams have been computed only for the CLS ensemble E5g and the function  $\widetilde{R}(t)$  is plotted in Figure 5.12. The results are quite precise and the linear dependence in eq. (5.27) cannot be neglected. Taking this into account, the result reads

$$|ax| = 0.0237(8),$$

and is in perfect agreement with the one obtained by the previous method (see Table 5.5). To determine the statistical error, I used a jackknife analysis and varied the fit range from  $t \in [9 - 18]$  to  $t \in [13 - 18]$  where the result is stable.

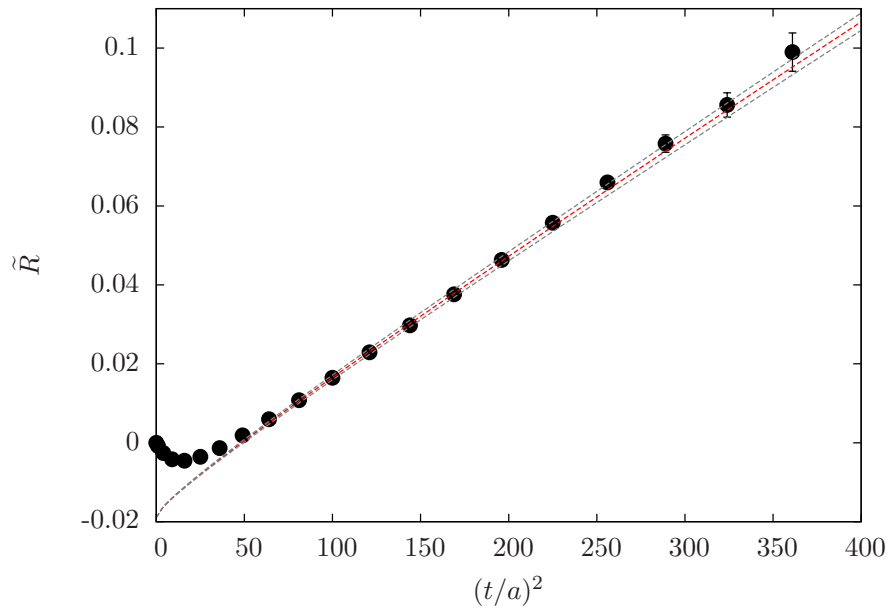


Figure 5.12 – Function  $\tilde{R}(t)$  for the CLS ensemble E5g.

This coupling was first computed on the lattice in ref. [115] and the authors quote two results for the two different actions used in their work:  $h_0 = 0.69(2)_{-7}^{+11}$  and  $h_0 = 0.58(2)_{-2}^{+6}$ . They obtain lower results than us but this difference might be explained by the larger quark masses used in ref. [115] where the chiral extrapolation tends to lower the extrapolated value. Our result is also a bit larger than the QCD sum rules estimate. In ref. [171], the parameter  $g_{B_0^* B \pi}$  has been computed and the authors found  $h = 0.56(28)$ . In ref. [172],  $g_{B_0^* B \pi}$  has also been computed in the framework of QCD sum rules and the authors quote  $g_{B_0^* B \pi} = 24(7)$  GeV corresponding to  $h_0 = 0.74(23)$ .

Finally, we can compare our results with decays of heavy-light mesons with a charm quark for which the spectrum is more accurately known. However, the static approximation is expected to give only a rough estimate since  $1/m$  corrections are probably sizable. For example, in the case of the  $D$  meson decay constant, the authors in ref. [173] found heavy quark spin breaking effects larger than 20%. The PDG [2] quotes a value of  $m_{D_0^*} = 2318(29)$  MeV for the mass of the scalar  $D$  meson and a total decay width of  $267(40)$  MeV which leads to  $\Gamma/k = 0.68(11)$  and  $h_0 = 0.74(8)$  (here, I assume that the branching ratio  $D_0^* \rightarrow D\pi$  is  $\approx 100\%$  as expected). This result is smaller than the one obtained in this work but compatible within error bars.

## Conclusion

I have presented a lattice computation of the soft pion coupling  $h$  which parametrizes the hadronic transition  $B_0^* \rightarrow B\pi$ . We used four lattice ensembles to control both discretization effects and chiral extrapolation. Our result reads  $h = 0.86(4)(2)$  where the first error is statistical and the second error includes the systematics. In particular, for the ensemble E5g where the box and cross diagrams have been computed, an independent cross-check was possible and a compatible result was obtained. Our value is larger than the one previously obtained in ref. [115] where larger pion masses were used, but

it is compatible with the experimental results for the  $D$  mesons.

A next step would be to compute the coupling constant  $\tilde{g}$  which parametrizes the hadronic matrix element  $B_1^* \rightarrow B_0^* \pi$ . It is similar to the soft coupling  $g$ , introduced in the previous chapter, but for the positive parity states  $J^P = (0^+, 1^+)$ . The effective couplings  $g$ ,  $h$  and  $\tilde{g}$  could then be used in the chiral extrapolations of the pseudoscalar and scalar  $B$  meson decay constant. This work is in progress.

# Chapter 6

## Mass and decay constant of the radially excited $D$ meson

### Contents

---

<b>Introduction</b> . . . . .	<b>130</b>
<b>6.1 Computation of the masses and decay constants of <math>D_{(s)}</math> and <math>D'_{(s)}</math></b> . . . . .	<b>131</b>
<b>6.2 Simulation details</b> . . . . .	<b>133</b>
<b>6.3 Results</b> . . . . .	<b>134</b>
6.3.1 Plateaus . . . . .	134
6.3.2 Re-evaluation of $f_{D_s}$ and $f_{D_s}/f_D$ . . . . .	134
6.3.3 Ratios $m_{D'_{(s)}}/m_{D_{(s)}}$ and $f_{D'_{(s)}}/f_{D_{(s)}}$ . . . . .	139
<b>Conclusion</b> . . . . .	<b>142</b>

---

## Introduction

The spectrum of  $D$  and  $B$  mesons has the same structure and was discussed in Chapter 4 (see Figure 4.2). In the charm sector, the orbital excitations have been measured experimentally and a new state, with quantum numbers  $J^P = 0^-$ , has been observed by the BaBar Collaboration [6] and is compatible with the first radial excitation ( $D'$ ). The measured mass,  $m_{D'} = 2539(8)$  MeV, turned out to be close to the quark model prediction  $m_{D'} = 2580$  MeV [174] but the measured width  $\Gamma(D') = 130(18)$  MeV appears to be much larger than the quark model prediction of ref. [175] and the identification of the state is still an open question.

Another intriguing fact concerns the weak properties of the  $D$  meson. The so called “1/2 vs. 3/2” puzzle is the fact that experimentally, one observes  $\Gamma(B \rightarrow D_{1/2}\ell\nu)^{\text{exp}} \approx \Gamma(B \rightarrow D_{3/2}\ell\nu)^{\text{exp}}$  while the theory predicts  $\Gamma(B \rightarrow D_{1/2}\ell\nu)^{\text{th}} \ll \Gamma(B \rightarrow D_{3/2}\ell\nu)^{\text{th}}$  [176, 177, 178, 179]. Here,  $D_{1/2}$  and  $D_{3/2}$  refer to states belonging to the positive parity doublets  $J^P = (0^+, 1^+)_{1/2}$  and  $J^P = (1^+, 2^+)_{3/2}$  respectively (see Table 4.1). It was suggested in ref. [7] that a potentially large  $\mathcal{B}(B \rightarrow D'\ell\nu)$  could help to solve this issue since the subsequent  $\Gamma(D' \rightarrow D_{1/2}\pi)$  is much larger than  $\Gamma(D' \rightarrow D_{3/2}\pi)$  because the emerging pion is in its s-wave and d-wave respectively. Indeed, a large  $\mathcal{B}(B \rightarrow D'\ell\nu)$  would result in an excess of the detected  $\Gamma(B \rightarrow D_{1/2}\ell\nu)$  with respect to  $\Gamma(B \rightarrow D_{3/2}\ell\nu)$ . To test this proposition, the authors in ref. [5] developed the possibility to check experimentally on the  $B \rightarrow D$  hadronic decays the size of the form factor  $f_+^R(q^2)$ , that parameterizes the  $B \rightarrow D'$  weak transition matrix element, using the factorization approximation [180] (here as in the following, the superscript  $R$  denotes the radial excitation). Indeed, for the so-called Class I decays [181, 180], the factorization amplitude associated to the branching ratio  $\mathcal{B}(\bar{B}^0 \rightarrow D'^+\pi^-)$  becomes

$$A_{\text{fact}}^I = -i \frac{G_F}{\sqrt{2}} V_{cb} V_{ud}^* a_1 f_\pi \times (m_B^2 - m_{D'}^2) f_0^R(m_\pi^2),$$

where  $f_0^R(m_\pi^2) \approx f_0^R(0) = f_+^R(0)$  is the  $B \rightarrow D'$  form factor and  $a_1$  is a Wilson coefficient that contains information about physics at short distances. For Class III decays, the factorization amplitude associated to the branching ratio  $\mathcal{B}(B^- \rightarrow D'^0\pi^-)$  is

$$A_{\text{fact}}^{III} = -i \frac{G_F}{\sqrt{2}} V_{cb} V_{ud}^* [a_1 f_\pi \times (m_B^2 - m_{D'}^2) f_0^R(m_\pi^2) + a_2 f_{D'} \times (m_B^2 - m_\pi^2) f_0^{B \rightarrow \pi}(m_{D'}^2)],$$

where  $f_0^{B \rightarrow \pi}$  is the  $B \rightarrow \pi\ell\nu$  decay form factor and  $a_2$  is another Wilson coefficient. When combined with the results for the more familiar decay  $\mathcal{B}(\bar{B}^0 \rightarrow D^+\pi^-)$ , one gets for the Class I decays

$$\text{Class I: } \frac{\mathcal{B}(\bar{B}^0 \rightarrow D'^+\pi^-)}{\mathcal{B}(\bar{B}^0 \rightarrow D^+\pi^-)} = \left( \frac{m_B^2 - m_{D'}^2}{m_B^2 - m_D^2} \right) \left( \frac{\lambda(m_B, m_{D'}, m_\pi)}{\lambda(m_B, m_D, m_\pi)} \right)^{1/2} \left| \frac{f_+^R(0)}{f_+(0)} \right|^2, \quad (6.1)$$

where the phase space term  $\lambda(x, y, z)$  is given in ref. [5] and  $f_+(0)$  is the  $B \rightarrow D$  form factor which has been measured experimentally. Similarly, taking the ratio between Class III and Class I decays, one finds

$$\text{Class III: } \frac{\mathcal{B}(\bar{B}^- \rightarrow D'^0\pi^-)}{\mathcal{B}(\bar{B}^0 \rightarrow D'^+\pi^-)} = \frac{\tau_{B^-}}{\tau_{\bar{B}^0}} \left[ 1 + \frac{a_2}{a_1} \frac{m_B^2 - m_\pi^2}{m_B^2 - m_{D'}^2} \frac{f_0^{B \rightarrow \pi}(m_{D'}^2)}{f_+^R(0)} \frac{f_{D'} f_D}{f_D f_\pi} \right]^2. \quad (6.2)$$

Therefore, using the experimental data, one can predict the value of  $f_+^R(0)$  in terms of  $\mathcal{B}(\overline{B}^0 \rightarrow D'^+\pi^-)$  and  $\mathcal{B}(\overline{B}^- \rightarrow D'^0\pi^-)$  if the values of the mass and decay constant of the radial excitation are known. One can then conclude that, if indeed  $f_+^R(0)$  is large, then the previous branching ratio  $\mathcal{B}(\overline{B}^0 \rightarrow D'^+\pi^-)$  can be accessible from experiment.

## 6.1 Computation of the masses and decay constants of $D_{(s)}$ and $D'_{(s)}$

The mass and decay constant of heavy-light hadrons with a charmed quark can be extracted on the lattice from the following two-point correlation function

$$C(t) = \sum_{\vec{x}} \langle O_\Gamma(\vec{0}, 0) O_\Gamma^\dagger(\vec{x}, t) \rangle = - \langle \sum_{\vec{x}} \text{Tr} [\Gamma G_c(0, x) \Gamma G_q(x, 0)] \rangle, \quad (6.3)$$

where  $O_\Gamma = \bar{c}\Gamma q$  is the bilinear quark operator, with  $c$  and  $q$  being the charm and the light quark field respectively, and  $\Gamma$  is chosen to ensure the coupling to the state with desired quantum numbers. In our study  $q$  is either the strange quark, or it coincides with the light sea quark. In the above notation  $G_q(x, 0) \equiv \langle q(x)\bar{q}(0) \rangle$  is the quark propagator computed in the background gauge field configuration by inverting the Wilson-Dirac operator of MtmQCD on the lattice (see Section 1.5.5). The quark propagators are computed by using stochastic sources, and in the computation of the correlation functions we used the so-called one-end trick [182].

The simplest and the most convenient choice is to use the local operators  $O_\Gamma = P_5 = \bar{c}\gamma_5 q$ , and extract the mass and decay constant of the lowest lying state from the exponential fall-off of the correlation function (6.3). Indeed, for large time separations

$$C_{55}(t) = \langle \sum_{\vec{x}} P_5(\vec{x}; t) P_5^\dagger(\vec{0}; 0) \rangle \xrightarrow{t \gg 0} |Z_{D_q}|^2 \frac{\cosh[m_{D_q}(T/2 - t)]}{m_{D_q}} e^{-m_{D_q}T/2}, \quad (6.4)$$

with  $T$  being the size of the temporal extension of the lattice, and  $Z_{D_q} = \langle 0|P_5|D_q \rangle$  is the overlap between the ground state and the interpolating operator and is related to the decay constant  $f_{D_q}$  via the axial Ward identity

$$(\mu_c + \mu_q) \langle 0|P_5|D_q \rangle = m_{D_q}^2 f_{D_q}. \quad (6.5)$$

In eq. (6.4) we used the symmetry of the correlation function with respect to  $t \leftrightarrow T - t$  of our periodic lattice. Indeed, contrary to eq. (2.22), both quarks can propagate forward and backward in time due to periodic boundary conditions resulting in the cosh function instead of the exponential. To extract the radial excitation properties, one can subtract the r.h.s. of eq. (6.4) from the correlator  $C_{55}(t)$ ,

$$C'_{55}(t) = C_{55}(t) - |Z_{D_q}|^2 \frac{\cosh[m_{D_q}(T/2 - t)]}{m_{D_q}} e^{-m_{D_q}T/2}, \quad (6.6)$$

and check whether or not there is a plateau of the effective mass,  $m_{D_q}^{\text{eff}}(t)$ , defined as

$$\frac{\cosh\left[m_{D_q}^{\text{eff}}(t)\left(\frac{T}{2} - t\right)\right]}{\cosh\left[m_{D_q}^{\text{eff}}(t)\left(\frac{T}{2} - t - 1\right)\right]} = \frac{C'_{55}(t)}{C'_{55}(t+1)}, \quad (6.7)$$

and possibly fit to the form similar to eq. (6.4) to extract the mass and the decay constant of  $D'_q$ . This strategy can be extended and combined by the computation of correlation functions with different source operators and by fitting them simultaneously.

Another way to proceed, is to use the Generalized Eigenvalue Problem (Section 2.26). This method is particularly well suited for the extraction of the radial excitation properties on the lattice as discussed in the previous chapters. Therefore, we worked with several interpolating operators  $O_k$  with  $\Gamma = \gamma_5$  but corresponding to different level of gaussian smearing for the light quark field (see Section 2.6). In particular, we choose the following values for the parameters

$$\kappa_G = 0.16, \quad n_k \in (0, 2, 10, 32), \quad \alpha = 0.5, \quad n_a = 20, \quad (6.8)$$

where  $\kappa_G$  and  $n_k$  refer to the gaussian smearing parameters in eq. (2.35) and  $\alpha$  and  $n_a$  to the APE smearing parameters in eq. (2.33) ( $n_a$  is the number of iterations). Note that the choice  $n_k = 0$  corresponds to the local operator which is needed for the computation of physically relevant decay constants. We checked that the correlation function computed with both quark fields smeared is equal to the one obtained with only one field smeared but with twice as many smearing steps,  $n_k$ . However, we observe that the correlation functions computed with both fields smeared are less noisy and for that reason the results presented in this work are obtained by using both  $q$  and  $c$  fields smeared. The various operators  $O_k$  can be combined in a matrix of correlation functions:

$$C_{ij}(t) = \langle O_i(t) O_j^\dagger(0) \rangle = \sum_n \frac{Z_{ni} Z_{nj}^*}{m_{D_q^{(n)}}} e^{-m_{D_q^{(n)}} \frac{T}{2}} \cosh \left[ m_{D_q^{(n)}} \left( \frac{T}{2} - t \right) \right]. \quad (6.9)$$

The Generalized Eigenvalue Problem (GEVP), presented in Section 2.5, is

$$C(t) v_n(t, t_0) = \lambda_n(t, t_0) C(t_0) v_n(t, t_0), \quad (6.10)$$

where  $\lambda_n(t, t_0)$  and  $v_n(t, t_0)$  are the generalized eigenvalues and eigenvectors respectively. From the eigenvalues, the mass of the  $n^{\text{th}}$  state is obtained from

$$\lambda_n(t, t_0) = \frac{\cosh \left[ m_{D_q^{(n)}} (T/2 - t) \right]}{\cosh \left[ m_{D_q^{(n)}} (T/2 - t_0) \right]}, \quad (6.11)$$

where  $n = 1$  corresponds to the lowest lying pseudoscalar  $D_q$  mesons, and  $n = 2$  to their first radial excitations  $D'_q$ . Again, the difference between this formula and the previous one given in Section 2.5 is due to the periodic boundary conditions and the fact that the charm quark is not static. Finally, from eq. (6.11), we consider the following effective mass

$$m_{D_q^{(n)}}^{\text{eff}}(t) = \text{arccosh} \left[ \frac{\lambda_n(t+1, t_0) + \lambda_n(t-1, t_0)}{2\lambda_n(t, t_0)} \right]. \quad (6.12)$$

The eigenvectors are used to construct an optimal interpolating operator for the desired state. In particular, to extract the decay constant one needs the matrix element of the local operator and a state  $|D_q^{(n)}\rangle$ . Similarly to eq. (2.28), it is obtained by considering

$$\langle D_q^{(n)} | O_L^\dagger | 0 \rangle^{\text{eff}}(t) = \frac{\sqrt{A_n} \sum_i (C_L(t), v_n(t, t_0))}{(v_n(t, t_0), C(t) v_n(t, t_0))} \xrightarrow{t \gg 0} \langle D_q^{(n)} | O_L^\dagger | 0 \rangle, \quad (6.13)$$

where  $A_n \delta_{nm} = \langle D_q^{(m)} | \widehat{O}^{(n)\dagger} | 0 \rangle$  and where, as before, the scalar product is defined by  $(a, b) = a_i^* b_j$  and the local correlation function by

$$C_{Li}(t) = \langle O_L(t) O_i^\dagger(0) \rangle = \langle P_5(t) O_i^\dagger(0) \rangle. \quad (6.14)$$

In the case of MtmQCD on the lattice, the local operator of interest is  $O_L = P_5 = \bar{c} \gamma_5 q$  because  $(\mu_q + \mu_c) P_5$  is renormalization group invariant, and therefore no renormalization constant is needed to compute the pseudoscalar decay constant.<sup>1</sup> This is not so in the case of Wilson-Clover action where it is more convenient to use  $O_L = A_0 = Z_A(g_0^2) \bar{c} \gamma_0 \gamma_5 q$ , with  $Z_A(g_0^2)$ , the axial current renormalization constant. However, since we shall be interested in the ratio of the decay constants,  $f_{D'_q}/f_{D_q}$ , one can use  $O_L = P_5$  in the case with the Wilson-Clover action as well.

## 6.2 Simulation details

In this work, we used the ensembles of gauge field configurations produced by the European Twisted Mass Collaboration (ETMC) [182] from the simulations of maximally twisted mass QCD (MtmQCD) [183] with  $N_f = 2$  dynamical quarks degenerate in mass. At fixed lattice spacing, we will also compare the MtmQCD values with the results obtained by using the standard Wilson-Clover action with  $N_f = 2$  dynamical quarks and with those obtained in quenched QCD. The main parameters of the ensembles are collected in Table 6.1 and Table 6.2. We use the results of ref. [184] to fix the charm ( $c$ ) and strange ( $s$ ) quark masses at each lattice spacing and then compute the correlation functions needed for the extraction of strange and non-strange  $D_q^{(n)}$ -meson properties.

$\beta$	$a$ (fm)	$L/a$	$\mu_{\text{sea1}}$	$\mu_{\text{sea2}}$	$\mu_{\text{sea3}}$	$\mu_s$	$\mu_c$	# cfgs
3.8	0.098(3)	24	0.0080	0.0110	×	0.0194(7)	0.2331(82)	240
3.9	0.085(3)	24	0.0040	0.0064	×	0.0177(6)	0.2150(75)	240
		32	0.0030	0.0040	×	0.0177(6)	0.2150(75)	150
4.05	0.067(2)	32	0.0030	0.0040	0.0080	0.0154(5)	0.1849(65)	150
4.2	0.054(1)	32	0.0065	×	×	0.0129(5)	0.1566(55)	150
		48	0.0020	×	×	0.0129(5)	0.1566(55)	100

Table 6.1 – Lattice ensembles used in this work with the indicated number of gauge field configurations. Lattice spacing is fixed by using the Sommer parameter  $r_0/a$  [105], with  $r_0 = 0.440(12)$  fm set by matching  $f_\pi$  obtained on the lattice with its physical value (cf. ref. [184]). Quark mass parameters  $\mu$  are given in lattice units.

1.  $\mu_{q,c}$  is the quark mass parameter.

$N_f$	$\beta$	$L/a$	$\kappa_{\text{sea}}$	$\kappa_s$	$\kappa_c$	# cfigs
0	6.2	24	$\times$	0.1348	0.125	200
2	5.4	24	0.13625	0.1359	0.126	160

Table 6.2 – Lattice set-up for the results obtained by using the Wilson gauge and the Wilson-Clover quark action.  $\kappa_{\text{sea}}$ ,  $\kappa_s$  and  $\kappa_c$  stand for the value of the hopping parameter of the sea, strange and the charm quark respectively.

## 6.3 Results

### 6.3.1 Plateaus

The effective mass plots are obtained using eq. (6.12). For the case of the lowest lying state ( $n = 1$ ) and the first radial excitation ( $n = 2$ ) the signals are illustrated in Figure 6.1. In the plateau region, each  $m_{D'_q}^{\text{eff}}(t)$  is then fitted to a constant  $m_{D'_q}$ . We checked that the results for the first radial excitation remain stable when we change the size of the matrix of correlators. We also checked that from this study we cannot extract a signal for the second radial excitation: only a few points at  $t \lesssim 5$  can be seen before the error bars become overwhelmingly large. We also checked that the choice of  $t_0$  in the GEVP (6.10) does not have any impact on the results presented here. Finally, we also note that the radial excitations extracted on the plateaus of subtracted correlation functions (6.6) are completely consistent with those obtained from the solution to the GEVP (6.10). Concerning the decay constants they are extracted from the matrix element obtained by using eq. (6.13), and the definition of the decay constant (6.5). The fitting intervals to extract the masses and decay constants for the lowest lying states are

$$\begin{aligned} t/a \in [8, 22]_{\beta=3.8} & \quad , \quad t/a \in [8, 22]_{\beta=3.9} , \\ t/a \in [12, 26]_{\beta=4.05} & \quad , \quad t/a \in [14, 30]_{\beta=4.2} , \end{aligned}$$

while for the radially excited states the following fit intervals have been chosen,

$$\begin{aligned} t/a \in [6, 10]_{\beta=3.8} & \quad , \quad t/a \in [9, 12]_{\beta=3.9} , \\ t/a \in [9, 12]_{\beta=4.05} & \quad , \quad t/a \in [11, 14]_{\beta=4.2} . \end{aligned}$$

For some values of the sea quark mass we have a few more points to fit but globally the time intervals noted above are used to obtain the results that we present in Table 6.3 and Table 6.4, in lattice units and for each of the lattice setups employed in this work.

### 6.3.2 Re-evaluation of $f_{D_s}$ and $f_{D_s}/f_D$

The results of ref. [185] included the simulations at three different lattice spacings and the value  $f_{D_s} = 244(8)$  MeV has been reported. That value has been improved in ref. [65] where the simulations at a smaller lattice spacing have been included in the analysis, leading to  $f_{D_s} = 248(6)$  MeV. Furthermore, while improving the MtmQCD estimate of  $f_{D_s}/f_D$ , the authors of ref. [65] also added the systematic uncertainty related to the chiral

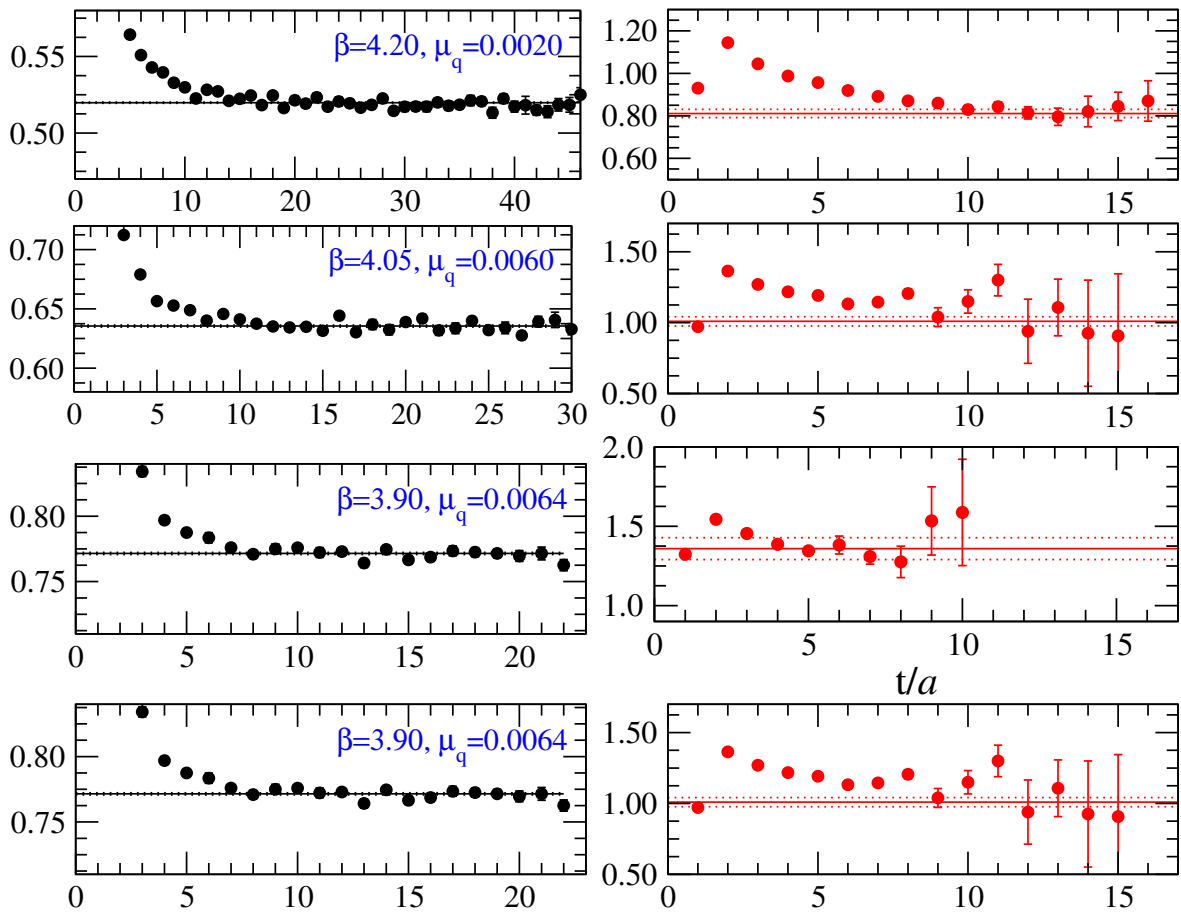


Figure 6.1 – Effective mass plots leading to the masses of  $D_s$  (left column) and  $D'_s$  states (right column), deduced from the matrix of correlation functions as discussed in the text. Plots are provided for all four lattice spacings considered in this work with MtmQCD action.

extrapolation, which was omitted in ref. [185]. Their final result,  $f_{D_s}/f_D = 1.17(5)$ , allowed to deduce  $f_D = 212(8)$  MeV.

Results in refs. [185, 65] have been obtained from the correlation functions with local source operators only. In the present work we implement several levels of the smearing procedure discussed above, with parameters (6.8), and then combine the resulting correlators in a matrix. Solving the GEVP, together with a slightly modified procedure to extract  $f_{D_s}$  and  $f_{D_s}/f_D$ , yield to more accurate results which is why in this subsection we update the values presented in refs. [185, 65].

To get the physically relevant  $f_{D_s}$  we need to extrapolate the values we obtained from all of our lattice ensembles (cf. Table 6.4). We choose to combine  $f_{D_s}$  and  $m_{D_s}$  in the dimensionless ratio that we then fit to the form,

$$\left(\frac{f_{D_s}}{m_{D_s}}\right)^{\text{latt.}} = A_{D_s} \left[ 1 + B_{D_s} m_q + C_{D_s} \left(\frac{a}{a_{\beta=3.9}}\right)^2 \right], \quad (6.15)$$

where  $A_{D_s}$ ,  $B_{D_s}$  and  $C_{D_s}$  are obtained from the fit and their values are given in Table 6.5. The above form takes into account the fact that the lattice discretization effects to the

$(L, \beta, \mu_q)$	$m_q^{\overline{\text{MS}}}(2 \text{ GeV})$	$m_{D_q}$	$m_{D'_q}$	$f_{D_q}$	$f_{D'_q}$
(24, 3.80, 0.0080)	0.0398(11)	0.843(1)	1.32(6)	0.136(1)	0.098(8)
(24, 3.80, 0.0110)	0.0547(15)	0.852(1)	1.34(3)	0.139(1)	0.105(6)
(32, 3.90,0.0040)	0.0216(5)	0.741(1)	1.05(5)	0.110(1)	0.054(8)
(24, 3.90,0.0064)	0.0345(8)	0.7748(1)	1.09(7)	0.112(1)	0.063(18)
(24, 3.90,0.0085)	0.0458(11)	0.748(2)	1.06(4)	0.113(1)	0.056(9)
(24, 3.90,0.0100)	0.0539(13)	0.755(1)	1.10(3)	0.116(1)	0.069(5)
(32, 4.05,0.0030)	0.0162(4)	0.608(2)	0.95(3)	0.083(1)	0.055(5)
(32, 4.05,0.0060)	0.0216(5)	0.616(1)	1.02(4)	0.087(1)	0.063(6)
(32, 4.05,0.0080)	0.0249(7)	0.621(1)	1.02(6)	0.090(1)	0.068(9)
(32, 4.20,0.0065)	0.049(2)	0.521(1)	0.79(3)	0.071(1)	0.038(4)
(48, 4.20,0.0020)	0.0150(7)	0.497(1)	0.81(5)	0.064(1)	0.037(7)

Table 6.3 – Masses and decay constants,  $m_{D'_q}$  and  $f_{D'_q}$ , as computed from the solution to the GEVP discussed in the text. Note that the light valence quark and the sea quarks are degenerate in mass,  $m_q$ , with the renormalized value given in the  $\overline{\text{MS}}$  scheme. Note that the hadron masses and decay constants are given in lattice units while  $m_q^{\overline{\text{MS}}}(2 \text{ GeV})$  is given in physical units [GeV].

hadronic quantities computed in MtmQCD are quadratic in the lattice spacing. Note that we divided by the lattice spacing of  $\beta = 3.9$  so that the parameter  $C_{D_s}$  actually indicates a size of discretization effects at  $\beta = 3.9$ . After taking  $m_q \equiv m_q^{\overline{\text{MS}}}(2 \text{ GeV})$ , also listed in Table 6.3, the fit of our data to eq. (6.15) in the continuum limit and at the physical  $m_{u,d}^{\overline{\text{MS}}}(2 \text{ GeV}) = 3.6(2) \text{ MeV}$  [184], gives

$$\left(\frac{f_{D_s}}{m_{D_s}}\right)^{\text{ph.}} = 0.1281(11). \quad (6.16)$$

With the help of  $m_{D_s}^{\text{ph.}} = 1968.5(3) \text{ MeV}$  [2], we finally have

$$f_{D_s} = 252(3) \text{ MeV}. \quad (6.17)$$

We checked that this result remains stable if we omit from the continuum extrapolation the results obtained at  $\beta = 3.8$ . This result is also consistent with those obtained from simulations with  $N_f = 2 + 1$  flavors of staggered quarks in the continuum limit [108], with those computed with  $N_f = 2 + 1$  flavors of Wilson-Clover quarks at the single lattice spacing [187], as well as with the recent experimental results presented in refs. [188, 189].

As for the SU(3) light flavor symmetry breaking, the ratio of  $f_{D_s}/f_D$  is combined with the meson masses inspired from the heavy quark expansion,

$$r_q = \frac{\phi_{D_s}}{\phi_{D_q}} \equiv \sqrt{\frac{m_{D_s}}{m_{D_q}}} \frac{f_{D_s}}{f_{D_q}}, \quad (6.18)$$

$(L, \beta, \mu_q)$	$m_{D_s}$	$m_{D'_s}$	$f_{D_s}$	$f_{D'_s}$	$f_K/f_\pi$
(24, 3.80, 0.0080)	0.8703(8)	1.36(7)	0.1459(9)	0.107(13)	1.075(4)
(24, 3.80, 0.0110)	0.8717(7)	1.35(3)	0.1462(9)	0.109(5)	1.051(3)
(32, 3.90, 0.0040)	0.7708(8)	1.09(4)	0.1206(7)	0.062(7)	1.114(7)
(24, 3.90, 0.0064)	0.7715(8)	1.11(4)	0.1203(5)	0.066(11)	1.072(2)
(24, 3.90, 0.0085)	0.7963(10)	1.09(3)	0.1199(7)	0.064(8)	1.057(2)
(24, 3.90, 0.0100)	0.7713(8)	1.12(2)	0.1214(6)	0.074(4)	1.045(1)
(32, 4.05, 0.0030)	0.6344(11)	0.99(3)	0.0923(7)	0.063(5)	1.129(6)
(32, 4.05, 0.0060)	0.6355(9)	1.03(4)	0.0930(6)	0.066(5)	1.072(1)
(32, 4.05, 0.0080)	0.6361(9)	1.03(5)	0.0941(8)	0.072(8)	1.050(2)
(32, 4.20, 0.0065)	0.5243(7)	0.81(2)	0.0750(6)	0.041(4)	1.049(2)
(48, 4.20, 0.0020)	0.5198(4)	0.82(2)	0.0726(3)	0.042(3)	1.134(6)

Table 6.4 – Similar as in Table 6.3 except that the valence quark mass is fixed to the strange quark mass value. We also list the values of  $f_K/f_\pi$  obtained on each lattice which are extracted in the same way as in ref. [185] and corrected for the small finite volume effects [186]. All data are given in lattice units.

where the index “ $q$ ” labels the valence light quark, which in our study is mass degenerate with the sea quark. As in refs. [185, 65] we fit our results to a form

$$r_q^{\text{latt.}} = A_r \left[ 1 + X \frac{3}{4} \frac{1 + 3g^2}{(4\pi f)^2} m_\pi^2 \log(m_\pi^2) + B_r m_\pi^2 + C_r \left( \frac{a}{a_{\beta=3.9}} \right)^2 \right], \quad (6.19)$$

where for  $X = 0$  we have the expression similar to the one used in eq. (6.15), and for  $X = 1$  the extrapolation formula includes the chiral logarithmic correction that has been computed in the framework of heavy meson chiral perturbation theory [154]. To use the latter formula one needs to fix the value of the soft pion coupling to the doublet of the lowest lying heavy-light mesons,  $g$ . Here, we took the value of ref. [122] computed on the same sets of gauge field configurations that are used here, and the result is  $g = 0.53(3)(3)$ . The results of the fit of our data to eq. (6.19) are collected in Table 6.5. Here we note that

$$\begin{aligned} \text{for } X = 0 & \quad , \quad \frac{f_{D_s}}{f_D} = 1.128(10), \\ \text{for } X = 1 & \quad , \quad \frac{f_{D_s}}{f_D} = 1.227(13). \end{aligned} \quad (6.20)$$

The logarithmic correction is large and after averaging the last two results, we finally have

$$\frac{f_{D_s}}{f_D} = 1.177(13)(50), \quad (6.21)$$

from which we can deduce  $f_D = 214(4)(9)$  MeV, where the second error reflects the systematics arising from the chiral extrapolation. In order to circumvent the large

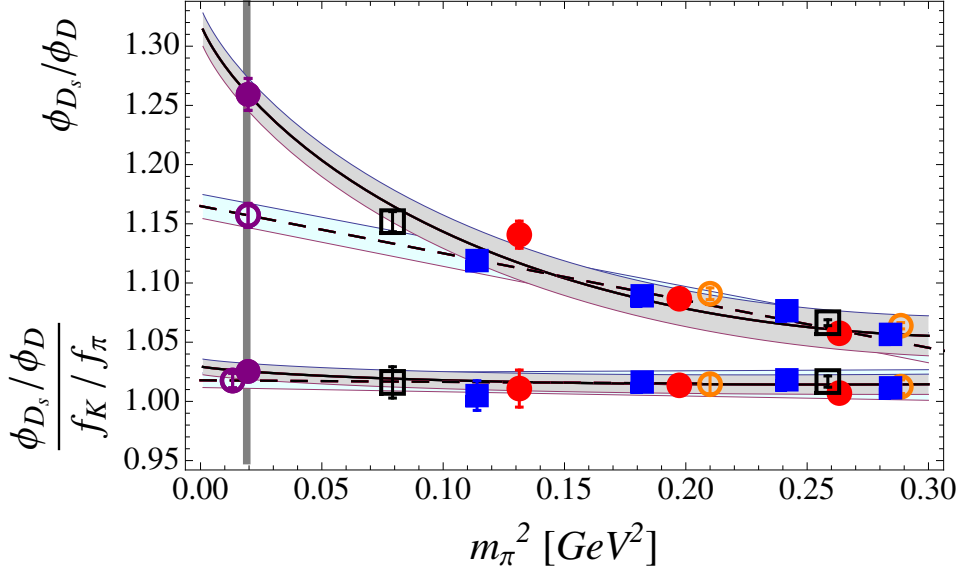


Figure 6.2 – Chiral extrapolation of the ratio of decay constants: Upper curves correspond to the fit of our data for  $\phi_{D_s}/\phi_D$  according to eq. (6.19) with  $X = 0$  and  $X = 1$ ; Lower curves correspond to the chiral extrapolation of the double ratio  $(\phi_{D_s}/\phi_D)/(f_K/f_\pi)$  with the formula (6.23) with  $X = 0$  and  $X = 1$ . The vertical line indicates the physical pion mass. Dashed (solid) curves depict the extrapolation without (with) inclusion of the chiral logarithms. The symbols corresponding to the lattice data are:  $\circ$  for  $\beta = 3.80$ ,  $\blacksquare$  for  $\beta = 3.90$ ,  $\bullet$  for  $\beta = 4.05$ , and  $\square$  for  $\beta = 4.20$ . Note that the result of the linear extrapolation of the double ratio has been slightly off-set to make it distinguishable from the one in which the chiral logarithms have been included.

logarithmic correction in eq. (6.19), one can study a double ratio [190],

$$R_q = \sqrt{\frac{m_{D_s}}{m_{D_q}} \frac{f_{D_s}/f_{D_q}}{f_K/f_\pi}}, \quad (6.22)$$

for which the logarithmic term is about 10 times smaller than in eq. (6.19),

$$R_q^{\text{latt.}} = A_R \left[ 1 + X \frac{9g^2 - 2}{4(4\pi f)^2} m_\pi^2 \log(m_\pi^2) + B_R m_\pi^2 + C_R \left( \frac{a}{a_{\beta=3.9}} \right)^2 \right], \quad (6.23)$$

and therefore the difference between the values obtained by setting  $X = 1$  and  $X = 0$  is much smaller, which can also be appreciated from the plot shown in Figure 6.2. We get

$$\frac{f_{D_s}}{f_D} = 0.995(6)(4) \times \frac{f_K}{f_\pi}, \quad (6.24)$$

where the central value is obtained by averaging the results of extrapolations with  $X = 0$  and  $X = 1$ , and the second error reflects the error due to chiral extrapolation. The results of the fit of our data to eq. (6.23) are listed in Table 6.5. Following the same strategy described in ref. [185], from the results for  $f_K/f_\pi$  listed in Table 6.4 we obtain  $f_K/f_\pi = 1.23(1)$ , which then gives<sup>2</sup>

$$\frac{f_{D_s}}{f_D} = 1.23(1)(1), \quad (6.25)$$

<sup>2</sup> In addition to the results considered in ref. [185], in this analysis we also included the values of  $f_K/f_\pi$  obtained at  $\beta = 4.20$ .

Quantity ( $Q$ )	Fit form	$A_Q$	$B_Q$	$C_Q$
$f_{D_s}/m_{D_s}$	eq. (6.15)	0.1278(11)	0.4(2)	0.21(1)
$r = \phi_{D_s}/\phi_D$	eq. (6.19) [ $X = 0$ ]	1.165(10)	-0.34(3)	0.006(5)
$r = \phi_{D_s}/\phi_D$	eq. (6.19) [ $X = 1$ ]	1.319(14)	0.06(3)	0.002(5)
$R = r/(f_K/f_\pi)$	eq. (6.23) [ $X = 0$ ]	1.018(6)	-0.013(22)	-0.002(4)
$R = r/(f_K/f_\pi)$	eq. (6.23) [ $X = 1$ ]	1.029(7)	0.021(24)	-0.002(4)
$m_{D'}/m_D$	eq. (6.27)	1.55(9)	0.6(1.5)	-0.04(5)
$m_{D'_s}/m_{D_s}$	eq. (6.27)	1.53(7)	1.0(1.2)	-0.05(4)
$f_{D'}/f_D$	eq. (6.27)	0.50(12)	1.7(5.6)	0.24(23)
$f_{D'_s}/f_{D_s}$	eq. (6.27)	0.52(9)	1.5(4.6)	0.19(21)

Table 6.5 – Fit results of the quantities computed in this chapter on the lattice.

that combined with  $f_{D_s}$  in eq. (6.17) gives

$$f_D = 205(5)(2) \text{ MeV}. \quad (6.26)$$

We note also that the above result remains remarkably stable if the data on our coarser lattices (corresponding to  $\beta = 3.8$ ) are left out from the chiral and continuum extrapolation.

### 6.3.3 Ratios $m_{D'_{(s)}}/m_{D_{(s)}}$ and $f_{D'_{(s)}}/f_{D_{(s)}}$

We now discuss the masses and the decay constants of the radially excited  $D$ -mesons. We focus on the dimensionless  $m_{D'_q}/m_{D_q}$  and  $f_{D'_q}/f_{D_q}$  ratios, that are easily built from our results presented in Table 6.3 (*non-strange*) and Table 6.4 (*strange*). In the following we denote by  $\mathcal{F}$  one of the four quantities discussed in this section, namely  $m_{D'}/m_D$ ,  $m_{D'_s}/m_{D_s}$ ,  $f_{D'}/f_D$ , and  $f_{D'_s}/f_{D_s}$ , and fit each to the form similar to eq. (6.15),

$$\mathcal{F}^{\text{latt.}} = A_{\mathcal{F}} \left[ 1 + B_{\mathcal{F}} m_q + C_{\mathcal{F}} \left( \frac{a}{a_{\beta=3.9}} \right)^2 \right], \quad (6.27)$$

We get the following physically relevant results,

$$\begin{aligned} \frac{m_{D'_s}}{m_{D_s}} = 1.53(7) \quad , \quad \frac{f_{D'_s}}{f_{D_s}} = 0.53(9) \quad , \\ \frac{m_{D'}}{m_D} = 1.56(9) \quad , \quad \frac{f_{D'}}{f_D} = 0.50(12) \quad . \end{aligned} \quad (6.28)$$

An illustration of that fit in the case of  $m_{D'}/m_D$  and  $f_{D'}/f_D$  is provided in Figure 6.3, while the values of  $A_{\mathcal{F}}$ ,  $B_{\mathcal{F}}$ , and  $C_{\mathcal{F}}$  for all four quantities can be found in Table 6.5. We observe that the above ratios do not exhibit a regular behavior in  $a^2$ , and are practically independent of the light quark mass.

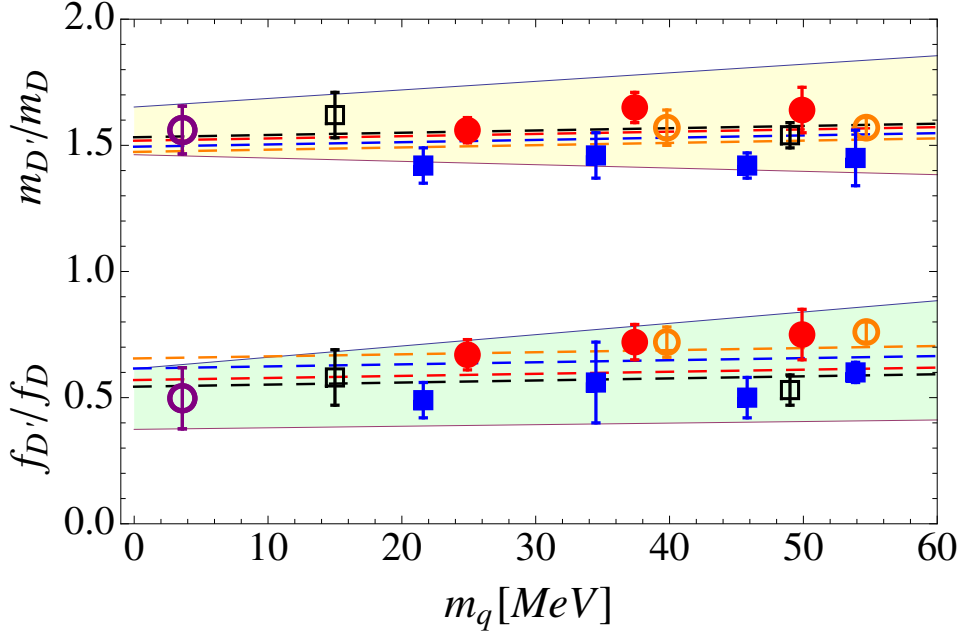


Figure 6.3 – Chiral extrapolation of the ratios  $m_{D'}/m_D$  and  $f_{D'}/f_D$  by using eq. (6.27). Dashed lines correspond to central values of various lattice spacings, and the bands indicate the error bars of extrapolation. The symbols of the lattice data points are the same as in Figure 6.2.

For that reason it is tempting to fit our data to a constant, i.e. to impose  $B_{\mathcal{F}} = C_{\mathcal{F}} = 0$  in eq. (6.27). We obtain

$$\begin{aligned} \frac{m_{D'_s}}{m_{D_s}} &= 1.52(2) \quad , \quad \frac{f_{D'_s}}{f_{D_s}} = 0.65(3) \quad , \\ \frac{m_{D'}}{m_D} &= 1.56(9) \quad , \quad \frac{f_{D'}}{f_D} = 0.65(3) \quad . \end{aligned} \quad (6.29)$$

In other words the mass ratios remain stable while the ratios of decay constants change quite considerably. We decide to take the difference between the central values in eq. (6.28) and in eq. (6.29) as an estimate of systematic uncertainty and after symmetrizing the error bars we finally obtain:

$$\begin{aligned} \frac{m_{D'_s}}{m_{D_s}} &= 1.53(7) \quad , \quad \frac{f_{D'_s}}{f_{D_s}} = 0.59(11) \quad , \\ \frac{m_{D'}}{m_D} &= 1.55(9) \quad , \quad \frac{f_{D'}}{f_D} = 0.57(16) \quad . \end{aligned} \quad (6.30)$$

With respect to the mass of the state suggested to be interpreted as  $D'$  and measured at BaBar,  $m_{D'}/m_D = 1.36$ , our result is significantly larger.

One could suspect that tuning the twisting angle to its maximal value on the lattice could be made only up to discretization effects which then induce a pollution to the extraction of the desired hadron state by the state with opposite parity. However, since that pollution is an  $\mathcal{O}(a^2)$  effect [183] and since we perform the extrapolation to the continuum limit, that argument could not be used to explain the potential discrepancy between our findings and the value measured at BaBar.

To further study this issue, we used the data at fixed lattice spacing (corresponding to  $\beta = 4.05$ ) and compared them with the results obtained by using the Wilson-Clover quark action with  $N_f = 2$  light flavors at nearly equal lattice spacing.<sup>3</sup> The results are

$$\text{MtmQCD} : \frac{m_{D'_s}}{m_{D_s}} = 1.55(6) \quad , \quad \frac{f_{D'_s}}{f_{D_s}} = 0.69(5) \quad , \quad (6.31)$$

$$\text{Clover} : \frac{m_{D'_s}}{m_{D_s}} = 1.48(7) \quad , \quad \frac{f_{D'_s}}{f_{D_s}} = 0.77(9) \quad . \quad (6.32)$$

In other words, at fixed lattice spacing and fixed light sea quark mass [ $m_q^{\overline{\text{MS}}}(2 \text{ GeV}) \simeq 25 \text{ MeV}$ ], the results for  $m_{D'_s}/m_{D_s}$  and  $f_{D'_s}/f_{D_s}$  obtained by using MtmQCD action are consistent with those obtained with the Wilson-Clover action. We therefore conclude that, within the above error bars, the mass of the radial excitation obtained on the lattice with  $N_f = 2$  dynamical quarks is larger than the state measured by BaBar.

Another potential difficulty when computing the properties of higher excited states on the lattice with light dynamical quarks is that the decay channels with emission of a pion might open up and modify the value of the extracted mass and decay constant. In the problem at hand, such channels are  $D' \rightarrow D^*\pi$  and/or  $D' \rightarrow D_0^*\pi$  in the case of non-strange radial excitation, and  $D'_s \rightarrow D^*K$  or  $D'_s \rightarrow D_{s0}^*K$  for the strange radial excitation. That difficulty does not exist in quenched QCD ( $N_f = 0$ ) which is why we produced a set of quenched QCD configurations at a similar lattice spacing (cf. Table 6.2) and computed the mass and decay constant of  $D_s$  meson and its radial excitation by following the same steps as described above. We have

$$N_f = 0 : \frac{m_{D'_s}}{m_{D_s}} = 1.41(9) \quad , \quad \frac{f_{D'_s}}{f_{D_s}} = 0.67(12) \quad , \quad (6.33)$$

$$N_f = 2 : \frac{m_{D'_s}}{m_{D_s}} = 1.48(7) \quad , \quad \frac{f_{D'_s}}{f_{D_s}} = 0.77(9) \quad . \quad (6.34)$$

From our data we cannot see the effects of the sea quark mass. We therefore conclude that within the statistical errors of this study the radially excited  $D'$  state is heavier than the one measured by BaBar as well as the one predicted by the constituent quark model of ref. [174]. It should be emphasized that this conclusion is based on the comparison made for the case of the strange valence light quark. We did not explore the lighter quarks to be able to make stronger statement for the non-strange  $m_{D'}/m_D$ . We believe more research is needed in that direction, to explore the simulations with very light sea and valence quarks and check whether or not the dependence of  $m_{D'}$  on the light quark mass changes considerably when close to the chiral limit, similar to the findings of ref. [130] for the Roper resonance. An indication that this indeed could be the case is provided by the results reported in ref. [129], where the simulations at one lattice spacing have been used to compute the spectrum of  $D_{(s)}$ -mesons.<sup>4</sup>

Concerning our results for the decay constants of the radial excitations, we see from eq. (6.28) that they are considerably smaller than those of the lowest states. This

3. The gauge field configurations with Wilson-Clover action have been produced by the QCDSF Collaboration [191, 192]. See Table 6.2.

4. Very recently two preliminary studies appeared in refs. [193, 194]. They do not report the numerical values for  $m_{D'_{(s)}}$  but from the plots provided we could see that their  $m_{D'}$  is larger than the mass of the state observed at BaBar, 2538(8) MeV.

situation is qualitatively different from what happens in the heavy quark limit ( $m_c \rightarrow \infty$ ), in which [162, 104]

$$\lim_{m_c \rightarrow \infty} \left( \frac{\sqrt{m_{D'_q}} f_{D'_q}}{\sqrt{m_{D_q}} f_{D_q}} \right) > 1, \quad (6.35)$$

while in our case, with the propagating charm quark, the above ratio is smaller than one.

## Conclusion

We computed  $m_{D'}/m_D$  and  $f_{D'}/f_D$  by using the gauge field configurations with  $N_f = 2$  mass-degenerate light quark flavors, generated at four lattice spacings and for several light sea quark masses. We find

$$\frac{m_{D'}}{m_D} = 1.55(9) \quad , \quad \frac{f_{D'}}{f_D} = 0.57(16). \quad (6.36)$$

If the state observed by BaBar Collaboration is indeed  $D'$ , then our result is larger than theirs,  $m_{D'}/m_D = 1.36$ . More research on both sides is needed to clarify the (potential) discrepancy. On the lattice QCD side it would be interesting to check whether or not  $m_{D'}/m_D$  becomes sensitive to the variation of the light quark mass in the region with very light quarks (closer to the chiral limit), the region not explored in the present study. Such a situation, that a hadron mass strongly depends on the sea quark mass when the latter is close to the chiral limit, was observed in the case of the Roper resonance on the lattice [130]. Concerning the interpretation of the state observed by BaBar at 2539(8) MeV, it is important to understand why its width is much larger than predicted. As a starting point one could verify if the predictions of ref. [175] remain stable if one uses different sets of wave functions (for example those of the model of ref. [174]) or different models.

We also improved the computation of the decay constants  $f_{D(s)}$  by relying on the chiral and continuum extrapolation of the ratios  $f_{D_s}/m_{D_s}$  and  $(\phi_{D_s}/\phi_D)/(f_K/f_\pi)$ . More specifically we obtain:

$$f_{D_s} = 252(3) \text{ MeV} \quad , \quad \frac{f_{D_s}}{f_D} = 1.23(1)(1), \quad (6.37)$$

where the second error in the latter result reflects the uncertainty due to inclusion/omission of the chiral logarithms in the light mass extrapolation to the physical limit. These two results give  $f_D = 205(5)(2) \text{ MeV}$ .<sup>5</sup>

We can finally use our results in equations (6.1) and (6.2) to predict the value of the form factor  $f_+^R(0)$  in terms of the branching ratios  $\mathcal{B}(\overline{B}^0 \rightarrow D'^+\pi^-)$  and  $\mathcal{B}(\overline{B}^- \rightarrow D'^0\pi^-)$ . Using the value  $|V_{cb}|f_+(q^2) \approx |V_{cb}|f_+(0) = 0.02642(8)$  from the BaBar Collaboration [195] and  $|V_{cb}| = 0.0411(16)$  [196], one obtains  $f_+(0) = 0.64(2)$  and we finally get

$$\begin{aligned} \mathcal{B}(\overline{B}^0 \rightarrow D'^+\pi^-) &= [3.6(6) \times 10^{-3}] |f_+^R(0)|^2, \\ \mathcal{B}(\overline{B}^- \rightarrow D'^0\pi^-) &= [3.8(7) \times 10^{-3}] \left[ 1 + \frac{0.16(5)}{f_+^R(0)} \right]^2 |f_+^R(0)|^2, \end{aligned}$$

5. Recent estimates of the vector meson decay constants  $f_{D_s^*}$ ,  $f_{D_s^*}/f_{D^*}$ , can be found in ref. [173].

---

where, in the last ratio, the quantity  $a_2/a_1$  is extracted from the measured branching ratios  $\mathcal{B}(B^- \rightarrow D^0\pi^-) = 0.481(15)\%$  and  $\mathcal{B}(\bar{B}^0 \rightarrow D^+\pi^-) = 0.268(13)\%$  [2].



# Conclusion

In this thesis, I have presented the results of our study on the heavy-light  $B$  and  $D$  mesons from lattice QCD with two dynamical quarks. In Chapters 3-5, the heavy  $b$  quark was simulated using the Heavy Quark Effective Theory (HQET) at static and first orders in the inverse quark mass and we used the Wilson Clover regularization for the light quarks. All results were extrapolated to the continuum and chiral limits analyzing a subset of the CLS lattice ensembles [69] and since physical volumes are large,  $Lm_\pi > 4$ , volume effects are expected to be negligible. In the last chapter, the  $D$  meson was simulated using the Twisted Mass formulation at maximal twist on ensembles provided by the ETM Collaboration.

In the first project, I have presented the results on the computation of the  $b$ -quark mass and  $B$  meson decay constant in the framework of HQET at static and first orders in the inverse heavy quark mass. We used the HQET parameters of ref. [68], computed non-perturbatively at different values of the heavy quark mass and in a large range of values, including the physical mass. The  $b$ -quark mass is then obtained by interpolating hadronic quantities, typically the mass of the heavy-light meson, at the physical  $B$  meson mass. All steps are carried out non-perturbatively except for the conversion of the RGI quark mass in the  $\overline{\text{MS}}$  scheme where the comparison with other results is easier. A particular attention was paid to the determination of the total error where all correlations have been taken into account. Systematic errors from the different extrapolations are also estimated using ten ensembles in a large range of lattice spacings [0.05 – 0.075] fm and pion masses down to 194 MeV. Our result reads  $\overline{m}_b^{\overline{\text{MS}}}(\overline{m}_b^{\overline{\text{MS}}}) = 4.21(11)$  GeV and is in agreement with the value cited by the PDG [2]. First order corrections in the HQET expansion are found to be small, making us confident that higher order corrections can be neglected at our level of accuracy. Moreover, comparing our result with previous quenched data obtained by the ALPHA Collaboration, no significant dependence on the number of active flavors can be stated. Finally, we used the HQET parameters, interpolated at the physical point, to compute other phenomenological interesting quantities like the  $B$  and  $B_s$  meson decay constants. Our results are  $f_B = 186(13)(2)_\chi$  MeV,  $f_{B_s} = 224(14)(2)_\chi$  MeV and  $f_{B_s}/f_B = 1.203(62)(19)_\chi$  where, in the last ratio, many systematic errors cancel. Our results are in agreement with the FLAG averages [106] and the first order corrections in the  $1/m$  expansion are small compared to the total error. These quantities allow us to predict the values of the CKM matrix elements  $|V_{ub}|$  and  $|V_{tb}^*V_{ts}|$  using the up-to-date experimental data for the branching ratios  $\mathcal{B}(B^- \rightarrow \tau^- \bar{\nu}_\tau)$  and  $\mathcal{B}(B_s \rightarrow \mu^+ \mu^-)$ .

In the second project presented in this thesis, I have studied the coupling constant associated to the hadronic transition  $B^{*'} \rightarrow B\pi$  where  $B^{*'}$  is the first radial excitation of the  $B^*$  meson. On the lattice, dealing with excited states is more complicated since the dominant contribution to the correlation functions comes from the ground state and the

Generalized Eigenvalue Problem is particularly well suited. Our result, extrapolated to the continuum and chiral limits is  $g_{12} = -0.17(4)$ , in agreement with a previous statement made in ref. [125] to explain the discrepancy between the sum rules estimates [197] and the experimental data for  $g_{D^*D\pi}$ . Then, we studied the scalar  $B$  meson on the lattice. Quark-antiquark, but also meson-meson interpolating operators have been implemented. The later are needed to extract information about the two-meson state composed of a pseudoscalar  $B$  meson and a pion. Studying the two point correlation function between a scalar  $B$  meson at time  $t = 0$  and a two-meson state at time  $t$ , we were able to extract the soft pion coupling  $h$ . Our result,  $h = 0.86(4)(2)$  shows a small dependence on the light quark mass and on the lattice spacing such that the extrapolations are smooth. No experimental data are presently available for the  $B$  meson but our result is compatible with the one for the  $D$  meson even if higher order corrections from the HQET expansion are expected to be sizable in the charm sector.

Finally, in the future, the HQET parameters could be used to compute other quantities like the mass splitting between the pseudoscalar and the vector  $B$  mesons. Also, a lattice computation of the soft pion coupling  $\tilde{g}$  and of the scalar  $B$  meson constant would enable us to test the influence of positive parity states in the chiral extrapolations of lattice data based on the Heavy Meson Chiral Lagrangian presented in Chapter 4. In particular, in Chapter 3, only negative parity states were taken into account in the extrapolation of the  $B$  meson decay constant, via the coupling  $\hat{g}$ . Since  $h$  is rather large and the mass splitting between the scalar and the pseudoscalar  $B$  meson is not large compared to pion mass, its influence may be noticeable.

In the last project, I have presented our results for the mass and decay constant of the radially excited  $D$  meson. A signal, compatible with this state, has been measured by the BaBar Collaboration [6] but with a decay width much larger than predicted by quark models [175]. We have computed the mass of this meson on the lattice and obtained  $m_{D'}/m_D = 1.55(9)$ , a value larger than experiment. Our result, obtained using the Twisted Mass formulation, is stable when compared to the result obtained with other lattice regularizations. Moreover, to test the influence of the potentially dangerous strong decays on the lattice, we performed a cross-check using quenched simulations and a compatible result was obtained. Therefore, additional efforts are necessary to explain the discrepancy between experiment and theory. Finally we have also computed the decay constant of the radially excited  $D$  meson and we obtained  $f_{D'}/f_D = 0.57(16)$ . This quantity, with the mass  $m_{D'}$ , can be used to compute the form factor  $f_+^R(0)$ , which governs the weak decays to the  $D'$  meson, in terms of the branching ratios  $\mathcal{B}(\overline{B}^0 \rightarrow D'^+\pi^-)$  and  $\mathcal{B}(\overline{B}^- \rightarrow D'^0\pi^-)$ . If  $f_+^R(0)$  is indeed large, as proposed in refs. [7, 5] to explain the “1/2 vs. 3/2” puzzle, then the previous strong decays should be accessible experimentally and could be used to check whether or not the assumption of a large  $f_+^R(0)$  is true.

# Appendices



# Appendix A

## Definitions and conventions

In Minkowski space-time, I use the following metric convention

$$\eta_{\mu\nu} = \{+, -, -, -\},$$

so that  $x^\mu = (x^0, \mathbf{x})$ ,  $x_\mu = (x^0, -\mathbf{x})$  and  $p \cdot x = p^0 x^0 - \mathbf{p} \cdot \mathbf{x}$ . In the Euclidean space-time, the metric becomes  $\delta_{\mu\nu}$ . In this work, repeated indices are understood to be summed except if stated otherwise.  $L$  and  $T$  are respectively the spatial and temporal extent of the lattice and  $a$  is the lattice spacing.

### A.1 The Dirac Algebra

In Minkowski space-time, the gamma matrices  $\gamma_\mu$  are defined by the anti-commutation relations  $\{\gamma_\mu, \gamma_\nu\} = 2\eta_{\mu\nu}$  of a Clifford algebra. It is also convenient to define the matrix  $\gamma_5$  and the total antisymmetric tensor  $\sigma_{\mu\nu}$  respectively given by

$$\gamma_5 = i\gamma_0\gamma_1\gamma_2\gamma_3 \quad \text{and} \quad \sigma_{\mu\nu} = \frac{i}{2}[\gamma_\mu, \gamma_\nu].$$

In the chiral representation, one has

$$\gamma^0 = \begin{pmatrix} 0 & 1 \\ 1 & 0 \end{pmatrix}, \quad \gamma^i = \begin{pmatrix} 0 & \sigma_i \\ -\sigma_i & 0 \end{pmatrix}, \quad \gamma^5 = \begin{pmatrix} -1 & 0 \\ 0 & 1 \end{pmatrix}$$

and in the Dirac representation,

$$\gamma^0 = \begin{pmatrix} 1 & 0 \\ 0 & -1 \end{pmatrix}, \quad \gamma^i = \begin{pmatrix} 0 & \sigma_i \\ -\sigma_i & 0 \end{pmatrix}, \quad \gamma^5 = \begin{pmatrix} 0 & 1 \\ 1 & 0 \end{pmatrix}$$

In Euclidean space-time, the gamma matrices  $\gamma_\mu^E$  must satisfy the Clifford algebra with respect to the metric  $\delta_{\mu\nu}$ , namely  $\{\gamma_\mu^E, \gamma_\nu^E\} = 2\delta_{\mu\nu}$ . The Euclidean matrices  $\gamma_\mu^E$  are obtained from previous one by the substitution

$$\gamma_0^E = \gamma_0, \quad \gamma_i^E = -i\gamma_i, \quad \gamma_5^E = \gamma_0^E \gamma_1^E \gamma_2^E \gamma_3^E,$$

and satisfy to the following relations

$$\begin{aligned} (\gamma_\mu^E)^\dagger &= \gamma_\mu^E, & (\gamma_5^E)^\dagger &= \gamma_5^E \\ (\gamma_\mu^E)^2 &= \mathbb{1}, & (\gamma_5^E)^2 &= \mathbb{1}. \end{aligned}$$

Moreover, the matrix  $\gamma_5^E$  anti-commutes with all matrices  $\gamma_\mu^E$ ,  $\{\gamma_5^E, \gamma_\mu^E\} = 0$ . Finally, a basis of the Dirac-Clifford Algebra is given by the sixteen linearly independent matrices

$$\{\mathbb{1}, \gamma_\mu, \sigma_{\mu\nu}, \gamma_\mu \gamma_5, \gamma_5\},$$

which transform respectively as a scalar, a vector, a tensor, a pseudo-vector and a pseudo-scalar quantity under space-time transformations. Two possible representations are the chiral and Dirac representations.

### Chiral representation

$$\gamma_0^E = \begin{pmatrix} 0 & 1 \\ 1 & 0 \end{pmatrix}, \quad \gamma_i^E = \begin{pmatrix} 0 & i\sigma_i \\ -i\sigma_i & 0 \end{pmatrix}, \quad \gamma_5^E = \begin{pmatrix} 1 & 0 \\ 0 & -1 \end{pmatrix}$$

### Dirac representation

$$\gamma_0^E = \begin{pmatrix} 1 & 0 \\ 0 & -1 \end{pmatrix}, \quad \gamma_i^E = \begin{pmatrix} 0 & i\sigma_i \\ -i\sigma_i & 0 \end{pmatrix}, \quad \gamma_5^E = \begin{pmatrix} 0 & -1 \\ -1 & 0 \end{pmatrix}$$

## A.2 Lattice derivatives

The discrete forward and backward derivatives are defined by

$$\partial_\mu \psi(x) = \frac{1}{a} [\psi(x + a\hat{\mu}) - \psi(x)], \quad (\text{A.1})$$

$$\partial_\mu^* \psi(x) = \frac{1}{a} [\psi(x) - \psi(x - a\hat{\mu})]. \quad (\text{A.2})$$

Similarly, the covariant derivative operators acting on fermions are

$$\nabla_\mu \psi(x) = \frac{1}{a} [U_\mu(x)\psi(x + a\hat{\mu}) - \psi(x)], \quad (\text{A.3})$$

$$\nabla_\mu^* \psi(x) = \frac{1}{a} [\psi(x) - U_\mu(x - a\hat{\mu})^{-1}\psi(x - a\hat{\mu})], \quad (\text{A.4})$$

$$\bar{\psi}(x) \overleftarrow{\nabla}_\mu = \frac{1}{a} [\bar{\psi}(x + a\hat{\mu})U_\mu(x)^{-1} - \bar{\psi}(x)], \quad (\text{A.5})$$

$$\bar{\psi}(x) \overleftarrow{\nabla}_\mu^* = \frac{1}{a} [\bar{\psi}(x) - \bar{\psi}(x - a\hat{\mu})U_\mu(x - a\hat{\mu})]. \quad (\text{A.6})$$

The symmetric covariant derivative is then given by

$$\tilde{\nabla}_\mu \psi(x) = \frac{\nabla_\mu + \nabla_\mu^*}{2} \psi(x) = \frac{1}{2a} [U_\mu(x)\psi(x + a\hat{\mu}) - U_\mu(x - a\hat{\mu})^{-1}\psi(x - a\hat{\mu})], \quad (\text{A.7})$$

and is useful to maintain the hermiticity of the Hamiltonian operator. Finally, the Laplace operator is defined via

$$\Delta = -\nabla_\mu \nabla_\mu^*,$$

and is explicitly given by

$$\Delta \psi(x) = \frac{1}{a^2} \sum_{\mu=1}^4 [U_\mu(x)\psi(x + a\hat{\mu}) - 2\psi(x) + U_\mu(x - a\hat{\mu})^{-1}\psi(x - a\hat{\mu})]. \quad (\text{A.8})$$

When the Laplace operator acts on space indices only, the same notation is used but  $i$  runs from 1 to 3

$$\Delta\psi(x) = \frac{1}{a^2} \sum_{i=1}^3 \left[ U_i(x)\psi(x + a\hat{i}) - 2\psi(x) + U_i(x - a\hat{i})^{-1}\psi(x - a\hat{i}) \right]. \quad (\text{A.9})$$

### A.3 The group SU(3)

The special unitary group SU(3) is a non-abelian Lie group of dimension 8. It is a compact group and the generators are defined by the following commutation relations

$$[T_i, T_j] = if_{ijk}T_k,$$

where  $f_{ijk}$ , the structure constants of the group, are given in ref. [8]. In the fundamental representation, a conventional choice for the generators  $T_i$  is given by  $T_i = \frac{1}{2}\lambda_i$  where  $\lambda_i$  are the eight Gell-Mann matrices

$$\lambda_1 = \begin{pmatrix} 0 & 1 & 0 \\ 1 & 0 & 0 \\ 0 & 0 & 0 \end{pmatrix}, \quad \lambda_2 = \begin{pmatrix} 0 & -i & 0 \\ i & 0 & 0 \\ 0 & 0 & 0 \end{pmatrix}, \quad \lambda_3 = \begin{pmatrix} 1 & 0 & 0 \\ 0 & -1 & 0 \\ 0 & 0 & 0 \end{pmatrix}$$

$$\lambda_4 = \begin{pmatrix} 0 & 0 & 1 \\ 0 & 0 & 0 \\ 1 & 0 & 0 \end{pmatrix}, \quad \lambda_5 = \begin{pmatrix} 0 & 0 & -i \\ 0 & 0 & 0 \\ i & 0 & 0 \end{pmatrix}, \quad \lambda_6 = \begin{pmatrix} 0 & 0 & 0 \\ 0 & 0 & 1 \\ 0 & 1 & 0 \end{pmatrix}$$

$$\lambda_7 = \begin{pmatrix} 0 & 0 & 0 \\ 0 & 0 & -i \\ 0 & i & 0 \end{pmatrix}, \quad \lambda_8 = \frac{1}{\sqrt{3}} \begin{pmatrix} 1 & 0 & 0 \\ 0 & 1 & 0 \\ 0 & 0 & -2 \end{pmatrix}.$$

Finally, the generators  $T_i$  obey the following relations

$$\text{Tr}(T_i T_j) = \frac{1}{2}\delta_{ij}, \quad (T_i)^\dagger = T_i.$$

### A.4 Fourier transformation

In the continuum, the Fourier transform of a function  $f$  (and its inverse) are defined by

$$\tilde{f}(k) = \int \frac{d^4x}{(2\pi)^4} e^{-ik \cdot x} f(x), \quad f(x) = \int d^4k e^{ik \cdot x} \tilde{f}(k),$$

and the delta function obeys

$$\int d^n x \delta^{(n)}(x) = 1 \quad , \quad \int d^4 x e^{ik \cdot x} = 2\pi \delta^{(4)}(k) .$$

Similarly, on the lattice, fields in momentum space are defined by

$$\tilde{\psi}(k) = a^4 \sum_x e^{-ikx} \psi(x) \quad , \quad \psi(x) = \frac{1}{(aL)^3 (aT)} \sum_k e^{ikx} \tilde{\psi}(k) .$$

# Appendix B

## Convergence rate in the sGEVP

In this section, I discuss the time dependence of  $\mathcal{M}_{mn}^{\text{sGEVP}}$  given by eq. (4.32) and used to extract the matrix element  $\mathcal{M}_{mn} = \langle B_n | A_i(0) | B_m^* \rangle$  where  $B_n$  is the  $n^{\text{th}}$  excited state ( $n = 1$  corresponds to the ground state). To simplify the notations, the lattice spacing is set to  $a = 1$ .

$$\mathcal{M}_{mn}^{\text{sGEVP}}(t, t_0) = -\partial_t \left( \frac{(v_m(t, t_0), [K(t, t_0)/\lambda_n(t, t_0) - K(t_0, t_0)] v_n(t, t_0))}{(v_n(t, t_0), C(t_0)v_n(t, t_0))^{1/2} (v_m(t, t_0), C(t_0)v_m(t, t_0))^{1/2}} e^{\Sigma(t_0, t_0)t_0/2} \right).$$

### B.1 Conventions

We have followed the strategy of ref. [42] to treat in perturbation theory the full GEVP, with an exact computation of the  $N$  lowest states:

$$C_{ij}(t) = \langle \mathcal{O}_i(t) \mathcal{O}_j(0) \rangle = C_{ij}^{(0)}(t) + \epsilon C_{ij}^{(1)}(t) = \sum_{n=1}^N e^{-E_n t} \psi_{ni} \psi_{nj} + \sum_{n=N+1}^{\infty} e^{-E_n t} \psi_{ni} \psi_{nj}, \quad (\text{B.1})$$

where  $\psi_{ni} = \langle 0 | \mathcal{O}_i | n \rangle$  and  $|n\rangle$  are the eigenstates of the transfer matrix with energy  $E_n$ . In the previous equation,  $\epsilon$  is the expansion parameter and

$$\begin{aligned} v_n(t, t_0) &= v_n^{(0)} + \epsilon v_n^{(1)}(t, t_0), \\ \lambda_n(t, t_0) &= \lambda_n^{(0)} + \epsilon \lambda_n^{(1)}(t, t_0), \end{aligned}$$

are the eigenvectors and eigenvalues of the Generalized Eigenvalue Problem

$$C(t)v_n(t, t_0) = \lambda_n(t, t_0)C(t_0)v_n(t, t_0). \quad (\text{B.2})$$

Eigenvectors are normalized such that

$$\begin{aligned} (v_m^{(0)}, C^{(0)}(t_0)v_n^{(0)}) &= \rho_n \delta_{nm}, \\ (v_n^{(1)}, C^{(0)}(t_0)v_n^{(0)}) &= 0, \end{aligned}$$

where  $\rho_n = e^{-E_n t}$ . Introducing the dual vectors  $u_n$  defined by

$$(u_n, \psi_m) = \sum_{i=1}^N u_{ni} \psi_{mi} = \delta_{nm} \quad \forall n \leq N,$$

we note, from equations B.1 and B.2, that

$$C^{(0)}(t)u_n = e^{-E_n t} \psi_n \quad , \quad v_n^{(0)}(t, t_0) = u_n \quad , \quad \lambda_n^{(0)}(t, t_0) = e^{-E_n(t-t_0)} .$$

Then, at zeroth-order, the matrix element is

$$\mathcal{M}_{mn}^{\text{eff},s,0} = \partial_t \left\{ \frac{\left( u_m, \left[ K(t, t_0)/\lambda_n^{(0)}(t, t_0) - K(t_0, t_0) \right] u_n \right)}{\left[ (u_m, C(t_0)u_m) (u_m, C(t_0)u_m) \right]^{1/2}} \right\} = \mathcal{M}_{mn} ,$$

with

$$(u_m, K(t, t_0)u_n) = \sum_{t_1} e^{-\Sigma_{mn}(t-t_1)} (u_m, C^{(3)}(t, t_1)u_n) = t \times \mathcal{M}_{nm} e^{-E_n t} ,$$

$$(u_n, C(t_0)u_n) = \rho_n = e^{-E_n t_0} ,$$

and where  $\Sigma_{mn} = E_n - E_m$ .

## B.2 First order corrections

At first order in  $\epsilon$ , we have

$$\lambda_n^{(1)} = \rho_n^{-1} (v_n^{(0)}, \Delta_n v_n^{(0)}) ,$$

$$v_n^{(1)} = \sum_{m \neq n} v_m^{(0)} \rho_m^{-1} \frac{(v_m^{(0)}, \Delta_n v_n^{(0)})}{\lambda_n^{(0)} - \lambda_m^{(0)}} = \sum_{n \neq m} \alpha_{nm} v_m^{(0)} ,$$

where  $\Delta_n = C^{(1)}(t) - \lambda_n(t)C^{(1)}(t_0)$  and  $\rho_n = e^{-E_n t_0}$ . With  $c_{n,m,l} = (u_n, \psi_l)(u_m, \psi_l)$  we get

$$\epsilon \frac{\lambda_n^{(1)}(t, t_0)}{\lambda_n^{(0)}(t, t_0)} = - \sum_{l > N} c_{n,n,l} e^{-(E_l - E_n)t_0} [1 - e^{-(E_l - E_n)(t-t_0)}] ,$$

$$\epsilon \alpha_{nm}(t, t_0) = - \sum_{l > N} c_{n,m,l} \frac{1 - e^{-(E_l - E_n)(t-t_0)}}{1 - e^{-(E_m - E_n)(t-t_0)}} e^{-(E_l - E_m)t_0} .$$

Finally the normalization conditions read

$$(v_n(t, t_0), C(t_0)v_n(t, t_0)) = \rho_n + \epsilon (v_n^{(0)}, C^{(1)}(t_0)v_n^{(0)}) .$$

We are ready to develop eq. (4.32) to first order in  $\epsilon$ :

$$\mathcal{M}_{mn}^{\text{eff},s} = \partial_t \left\{ \frac{\langle v_m(t, t_0), [K(t, t_0)/\lambda_n(t, t_0) - K(t_0, t_0)] v_n(t, t_0) \rangle}{\left[ \langle v_m(t, t_0), C^{(2)}(t_0)v_m(t, t_0) \rangle \langle v_n(t, t_0), C^{(2)}(t_0)v_n(t, t_0) \rangle \right]^{1/2}} e^{\frac{t_0}{2} \Sigma(t_0, t_0)} \right\}$$

$$= \mathcal{M}_{mn}^{\text{eff},s,0} + \epsilon \mathcal{M}_{mn}^{\text{eff},s,1} ,$$

and the sub-leading order reads

$$\epsilon \mathcal{M}_{mn}^{\text{eff},s,1} = \epsilon \partial_t \sum_{a=1}^5 T_a .$$

**First correction:**

The first sub-leading correction reads

$$\begin{aligned} T_1 &= -\frac{\lambda_n^{(1)}(t, t_0)}{(\lambda_n^{(0)}(t, t_0))^2} \frac{\left(v_m^{(0)}(t, t_0), K(t, t_0)v_n^{(0)}(t, t_0)\right)}{(\rho_n\rho_m)^{1/2}} e^{\frac{t_0}{2}\Sigma(t_0, t_0)} \\ &= -\frac{\lambda_n^{(1)}(t, t_0)}{\lambda_n^{(0)}(t, t_0)} \left(v_m^{(0)}(t, t_0), K(t, t_0)v_n^{(0)}(t, t_0)\right) e^{E_n t}. \end{aligned}$$

and is given by

$$T_1 = -\mathcal{M}_{mn} t \times \frac{\lambda_n^{(1)}(t, t_0)}{\lambda_n^{(0)}(t, t_0)} \sim c_{n,n,N+1} \mathcal{M}_{mn} \times t e^{-\Delta_{N+1,n}t_0} [1 - e^{-\Delta_{N+1,n}(t-t_0)}].$$

Defining the discrete derivative  $\partial_t A = A(t+1) - A(t)$ , and taking at the end of the computation  $t_0 = t - 1$ , we get

$$\partial_t T_1 \sim c_{n,n,N+1} \mathcal{M}_{mn} (1 - e^{-\Delta_{N+1,n}}) \times (t + 1 + e^{\Delta_{N+1,n}}) e^{-\Delta_{N+1,n}t}.$$

**Second correction:**

The second sub-leading contribution reads

$$\begin{aligned} T_2 &= \frac{\left(v_m^{(1)}(t, t_0), \left[K(t, t_0)/\lambda_n^{(0)}(t, t_0) - K(t_0, t_0)\right] v_n^{(0)}(t, t_0)\right)}{(\rho_n\rho_m)^{1/2}} e^{\frac{t_0}{2}\Sigma(t_0, t_0)} \\ &= \left(v_m^{(1)}(t, t_0), \left[K(t, t_0)e^{E_n t} - K(t_0, t_0)e^{E_n t_0}\right] v_n^{(0)}(t, t_0)\right). \end{aligned}$$

With some algebra, we deduce

$$\begin{aligned} \left(v_p^{(0)}(t, t_0), K(t, t_0)v_n^{(0)}(t, t_0)\right) e^{E_n t} &= \sum_{t_1} e^{-(t-t_1)(E_n - E_m)} \sum_{rs} (u_p, \psi_r)(\psi_s, u_n) \mathcal{M}_{rs} e^{-E_r(t-t_1)} e^{-E_s t_1} e^{E_n t} \\ &= \sum_{t_1} e^{-(t-t_1)(E_n - E_m)} \mathcal{M}_{pn} e^{-E_p(t-t_1)} e^{-E_n t_1} e^{E_n t} \\ &= \sum_{t_1} \mathcal{M}_{pn} e^{-(E_p - E_m)t_1}, \end{aligned}$$

and

$$\left(v_p^{(0)}(t, t_0), \left[K(t, t_0)e^{E_n t} - K(t_0, t_0)e^{E_n t_0}\right] v_n^{(0)}(t, t_0)\right) = \sum_{t_1=t_0+1}^t \mathcal{M}_{pn} e^{-(E_p - E_m)t_1}.$$

Finally,

$$\begin{aligned} T_2 &= \sum_{p \neq m} \left[ \alpha_{mp}(t, t_0) \sum_{t_1=t_0+1}^t \mathcal{M}_{pn} e^{-(E_p - E_m)t_1} \right], \\ \partial_t T_2 &= \sum_{p \neq m} \left[ (\alpha_{mp}(t+1, t_0) - \alpha_{mp}(t, t_0)) \sum_{t_1=t_0+1}^t \mathcal{M}_{pn} e^{-(E_p - E_m)t_1} + \alpha_{mp}(t+1, t_0) \mathcal{M}_{pn} \right. \\ &\quad \left. e^{-(E_p - E_m)(t+1)} \right]. \end{aligned}$$

Setting  $t_0 = t - 1$ , the first term of the previous equation reads

$$\begin{aligned} & \sum_{p \neq m} (\alpha_{mp}(t+1, t_0) - \alpha_{mp}(t, t_0)) \times \sum_{t_1=t_0+1}^t \mathcal{M}_{pn} e^{-(E_p - E_m)t_1} \\ & \sim - \sum_{p \neq m} \left[ c_{m,p,N+1} e^{-(E_{N+1} - E_p)(t-1)} \times \left( \frac{1 - e^{-2(E_{N+1} - E_m)}}{1 - e^{-2(E_p - E_m)}} - \frac{1 - e^{-(E_{N+1} - E_m)}}{1 - e^{-(E_p - E_m)}} \right) \right] \times \mathcal{M}_{pn} e^{-(E_p - E_m)t} \\ & \sim - e^{-(E_{N+1} - E_m)t} \sum_{p \neq m} \left[ c_{m,p,N+1} \mathcal{M}_{pn} e^{(E_{N+1} - E_p)} \times \left( \frac{1 - e^{-2(E_{N+1} - E_m)}}{1 - e^{-2(E_p - E_m)}} - \frac{1 - e^{-(E_{N+1} - E_m)}}{1 - e^{-(E_p - E_m)}} \right) \right], \end{aligned}$$

and the second term reads

$$\begin{aligned} & \sum_{p \neq m} \alpha_{mp}(t+1, t_0) \mathcal{M}_{pn} e^{-(E_p - E_m)(t+1)} \\ & \sim - \sum_{p \neq m} e^{-(E_{N+1} - E_p)(t-1)} \frac{1 - e^{-2(E_{N+1} - E_m)}}{1 - e^{-2(E_p - E_m)}} c_{m,p,N+1} \mathcal{M}_{pn} \times e^{-(E_p - E_m)(t+1)} \\ & \sim - e^{-(E_{N+1} - E_m)t} \sum_{p \neq m} e^{(E_{N+1} + E_m - 2E_p)} \frac{1 - e^{-2(E_{N+1} - E_m)}}{1 - e^{-2(E_p - E_m)}} c_{m,p,N+1} \mathcal{M}_{pn}. \end{aligned}$$

Finally, we find

$$\partial_t T_2 = e^{-\Delta_{N+1,m}t} \sum_{p \neq m} c_{m,p,N+1} \mathcal{M}_{pn} \frac{1 - e^{-(E_{N+1} - E_m)}}{1 - e^{-(E_m - E_p)}}.$$

### Third correction:

The third contribution

$$T_3 = \frac{\left( v_m^{(0)}(t, t_0), \left[ K(t, t_0) / \lambda_n^{(0)}(t, t_0) - K(t_0, t_0) \right] v_n^{(1)}(t, t_0) \right)}{(\rho_n \rho_m)^{1/2}} e^{\frac{t_0}{2} \Sigma(t_0, t_0)},$$

is obtained in the same manner as  $\partial_t T_2$  after permutation of the indices  $m$  and  $n$ .

### Fourth correction:

The fourth sub-leading contribution reads

$$T_4 = \frac{1}{\lambda_n^{(0)}(t, t_0)} \frac{\left( v_m^{(0)}(t, t_0), K^{(1)}(t, t_0) v_n^{(0)}(t, t_0) \right)}{(\rho_n \rho_m)^{1/2}} e^{\frac{t_0}{2} \Sigma(t_0, t_0)} = \left( v_m^{(0)}(t, t_0), K^{(1)}(t, t_0) v_n^{(0)}(t, t_0) \right) e^{E_n t}.$$

With some algebra we deduce

$$\begin{aligned}
(v_m^{(0)}(t, t_0), K^{(1)}(t, t_0)v_n^{(0)}(t, t_0)) &= \sum_{t_1} e^{-(E_n - E_m)(t - t_1)} \sum_{(r|s) > N} (u_m, \psi_r)(\psi_s, u_n) \mathcal{M}_{rs} e^{-E_r(t - t_1)} e^{-E_s t_1} \\
&= + \sum_{t_1} e^{-(E_n - E_m)(t - t_1)} (u_m, \psi_{N+1}) \mathcal{M}_{N+1, n} e^{-E_{N+1}(t - t_1)} e^{-E_n t_1} \\
&\quad + \sum_{t_1} e^{-(E_n - E_m)(t - t_1)} (u_n, \psi_{N+1}) \mathcal{M}_{N+1, m} e^{-E_m(t - t_1)} e^{-E_{N+1} t_1} \\
&\quad + \sum_{t_1} e^{-(E_n - E_m)(t - t_1)} \sum_{(r \& s) > N} (u_n, \psi_r)(u_m, \psi_s) \mathcal{M}_{r, s} e^{-E_r(t - t_1)} e^{-E_s t_1} \\
&= + \sum_{t_1} e^{-(E_n - E_m)t_1} (u_m, \psi_{N+1}) \mathcal{M}_{N+1, n} e^{-E_{N+1} t_1} e^{-E_n(t - t_1)} \\
&\quad + \sum_{t_1} e^{-E_n(t - t_1)} (u_n, \psi_{N+1}) \mathcal{M}_{N+1, m} e^{-E_{N+1} t_1} \\
&\quad + \sum_{t_1} e^{-(E_n - E_m)(t - t_1)} (u_n, \psi_{N+1})(u_m, \psi_{N+1}) \mathcal{M}_{N+1, N+1} e^{-E_{N+1} t} \\
&= + e^{-E_n t} (u_m, \psi_{N+1}) \mathcal{M}_{N+1, n} \sum_{t_1} e^{-(E_{N+1} - E_m)t_1} \\
&\quad + e^{-E_n t} (u_n, \psi_{N+1}) \mathcal{M}_{N+1, m} \sum_{t_1} e^{-(E_{N+1} - E_n)t_1} \\
&\quad + c_{n, m, N+1} \mathcal{M}_{N+1, N+1} e^{-E_{N+1} t} \sum_{t_1} e^{-(E_n - E_m)t_1},
\end{aligned}$$

and we obtain

$$\begin{aligned}
\partial_t T_4 &\sim + \langle u_m, \psi_{N+1} \rangle \mathcal{M}_{N+1, n} e^{-\Delta_{N+1, m}(t+1)} \\
&\quad + \langle u_n, \psi_{N+1} \rangle \mathcal{M}_{N+1, m} e^{-\Delta_{N+1, n}(t+1)} \\
&\quad - c_{n, m, N+1} \mathcal{M}_{N+1, N+1} \frac{e^{-(E_{N+1} - E_n)} - 1}{e^{-(E_n - E_m)} - 1} e^{-\Delta_{N+1, n} t} \\
&\quad - c_{n, m, N+1} \mathcal{M}_{N+1, N+1} \frac{e^{-(E_{N+1} - E_m)} - 1}{e^{-(E_m - E_n)} - 1} e^{-\Delta_{N+1, m} t}.
\end{aligned}$$

### Fifth correction:

Finally, the last sub-leading contribution reads

$$\begin{aligned}
T_5 &= -t \mathcal{M}_{mn} \times \left( \frac{\langle v_m^{(0)}, C^{(2,1)}(t_0)v_m^{(0)} \rangle}{2\rho_m} + \frac{\langle v_n^{(0)}, C^{(2,1)}(t_0)v_n^{(0)} \rangle}{2\rho_n} \right) \\
&\sim -t \mathcal{M}_{mn} \times \left( \frac{1}{2} c_{m, m, N+1} e^{-(E_{N+1} - E_m)t_0} + \frac{1}{2} c_{n, n, N+1} e^{-(E_{N+1} - E_n)t_0} \right),
\end{aligned}$$

and with  $t_0 = t - 1$ , we get

$$\partial_t T_5 \sim -\frac{\mathcal{M}_{mn}}{2} \times (c_{m, m, N+1} e^{-\Delta_{N+1, m}(t-1)} + c_{n, n, N+1} e^{-\Delta_{N+1, n}(t-1)}).$$

## Conclusion

We see that for  $n > m$  the dominating contribution  $T_1$  to  $\epsilon M_{mn}^{\text{eff},s,1}$  is in  $t e^{-\Delta_{N+1,n}t}$  with sub-leading terms  $T_2 - T_5$  while for  $n < m$  the leading contribution is in  $e^{-\Delta_{N+1,m}t}$ .

## B.3 Numerical tests

We have tested numerically our finding in the toy model of ref. [160], with  $r_0 E_n = n$ ,  $r_0 = 0.3$ , the  $3 \times 5$  matrix of couplings

$$\psi = \langle 0 | \mathcal{O}_i | n \rangle = \begin{pmatrix} 0.92 & 0.03 & -0.10 & -0.01 & -0.02 \\ 0.84 & 0.42 & 0.03 & -0.06 & 0.00 \\ 0.56 & 0.54 & 0.48 & 0.26 & 0.04 \end{pmatrix}$$

and the hadronic matrix elements

$$M_{nn} = 0.7 \frac{6}{n+5} \quad , \quad M_{n,m+n} = \frac{M_{nn}}{3m} .$$

The comparison between the analytical formulae and the numerical solution is plotted in Figure B.1. It is encouraging to obtain such good agreement after  $t = 8$ .

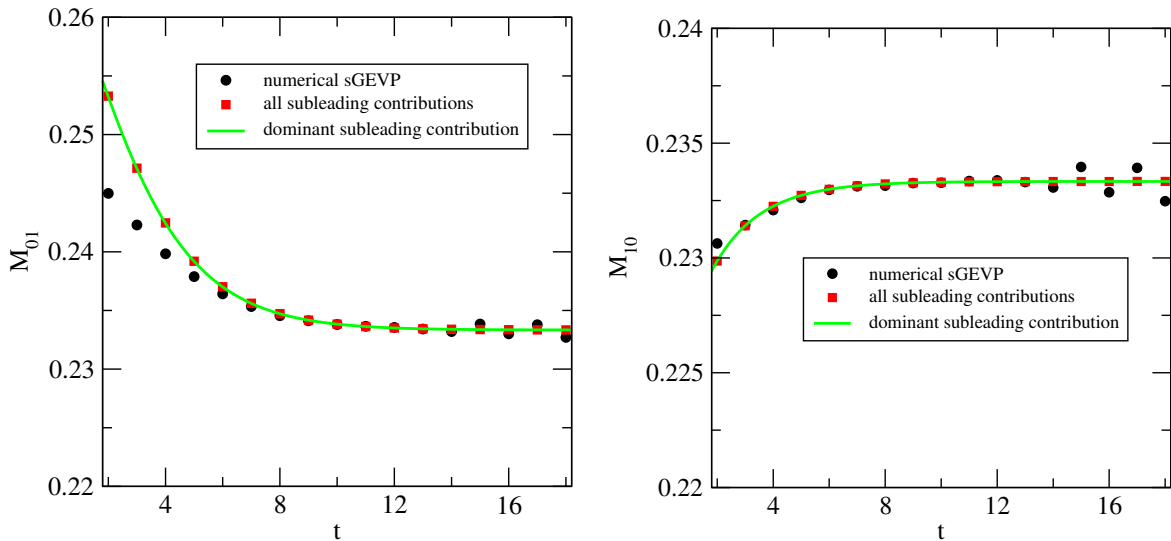


Figure B.1 – Analytical formulae for  $R_{mn}^{\text{sGEVP}}$  compared to the numerical solution of our toy model.



**First contribution**

$$\begin{aligned} & \overbrace{[\bar{d}(x_1)\Gamma u(x_1)] [\bar{u}(x_2)\Gamma b(x_2)] [\bar{b}(y_2)\bar{\Gamma}u(y_2)] [\bar{u}(y_1)\bar{\Gamma}d(y_1)]} \\ & = -\text{Tr} [G_d(y_1, x_1)\Gamma G_u(x_1, x_2)\Gamma G_b(x_2, y_2)\bar{\Gamma}G_u(y_2, y_1)\bar{\Gamma}] \end{aligned}$$

$$\begin{aligned} & \overbrace{[\bar{d}(x_1)\Gamma u(x_1)] [\bar{u}(x_2)\Gamma b(x_2)] [\bar{b}(y_2)\bar{\Gamma}u(y_2)] [\bar{u}(y_1)\bar{\Gamma}d(y_1)]} \\ & = +\text{Tr} [G_d(y_1, x_1)\Gamma G_u(x_1, y_1)\bar{\Gamma}] \text{Tr} [G_u(y_2, x_2)\Gamma G_b(x_2, y_2)\bar{\Gamma}] \end{aligned}$$

**Second contribution**

In the brackets corresponding to the neutral pion, Wick contractions between quarks  $u$  and  $\bar{u}$  or between quarks  $d$  and  $\bar{d}$  at the same space-time point cancel with each other and their contributions vanish due to isospin symmetry.

$$\begin{aligned} & \overbrace{[\bar{u}(x_1)\Gamma u(x_1) - \bar{d}(x_1)\Gamma d(x_1)] [\bar{d}(x_2)\Gamma b(x_2)] [\bar{b}(y_2)\bar{\Gamma}d(y_2)] [\bar{u}(y_1)\bar{\Gamma}u(y_1) - \bar{d}(y_1)\bar{\Gamma}d(y_1)]} \\ & = -\text{Tr} [G_d(y_1, x_1)\Gamma G_d(x_1, x_2)\Gamma G_b(x_2, y_2)\bar{\Gamma}G_d(y_2, y_1)\bar{\Gamma}] \end{aligned}$$

$$\begin{aligned} & \overbrace{[\bar{u}(x_1)\Gamma u(x_1) - \bar{d}(x_1)\Gamma d(x_1)] [\bar{d}(x_2)\Gamma b(x_2)] [\bar{b}(y_2)\bar{\Gamma}d(y_2)] [\bar{u}(y_1)\bar{\Gamma}u(y_1) - \bar{d}(y_1)\bar{\Gamma}d(y_1)]} \\ & = +2 \times \text{Tr} [G_d(y_1, x_1)\Gamma G_d(x_1, y_1)\bar{\Gamma}] \text{Tr} [G_d(y_2, x_2)\Gamma G_b(x_2, y_2)\bar{\Gamma}] \end{aligned}$$

The factor two comes from the same contraction pattern but with quarks  $u(x_1)$  and  $\bar{u}(x_1)$  contracted with quarks  $\bar{u}(y_1)$  and  $u(y_1)$  respectively.

$$\begin{aligned} & \overbrace{[\bar{u}(x_1)\Gamma u(x_1) - \bar{d}(x_1)\Gamma d(x_1)] [\bar{d}(x_2)\Gamma b(x_2)] [\bar{b}(y_2)\bar{\Gamma}d(y_2)] [\bar{u}(y_1)\bar{\Gamma}u(y_1) - \bar{d}(y_1)\bar{\Gamma}d(y_1)]} \\ & = -\text{Tr} [G_d(y_1, x_2)\Gamma G_b(x_2, y_2)\bar{\Gamma}G_d(y_2, x_1)\Gamma G_d(x_1, y_1)\bar{\Gamma}] \end{aligned}$$

**Third contribution**

$$\begin{aligned} & \overbrace{[\bar{d}(x_1)\Gamma u(x_1)] [\bar{u}(x_2)\Gamma b(x_2)] [\bar{b}(y_2)\bar{\Gamma}d(y_2)] [\bar{u}(y_1)\bar{\Gamma}u(y_1) - \bar{d}(y_1)\bar{\Gamma}d(y_1)]} \\ & = +\text{Tr} [G_d(y_1, x_1)\Gamma G_u(x_1, x_2)\Gamma G_b(x_2, y_2)\bar{\Gamma}G_d(y_2, y_1)\bar{\Gamma}] \end{aligned}$$

$$\begin{aligned} & \overbrace{[\bar{d}(x_1)\Gamma u(x_1)] [\bar{u}(x_2)\Gamma b(x_2)] [\bar{b}(y_2)\bar{\Gamma}d(y_2)] [\bar{u}(y_1)\bar{\Gamma}u(y_1) - \bar{d}(y_1)\bar{\Gamma}d(y_1)]} \\ & = -\text{Tr} [G_u(y_1, x_2)\Gamma G_b(x_2, y_2)\bar{\Gamma}G_d(y_2, x_1)\Gamma G_d(x_1, y_1)\bar{\Gamma}] \end{aligned}$$

where, as before, contractions between up and down quarks in the last bracket are not considered due to isospin symmetry.

#### Fourth contribution

$$\begin{aligned}
 & \overbrace{[\bar{u}(x_1)\Gamma u(x_1) - \bar{d}(x_1)\Gamma d(x_1)]}^{\text{---}} \overbrace{[\bar{d}(x_2)\Gamma b(x_2)]}^{\text{---}} \overbrace{[\bar{b}(y_2)\bar{\Gamma} u(y_2)]}^{\text{---}} \overbrace{[\bar{u}(y_1)\bar{\Gamma} d(y_1)]}^{\text{---}} \\
 & = +\text{Tr} [G_d(y_1, x_1)\Gamma G_d(x_1, x_2)\Gamma G_b(x_2, y_2)\bar{\Gamma} G_u(y_2, y_1)\bar{\Gamma}]
 \end{aligned}$$

$$\begin{aligned}
 & \overbrace{[\bar{u}(x_1)\Gamma u(x_1) - \bar{d}(x_1)\Gamma d(x_1)]}^{\text{---}} \overbrace{[\bar{d}(x_2)\Gamma b(x_2)]}^{\text{---}} \overbrace{[\bar{b}(y_2)\bar{\Gamma} u(y_2)]}^{\text{---}} \overbrace{[\bar{u}(y_1)\bar{\Gamma} d(y_1)]}^{\text{---}} \\
 & = -\text{Tr} [G_d(y_1, x_2)\Gamma G_b(x_2, y_2)\bar{\Gamma} G_u(y_2, x_1)\Gamma G_u(x_1, y_1)\bar{\Gamma}]
 \end{aligned}$$

#### Conclusion :

The meson-meson two-point correlation function is the sum of three terms with coefficients  $\alpha = 1$ ,  $\beta = -3/2$  and  $\gamma = 1/2$ :

$$\begin{aligned}
 C_{B\pi-B\pi}(t) &= \frac{\alpha}{V^4} \sum_{\vec{x}_i, \vec{y}_i} \text{Tr} [G_l(y_1, x_1)\Gamma G_l(x_1, y_1)\bar{\Gamma}] \times \text{Tr} [G_h(y_2, x_2)\Gamma G_l(x_2, y_2)\bar{\Gamma}] \\
 &+ \frac{\beta}{V^4} \sum_{\vec{x}_i, \vec{y}_i} \text{Tr} [G_l(y_1, x_1)\Gamma G_l(x_1, x_2)\Gamma G_h(x_2, y_2)\bar{\Gamma} G_l(y_2, y_1)\bar{\Gamma}] \\
 &+ \frac{\gamma}{V^4} \sum_{\vec{x}_i, \vec{y}_i} \text{Tr} [G_l(y_1, x_2)\Gamma G_h(x_2, y_2)\bar{\Gamma} G_l(y_2, x_1)\Gamma G_l(x_1, y_1)\bar{\Gamma}] .
 \end{aligned}$$

They correspond to the direct, box and cross diagrams respectively (Figure 5.3).



# Appendix D

## Renormalization

### D.1 The renormalization group

The renormalized parameters of the Lagrangian ( $\bar{g}$  and  $\bar{m}_i$ ) are function of the scale  $\mu$ . However, in renormalizable theories, physical predictions should be independent of this mass scale and therefore satisfy the following renormalization group equation

$$\frac{dP}{d\mu} = 0 \Leftrightarrow \left( \mu \frac{\partial}{\partial \mu} + \beta(\bar{g}) \frac{\partial}{\partial \bar{g}} + \tau(\bar{g}) \bar{m} \frac{\partial}{\partial \bar{m}} - \gamma_Q(\bar{g}) \right) P(\bar{g}(\mu), \bar{m}(\mu), \mu) = 0$$

where the beta function  $\beta$ , the anomalous dimension of the mass  $\tau$  and the anomalous dimension of the field  $\gamma_Q$  are respectively defined by

$$\beta(\bar{g}) = \mu \frac{\partial \bar{g}}{\partial \mu} \quad , \quad \tau(\bar{g}) = \frac{\mu}{\bar{m}} \frac{\partial \bar{m}}{\partial \mu} \quad , \quad \gamma_Q(\bar{g}) = \frac{\mu}{2Z} \frac{\partial Z}{\partial \mu} \quad ,$$

and where  $Z$  is the wave function renormalization factor.

### D.2 Perturbative running of the strong coupling and quark masses

The  $\beta$  and  $\tau$  functions can be computed in perturbation theory (but they are also perfectly well defined non-perturbatively), their expansions read

$$\beta(\bar{g}) = -b_0 \bar{g}^3 - b_1 \bar{g}^5 - b_2 \bar{g}^7 + \mathcal{O}(\bar{g}^9) \quad , \quad \tau(\bar{g}) = -d_0 \bar{g}^2 - d_1 \bar{g}^4 + \mathcal{O}(\bar{g}^6) \quad ,$$

and the parameters  $b_0$ ,  $b_1$  et  $d_0$  are scheme independent (for massless renormalization schemes). One can define the Lambda parameter and the renormalization group invariant mass (RGI) by

$$\Lambda = \mu (b_0 \bar{g}^2)^{-b_1/2b_0} \exp \left( -\frac{1}{2b_0 \bar{g}^2} \right) \times \exp \left\{ -\int_0^{\bar{g}(\mu)} dx \left[ \frac{1}{\beta(x)} + \frac{1}{b_0 x^3} - \frac{b_1}{b_0^2 x} \right] \right\} \quad , \quad (\text{D.1})$$

$$M_i = \bar{m}_i(\mu) (2b_0 \bar{g}^2(\mu))^{-d_0/2b_0} \times \exp \left\{ -\int_0^{\bar{g}(\mu)} dx \left[ \frac{\tau(x)}{\beta(x)} - \frac{d_0}{b_0 x} \right] \right\} \quad . \quad (\text{D.2})$$

The quantities  $\Lambda$  and  $M_i$  are Renormalization Group Invariant (RGI) and do not depend on the renormalization scale. In particular they satisfy the renormalization group equation (D.3)

$$\left\{ \mu \frac{\partial}{\partial \mu} + \beta(\bar{g}) \frac{\partial}{\partial \bar{g}} + \tau(\bar{g}) \bar{m} \frac{\partial}{\partial \bar{m}} \right\} P = 0. \quad (\text{D.3})$$

The mass  $M_i$  is also scheme independent but not  $\Lambda$ . The relationship between  $\Lambda$  and  $\Lambda'$  in two different renormalization schemes is exactly given by the one loop calculation

$$\Lambda' = \Lambda e^{c_1/(2b_0)},$$

where  $c_1$  is defined by

$$\bar{g}' = \bar{g} (1 + c_1 \bar{g}^3 + \dots).$$

## D.3 Tables

### Coefficients of the $\beta$ function in the $\overline{MS}$ scheme

The coefficients  $b_0$  and  $b_1$  are scheme independent and the other coefficients are given by [102]:

$$\begin{aligned} b_0 &= \frac{1}{(4\pi)^2} \left( 11 - \frac{2}{3} N_f \right), \\ b_1 &= \frac{1}{(4\pi)^4} \left( 102 - \frac{38}{3} N_f \right), \\ b_2 &= \frac{1}{(4\pi)^6} \left( \frac{2857}{2} - \frac{5033}{18} N_f + \frac{325}{54} N_f^2 \right), \\ b_3 &= \frac{1}{(4\pi)^8} \left( \left[ \frac{149753}{6} + 3564 \xi_3 \right] - \left[ \frac{1078361}{162} + \frac{6508}{27} \xi_3 \right] N_f + \left[ \frac{50065}{162} + \frac{6472}{81} \xi_3 \right] N_f^2 + \frac{1093}{729} N_f^3 \right), \end{aligned}$$

where  $N_f$  is the number of active flavours.

### Coefficients of the $\tau$ function in the $\overline{MS}$ scheme

The first coefficient of the quark mass anomalous dimension,  $d_0$ , is scheme independent. The other coefficients are known up to five loops in the  $\overline{MS}$  scheme [198, 103]:

$$\begin{aligned} d_0 &= \frac{8}{(4\pi)^2}, \\ d_1 &= \frac{1}{(4\pi)^4} \left( \frac{404}{3} - \frac{40}{9} N_f \right), \\ d_2 &= \frac{1}{(4\pi)^6} \left( 2498 - \left[ \frac{4432}{27} + \frac{320}{3} \xi_3 \right] N_f - \frac{280}{81} N_f^2 \right), \\ d_3 &= \frac{1}{(4\pi)^8} \left( \left[ \frac{9206110}{162} + \frac{271360}{27} \xi_3 - 17600 \xi_5 \right] + \left[ -\frac{183446}{27} - \frac{68384}{9} \xi_3 + 1760 \xi_4 + \frac{36800}{9} \xi_5 \right] N_f \right. \\ &\quad \left. + \left[ \frac{10484}{243} + \frac{1600}{9} \xi_3 - \frac{320}{3} \xi_4 \right] N_f^2 + \left[ -\frac{664}{243} + \frac{128}{27} \right] N_f^3 \right), \end{aligned}$$

$$\begin{aligned}
d_4 = \frac{1}{(4\pi)^{10}} & \left( \frac{99512327}{162} + \frac{46402466}{243}\xi_3 + 96800\xi_3^2 - \frac{698126}{9}\xi_4 - \frac{231757160}{243}\xi_5 + 242000\xi_6 \right. \\
& + 412720\xi_7 + N_f \left[ -\frac{150736283}{1458} - \frac{12538016}{81}\xi_3 - \frac{75680}{9}\xi_3^2 + \frac{2038742}{27}\xi_4 + \frac{49876180}{243}\xi_5 \right. \\
& - \frac{638000}{9}\xi_6 - \left. \frac{1820000}{27}\xi_7 \right] + N_f^2 \left[ \frac{1320742}{729} + \frac{2010824}{243}\xi_3 + \frac{46400}{27}\xi_3^2 - \frac{166300}{27}\xi_4 - \frac{264040}{81}\xi_5 \right. \\
& \left. \left. + \frac{92000}{27}\xi_6 \right] + N_f^3 \left[ \frac{91865}{1458} + \frac{12848}{81}\xi_3 + \frac{448}{9}\xi_4 - \frac{5120}{27}\xi_5 \right] + N_f^4 \left[ -\frac{260}{243} - \frac{320}{243}\xi_3 + \frac{64}{27}\xi_4 \right] \right).
\end{aligned}$$

### Coefficients in the Schrödinger Functional scheme

The parameters  $b_0$ ,  $b_1$  and  $d_0$  are scheme independent, so they are the same in the SF and  $\overline{\text{MS}}$  schemes. The parameter  $b_2$  and  $d_1$  have been computed respectively in [199] and [200]:

$$\begin{aligned}
b_2 &= \frac{1}{(4\pi)^3} (0.483(7) - 0.275(5)N_f + 0.0361(5)N_f^2 - 0.00175(1)N_f^3), \\
d_1 &= d_0 (0.0271 + 0.0105N_f).
\end{aligned}$$

Finally, the relation between the  $\Lambda$  parameter in the SF and  $\overline{\text{MS}}$  schemes is [201]

$$\Lambda_{\overline{\text{MS}}}^{(2)} = 2.382035(3)\Lambda_{\text{SF}}^{(2)}.$$

## D.4 Other conventions

The  $\beta$  and  $\tau$  functions can be defined in terms of  $\bar{\alpha} = \bar{g}^2/(4\pi)$ :

$$\beta(\bar{\alpha}) = \mu^2 \frac{d\bar{\alpha}}{d\mu^2} = - \sum_{i \geq 0} \beta_i \left( \frac{\bar{\alpha}}{\pi} \right)^{i+2}, \quad b_i = \frac{\beta_i}{(4\pi^2)^{i+1}},$$

and

$$\gamma(\bar{\alpha})\bar{m}_i = \mu^2 \frac{d\bar{m}_i}{d\mu^2} = -\bar{m} \sum_{i \geq 0} \gamma_i \left( \frac{\bar{\alpha}}{\pi} \right)^{i+1}, \quad d_i = \frac{2\gamma_i}{(4\pi^2)^{i+1}}.$$

A different convention to define the RGI mass  $\hat{m}$  is also used in ref. [101], the relation between  $\hat{m}$  and  $M$  is given by

$$\hat{m} = \lim_{\mu \rightarrow \infty} \bar{m}_i(\mu) \left( \frac{\bar{\alpha}(\mu)}{\pi} \right)^{-\frac{\gamma_0}{\beta_0}} = \left( \frac{1}{8\pi^2 b_0} \right)^{-\frac{d_0}{2b_0}} M. \quad (\text{D.4})$$



# Bibliography

- [1] F. Bernardoni, B. Blossier, J. Bulava, M. Della Morte, P. Fritzsche, et al., *The  $b$ -quark mass from non-perturbative  $N_f = 2$  Heavy Quark Effective Theory at  $O(1/m_h)$* , Phys.Lett. **B730** (2014) 171–177, [arXiv:1311.5498].
- [2] **Particle Data Group**, J. Beringer et al., *Review of Particle Physics (RPP)*, Phys.Rev. **D86** (2012) 010001.
- [3] F. Bernardoni, B. Blossier, J. Bulava, M. Della Morte, P. Fritzsche, et al., *Decay constants of  $B$ -mesons from non-perturbative HQET with two light dynamical quarks*, [arXiv:1404.3590].
- [4] B. Blossier, A. Gérardin, J. Bulava, and M. Donnellan, *On the  $B^{*'} \rightarrow B$  transition*, PoS **LATTICE2013** (2013) 256, [arXiv:1312.3495].
- [5] D. Becirevic, B. Blossier, A. Gerardin, A. Le Yaouanc, and F. Sanfilippo, *On the significance of  $B$ -decays to radially excited  $D$* , Nucl.Phys. **B872** (2013) 313–332, [arXiv:1301.7336].
- [6] **BaBar Collaboration**, P. del Amo Sanchez et al., *Observation of new resonances decaying to  $D\pi$  and  $D^*\pi$  in inclusive  $e^+e^-$  collisions near  $\sqrt{s} = 10.58$  GeV*, Phys.Rev. **D82** (2010) 111101, [arXiv:1009.2076].
- [7] F. U. Bernlochner, Z. Ligeti, and S. Turczyk, *A Proposal to solve some puzzles in semileptonic  $B$  decays*, Phys.Rev. **D85** (2012) 094033, [arXiv:1202.1834].
- [8] M. E. Peskin and D. V. Schroeder, *An Introduction to quantum field theory*. 1995.
- [9] S. Weinberg, *The Quantum theory of fields. Vol. 1: Foundations*. 1995.
- [10] S. Weinberg, *The quantum theory of fields. Vol. 2: Modern applications*. 1996.
- [11] S. L. Adler and D. Boulware, *Anomalous commutators and the triangle diagram*, Phys.Rev. **184** (1969) 1740–1744.
- [12] R. Jackiw and K. Johnson, *Anomalies of the axial vector current*, Phys.Rev. **182** (1969) 1459–1469.
- [13] R. Streater and A. Wightman, *PCT, spin and statistics, and all that*. 1989.
- [14] K. Osterwalder and R. Schrader, *Axioms for euclidean Green's functions*, Commun.Math.Phys. **31** (1973) 83–112.
- [15] K. Osterwalder and R. Schrader, *Axioms for Euclidean Green's Functions. 2.*, Commun.Math.Phys. **42** (1975) 281.
- [16] J. Glimm and A. Jaffe, *Quantum Physics, A Functional Integral of View*. Springer, New York, 1981.
- [17] L. Maiani and M. Testa, *Final state interactions from Euclidean correlation functions*, Phys.Lett. **B245** (1990) 585–590.
- [18] K. G. Wilson, *Confinement of Quarks*, Phys.Rev. **D10** (1974) 2445–2459.

- [19] E. Seiler, *Gauge Theories as a Problem of Constructive Quantum Field Theory and Statistical Mechanics*, Lect.Notes Phys. **159** (1982) 1–192.
- [20] L. Susskind, *Lattice Fermions*, Phys.Rev. **D16** (1977) 3031–3039.
- [21] K. G. Wilson, *Quarks and Strings on a Lattice*. 1975.
- [22] B. Sheikholeslami and R. Wohlert, *Improved Continuum Limit Lattice Action for QCD with Wilson Fermions*, Nucl.Phys. **B259** (1985) 572.
- [23] M. Luscher and P. Weisz,  *$O(a)$  improvement of the axial current in lattice QCD to one loop order of perturbation theory*, Nucl.Phys. **B479** (1996) 429–458, [hep-lat/9606016].
- [24] **ALPHA Collaboration**, K. Jansen and R. Sommer,  *$O(\alpha)$  improvement of lattice QCD with two flavors of Wilson quarks*, Nucl.Phys. **B530** (1998) 185–203, [hep-lat/9803017].
- [25] M. G. Alford, T. Klassen, and G. Lepage, *Improving lattice quark actions*, Nucl.Phys. **B496** (1997) 377–407, [hep-lat/9611010].
- [26] H. B. Nielsen and M. Ninomiya, *Absence of Neutrinos on a Lattice. 1. Proof by Homotopy Theory*, Nucl.Phys. **B185** (1981) 20.
- [27] H. B. Nielsen and M. Ninomiya, *Absence of Neutrinos on a Lattice. 2. Intuitive Topological Proof*, Nucl.Phys. **B193** (1981) 173.
- [28] H. B. Nielsen and M. Ninomiya, *No Go Theorem for Regularizing Chiral Fermions*, Phys.Lett. **B105** (1981) 219.
- [29] P. H. Ginsparg and K. G. Wilson, *A Remnant of Chiral Symmetry on the Lattice*, Phys.Rev. **D25** (1982) 2649.
- [30] R. Frezzotti, P. A. Grassi, S. Sint, and P. Weisz, *A Local formulation of lattice QCD without unphysical fermion zero modes*, Nucl.Phys.Proc.Suppl. **83** (2000) 941–946, [hep-lat/9909003].
- [31] **ALPHA Collaboration**, R. Frezzotti, P. A. Grassi, S. Sint, and P. Weisz, *Lattice QCD with a chirally twisted mass term*, JHEP **0108** (2001) 058, [hep-lat/0101001].
- [32] **ALPHA Collaboration**, R. Frezzotti, S. Sint, and P. Weisz,  *$O(a)$  improved twisted mass lattice QCD*, JHEP **0107** (2001) 048, [hep-lat/0104014].
- [33] Y. Saad, *Iterative Methods for Sparse Linear Systems*. Society for Industrial and Applied Mathematics, Philadelphia, PA, USA, 2nd ed., 2003.
- [34] G. Bhanot, *The Metropolis Algorithm*, Rept.Prog.Phys. **51** (1988) 429.
- [35] S. Duane, A. Kennedy, B. Pendleton, and D. Roweth, *Hybrid Monte Carlo*, Phys.Lett. **B195** (1987) 216–222.
- [36] J. Foley, K. Jimmy Juge, A. O’Cais, M. Peardon, S. M. Ryan, et al., *Practical all-to-all propagators for lattice QCD*, Comput.Phys.Commun. **172** (2005) 145–162, [hep-lat/0505023].
- [37] M. Luscher, “DD-HMC algorithm for two-flavour lattice qcd.” [<http://luscher.web.cern.ch/luscher/DD-HMC/index.html>] .
- [38] M. Luscher, *Schwarz-preconditioned HMC algorithm for two-flavour lattice QCD*, Comput.Phys.Commun. **165** (2005) 199–220, [hep-lat/0409106].
- [39] M. Luscher, *Solution of the Dirac equation in lattice QCD using a domain decomposition method*, Comput.Phys.Commun. **156** (2004) 209–220, [hep-lat/0310048].

- [40] M. Luscher, *Local coherence and deflation of the low quark modes in lattice QCD*, JHEP **0707** (2007) 081, [arXiv:0706.2298].
- [41] M. Luscher, *Deflation acceleration of lattice QCD simulations*, JHEP **0712** (2007) 011, [arXiv:0710.5417].
- [42] B. Blossier, M. Della Morte, G. von Hippel, T. Mendes, and R. Sommer, *On the generalized eigenvalue method for energies and matrix elements in lattice field theory*, JHEP **0904** (2009) 094, [arXiv:0902.1265].
- [43] **APE Collaboration**, M. Albanese et al., *Glueball Masses and String Tension in Lattice QCD*, Phys.Lett. **B192** (1987) 163–169.
- [44] A. Hasenfratz and F. Knechtli, *Flavor symmetry and the static potential with hypercubic blocking*, Phys.Rev. **D64** (2001) 034504, [hep-lat/0103029].
- [45] M. Della Morte, A. Shindler, and R. Sommer, *On lattice actions for static quarks*, JHEP **0508** (2005) 051, [hep-lat/0506008].
- [46] S. Gusken, U. Low, K. Mutter, R. Sommer, A. Patel, et al., *Nonsinglet Axial Vector Couplings of the Baryon Octet in Lattice QCD*, Phys.Lett. **B227** (1989) 266.
- [47] **ALPHA Collaboration**, U. Wolff, *Monte Carlo errors with less errors*, Comput.Phys.Commun. **156** (2004) 143–153, [hep-lat/0306017].
- [48] R. Miller, *The Jackknife: A Review.*, Biometrika. **61** (1974) 1–15.
- [49] P. Young, *Jackknife and bootstrap resampling methods in statistical analysis to correct for bias*, Statistical Science **11** (1996) 189–228.
- [50] **ALPHA Collaboration**, S. Schaefer, R. Sommer, and F. Virotta, *Critical slowing down and error analysis in lattice QCD simulations*, Nucl.Phys. **B845** (2011) 93–119, [arXiv:1009.5228].
- [51] S. Capitani, M. Della Morte, G. von Hippel, B. Knippschild, and H. Wittig, *Scale setting via the  $\Omega$  baryon mass*, PoS **LATTICE2011** (2011) 145, [arXiv:1110.6365].
- [52] P. Fritzscht, F. Knechtli, B. Leder, M. Marinkovic, S. Schaefer, et al., *The strange quark mass and Lambda parameter of two flavor QCD*, Nucl.Phys. **B865** (2012) 397–429, [arXiv:1205.5380].
- [53] M. Luscher, *Volume Dependence of the Energy Spectrum in Massive Quantum Field Theories. 1. Stable Particle States*, Commun.Math.Phys. **104** (1986) 177.
- [54] J. Gasser and H. Leutwyler, *Chiral Perturbation Theory to One Loop*, Annals Phys. **158** (1984) 142.
- [55] J. Goity, *Chiral perturbation theory for SU(3) breaking in heavy meson systems*, Phys.Rev. **D46** (1992) 3929–3936, [hep-ph/9206230].
- [56] **BaBar Collaboration**, J. Lees et al., *Evidence of  $B \rightarrow \tau \nu$  decays with hadronic B tags*, Phys.Rev. **D88** (2013) 031102, [arXiv:1207.0698].
- [57] **Belle Collaboration**, I. Adachi et al., *Evidence for  $B^- \rightarrow \tau^- \bar{\nu}_\tau$  with a Hadronic Tagging Method Using the Full Data Sample of Belle*, Phys.Rev.Lett. **110** (2013), no. 13 131801, [arXiv:1208.4678].
- [58] **BaBar Collaboration**, P. del Amo Sanchez et al., *Measurement of the  $B^0 \rightarrow \pi^\ell \ell^+ \nu$  and  $B^+ \rightarrow \eta^{(\prime)} \ell^+ \nu$  Branching Fractions, the  $B^0 \rightarrow \pi^- \ell^+ \nu$  and  $B^+ \rightarrow \eta \ell^+ \nu$  Form-Factor Shapes, and Determination of  $|V_{ub}|$* , Phys.Rev. **D83** (2011) 052011, [arXiv:1010.0987].

- [59] **BELLE Collaboration**, H. Ha et al., *Measurement of the decay  $B^0 \rightarrow \pi^- \ell^+ \nu$  and determination of  $|V_{ub}|$* , Phys.Rev. **D83** (2011) 071101, [arXiv:1012.0090].
- [60] **LHCb collaboration**, R. Aaij et al., *Measurement of the  $B_s^0 \rightarrow \mu^+ \mu^-$  branching fraction and search for  $B^0 \rightarrow \mu^+ \mu^-$  decays at the LHCb experiment*, Phys.Rev.Lett. **111** (2013) 101805, [arXiv:1307.5024].
- [61] **CMS Collaboration**, S. Chatrchyan et al., *Measurement of the  $B_s \rightarrow \mu^+ \mu^-$  branching fraction and search for  $B_0 \rightarrow \mu^+ \mu^-$  with the CMS Experiment*, Phys.Rev.Lett. **111** (2013) 101804, [arXiv:1307.5025].
- [62] A. J. Buras, J. Girrbach, D. Guadagnoli, and G. Isidori, *On the Standard Model prediction for  $\mathcal{B}(B_{s,d} \rightarrow \mu^+ \mu^-)$* , Eur.Phys.J. **C72** (2012) 2172, [arXiv:1208.0934].
- [63] A. J. Buras, R. Fleischer, J. Girrbach, and R. Knegjens, *Probing New Physics with the  $B_s \rightarrow \mu^+ \mu^-$  Time-Dependent Rate*, JHEP **1307** (2013) 77, [arXiv:1303.3820].
- [64] **ETM Collaboration**, N. Carrasco et al., *B-physics from  $N_f = 2$  tmQCD: the Standard Model and beyond*, JHEP **1403** (2014) 016, [arXiv:1308.1851].
- [65] **ETM Collaboration**, P. Dimopoulos et al., *Lattice QCD determination of  $m_b$ ,  $f_B$  and  $f_{B_s}$  with twisted mass Wilson fermions*, JHEP **1201** (2012) 046, [arXiv:1107.1441].
- [66] C. McNeile, C. Davies, E. Follana, K. Hornbostel, and G. Lepage, *High-Precision  $c$  and  $b$  Masses, and QCD Coupling from Current-Current Correlators in Lattice and Continuum QCD*, Phys.Rev. **D82** (2010) 034512, [arXiv:1004.4285].
- [67] G. M. de Divitiis, M. Guagnelli, R. Petronzio, N. Tantalo, and F. Palombi, *Heavy quark masses in the continuum limit of quenched lattice QCD*, Nucl.Phys. **B675** (2003) 309–332, [hep-lat/0305018].
- [68] **ALPHA Collaboration**, B. Blossier et al., *Parameters of Heavy Quark Effective Theory from  $N_f = 2$  lattice QCD*, JHEP **1209** (2012) 132, [arXiv:1203.6516].
- [69] **Coordinated Lattice Simulations**,  
[<https://twiki.cern.ch/twiki/bin/view/CLS/WebHome>] .
- [70] E. Eichten and B. R. Hill, *An Effective Field Theory for the Calculation of Matrix Elements Involving Heavy Quarks*, Phys.Lett. **B234** (1990) 511.
- [71] N. Isgur and M. B. Wise, *Weak Decays of Heavy Mesons in the Static Quark Approximation*, Phys.Lett. **B232** (1989) 113.
- [72] H. Georgi, *An Effective Field Theory for Heavy Quarks at Low-energies*, Phys.Lett. **B240** (1990) 447–450.
- [73] E. Eichten and B. R. Hill, *Static effective field theory:  $1/m$  corrections*, Phys.Lett. **B243** (1990) 427–431.
- [74] B. Grinstein, *The Static Quark Effective Theory*, Nucl.Phys. **B339** (1990) 253–268.
- [75] M. Luscher, *Volume Dependence of the Energy Spectrum in Massive Quantum Field Theories. 2. Scattering States*, Commun.Math.Phys. **105** (1986) 153–188.
- [76] T. Mannel, W. Roberts, and Z. Ryzak, *A Derivation of the heavy quark effective Lagrangian from QCD*, Nucl.Phys. **B368** (1992) 204–220.
- [77] A. F. Falk and M. Neubert, *Second order power corrections in the heavy quark effective theory. 1. Formalism and meson form-factors*, Phys.Rev. **D47** (1993) 2965–2981, [hep-ph/9209268].

- [78] **ALPHA Collaboration**, M. Kurth and R. Sommer, *Renormalization and  $O(a)$  improvement of the static axial current*, Nucl.Phys. **B597** (2001) 488–518, [hep-lat/0007002].
- [79] **ALPHA Collaboration**, M. Della Morte et al., *Lattice HQET with exponentially improved statistical precision*, Phys.Lett. **B581** (2004) 93–98, [hep-lat/0307021].
- [80] B. Thacker and G. Lepage, *A Lattice QCD simulation with dynamical heavy quarks*, Nucl.Phys.Proc.Suppl. **20** (1991) 509–512.
- [81] G. P. Lepage, L. Magnea, C. Nakhleh, U. Magnea, and K. Hornbostel, *Improved nonrelativistic QCD for heavy quark physics*, Phys.Rev. **D46** (1992) 4052–4067, [hep-lat/9205007].
- [82] E. Eichten and B. R. Hill, *Renormalization of Heavy - Light Bilinears and  $F(B)$  for Wilson Fermions*, Phys.Lett. **B240** (1990) 193.
- [83] G. Martinelli and C. T. Sachrajda, *Computation of the  $b$  quark mass with perturbative matching at the next-to-next-to-leading order*, Nucl.Phys. **B559** (1999) 429–452, [hep-lat/9812001].
- [84] L. Maiani, G. Martinelli, and C. T. Sachrajda, *Nonperturbative subtractions in the heavy quark effective field theory*, Nucl.Phys. **B368** (1992) 281–292.
- [85] R. Sommer, *Nonperturbative renormalization of HQET and QCD*, Nucl.Phys.Proc.Suppl. **119** (2003) 185–197, [hep-lat/0209162].
- [86] **ALPHA Collaboration**, J. Heitger and R. Sommer, *Nonperturbative heavy quark effective theory*, JHEP **0402** (2004) 022, [hep-lat/0310035].
- [87] M. Della Morte, N. Garron, M. Papinutto, and R. Sommer, *Heavy quark effective theory computation of the mass of the bottom quark*, JHEP **0701** (2007) 007, [hep-ph/0609294].
- [88] B. Blossier, M. della Morte, N. Garron, and R. Sommer, *HQET at order  $1/m$ : I. Non-perturbative parameters in the quenched approximation*, JHEP **1006** (2010) 002, [arXiv:1001.4783].
- [89] M. Neubert, *Symmetry breaking corrections to meson decay constants in the heavy quark effective theory*, Phys.Rev. **D46** (1992) 1076–1087.
- [90] S. Sint, *On the Schrodinger functional in QCD*, Nucl.Phys. **B421** (1994) 135–158, [hep-lat/9312079].
- [91] **ALPHA Collaboration**, M. Della Morte et al., *Non-perturbative quark mass renormalization in two-flavor QCD*, Nucl.Phys. **B729** (2005) 117–134, [hep-lat/0507035].
- [92] M. Della Morte, R. Hoffmann, and R. Sommer, *Non-perturbative improvement of the axial current for dynamical Wilson fermions*, JHEP **0503** (2005) 029, [hep-lat/0503003].
- [93] M. Luscher, S. Sint, R. Sommer, and P. Weisz, *Chiral symmetry and  $O(a)$  improvement in lattice QCD*, Nucl.Phys. **B478** (1996) 365–400, [hep-lat/9605038].
- [94] A. Grimbach, D. Guazzini, F. Knechtli, and F. Palombi,  *$O(a)$  improvement of the HYP static axial and vector currents at one-loop order of perturbation theory*, JHEP **0803** (2008) 039, [arXiv:0802.0862].
- [95] M. Marinkovic and S. Schaefer, *Comparison of the mass preconditioned HMC and the DD-HMC algorithm for two-flavour QCD*, PoS **LATTICE2010** (2010) 031, [arXiv:1011.0911].

- [96] M. Luscher, S. Sint, R. Sommer, P. Weisz, and U. Wolff, *Nonperturbative  $O(a)$  improvement of lattice QCD*, Nucl.Phys. **B491** (1997) 323–343, [hep-lat/9609035].
- [97] S. Lottini, *Chiral behaviour of the pion decay constant in  $N_f = 2$  QCD*, PoS **LATTICE2013** (2013) 315, [arXiv:1311.3081].
- [98] **ALPHA Collaboration**, B. Blossier et al., *HQET at order  $1/m$ : II. Spectroscopy in the quenched approximation*, JHEP **1005** (2010) 074, [arXiv:1004.2661].
- [99] F. Bernardoni, P. Hernandez, and S. Necco, *Heavy-light mesons in the epsilon-regime*, JHEP **1001** (2010) 070, [arXiv:0910.2537].
- [100] **ALPHA Collaboration**, J. Bulava, M. Donnellan, and R. Sommer, *The  $B^*B\pi$  Coupling in the Static Limit*, PoS **LATTICE2010** (2010) 303, [arXiv:1011.4393].
- [101] K. Chetyrkin and A. Retey, *Renormalization and running of quark mass and field in the regularization invariant and  $\overline{\text{MS}}$  schemes at three loops and four loops*, Nucl.Phys. **B583** (2000) 3–34, [hep-ph/9910332].
- [102] T. van Ritbergen, J. Vermaseren, and S. Larin, *The Four loop beta function in quantum chromodynamics*, Phys.Lett. **B400** (1997) 379–384, [hep-ph/9701390].
- [103] P. Baikov, K. Chetyrkin, and J. Kühn, *Quark Mass and Field Anomalous Dimensions to  $\mathcal{O}(\alpha_s^5)$* , [arXiv:1402.6611].
- [104] **ALPHA Collaboration**, B. Blossier et al., *HQET at order  $1/m$ : III. Decay constants in the quenched approximation*, JHEP **1012** (2010) 039, [arXiv:1006.5816].
- [105] R. Sommer, *A New way to set the energy scale in lattice gauge theories and its applications to the static force and  $\alpha_s$  in  $SU(2)$  Yang-Mills theory*, Nucl.Phys. **B411** (1994) 839–854, [hep-lat/9310022].
- [106] S. Aoki, Y. Aoki, C. Bernard, T. Blum, G. Colangelo, et al., *Review of lattice results concerning low energy particle physics*, [arXiv:1310.8555].
- [107] C. McNeile, C. Davies, E. Follana, K. Hornbostel, and G. Lepage, *High-Precision  $f_{B_s}$  and HQET from Relativistic Lattice QCD*, Phys.Rev. **D85** (2012) 031503, [arXiv:1110.4510].
- [108] **Fermilab Lattice Collaboration**, **MILC Collaboration**, A. Bazavov et al.,  *$B$ - and  $D$ -meson decay constants from three-flavor lattice QCD*, Phys.Rev. **D85** (2012) 114506, [arXiv:1112.3051].
- [109] H. Na, C. J. Monahan, C. T. Davies, R. Horgan, G. P. Lepage, et al., *The  $B$  and  $B_s$  Meson Decay Constants from Lattice QCD*, Phys.Rev. **D86** (2012) 034506, [arXiv:1202.4914].
- [110] **BaBar Collaboration**, B. Aubert et al., *A Search for  $B^+ \rightarrow \tau^+ \nu$  with Hadronic  $B$  tags*, Phys.Rev. **D77** (2008) 011107, [arXiv:0708.2260].
- [111] **BaBar Collaboration**, B. Aubert et al., *A Search for  $B^+ \rightarrow \ell^+ \nu_\ell$  Recoiling Against  $B^- \rightarrow D^0 \ell^- \bar{\nu} X$* , Phys.Rev. **D81** (2010) 051101, [arXiv:0912.2453].
- [112] **Belle collaboration**, K. Hara et al., *Evidence for  $B^- \rightarrow \tau^- \bar{\nu}_\tau$  with a Semileptonic Tagging Method*, Phys.Rev. **D82** (2010) 071101, [arXiv:1006.4201].
- [113] **CMS and LHCb Collaborations**, *Combination of results on the rare decays  $B_{(s)}^0 \rightarrow \mu^+ \mu^-$  from the CMS and LHCb experiments*, Tech. Rep. CMS-PAS-BPH-13-007. CERN-LHCb-CONF-2013-012, CERN, Geneva, Jul, 2013.
- [114] D. Becirevic, S. Fajfer, and S. Prelovsek, *On the mass differences between the scalar and pseudoscalar heavy-light mesons*, Phys.Lett. **B599** (2004) 55, [hep-ph/0406296].

- [115] D. Becirevic, E. Chang, and A. L. Yaouanc, *Pionic couplings to the lowest heavy-light mesons of positive and negative parity*, [arXiv:1203.0167].
- [116] **UKQCD Collaboration**, G. de Divitiis et al., *Towards a lattice determination of the  $B^*B\pi$  coupling*, JHEP **9810** (1998) 010, [hep-lat/9807032].
- [117] H. Ohki, H. Matsufuru, and T. Onogi, *Determination of  $B^*B\pi$  coupling in unquenched QCD*, Phys.Rev. **D77** (2008) 094509, [arXiv:0802.1563].
- [118] D. Becirevic, B. Blossier, E. Chang, and B. Haas,  *$g(B^*B\pi)$ -coupling in the static heavy quark limit*, Phys.Lett. **B679** (2009) 231–236, [arXiv:0905.3355].
- [119] F. Bernardoni, J. Bulava, M. Donnellan, and R. Sommer, *Precision lattice QCD computation of the  $B^*B\pi$  coupling*, [arXiv:1404.6951].
- [120] R. Godang, *Charm Decays and Spectroscopy at BABAR*, PoS **ICHEP2012** (2013) 330, [arXiv:1301.0141].
- [121] W. Detmold, C. D. Lin, and S. Meinel, *Calculation of the heavy-hadron axial couplings  $g_1$ ,  $g_2$ , and  $g_3$  using lattice QCD*, Phys.Rev. **D85** (2012) 114508, [arXiv:1203.3378].
- [122] D. Becirevic and F. Sanfilippo, *Theoretical estimate of the  $D^* \rightarrow D\pi$  decay rate*, Phys.Lett. **B721** (2013) 94–100, [arXiv:1210.5410].
- [123] A. Khodjamirian, R. Ruckl, S. Weinzierl, and O. I. Yakovlev, *Perturbative QCD correction to the light cone sum rule for the  $B^*B\pi$  and  $D^*D\pi$  couplings*, Phys.Lett. **B457** (1999) 245–252, [hep-ph/9903421].
- [124] P. Gambino, T. Mannel, and N. Uraltsev,  *$B \rightarrow D^*$  Zero-Recoil Formfactor and the Heavy Quark Expansion in QCD: A Systematic Study*, JHEP **1210** (2012) 169, [arXiv:1206.2296].
- [125] D. Becirevic, J. Charles, A. LeYaouanc, L. Oliver, O. Pene, et al., *Possible explanation of the discrepancy of the light cone QCD sum rule calculation of  $g(D^*D\pi)$  coupling with experiment*, JHEP **0301** (2003) 009, [hep-ph/0212177].
- [126] **ALPHA Collaboration**, F. Bernardoni, J. Bulaba, M. Donnellan, and R. Sommer, “In preparation.”
- [127] J. Bulava, *Progress on Excited Hadrons in Lattice QCD*, PoS **LATTICE2011** (2011) 021, [arXiv:1112.0212].
- [128] T. Burch, C. Gattringer, L. Y. Glozman, C. Hagen, D. Hierl, et al., *Excited hadrons on the lattice: Baryons*, Phys.Rev. **D74** (2006) 014504, [hep-lat/0604019].
- [129] D. Mohler and R. Woloshyn,  *$D$  and  $D_s$  meson spectroscopy*, Phys.Rev. **D84** (2011) 054505, [arXiv:1103.5506].
- [130] **CSSM Lattice Collaboration**, M. S. Mahbub, W. Kamleh, D. B. Leinweber, P. J. Moran, and A. G. Williams, *Roper Resonance in 2+1 Flavor QCD*, Phys.Lett. **B707** (2012) 389–393, [arXiv:1011.5724].
- [131] B. Blossier, J. Bulava, M. Donnellan, and A. Gérardin,  *$B^{*'} \rightarrow B$  transition*, Phys.Rev. **D87** (2013), no. 9 094518, [arXiv:1304.3363].
- [132] **OPAL Collaboration**, R. Akers et al., *Observations of  $\pi - B$  charge - flavor correlations and resonant  $B\pi$  and  $BK$  production*, Z.Phys. **C66** (1995) 19–30.
- [133] **ALEPH Collaboration**, D. Buskulic et al., *Production of excited beauty states in  $Z$  decays*, Z.Phys. **C69** (1996) 393–404.

- [134] **ALEPH Collaboration**, R. Barate et al., *Resonant structure and flavor tagging in the  $B\pi^\pm$  system using fully reconstructed  $B$  decays*, Phys.Lett. **B425** (1998) 215–226.
- [135] **DELPHI Collaboration**, P. Abreu et al., *Observation of orbitally excited  $B$  mesons*, Phys.Lett. **B345** (1995) 598–608.
- [136] **DELPHI Collaboration**, M. Feindt, *First evidence for the  $B^*$  Dalitz decay and radially excited  $B$ -mesons*, .
- [137] **DELPHI Collaboration**, W. Oberschulte-Beckmann, *Evidence for the  $B^*$  Dalitz decay and radially excited  $B$  mesons*, .
- [138] Z. Albrecht, G. Barker, M. Feindt, U. Kerzel, M. Moch, et al., *A study of excited  $b$ -hadron states with the DELPHI detector at LEP*, .
- [139] **L3 Collaboration**, M. Acciarri et al., *Measurement of the spectroscopy of orbitally excited  $B$  mesons at LEP*, Phys.Lett. **B465** (1999) 323–334, [hep-ex/9909018].
- [140] M. Paulini, *Spectroscopy and Decay of  $B$  Hadrons at the Tevatron*, eConf **C0610161** (2006) 027, [hep-ex/0702047].
- [141] **CDF Collaboration**, T. Aaltonen et al., *Measurement of Resonance Parameters of Orbitally Excited Narrow  $B^0$  Mesons*, Phys.Rev.Lett. **102** (2009) 102003, [arXiv:0809.5007].
- [142] **D0 Collaboration**, V. Abazov et al., *Observation and Properties of  $L = 1$   $B_1$  and  $B_2^*$  Mesons*, Phys.Rev.Lett. **99** (2007) 172001, [arXiv:0705.3229].
- [143] **D0 Collaboration**, V. Abazov et al., *Observation and properties of the orbitally excited  $B_{s2}^*$  meson*, Phys.Rev.Lett. **100** (2008) 082002, [arXiv:0711.0319].
- [144] **CDF Collaboration**, T. A. Aaltonen et al., *Study of orbitally excited  $B$  mesons and evidence for a new  $B\pi$  resonance*, Phys.Rev.D (2013) [arXiv:1309.5961].
- [145] **LHCb Collaboration**, *Observations of Orbitally Excited  $B_{(s)}^{**}$  Mesons*, .
- [146] **UKQCD Collaboration**, A. M. Green, J. Koponen, C. McNeile, C. Michael, and G. Thompson, *Excited  $B$  mesons from the lattice*, Phys.Rev. **D69** (2004) 094505, [hep-lat/0312007].
- [147] P. Gelhausen, A. Khodjamirian, A. Pivovarov, and D. Rosenthal, *Radial excitations of heavy-light mesons from QCD sum rules*, [arXiv:1404.5891].
- [148] D. Ebert, R. Faustov, and V. Galkin, *Heavy-light meson spectroscopy and Regge trajectories in the relativistic quark model*, Eur.Phys.J. **C66** (2010) 197–206, [arXiv:0910.5612].
- [149] M. B. Wise, *Chiral perturbation theory for hadrons containing a heavy quark*, Phys.Rev. **D45** (1992) 2188–2191.
- [150] H.-Y. Cheng, C.-Y. Cheung, G.-L. Lin, Y. Lin, T.-M. Yan, et al., *Chiral Lagrangians for radiative decays of heavy hadrons*, Phys.Rev. **D47** (1993) 1030–1042, [hep-ph/9209262].
- [151] G. Burdman and J. F. Donoghue, *Union of chiral and heavy quark symmetries*, Phys.Lett. **B280** (1992) 287–291.
- [152] J. Callan, Curtis G., S. R. Coleman, J. Wess, and B. Zumino, *Structure of phenomenological Lagrangians. 2.*, Phys.Rev. **177** (1969) 2247–2250.
- [153] S. R. Coleman, J. Wess, and B. Zumino, *Structure of phenomenological Lagrangians. 1.*, Phys.Rev. **177** (1969) 2239–2247.

- [154] R. Casalbuoni, A. Deandrea, N. Di Bartolomeo, R. Gatto, F. Feruglio, et al., *Phenomenology of heavy meson chiral Lagrangians*, Phys.Rept. **281** (1997) 145–238, [hep-ph/9605342].
- [155] A. F. Falk, *Hadrons of arbitrary spin in the heavy quark effective theory*, Nucl.Phys. **B378** (1992) 79–94.
- [156] A. F. Falk, H. Georgi, B. Grinstein, and M. B. Wise, *Heavy Meson Form-factors From QCD*, Nucl.Phys. **B343** (1990) 1–13.
- [157] T.-M. Yan, H.-Y. Cheng, C.-Y. Cheung, G.-L. Lin, Y. Lin, et al., *Heavy quark symmetry and chiral dynamics*, Phys.Rev. **D46** (1992) 1148–1164.
- [158] D. Becirevic, E. Chang, and A. L. Yaouanc, *On internal structure of the heavy-light mesons*, Phys.Rev. **D80** (2009) 034504, [arXiv:0905.3352].
- [159] M. Della Morte, R. Sommer, and S. Takeda, *On cutoff effects in lattice QCD from short to long distances*, Phys.Lett. **B672** (2009) 407–412, [arXiv:0807.1120].
- [160] J. Bulava, M. Donnellan, and R. Sommer, *On the computation of hadron-to-hadron transition matrix elements in lattice QCD*, JHEP **1201** (2012) 140, [arXiv:1108.3774].
- [161] **ETM Collaboration**, C. Michael, A. Shindler, and M. Wagner, *The continuum limit of the static-light meson spectrum*, JHEP **1008** (2010) 009, [arXiv:1004.4235].
- [162] T. Burch, C. Hagen, C. B. Lang, M. Limmer, and A. Schafer, *Excitations of single-beauty hadrons*, Phys.Rev. **D79** (2009) 014504, [arXiv:0809.1103].
- [163] M. Luscher, *Two particle states on a torus and their relation to the scattering matrix*, Nucl.Phys. **B354** (1991) 531–578.
- [164] M. Luscher, *Signatures of unstable particles in finite volume*, Nucl.Phys. **B364** (1991) 237–254.
- [165] D. Mohler, S. Prelovsek, and R. Woloshyn,  *$D\pi$  scattering and  $D$  meson resonances from lattice QCD*, Phys.Rev. **D87** (2013), no. 3 034501, [arXiv:1208.4059].
- [166] **UKQCD Collaboration**, C. McNeile, C. Michael, and G. Thompson, *Hadronic decay of a scalar  $B$  meson from the lattice*, Phys.Rev. **D70** (2004) 054501, [hep-lat/0404010].
- [167] **UKQCD Collaboration**, C. McNeile, C. Michael, and P. Pennanen, *Hybrid meson decay from the lattice*, Phys.Rev. **D65** (2002) 094505, [hep-lat/0201006].
- [168] **UKQCD Collaboration**, C. McNeile and C. Michael, *Mixing of scalar glueballs and flavor singlet scalar mesons*, Phys.Rev. **D63** (2001) 114503, [hep-lat/0010019].
- [169] **UKQCD Collaboration**, C. McNeile and C. Michael, *Hadronic decay of a vector meson from the lattice*, Phys.Lett. **B556** (2003) 177–184, [hep-lat/0212020].
- [170] S. Fajfer and J. F. Kamenik, *Chiral loop corrections to strong decays of positive and negative parity charmed mesons*, Phys.Rev. **D74** (2006) 074023, [hep-ph/0606278].
- [171] P. Colangelo, F. De Fazio, G. Nardulli, N. Di Bartolomeo, and R. Gatto, *Strong coupling of excited heavy mesons*, Phys.Rev. **D52** (1995) 6422–6434, [hep-ph/9506207].
- [172] T. Aliev and M. Savci, *The Strong  $g_{B^{(*)}B\pi}$  coupling constant in full QCD*, J.Phys. **G22** (1996) 1759–1763, [hep-ph/9604258].

- [173] D. Becirevic, V. Lubicz, F. Sanfilippo, S. Simula, and C. Tarantino, *D-meson decay constants and a check of factorization in non-leptonic B-decays*, JHEP **1202** (2012) 042, [arXiv:1201.4039].
- [174] S. Godfrey and N. Isgur, *Mesons in a Relativized Quark Model with Chromodynamics*, Phys.Rev. **D32** (1985) 189–231.
- [175] Z.-F. Sun, J.-S. Yu, X. Liu, and T. Matsuki, *Newly observed  $D(2550)$ ,  $D(2610)$ , and  $D(2760)$  as  $2S$  and  $1D$  charmed mesons*, Phys.Rev. **D82** (2010) 111501, [arXiv:1008.3120].
- [176] V. Morenas, A. Le Yaouanc, L. Oliver, O. Pene, and J. Raynal, *Quantitative predictions for B semileptonic decays into D,  $D^*$  and the orbitally excited  $D^{**}$  in quark models a la Bakamjian-Thomas*, Phys.Rev. **D56** (1997) 5668–5680, [hep-ph/9706265].
- [177] A. K. Leibovich, Z. Ligeti, I. W. Stewart, and M. B. Wise, *Semileptonic B decays to excited charmed mesons*, Phys.Rev. **D57** (1998) 308–330, [hep-ph/9705467].
- [178] D. Becirevic, A. Le Yaouanc, L. Oliver, J.-C. Raynal, P. Roudeau, et al., *Proposal to study  $B_s \rightarrow \bar{D}_{sJ}$  transitions*, Phys.Rev. **D87** (2013), no. 5 054007, [arXiv:1206.5869].
- [179] I. Bigi, B. Blossier, A. Le Yaouanc, L. Oliver, O. Pene, et al., *Memorino on the ‘1/2 vs. 3/2 Puzzle’ in  $\bar{B} \rightarrow \ell\nu X_c$ : A Year Later and a Bit Wiser*, Eur.Phys.J. **C52** (2007) 975–985, [arXiv:0708.1621].
- [180] M. Neubert and B. Stech, *Nonleptonic weak decays of B mesons*, Adv.Ser.Direct.High Energy Phys. **15** (1998) 294–344, [hep-ph/9705292].
- [181] M. Bauer, B. Stech, and M. Wirbel, *Exclusive Nonleptonic Decays of D,  $D_{(s)}$ , and B Mesons*, Z.Phys. **C34** (1987) 103.
- [182] **ETM Collaboration**, P. Boucaud et al., *Dynamical Twisted Mass Fermions with Light Quarks: Simulation and Analysis Details*, Comput.Phys.Commun. **179** (2008) 695–715, [arXiv:0803.0224].
- [183] R. Frezzotti and G. Rossi, *Chirally improving Wilson fermions. 1.  $O(a)$  improvement*, JHEP **0408** (2004) 007, [hep-lat/0306014].
- [184] **ETM Collaboration**, B. Blossier et al., *Average up/down, strange and charm quark masses with  $N_f = 2$  twisted mass lattice QCD*, Phys.Rev. **D82** (2010) 114513, [arXiv:1010.3659].
- [185] **ETM Collaboration**, B. Blossier et al., *Pseudoscalar decay constants of kaon and D-mesons from  $N_f = 2$  twisted mass Lattice QCD*, JHEP **0907** (2009) 043, [arXiv:0904.0954].
- [186] G. Colangelo and C. Haefeli, *Finite volume effects for the pion mass at two loops*, Nucl.Phys. **B744** (2006) 14–33, [hep-lat/0602017].
- [187] **PACS-CS Collaboration**, Y. Namekawa et al., *Charm quark system at the physical point of 2+1 flavor lattice QCD*, Phys.Rev. **D84** (2011) 074505, [arXiv:1104.4600].
- [188] **Belle Collaboration**, A. Zupanc, *Improved measurements of  $D_s$  meson decay constant and branching fractions of  $D_s^+ \rightarrow K^- K^+ \pi^+$ ,  $\bar{K}^0 K^+$  and  $\eta \pi^+$  decays from Belle*, [arXiv:1212.3942].
- [189] J. L. Rosner and S. Stone, *Leptonic decays of charged pseudoscalar mesons - 2012*, [arXiv:1201.2401].

- [190] D. Becirevic, S. Fajfer, S. Prelovsek, and J. Zupan, *Chiral corrections and lattice QCD results for  $f_{B_s}/f_{B_d}$  and  $\Delta m_{B_s}/\Delta m_{B_d}$* , Phys.Lett. **B563** (2003) 150–156, [hep-ph/0211271].
- [191] **QCDSF Collaboration**, A. Ali Khan et al., *Accelerating the hybrid Monte Carlo algorithm*, Phys.Lett. **B564** (2003) 235–240, [hep-lat/0303026].
- [192] M. Gockeler, R. Horsley, Y. Nakamura, H. Perlt, D. Pleiter, et al., *Perturbative and Nonperturbative Renormalization in Lattice QCD*, Phys.Rev. **D82** (2010) 114511, [arXiv:1003.5756].
- [193] G. Bali, S. Collins, and P. Perez-Rubio, *Charmed hadron spectroscopy on the lattice for  $N_f = 2 + 1$  flavours*, J.Phys.Conf.Ser. **426** (2013) 012017, [arXiv:1212.0565].
- [194] G. Moir, M. Peardon, S. M. Ryan, and C. E. Thomas, *Excited  $D$  and  $D_s$  meson spectroscopy from lattice QCD*, PoS **ConfinementX** (2012) 139, [arXiv:1301.3397].
- [195] **BaBar Collaboration**, B. Aubert et al., *Measurement of  $|V_{cb}|$  and the Form-Factor Slope in  $\bar{B} \rightarrow D\ell^-\bar{\nu}_\ell$  Decays in Events Tagged by a Fully Reconstructed  $B$  Meson*, Phys.Rev.Lett. **104** (2010) 011802, [arXiv:0904.4063].
- [196] J. Charles, O. Deschamps, S. Descotes-Genon, R. Itoh, H. Lacker, et al., *Predictions of selected flavour observables within the Standard Model*, Phys.Rev. **D84** (2011) 033005, [arXiv:1106.4041].
- [197] V. Belyaev, V. M. Braun, A. Khodjamirian, and R. Ruckl,  *$D^*D\pi$  and  $B^*B\pi$  couplings in QCD*, Phys.Rev. **D51** (1995) 6177–6195, [hep-ph/9410280].
- [198] J. Vermaseren, S. Larin, and T. van Ritbergen, *The four loop quark mass anomalous dimension and the invariant quark mass*, Phys.Lett. **B405** (1997) 327–333, [hep-ph/9703284].
- [199] **ALPHA Collaboration**, M. Della Morte et al., *Computation of the strong coupling in QCD with two dynamical flavors*, Nucl.Phys. **B713** (2005) 378–406, [hep-lat/0411025].
- [200] **ALPHA Collaboration**, S. Sint and P. Weisz, *The Running quark mass in the  $SF$  scheme and its two loop anomalous dimension*, Nucl.Phys. **B545** (1999) 529–542, [hep-lat/9808013].
- [201] M. Luscher, R. Narayanan, P. Weisz, and U. Wolff, *The Schrodinger functional: A Renormalizable probe for non Abelian gauge theories*, Nucl.Phys. **B384** (1992) 168–228, [hep-lat/9207009].